UNIVERSITÀ DEGLI STUDI
DI GENOVA

Corso di Dottorato in Scienze e Tecnologie per l'Ambiente e il Territorio (STAT)

Curriculum: Scienze della Terra

XXXIII ciclo

Title:

The study of cave deposits as a contribution to paleoclimatic reconstruction in western Liguria

PhD candidate: Eleonora Sessa

Supervisor: Dr. Ivano Rellini

Acknowledgements

Well, here we are.

I would like to thank my supervisor, dr. Rellini, who helped, encouraged and inspired me to do better and better.

I was lucky enough to work within multidisciplinary groups (from different universities and research institutions) composed of helpful, kind and understanding people who are always willing to assist me.

I also found the same willingness and kindness in the many profs and researchers of University of Genova who, at times, have done the impossible for the data collected within this thesis. I will never thank you enough, especially in the face of the difficulties faced in the last year.

Not only the members of the academy contributed to the realization of this thesis: I would like to thank the librarians and all the administrative staff who contributed, aiding me, despite my, sometimes absurd, questions and problems.

A special thanks also goes to my two external evaluators and the commission who made themselves available and took the time to make this work much better.

A huge thank you goes to my colleagues and former colleagues. I consider myself lucky to have met you and I am glad that our cultural differences have not been an insurmountable problem, despite your grumbling and my pronouncements. (Just kidding, maybe).

I thank my friends who have already grown tired of my continuing to study and hardly ever going out. I miss you all so much.

I would like to thank my boyfriend, also. Thank you. (Anything I wrote he wouldn't like it anyway).

Finally, I thank my family, who every time invents for me a new field of research not knowing exactly what I'm doing. If you want, there are 27x pages here where I explain it. Have fun!

Abstract

The deposits of four caves in western Liguria have been investigated, in particular Tana di Badalucco (Imperia), Arma degli Zerbi (Savona), Caverna delle Fate (Savona) and Arma delle Manie (Savona). These are caves already extensively studied in the past, but exclusively from an archaeological point of view. In this case, the study involved the application of different techniques aimed at the final objective of obtaining a paleoclimatic and paleoenvironmental reconstruction for this study area. The techniques used were different, starting from routine bulk analyses, passing from XRD analysis, and ending, and focusing in particular, on the use of the micromorphological technique. This allowed us to identify, in detail, the more or less significant changes that occurred in this region during the last glacial period and the Holocene, and therefore the alternation of more or less cold and more or less humid conditions of the last 120 kyr.

Table of contents

Acknowledgements 2

Abstract 3

1. Aims of the study 7

2. Paleoecology and paleoenvironmental reconstruction from the Late Pleistocene 8

2.1 Liguria region, and its surroundings, paleoclimate and paleoenvironment 15

The Last interglacial and the beginning of the Last glaciation (MIS 5) 15

The Last glaciation (MIS 4 – MIS 2) 17

The Holocene (MIS 1) 21

2.2 Present-day climate 22

2.3 Cave settings 23

3 Study area 27

3.1 Tana di Badalucco 27

Geological and environmental context 28

Previous studies 29

3.2 Finalese area 31

Geological context 31

Site description and previous studies 39

4. Materials and methods 55

4.1 Fieldwork and site stratigraphy 55

4.2 Sampling 57

4.3 Laboratory analysis 58

4.4 X-Ray Powder Diffraction (XRD) 60

4.5 Radiocarbon dating 60

4.6 Micromorphological analysis 61

5. Results 63

Tana di Badalucco 63

Field work and site stratigraphy 63
Sampling 65
Micromorphological analysis 67
Arma degli Zerbi 75
Fieldwork and site stratigraphy 75
Sampling 79
Laboratory analysis 80
X-ray powder diffraction 84
Radiocarbon dating 86
Micromorphological analysis 87
Caverna delle Fate 99
Fieldwork and site stratigraphy 100
Sampling 102
Laboratory analysis 103
X-ray powder diffraction 105
Radiocarbon dating 106
Micromorphological analysis 106
Arma delle Manie 120
Fieldwork and site stratigraphy 120
Sampling 123
Laboratory analysis 123
X-ray powder diffraction 125
Radiocarbon dating 127
Micromorphological analysis 127
6. Discussion and conclusions 138
Tana di Badalucco 138
Arma degli Zerbi 148
Caverna delle Fate 161

Arma delle Manie 175
7. Comparison between the study sites and general conclusions 186
Figure index 190
Table index 199
Bibliography 201
Appendices 231
Appendix A: Micromorphological description table 231
Appendix B: Micromorphological analysis description 235
Tana di Badalucco cave 235
Arma degli Zerbi 243
Caverna delle Fate 255
Arma delle Manie 268

1. Aims of the study

The main objective of this work was to give a paleoclimatic reconstruction of the period that goes from the Last Glaciation to today for western Liguria. In this way, the results obtained would then be placed within a wider context and compared with what is already known. Indeed, as Courty and Vallverdu (2001) affirm, this information at the regional scale is indispensable to refine the global picture we already possess. Most of the knowledge we have comes from studies of ice cores and marine sediments, but also cave sediments can be considered a reliable proxy for this purpose. The main features of these infillings, in effect, are the high temporal resolution and the environmental sensitivity they demonstrate, qualities of great value when trying to reconstruct climates and environments of the past. It can also help in understanding and deepening how the environment responds to certain stimuli and climate changes, as well in the long term.

Another important objective was to demonstrate the importance and effectiveness of the use of micromorphological analysis, always associated with other field and bulk analysis, and within a multidisciplinary working group. This technique makes it possible to recognize details that the naked eye cannot, such as fine sedimentary structures, and particular features (pedofeatures) capable of giving precise information on the process that led to their creation. Furthermore, thanks to its employ, large quantities of material are not necessary, an aspect that should not be underestimated in a context where deposits have already been almost completely removed. The distinction between primary or secondary material, and between syn- and post-depositional processes, becomes easier, if not possible only in this manner. In this way, it will be possible to have a more complete and faithful image of the processes occurring on the studied materials, as well as a relative chronology of these. Finally, it is thus possible to determine the origin of the finer elements, visible only using a microscope, and determine whether they are of geogenic, biogenic, or of anthropogenic nature.

2. Paleoecology and paleoenvironmental reconstruction from the Late Pleistocene

The paleoecological and paleoenvironmental reconstruction of the Last Glacial – Interglacial cycle, in particular for western Liguria, can be considered as the main focus of this thesis.

The Last Glacial - Interglacial cycle occurred around the last 120 kyr b2k (thousands of years before 2000 AD) (Baumgartner *et al.*, 2014; Kindler *et al.*, 2014), also considering the period just after the end of the last glaciation, which occurred around 10 kyr b2k, or 11.7 kyr Before Present, BP (Marchal *et al.*, 2002; Rousse *et al.*, 2006; Baumgartner *et al.*, 2014).

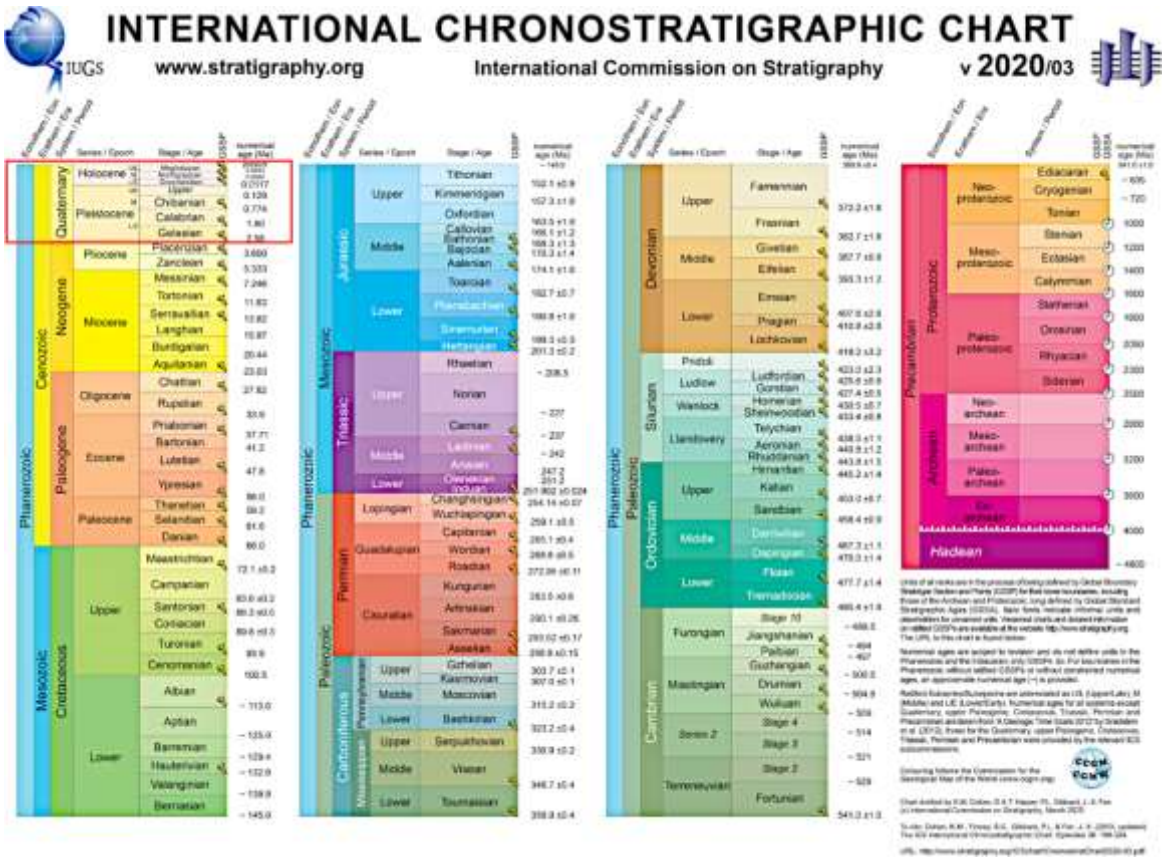

Figure 1 - International Stratigraphic Chart as released by the International Commission on Stratigraphy in 2020. The red square indicates the restricted temporal extension of the Quaternary period.

Referring to the Geological Time Scale (Cohen *et al.*, 2013), as presented by the International Chronostratigraphic Chart, the time frame mentioned above covers a very limited part of the chart (Figure 1). In fact, the concerned portion does not even include the entire Quaternary period, which

alone extends from 2.58 Ma to the present day (Cohen *et al.*, 2013). In turn, the Quaternary is divided into two eras: the Pleistocene (from 2.58 Ma up to 0.0117 Ma) and the Holocene (from 0.0117 Ma to today) (Anderson, Goudie and Parker, 2013; Cohen *et al.*, 2013). Nevertheless, not the whole Pleistocene epoch will be considered here.

The Pleistocene (and to a lesser extent the Holocene) was a very unstable era from a climatic and environmental point of view (Pisias and Moore, 1981; Saltzman and Maasch, 1988; Raymo, 1992; Greenland Ice-core Project (GRIP) Members, 1993; Saltzman and Verbitsky, 1994; Ding *et al.*, 1999; Davis *et al.*, 2003; Hemming, 2004; Davis, Menounos and Osborn, 2009). This is known thanks to the cross-comparison between different proxies, which have allowed a more or less detailed reconstruction of the climates and environments in different areas of the planet.

Since the late 1940s, the fractionation of stable oxygen isotopes has been used to reconstruct the paleotemperatures of the last hundreds of thousands years of the Earth (Urey, 1947; Epstein *et al.*, 1951; Arrhenius, 1953; Emiliani, 1955; Brenchley and Harper, 2010). This is possible thanks to the ratio between the heaviest stable isotope of oxygen, ^{18}O, and the lightest stable isotope, ^{16}O, and the way they behave reciprocally within a system (Urey, 1947; Emiliani, 1955). The equation displayed here defines how much the isotopic fractionation of a sample can deviate from the prefixed standard (usually SMOW, Standard Mean Oceanic Water) and thus how much a sample is enriched in ^{18}O (Emiliani, 1955):

$$\delta = 1000\ \frac{^{18}O/^{16}O(sample) - \ ^{18}O\ /\ ^{16}O\ (standard)}{^{18}O\ /\ ^{16}O\ (standard)}$$

The principle behind this method is that living things deposit a carbonate shell richer in the heavier isotope (^{18}O), rather than the lighter one (^{16}O), under colder conditions (Urey, 1947). It has been demonstrated by Epstein et al. (1951) that there is a relation between these stable isotopes fractionation and paleotemperature, and it was empirically demonstrated by this formula:

$$t\ (°C) = 16.5 - \ 4.3\delta + 0.14\delta^2$$

The first works attempting to use this method proposed a reconstruction of paleotemperatures starting from the ratio of the two isotopes content within bivalves' shells in marine sediments (Urey,

1947; Epstein *et al.*, 1951). Although the technique proved to be excellent, it was later realized that another type of organism was to be preferred, since these are not so easily found and not so often recurring in the ocean sediments' column (Emiliani, 1955). It was in this wake of studies that Emiliani (1955) carried out his analyses on isotope fractionation, considering planktonic Foraminifera instead of bivalves. Unfortunately, even this choice was affected by certain negative influences: the data were excessively prejudiced by the so-called "glacial effect", linked to the Rayleigh distillation (Shackleton, 1967; Shackleton *et al.*, 2003; Scott *et al.*, 2004). For this reason, the study of the fractionation of oxygen in benthic Foraminifera began: in this case, despite having the same variability as planktonic Foraminifera, it was not influenced by glacial and interglacial periods (Shackleton, 1967).

Already from the first results obtained by Emiliani (1955), it was noted how the isotopic curves based on planktonic Foraminifera from the Caribbean and the Mediterranean behaved in the same way and showed the same oscillatory trend, indicative of a fluctuation in global temperatures from the Pleistocene to today. Again, Emiliani (1955), in his work, quoted (and modified) the chronology proposed by Arrhenius (1953), the one on which the division in Marine Isotope Stages (MIS) is still based (Figure 2 and Figure 3). In fact, even then an alternation between warmer "stages" and colder "stages" had been noticed (Arrhenius, 1953; Emiliani, 1955). They found it convenient to indicate with the number 1 the current warm stage and to increase in number going backwards in time, keeping odd numbers for warmer periods and even numbers for colder ones (Figure 2) (Arrhenius, 1953; Emiliani, 1955).

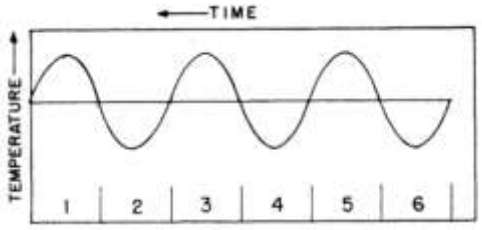

Figure 2 - "Ideal variation of temperature with time, and stage numbers". From Emiliani (1955). *The original (and ideal) Marine Isotope Stages (MIS) as proposed by Emiliani and Arrhenius.*

Obviously, since then, the techniques and the obtained results have refined, nonetheless the underlying principle has remained the same. Currently there are many master archives: ice cores (with the GRIP and NGRIP projects, for example) (Antoine et al., 2009; Dumitru et al., 2018; Grootes et al., 1993; Kindler et al., 2014; Mojtabavi et al., 2019; Rasmussen et al., 2014; Schwander et al., 1997; and others) which return quality information, but only of most recent times; and oceanic sediments

(ODP, for example) (Raymo, 1992; Waelbroeck *et al.*, 2002, 2008; Drysdale *et al.*, 2004; Dumitru *et al.*, 2018) which have a more limited temporal resolution, but cover longer time intervals.

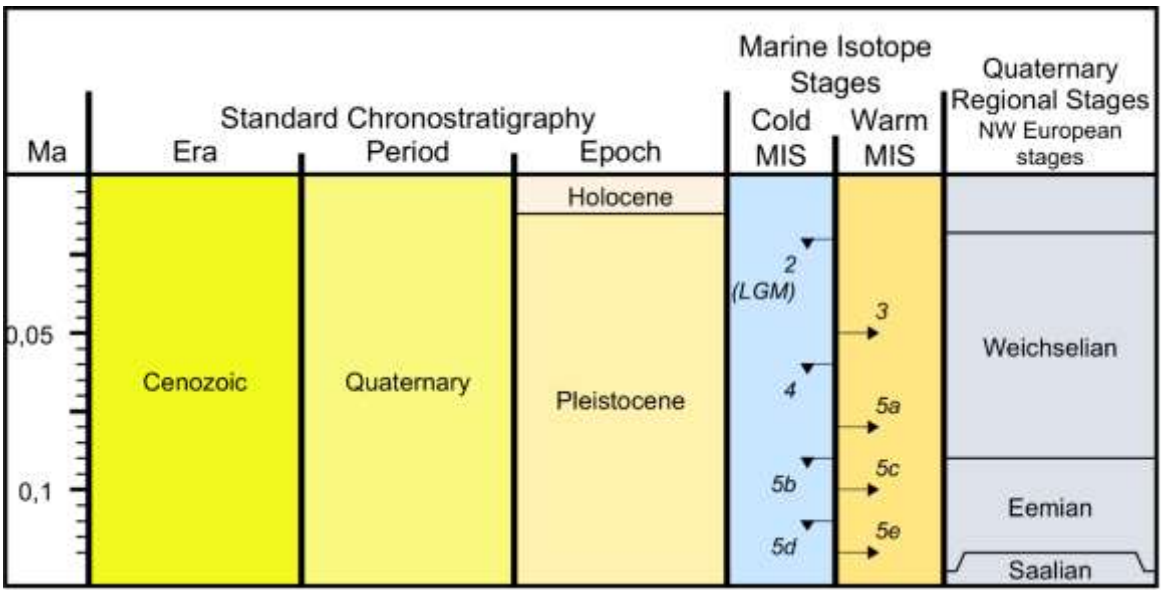

Figure 3 - The reciprocal relationships existing between geochronological and climatostratigraphic units as they are known today. Figure realized with TS-Creator (2020).

As demonstrated by Emiliani and Arrhenius, MIS did indeed indicate warmer (interglacial) and colder (glacial) periods (Arrhenius, 1953, 1961; Emiliani, 1955; Anderson, Goudie and Parker, 2013). Over time, the technique has been applied in different occasions and, with it, the data has become more detailed (Raymo, 1992; Ding *et al.*, 1999; Waelbroeck *et al.*, 2002; Shackleton *et al.*, 2003). So much so that it was realized that, even within the same glacial and interglacial periods, it was possible to recognize minor fluctuations in temperatures, known as stadials and interstadials (Johnsen *et al.*, 1992; Brook, Sowers and Orchardo, 1996; Hughes, 1996; Ditlevsen, Ditlevsen and Andersen, 2002; Voelker, 2002; Anderson, Goudie and Parker, 2013; Baumgartner *et al.*, 2014; Rasmussen *et al.*, 2014; Roberts, 2014). Thus, the behaviour of the recorded temperature in relation to time is very far from the ideal proposed by Emiliani (1955) and Arrhenius (1953) (Figure 2). Stadials can be considered as a relative cold phase, with ice sheets expansion, during a glacial period (Johnsen *et al.*, 1992; Anderson, Goudie and Parker, 2013). Whereas, interstadials are defined as relatively warmer periods, with ice sheets retreat, still during a glacial cycle (Dansgaard *et al.*, 1982; Anderson, Goudie and Parker, 2013). Stadials and interstadials have been recognised in Greenland ice cores and are often referred to as GSs (Greenland Stadials) and GIs (Greenland Interstadials) (Figure 4),

respectively (Spötl and Mangini, 2002; North Greenland Ice Core Project members, 2004; Van Meerbeeck *et al.*, 2011; Rasmussen *et al.*, 2014). They can only be considered to have occurred in the northern hemisphere (Brook, Sowers and Orchardo, 1996; Voelker, 2002; North Greenland Ice Core Project members, 2004; Flückiger, Knutti and White, 2006; Flückiger *et al.*, 2008; Steffensen *et al.*, 2008; Waelbroeck *et al.*, 2008; Cheng *et al.*, 2009; Miller *et al.*, 2011).

Recurring events in the different climate proxies are the Dansgaard-Oeschger and Heinrich events. The former represents a recurring series of abrupt climate changes of local/regional scale, where atmospheric and oceanic conditions shifted from milder conditions, typical of interstadials, to more rigid conditions, typical of stadials (Hughes, 1996; Kjellström *et al.*, 2010; Rasmussen *et al.*, 2014). There are 25 recognized events of this type, with a duration of a few decades and temperature changes between 5 °C and 16 °C (Rasmussen *et al.*, 2014). The Heinrich events, on the other hand, are large climatic fluctuations linked to layers of Ice-Rafted Debris (IRD), associated with the Laurentide ice sheet (Heinrich, 1988; Hemming, 2004). They are documented above all in the North Atlantic records and occurred during some of the longer stadials of the last glaciation (Hughes, 1996; Flückiger, Knutti and White, 2006; Kjellström *et al.*, 2010; Rasmussen *et al.*, 2014). The Heinrich events suggest cold and arid conditions in the North Atlantic and partly in Europe (Heinrich, 1988; Flückiger, Knutti and White, 2006; Clark *et al.*, 2013). In any case, according to some authors, it is possible to state the presence of a Heinrich event only in the presence of evident levels of IRD and not only if a cold period is recognised in the studied record (Lowe *et al.*, 2008; Rasmussen *et al.*, 2014). Unfortunately, it is still unclear the process or the triggering event behind these episodes, and so also on what can vary their duration (Flückiger, Knutti and White, 2006; Anderson, Goudie and Parker, 2013; Clark *et al.*, 2013).

In paleoclimatic and paleoenvironmental reconstruction, there is a complication common to all the events occurred during the last glaciation: time-transgression (Ruddiman and McIntyre, 1973; Lowe, 2001; Brown *et al.*, 2013). All the processes occurring on Earth are linked to each other and influence each other in turn, sometimes triggering new ones in cascade. The same is true for all processes that trigger climate and environmental changes (Ruddiman and McIntyre, 1973). Since each region of the planet has its own characteristics, it will respond differently and with different timing to changes in the atmosphere, water circulation, air temperatures, and so on (Lowe, 2001; Anderson, Goudie and Parker, 2013; Lowe and Walker, 2014). It is for this reason that the broad chronologies derived from the above master records (i.e. ice cores and ocean sediments) do not always find an exact match in the continental records and it is for this reason that studies like this are necessary (Courty and Vallverdu, 2001).

Just considering the European continent, we know that it is a very complex and multifaceted context (Housley *et al.*, 1997; Sommer and Benecke, 2004; Sommer and Nadachowski, 2006; Willner, Di Pietro and Bergmeier, 2009; Drees *et al.*, 2010), and the same is true for the Mediterranean area. The Mediterranean is globally recognized as a peculiar environment that has played a great role as a refuge for many animal and plant species, but also for man (Carrion and Sanchez-Gomez, 1992; Figueiral and Terral, 2002; Petit *et al.*, 2003; Habel, Dieker and Schmitt, 2009; Médail and Diadema, 2009; Cheddadi and Khater, 2016; Koç, Svenning and Avcı, 2018; Roberts *et al.*, 2018). Finally, a similar role, but on a smaller scale, was played by the Italian region Liguria which, being on the sea and limited by the mountains – thus protecting its area from the harsh climatic changes of North Europe -, acted as a refuge habitat during the last glacial period (Bahn, 1977; Kaniewski *et al.*, 2005; Casazza *et al.*, 2008; Ricci Lucchi, 2008; Rellini *et al.*, 2013; Burke *et al.*, 2017).

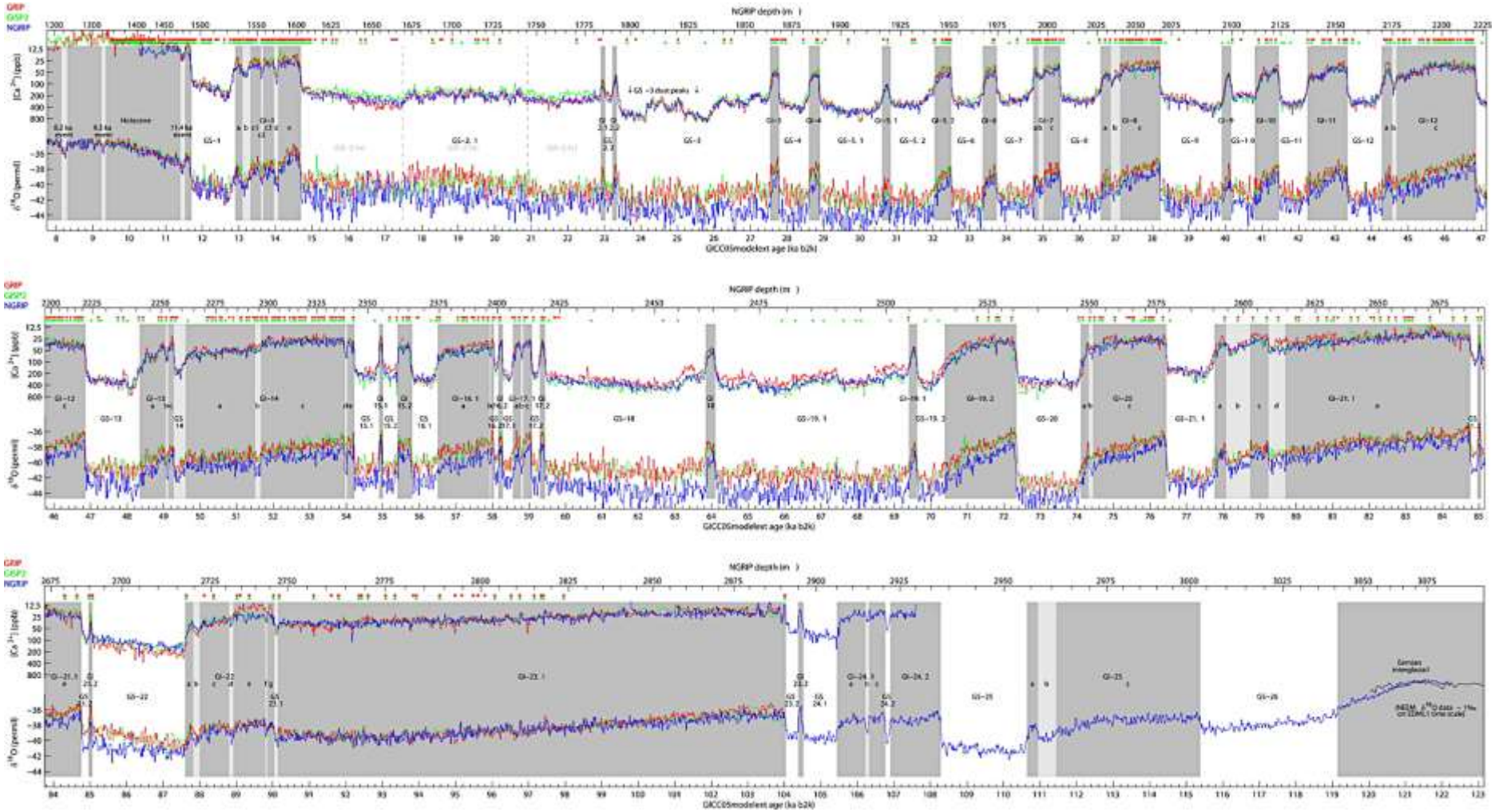

Figure 4 – From (Rasmussen *et al.*, 2014). *Here it is possible to see the correlation between temperatures and stable isotopes of the last 123 kyr (here reported as ka b2k, i.e. thousand of years before 2000 AD) as obtained from Greenland ice core studies (and from the GRIP, GISP2 and NGRIP projects, in red, green and blue respectively). All recognized events are differentiated by colour (white or grey), such as the last interglacial (Eemian) and the various stadials and interstadials.*

2.1 Liguria region, and its surroundings, paleoclimate and paleoenvironment

The Last interglacial and the beginning of the Last glaciation (MIS 5)

Marine Isotopic Stage 5 has always been divided into five substages, usually indicated with the first five lowercase letters of the alphabet (starting from the more recent, a, to the older one, e), characterised by very different climatic conditions (Shackleton *et al.*, 2003).

MIS 5e approximately coincides with the Last interglacial and sometimes is also referred to as MIS 5.5 (as in Figure 5). According to an almost disused denomination for the Mediterranean basin, we can refer to it as the Tyrrhenian period (another chronostratigraphic subunit, Figure 5), during which the ESL (Estimated Sea Level) was calculated to be between +4 m +9 m above the present mean sea level (Bardají *et al.*, 2009; Pascucci, Sechi and Andreucci, 2014; Benjamin *et al.*, 2017). This information is important with regards to the studied cave deposits, as the considered caves are all located not too far from the current shoreline and, thus, also their deposits are indirectly influenced by it (Bar-Matthews *et al.*, 1999; Vesica *et al.*, 2000). Another important piece of information gleaned from coastal studies - whose indicators include marine terraces, beachrocks, fossils, and tidal notches (Benjamin *et al.*, 2017) - concerns meteorological events: according to many scientists, at the end of the Last interglacial there have been important changes in weather conditions, such as an increase in storminess and runoff (Bardají *et al.*, 2009), as cold conditions were restoring.

There are not many data regarding the state of vegetation during the last interglacial and even the few present do not go into great detail. This might be due to the limited resolution of the studied deposits and to the partial presence and preservation of pollen (Kaniewski, Renault-Miskovsky and de Lumley, 2005). For what we know, the end of MIS 6 and the beginning of MIS 5e sees the transition from open vegetation to forests (Ricci Lucchi, 2008). High temperatures and rising sea levels allow trees to move away from their former refugia and spread (Ricci Lucchi, 2008). During the last interglacial, species linked to colder climates survive, while, in the meantime, there is an increase in thermophilous species and Mediterranean taxa at low altitudes and along the coasts (Ricci Lucchi, 2008). Genera such as *Picea*, *Abies* and *Quercus*, on the other hand, expanded: *Picea* and *Abies* at upper elevations and, mixed with deciduous *Quercus*, at middle to lower altitudes (Combourieu-Nebout *et al.*, 2015). With the upcoming end of MIS 5e, there is a disruption of the continental vegetation cover and a repeated denudation of the valley slopes, probably correlated with the said meteorological changes (Pascucci, Sechi and Andreucci, 2014). In this way the landscape is more similar to that of the steppe, even in the Ligurian area, with increasing aridity near the coast, and a crescendo of humidity as the altitude increases (Kaniewski *et al.*, 2005; Bardají *et al.*, 2009).

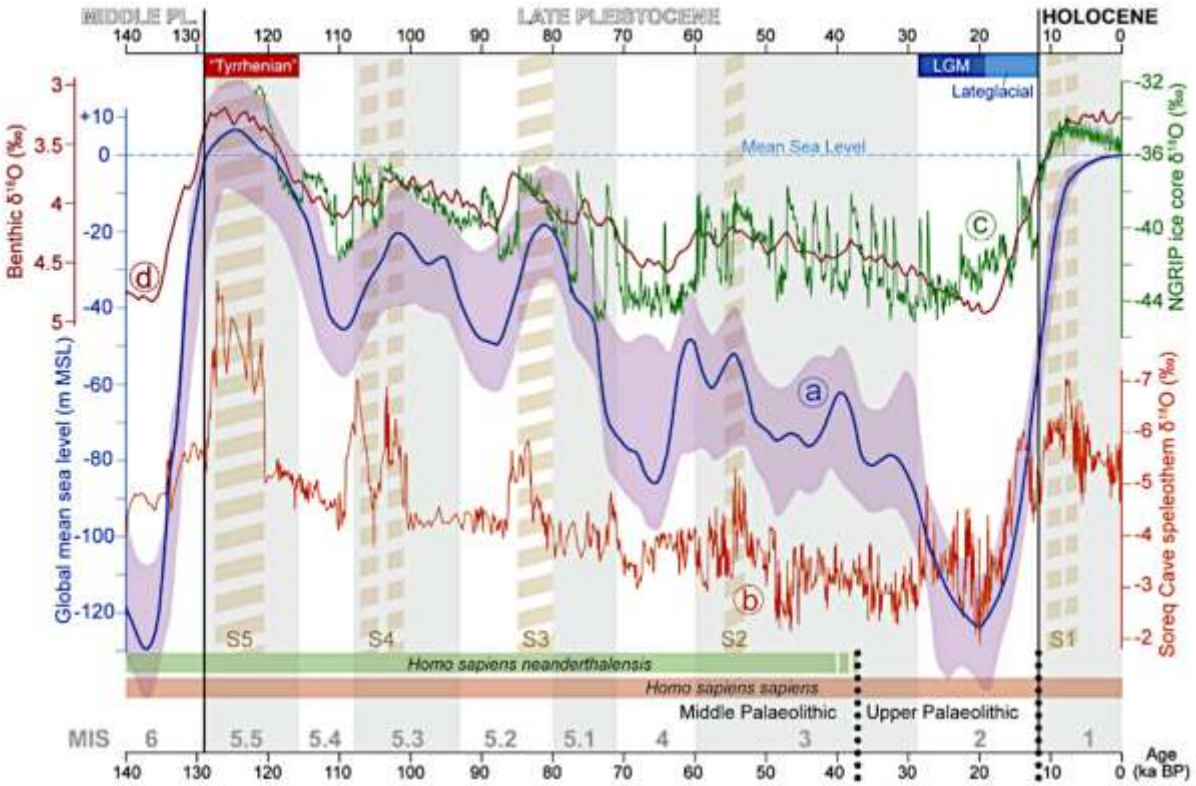

Figure 5 - Global mean sea level compared with paleoclimate proxies and human evolution and industry since 140 kyr BP. From Benjamin *et al.* (2017). *a) Global mean sea-level curve, with its uncertainty (from* Waelbroeck *et al.* (2002)*). b) Variation in oxygen isotopes indicating paleoclimatic variations for the SE Mediterranean basin. c) Paleoclimatic proxy for the northern hemisphere from the NGRIP project* (North Greenland Ice Core Project members, 2004; Kindler *et al.*, 2014)*. d) Variation of stable oxygen isotopes for the benthic composition* (Lisiecki and Stern, 2016). *Brown dashed shading indicates periods of sapropel deposition* (Rohling, Marino and Grant, 2015).

The faunal data regarding the transition from MIS 6 to MIS 5, and the subsequent development of the latter, are also rather limited as regards the areas under examination (Defleur and Desclaux, 2019). In any case, it is known that the climate change between the MIS 6 glaciation and the beginning of the Eemian period was rather rapid, and it passed from a glacial period to a warmer temperate period than the present one (Defleur and Desclaux, 2019). The sea level, as mentioned above, was much higher than today and many sites, such as those of the Balzi Rossi in the SE of France, were located below sea level, as evidenced by the discovery of many *Strombus bubonius* shells (Federici and Pappalardo, 2006; Valensi, 2009; Onoratini *et al.*, 2012; Moussous, Valensi and Simon, 2014). Therefore we move from faunal assemblages of red deer (*Cervus elaphus*) and ibex (*Capra ibex*) to animals of warmer climates (Valensi and Psathi, 2004; Valensi, Crégut-Bonnoure and Defleur, 2012). Throughout the MIS 5, a peculiar climate creates, allowing the formation of coastal corridors, capable of facilitating migration and leading to a redistribution of flora and fauna along the NW Ligurian and SE French coast (Valensi, 2009). Between MIS 5c and 5a, the typical associations of temperate

climates of that time are characterized by the presence of red deer (*Cervus elaphus*, that survived the climatic change), fallow deer (*Dama* sp.), roe deer (*Capreolus capreolus*), giant deer (*Megaloceros giganteus*), straight-tusked elephant (*Palaeoloxodon antiquus*), narrow-nosed rhinoceros (*Stephanorhinus hemitoechus*), asiatic black bear (*Ursus thibetanus*), among others (Valensi and Psathi, 2004; Kaniewski, Renault-Miskovsky and de Lumley, 2005; Onoratini *et al.*, 2012; Moussous, Valensi and Simon, 2014; Defleur and Desclaux, 2019; Brugal *et al.*, 2020).

The Last glaciation (MIS 4 – MIS 2)

The period between the start of MIS 4 (about 75 kyr b2k) and the end of MIS 2 (which approximately corresponds to the start of the Holocene, 11.7 kyr BP) is considered a generally cold period, with many and wide fluctuations, in temperatures, in rainfall, and in the estimated sea level (Figure 5) (Waelbroeck *et al.*, 2002; Pascucci, Sechi and Andreucci, 2014). The Early Pleniglacial (MIS 4) was relatively short (about 10 kyr) and tended to be a cold and dry period (Moreno *et al.*, 2012; Pascucci, Sechi and Andreucci, 2014). MIS 3 (between 60 and 28 kyr b2k) was much more unstable and relatively wetter (Martrat *et al.*, 2004; Sorin *et al.*, 2010; Pascucci, Sechi and Andreucci, 2014; Weber *et al.*, 2018). At the end of this period the onset of the Last Glacial Maximum drastically took place, leading to extreme drops in temperatures (even of 13 °C) and estimated sea level (- 80 m with respect to present mean sea level), as well as a decrease in humidity, thus returning to rather arid conditions (Vesica *et al.*, 2000; Rovere *et al.*, 2011; Pascucci, Sechi and Andreucci, 2014; Benjamin *et al.*, 2017).

These cold and arid conditions, as well as the extent of their variations over this period of time, have been vastly underestimated for the Mediterranean basin area (Ramstein *et al.*, 2007). Extremely cold periods and relatively warm periods (but not as warm as the present ones) have alternated also in these areas, with the extension of glaciers and areas influenced by the incidence of permafrost, even at low latitudes (Huijzer and Isarin, 1997; Wohlfarth *et al.*, 2008; Becker *et al.*, 2015; Oliva *et al.*, 2018). Unfortunately, most of the information from the various studies concerns exclusively the maximum peak of this phenomenon, i.e. the traces left during the Last Glacial Maximum (LGM) (Bini, Tognini and Zuccoli, 1998; Bini, 2005). Bini (2005) well explains how it is not possible to know the exact extension of the various expansions and regressions of ice sheets during the last glaciation, since the subsequent events have practically eliminated all traces. Therefore only the LGM signs remain, hence when glaciers in the Alps were at their maximum and a periglacial environment extended much more than now (Becker *et al.*, 2017; Sessa, Bona and Angiolini, 2021). With the expansion of glaciers, the extent of the permafrost also accentuated. There are traces of its presence

in the Pre-Alps, but also in certain parts of the Mediterranean (Oliva *et al.*, 2018). It is well documented also in Liguria, although, in these cases, it was just a seasonal and discontinuous permafrost (Van Vliet-Lanoë and Hallegouët, 2001; Rellini *et al.*, 2013, 2014; Oliva *et al.*, 2018) (Figure 6).

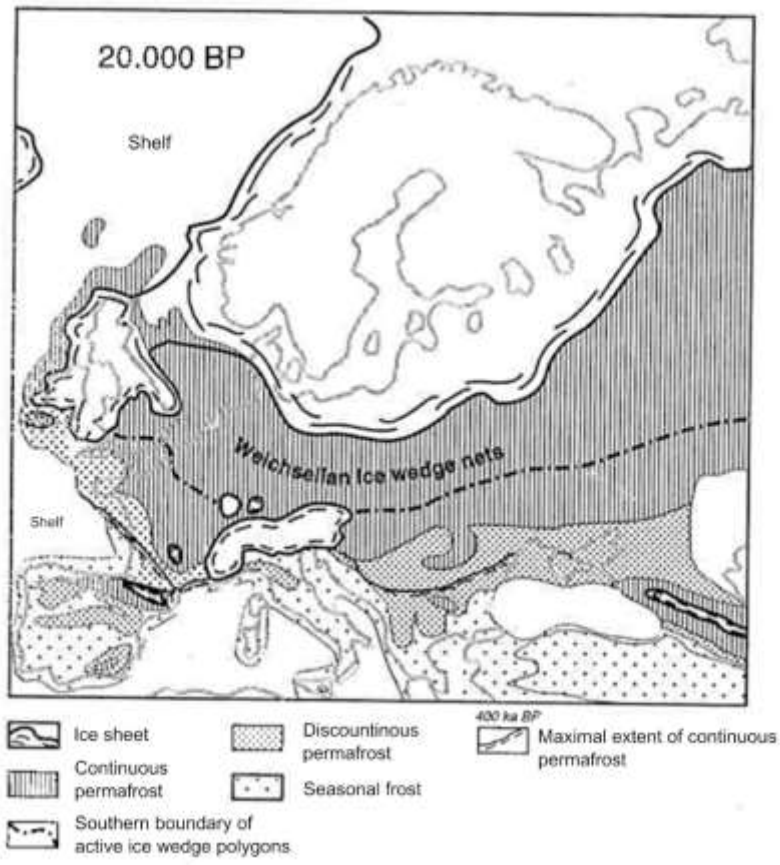

Figure 6 - Permafrost extension 20 kyr BP, related to the northern European ice sheets and the active networks of ice wedges. In Van Vliet-Lanoë and Hallegouët (2001).

Another important element that characterized this time period was loess (Fitzsimmons, Marković and Hambach, 2012; Hošek *et al.*, 2015; Profe *et al.*, 2016). It is usually defined as a silty aeolian deposit, composed mainly of quartz, feldspar, mica, clay minerals and carbonate grains (Pye, 1984). It is generally homogeneous, showing no stratifications, but it can be highly porous (Pye, 1984; Rellini *et al.*, 2009). Generally yellowish, but it can also be grey, red or brown (Pye, 1984; Zerboni *et al.*, 2018). An important aspect in its definition is its granulometry: it is generally located between 20-40 µm, but it can also have a high percentage of sands (> 20%, *sandy loess*) or clays (> 20%, *clayey loess*) (Pye, 1984; Yang, Karius and Sauer, 2020). Finally, it can be considered eventually a *primary loess*, if deposited directly from the wind; a *reworked loess*, as a material reworked from

primary loess; or *weathered loess*, if it has undergone weathering, pedogenesis or diagenesis (Pye, 1984). This sediment is particularly important also for the paleoclimatic information it brings with it: it is now known that the ideal environment for loess deposition is an arid and cold one, with little or no vegetation at all, where the main source can retraced near or far from the deposit (Cremaschi *et al.*, 1990; Antoine *et al.*, 2009; Rousseau *et al.*, 2017, 2018; Zerboni *et al.*, 2018). The main deposits of this material are found in China, Russia and Central Europe, where they can reach thicknesses up to 30 m (Pye, 1984; Rousseau *et al.*, 2018). In any case, many studies have also considered northern Italy, in particular the Po Plain loess basin and its surrounding areas (Cremaschi and Van Vliet-Lanoë, 1990; Rellini *et al.*, 2009; Cremaschi *et al.*, 2015; Zerboni *et al.*, 2018). Sheets of these sediments have also been documented for Liguria, where reworked loess has been recognized and studied (Rellini, 2007; Rellini *et al.*, 2009, 2014).

Thus, the beginning of the last glacial period sees a drastic drop in temperatures and sea level. Organisms react differently, and more or less promptly, throughout the Mediterranean area. During MIS 4, the vegetation changes, becoming more open and dominated by *Artemisia*, accompanied by Poaceae and Asteraceae, typical steppe and arid environments species (Margari *et al.*, 2009; Biltekin *et al.*, 2019; Guido *et al.*, 2020). Similar behaviours are found in different countries such as Spain and Greece, but also in the Ligurian and Tuscan Apennines and in the Ligurian Alps (Kaniewski *et al.*, 2005; Kaniewski, Renault-Miskovsky and de Lumley, 2005; Ricci Lucchi, 2008; Margari *et al.*, 2009; Biltekin *et al.*, 2019; Guido *et al.*, 2020). In this way, various episodes of alternation between steppe environment, mesothermophilous forest and then steppe again, alternated (Burjachs *et al.*, 2012; Biltekin *et al.*, 2019). In some areas, rather than others, tree species are found throughout the glacial record, despite the constant climatic changes (Kaniewski, Renault-Miskovsky and de Lumley, 2004; Ricci Lucchi, 2008; Guido *et al.*, 2020). In these cases, this is justified by local factors and geographical and geomorphological characteristics of the area, which have allowed the creation of tree refugia (Ricci Lucchi, 2008; Guido *et al.*, 2020), as is the case of western Liguria (Kaniewski, Renault-Miskovsky and de Lumley, 2004, 2005; Kaniewski *et al.*, 2005). In any case, the pollen, and flora data in general, agree in indicating the period of MIS 4 as cold and arid, with a grassland-steppic assemblage (Kaniewski *et al.*, 2005; Margari *et al.*, 2009; Burjachs *et al.*, 2012; Biltekin *et al.*, 2019). MIS 3 was much more unstable and periods of open woodland interchanged with short periods of climate improvement (Badino *et al.*, 2020), characterized by species such as *Quercus* spp., *Rhamnus*, *Olea-Phyllirea* and others (Biltekin *et al.*, 2019). Finally, MIS 2 is documented as the driest period of the glaciation, during which steppe vegetation prevailed again over all others (Moreno *et al.*, 2012), although in western Liguria many traces of trees from less rigid environments have been recognized, too (Kaniewski, Renault-Miskovsky and de Lumley, 2004, 2005; Kaniewski *et al.*, 2005).

As for the fauna of this period, nearby sites have returned a more or less clear picture of the general situation. An unequivocal aspect that permeates these works is the fundamental role played by these areas as a refuge, not only for plant species, but also for animals (Sommer and Nadachowski, 2006; Valensi, 2009). Furthermore, the data collected from caves' or shelters' deposits can be the result of the influence exerted by man, being the products of hunting and sustenance, and not the exact picture of the overall spectrum of the fauna population (Tagliacozzo *et al.*, 2012). Moreover, since we are actually talking about a refuge area, it is important to consider that we will not witness absolute faunal changes, but rather a change in the proportions of the same species, with the introduction of few more typical of cold climates (Valensi, 2009). The data regarding MIS 4 are fewer than those of MIS 3 and 2. Finds from the Grotte du Lazaret cave (France) and from the Santa Lucia Superiore cave (Toirano, Liguria, NW Italy) indicate a transitional period with the appearance of species associated to colder climates (Valensi *et al.*, 2008; Valensi, 2009; Onoratini *et al.*, 2012). Therefore we have species like *Elephas antiquus* (Falconer and Cautley, 1847) (Mol, de Vos and van der Plicht, 2007; Onoratini *et al.*, 2012), but also chamois (*Rupicapra rupicapra*), bison (*Bison priscus*), deer (*Cervus elaphus*), ibex (*Capra ibex*), and, above all, cave bear (*Ursus spelaeus*) (de Lumley *et al.*, 2008; Valensi, 2009). MIS 3 presents a more complex situation, partly due to the aforementioned climatic fluctuations. As for the previous stage, *Elephas antiquus* is also reported here, this time flanked to the *Mammuthus primigenius* (Blumenbach, 1799) (Onoratini *et al.*, 2012). Around 40 kyr BP, in Western Liguria, there are signs of forest related species, of relatively humid and temperate conditions, such as *Chionomys nivalis*, *Microtus arvalis* and *Microtus* (*Terricola*) gr. *multiplex - subterraneus* (Riparo Mochi) (Berto, Santaniello and Grimaldi, 2019), *Clethrionomys glareolus*, *Apodemus* (*sylvaemus*) and *Elyomis quercinus* at Riparo Bombrini (Holt *et al.*, 2019). Subsequently, there is a shift towards a slightly colder and more arid period, with a percentage decrease of *Microtus* (*Terricola*) *multiplex-subterraneus* and *Clethrionomys glareolus* (Berto, Santaniello and Grimaldi, 2019). At the beginning of LGM, *Microtus arvalis* becomes dominant in Riparo Mochi's deposits, while, throughout the region (and not only), cave bear remains are found in large quantities (Valensi, 2009). The LGM onset terminates with the beginning of MIS 2 and with a general further worsening in climatic conditions (Obreht *et al.*, 2017). Again, the zone acts as a glacial refugia and exhibits faunal assemblages typical of generally colder, though not so cold, areas (Sommer and Nadachowski, 2006; Valensi, 2009). In this case, Arene Candide cave is the best example available: between 25 kyr BP and 18 kyr BP circa, the fauna that occupied its chambers varied significantly. At the beginning of this time period, *Marmota marmota* dominated, but also hyena, cave bear and leopard were present (Tagliacozzo *et al.*, 2012). At around 23 kyr BP, there is almost an absence of cold species, but hyena and red deer are reported (Cassoli and Tagliacozzo, 1994). Subsequently (~ 20 kyr BP) a new cold

regime establishes, with lynx, elk and mammoth, and then return to forest species (Cassoli and Tagliacozzo, 1994; Royer *et al.*, 2016; Berto, Santaniello and Grimaldi, 2019).

The Holocene (MIS 1)

With the beginning of the Holocene, we witness a slow change towards present day climate and environment. A marine transgression occurs, leading to a sea level rise of 120 m (Mariotti Lippi *et al.*, 2007; Carobene, Firpo and Rovere, 2008; Andreucci *et al.*, 2014; Pascucci, Sechi and Andreucci, 2014). For what concerns the Ligurian Sea coast, the sea level rose continuously throughout the Holocene, slowing down around 7.5 kyr BP and around 3 kyr BP, until it reached nowadays level, still undergoing limited variations, mainly in the isostatic adjustment (Carobene, Firpo and Rovere, 2008; Vacchi *et al.*, 2016) (Figure 7). At ~13 kyr BP the relative sea level (RSL) is at -45.6 ± 1.2 m, which quickly goes to -18 ± 0.9 m (~9.3 kyr BP), slowing down around ~7.5 kyr BP with values of -6.1 ± 1 m and slowing even more at ~3 kyr BP with -0.4 ± 0.3m (Carobene, Firpo and Rovere, 2008; Vacchi *et al.*, 2016).

Figure 7 - How sea level rose during Holocene. Modified from Vacchi *et al.* (2016).

As already demonstrated by sea level change, the changes occurring at the beginning of the Holocene are considerable. For what concerns vegetation, around 11.6 kyr BP, in eastern Liguria, there is an expansion in the mesophilous woodland, with the increase of *Abies* and the decline of *Pinus*, perhaps *mugo* (Arobba and Caramiello, 2008; Bellini, Mariotti-Lippi and Montanari, 2009; Montanari *et al.*, 2014; Guido *et al.*, 2020). Along with these, also grow *Quercus, Alnus, Betula, Corylus* and *Fagus* (Guido *et al.*, 2020). Not long after, a great environmental change takes place (~ 9.9 kyr BP) leading to increasingly better climatic conditions, marked by a further decline in species such as *Pinus* and *Artemisia*, leaving behind more space for *Quercus, Corylus, Alnus, Fagus, Tilia, Ulmus Fraxinus* and Ericaceae (Bellini, Mariotti-Lippi and Montanari, 2009; Branch, 2013;

Montanari *et al.*, 2014; Arobba *et al.*, 2018; Guido *et al.*, 2020). In general, throughout the Early and Middle Holocene, *Abies* is seen declining in favour of *Fagus* (Branch and Marini, 2014; Branch *et al.*, 2014; Arobba *et al.*, 2018). At the same time, the human impact also increases making it difficult to distinguish between human action and actual climate and environmental changes (Roberts *et al.*, 2004; Mariotti Lippi *et al.*, 2007; Branch, 2013; Branch and Marini, 2014). More and more anthropogenic taxa are found, in caves and shelters deposits, but also in lake sediments, in the west as in the east of Liguria, mainly in cereal species (Branch *et al.*, 2014; Arobba *et al.*, 2018). Also the quantity of microcharcoals found is higher, probably linked to a new need for open and cultivable land (Branch and Marini, 2014; Guido *et al.*, 2020). The peak of this phenomenon seems to occur around 3.5 kyr BP, when a good amount of *Vitis* is found in Ligurian and Tuscan Apennines (Mariotti Lippi *et al.*, 2007). Finally, in the Late Holocene, the Mediterranean maquis really starts to expand, perhaps favoured by a different management of the landscape exerted by man (Bellini, Mariotti-Lippi and Montanari, 2009).

The trend detected by the vegetation is confirmed by the fauna. The beginning of the Holocene sees an increase in forest cover, thus more forest-adapted species are found, examples are some genera of bats found in Arene Candide deposits (e.g. *Nyctalus lasiopterus*) (Salari, 2010). From the mid-Holocene and on, the animal remains found in cave deposits and other environments studied, always indicate a greater influence on the part of man (Alhaique, 1994; Cassoli and Tagliacozzo, 1994; Sommer and Benecke, 2005; Angelone, Moncunill-Solé and Kotsakis, 2020). In this period pastoralism begins to develop and with it new species of animals linked to man's sustenance are introduced (Sommer and Benecke, 2005; Angelone, Moncunill-Solé and Kotsakis, 2020). In the M levels of the Arene Candide cave the most represented animals are: *Cervus elaphus*, *Capreolus capreolus* and *Sus scrofa*, indicating a strong human influence (Alhaique, 1994; Cassoli and Tagliacozzo, 1994).

2.2 Present-day climate

The study area present-day climate, as defined by the Köppen-Geiger classification is *Csa*, i.e. temperate, with a dry and hot summer (Kottek *et al.*, 2006; Peel, Finlayson and McMahon, 2007; Fratianni and Acquaotta, 2017). In general, temperatures are mitigated by the presence of the Tyrrhenian sea and it is evident the great difference with very close areas, such as the Po Plain (Fratianni and Acquaotta, 2017). On average, rainfall, especially for the study areas (Figure 8a), is comprehended between 700 mm and 1000 mm per year (ARPAL, 2013). Summers are hot and dry, with maximum temperatures above 30 °C and the four hottest months always having an average

temperature above 20 °C (ARPAL, 2013) (Figure 8b). The minimum temperatures are never really low and the average temperature of the coldest month (January), in the last sixteen years, has been 7.7 ° C (Regione Liguria, 2021) (Figure 8b). The days with a minimum temperature below 0 ° C (the so-called "*frost days*", Figure 8c) were between 6 and 9 for the Finalese area, and between 15 and 18 for the areas near Pigna (ARPAL, 2013).

2.3 Cave settings

Caves have long been considered as sedimentary traps (Goldberg and Macphail, 2013; Karkanas and Goldberg, 2017; Nejman *et al.*, 2018), and the deposits, or sediments, inside them – as consequence - as excellent sedimentary records (Courty and Vallverdu, 2001), or paleoclimatic archives (White, 2007). This because of two important characteristics they possess: temporal resolution and environmental sensitivity (Woodward and Goldberg, 2001). Where the latter can be defined as "*the propensity of a system to respond to a minor external change*" (Shumm, 1991). All caves are a combination of deposition environments, sensitive to the outside world at different rates and magnitudes (Courty and Vallverdu, 2001).

From the cave deposits study, it is also possible to propose a correlation between different sites stratigraphy and paleoclimatic reconstruction (Woodward and Goldberg, 2001), even if some difficulties can be found. Local factors can sometime hide the recognition of more general climatic conditions (Courty and Vallverdu, 2001; Goldberg and Sherwood, 2006; Karkanas and Goldberg, 2017). One way to distinguish local factors (microclimate) from broader climatic factors (macroclimate) affecting deposits is to use a multidisciplinary approach, employing all the best techniques of one field and collaborating with experts from other disciplines (Goldberg and Macphail, 2013; Karkanas and Goldberg, 2017).

Cave sediments can be of different origin. They can be geogenic, biogenic or anthropogenic (Farrand, 2001; Goldberg and Sherwood, 2006; Goldberg and Macphail, 2013; Karkanas and Goldberg, 2013, 2017) and it is important to be able to recognize each one of these in order to give the best interpretation possible of the stratigraphies studied. The geogenic, biogenic and anthropogenic sediments can be clastic or chemical, primary or secondary and endogenous or exogenous (Goldberg and Sherwood, 2006; White, 2007; Goldberg and Macphail, 2013; Karkanas and Goldberg, 2017), as shown in Table 1.

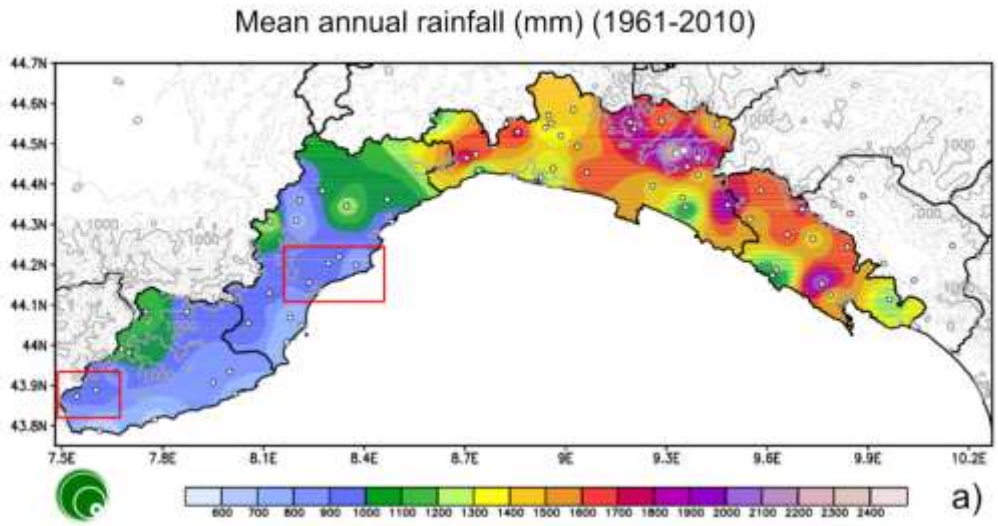

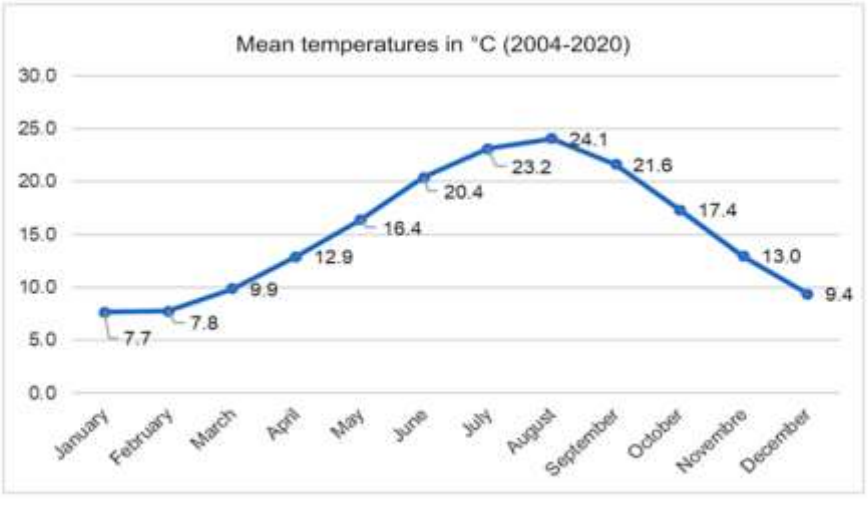

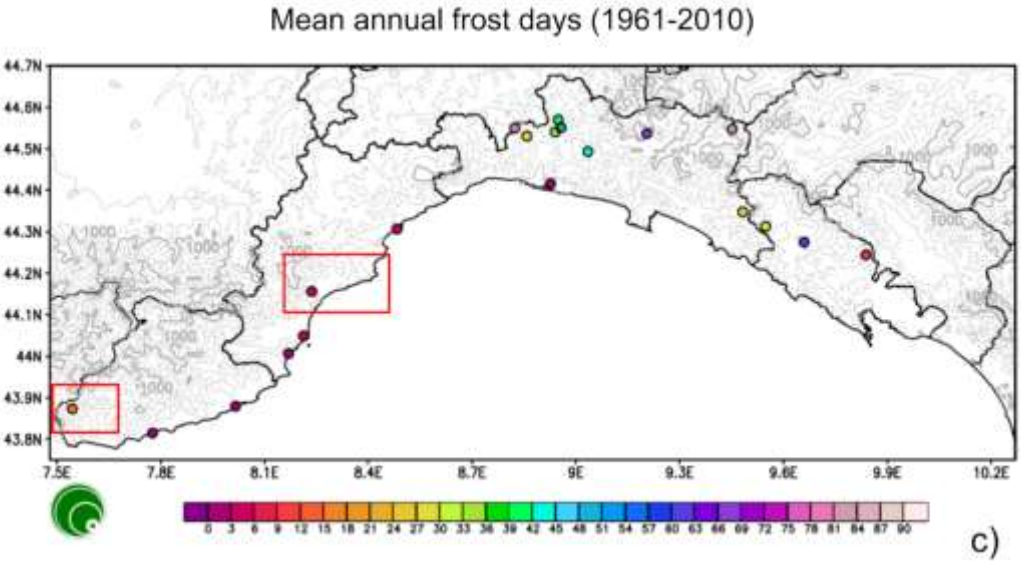

Figure 8 - a) Mean annual rainfall (in mm): the data collected cover the entire period from 1961 to 2010.With two red rectangles are indicated, starting from the West, the area near Pigna Municipality, where Tana di Badalucco cave is situated, and the Finalese

area where the remaining three studied caves are located. Modified from ARPAL (2013). *b) Mean temperatures (in °C) for the sole Finalese area, as obtained from the ARPAL site* (Regione Liguria, 2021). *No data were available for the other area. c) Mean annual frost days, i.e. the days with a minimum temperature below 0 ° C. What was said for a) also applies here. Modified from* ARPAL (2013).

Although cave deposits have the important characteristic of remaining almost unchanged and are able to keep track of the main changes in the environment for long periods of time, and regardless of their origin or nature, they undergo diagenesis, a low-temperature post-depositional change (Goldberg and Sherwood, 2006) and syn- and other post-depositional processes. This processes leave easily recognizable traces in the sediments and these, in turn, can convey information regarding particular conditions to which the cave environments have been subjected and, consequently, also the surrounding area (Karkanas *et al.*, 2000; Goldberg and Sherwood, 2006; Karkanas and Goldberg, 2013). Some examples of these processes can be found in Table 2.

*Table 1 - A non-exhaustive table of cave sediments types divided for origin and nature. * indicates high likelihood, - indicates low likelihood of finding. Modified from* (Goldberg and Sherwood, 2006).

Sediment type	Endogenous	Exogenous
Clastic sediments		
Geogenic:		
- Weathering detritus;	*	
- Block breakdown (*éboulis*);	*	
- Grain breakdown by dissolution, abrasion;	*	
- Entrance talus;	*	*
- Infiltrates;	*	*
- Fluvial, glacial, aeolian deposits.		*
Biogenic:		
- Bird and bat guano;	*	-
- Gastroliths;	*	-
- Carnivore, Omnivore and herbivore coprolites and bone;	*	*
- Plant residues (grass, wood, pollen);	-	*
Anthropogenic:		
- Microartifacts (bone, lithics, shell,…);	-	*
- Transported material (soil, sediment, organic material);	-	*
- Wood, charcoal, ash.	-	*
Chemical sediments		
Geogenic:		
- Carbonates (speleothems, for example);	*	
- Resistates;	*	
- Ice.	*	
Biogenic:		
- Oxide, phosphate, carbonate and nitrate minerals;	*	
- Guano.	*	

Table 2 - A non-exhaustive table of processes occurring inside a cave. Modified from (Goldberg and Sherwood, 2006).

Physical processes
Reworking by wind, water, biological activity, humans;
Slumping and faulting;
Trampling by humans and other animals;
Burrowing by humans and other animals;
Vertical translocation of particles by water and ice;
Dumping of material, midden formation;
Hearth cleaning and sweeping of hearths.
Chemical processes
Calcification;
Decalcification;
Phosphate mineralisation and bone dissolution;
Formation of other authigenic minerals.

3 Study area

3.1 Tana di Badalucco

Tana di Badalucco is located in NW Italy, in the Pigna (IM) municipality (Figure 9a), not far from the French border. Rio Corvo and Rio Muratone streams meet in this area, called Marellae, few meters from this site, significantly shaping the valley below, resulting in a good geographic passage-way exploited in the past by animals and humans (Chiarenza, 2007). The cave is placed 665 m a.s.l. and 18 m above the Rio Corvo stream. Tana di Badalucco cave has only one entrance, oriented to the West, oval-shaped, slightly oblique leftwards, and with its main axis 3 m high (Figure 9b). It probably owes its name to the original owner of the area, but the toponym similarity with another cave (Tana Bertrand, in the Badalucco municipality) has created many misunderstandings over time (Sessa *et al.*, 2019). In addition to this, the cave itself has many names and is often found mentioned differently (e.g., *Tana di Barraicu*, *Sgarbu di Barraico* (Calandri, Crippa and Ramella, 1979), *Sgarbu di Barauco*, *Tana di Ballanco*, *Grotta Torello*, *Grotta Tuvetto* (Issel, 1908), *Grotta Tovello* and *U' Garbu de Baraico*). Some of the aforementioned names are recorded in the scientific literature, while others are known only by locals.

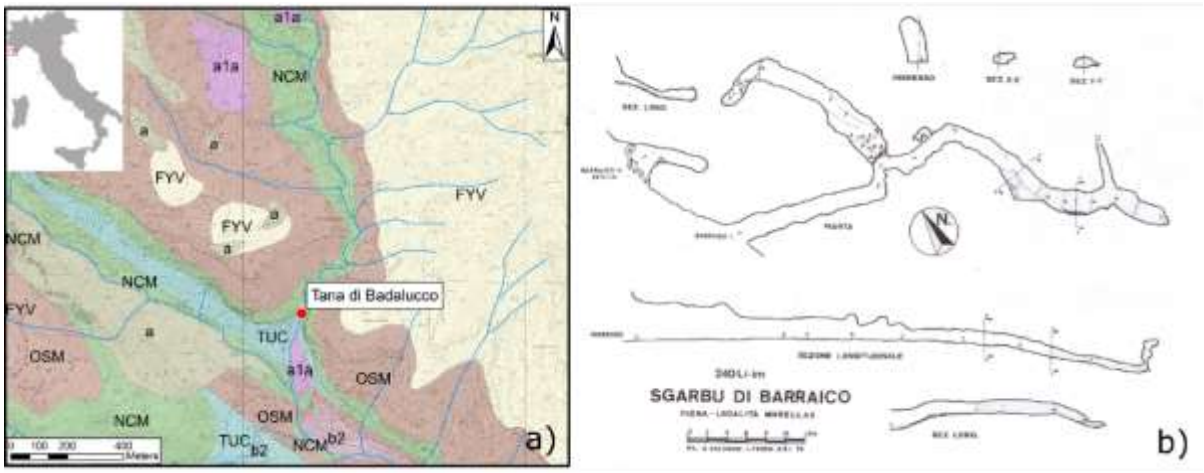

Figure 9 – Tana di Badalucco cave location and geology (a); Tana di Badalucco cave plan and sections, one of its synonyms is reported (b) (from Calandri et al., 1979*).*

Geological and environmental context

The whole area is characterized by a complex karst system and a high number of caves, mostly no longer active (Calandri and Camprendon, 1982). The cave's entrance is not far from the Giacheira cave (Bianchi, Rellini and Traverso, 2015), belonging to the same karst system (Figure 9a).

Tana di Badalucco has formed at the contact between the Eocene calcarenites and the Upper Cretaceous marly limestone, both belonging to the *Dauphinois Provençal domain* (Calandri, Crippa and Ramella, 1979; Calandri and Camprendon, 1982). The second formation reported is the most represented in the study area (Calandri and Camprendon, 1982); it is called Trucco marls and marly limestones formation (TUC, *Marne e calcari marnosi di Trucco*) (Figure 9a). At its top can be found the Capo Mortola calcarenites formation (NCM – *Calcareniti di Capo Mortola*), also known in literature as *nummulitic limestone*, name attributed for its richness in this Foraminifera genre (Dallagiovanna *et al.*, 2012). In this area are also present two other formations that influence the cave development and infillings: the Olivetta S. Michele silty marls (OSM – *Marne siltose di Olivetta S. Michele*) and the Ventimiglia flysch (FYV – *Flysch di Ventimiglia*). The first develops above the NCM, with a gradual transition from one to the other, and formed during the Lutetian and Bartonian ages, while the second formed during the Bartonian and Priabonian (Dallagiovanna *et al.*, 2012).

The Provençal Dauphinois domain has been interpreted as the result of the early stages of subsidence of the Alpine Foreland basin and can be divided into four lithostratigraphic units (Perotti *et al.*, 2012).

Trucco marls and marly limestones (TUC): This formation crops out only in small portions of the study area, in particular at the Muratone Pass. These are marly limestones and limestones, typical of bacinal plain, and of variable thickness (Dallagiovanna *et al.*, 2012; Perotti *et al.*, 2012). Its maximum thickness can reach up to 600 m, as marly intercalations are present, thicker in the upper part (Dallagiovanna *et al.*, 2012). Directly above, it is in contact with the nummulitic limestones (NCM). (Campanian – Lower Maastrichtian)

Capo Mortola calcarenites, or Nummulitic limestone (NCM): Tana di Badalucco formed within this formation. These calcarenites are the product of the Eocene transgression, with sediments of terrigenous platform and, in some points, of internal slope, with macroforams remains. Sandstones range from greywackes to arkoses, in layers from decametric to metric, with bioclasts composed of nummulitides (Dallagiovanna *et al.*, 2012). The calcarenites alternate with silty-arenaceous and marly

horizons, which increase in thickness towards the top of the unit, as it passes through the marls of Olivetta San Michele. (Upper Lutetian – Lower Bartonian)

Olivetta S. Michele silty marls (OSM): This formation is also known in literature as "*Globigerina marls*" (Stani *et al.*, 2009; Dallagiovanna *et al.*, 2012) or "*Marnes Bleues*" (Joseph and Lomas, 2004) and it covers a large part of the study area. It is constituted of hemipelagites, represented by bluish marls, silty marls and calcareous marls, deposited on a slope or distal ramp setting (Joseph and Lomas, 2004; Dallagiovanna *et al.*, 2012; Perotti *et al.*, 2012). (Upper Bartonian–Lower Priabonian)

Ventimiglia flysch (FYV): better known as "*Grès d'Annot*" and well studied in the last century (Stanley, 1975; Joseph and Lomas, 2004; Stani *et al.*, 2009). It is present only on the north-eastern part of the geological map reported in Figure 9a. These are gravity flow deposits (turbidites and debris flow deposits) that rest on the Marnes Bleues palaeoslope (Joseph and Lomas, 2004), in particular they are alternations of sandstone and mudstones of grey and brown colour (Dallagiovanna *et al.*, 2012). This formation well represents the interaction between foreland basin evolution and deep-marine sedimentation, on both regional and local scales (Joseph and Lomas, 2004).

Previous studies

As already mentioned before, the many names of this cave make it difficult to accurately reconstruct the first excavations of its deposits. Probably this cave has always been known by the locals who frequently used its infillings for the fields and its spaces as a shelter for livestock, although Issel mentions this cave only in 1892. In any case, the first certain exploration was conducted by the mountaineer Kledgen in 1929 and it is believed that on that occasion many *Ursus spelaeus* (Rosenmüller et Heinroth) remains had been found there (Calandri, Crippa and Ramella, 1979). Furthermore, some authors (among others Zambelli, 1934), suggest that another excavation, by some English men, has taken place around 1920, and these would have stolen an entire human skeleton from the first part of the cave (Calandri, Crippa and Ramella, 1979). However, there is no way to know this for sure.

Instead, we know with certainty that the excavations under Zambelli's direction were carried out between June and July 1933, on behalf of Imperia's Speleological Group "A. Mochi", and found a great variety of paleontological and palethnological finds digging the first two internal traits of the main branch (Zambelli, 1934; Calandri, Crippa and Ramella, 1979).

After WWII, in 1965–1966, the Gruppo ricerche sanremese (Istituto Internazionale di Studi Liguri, an Italian cultural association aimed at studying the history of Liguria) returned to Tana di Badalucco

to excavate what was left (Molinari, Montinari and Rossi, 2012). Many lithic tools referable to the Mousterian industry and about 20 pottery fragments, maybe from Neolithic to late Bronze Age, were recuperated and, among them, even VBQ (Vasi a Bocca Quadrata, Square-Mouthed Pottery) phase pottery fragments (Ricci, 1988; Bianchi, Rellini and Traverso, 2015). The current excavations started in 2012, thanks to Soprintendenza Archeologia della Liguria and University of Genova. On this occasion, it has been noted that small parts of the deposit, near the entrance and most of the innermost portion, are still in place (Bianchi, Rellini and Traverso, 2015; Sessa *et al.*, 2019).

3.2 Finalese area

The study area (Figure 10) is located in western Liguria, in a space whose geographical limits are the Torrente dell'Aquila (to the West, near Arma degli Zerbi cave) and the outermost border of the Manie Plateau (to the East, immediately next to the other two caves indicated on the map in Figure 10). The geomorphological aspects of the area are fundamentally linked to the activity of rivers, slope processes and meteoric degradation (Dallagiovanna *et al.*, 2011). However, it is evident how the lithological characteristics of the outcropping rocks and the structural arrangement strongly conditioned the general morphogenesis (Dallagiovanna *et al.*, 2011).

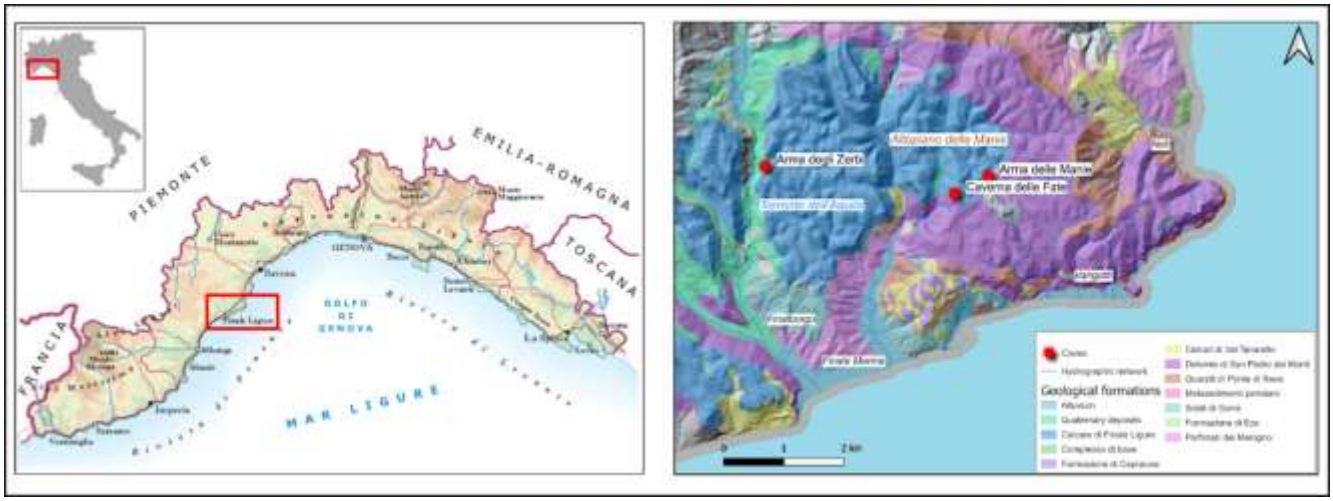

Figure 10 - Geological and geographical framework of the study area.

Geological context

The geological context of western Liguria derives from a complicated geodynamic process which, after the subduction of oceanic lithosphere and the subsequent collision between the European and insubric continental plates, led to the construction of an orogen formed by a set of tectonic units of continental and oceanic drift (Dallagiovanna *et al.*, 2011). In this area there are three main structural systems, separated by tectonic surfaces, starting from the geometric top down: the Piedmontese-Ligurian, the Pennidic and the Dauphinois-Provençal (Perotti, Seno and Vanossi, 1994; Dallagiovanna *et al.*, 2011). The most interested part, in this case, is that of the Pennidic domain of the Ligurian Alps, formed by tectonic units that have well recorded the metamorphic history of this area (Perotti, Seno and Vanossi, 1994; Dallagiovanna *et al.*, 2011). They are of continental relevance

and belong to the Brianzonese units (Boni *et al.*, 1971; Dallagiovanna *et al.*, 2011; Murialdo, Cabella and Arobba, 2019).

Here only the tectonic units directly involved in the area, and consequently the cave infillings, will be reported and a brief presentation will be made.

PRE-PLIOCENE EVOLUTION (Figure 11)

The oldest deposits are of Carboniferous age (or Permian, there is no certainty yet) (Boni *et al.*, 1971; Biancotti and Motta, 1988; Dallagiovanna *et al.*, 2011). In fact, during the ***Upper Carboniferous*** (or ***Middle Permian***) there is a very intense volcanic activity with consequent deposition of lavas and pyroclastites, interspersed with terrigenous sediments (Biancotti and Motta, 1988). A weak alpine metamorphism lead to the transformation of acid lavas into porphyroids (*Porfiroidi del Melogno*, Figure 10 and Figure 12), while the basic lavas transformed into prasinites and schists (*Formazione di Eze*, Figure 10 and Figure 12), and the terrigenous sediments and pyroclastites in schists, quartz schists and mica schists (*Scisti di Gorra*, Figure 10 and Figure 12) (Boni *et al.*, 1971; Biancotti and Motta, 1988).

During the ***Upper Permian***, volcanic activity and sedimentation continued, but then volcanic eruptions soon stopped (Biancotti and Motta, 1988; Cortesogno *et al.*, 1998; Decarlis *et al.*, 2013).

The Ponte di Nava quartzites (*Quarziti di Ponte di Nava*, Figure 10 and Figure 12) are the first term of the ***Uppermost Permian-Lower Triassic*** coverage of Briançonnais. They are beach deposits still bearing the typical structures of these depositional environments. (Biancotti and Motta, 1988; Decarlis *et al.*, 2013)

A partial or total emergence of the area is probably attributable to the ***Lower Triassic***. It passes with continuity of deposition to the Dolomites of San Pietro dei Monti (*Dolomiti di San Pietro dei Monti*, Figure 10 and Figure 12), even if from time to time there is a surface of erosion between the quartzites and the latter (Biancotti and Motta, 1988). During the ***Middle Triassic***, a carbonate platform develops and the deposition of grey dolomitic limestones, grey dolomites and marly limestones ("pseudoflysch"), in some cases dolomitic breccias, ceroid limestones, and, towards the top, marl and marly limestones takes place (Biancotti and Motta, 1988). The carbonate deposition ceases between the ***Upper Triassic*** and lasts until the ***Upper Jurassic***, creating a deposition gap, when the Briançonnais anticline formed (Biancotti and Motta, 1988; Dallagiovanna *et al.*, 2011).

This erosive phase leads, in some areas, to the direct deposition of pelagic limestones (*Calcari della Val Tanarello*, ***Upper Jurassic***) on the permo-carboniferous levels (Boni *et al.*, 1971; Biancotti and Motta, 1988).

Between the ***Upper Cretaceous*** and the ***Eocene***, clayey-calcareous sediments of pelagic environment, belonging to the Caprauna Formation (*Formazione di Caprauna*), are deposited (Biancotti and Motta, 1988).

With this last formation the Briançonnais series ends. Subsequently the Alpine orogeny occurred, it is responsible for the lamination and metamorphism of the previous units, as well as for the overthrust of the internal Briançonnais on the external one (Biancotti and Motta, 1988).

Between the ***Lower Oligocene*** and the ***Langhian***, the Finalese area is occupied by a large bay, in which the terrigenous, clayey-marly, sandy and conglomeratic sediments are deposited, constituting the "Pietra di Finale" basal complex (*Complesso di Base del calcare di Finale Ligure*). The well-known "*Pietra di Finale*" (formation of the Limestone of Finale Ligure, *Calcari di Finale Ligure*) is formed during the ***Langhian-Serravallian***, from a new wide gulf, where subsidence and land input of material are equal (Boni, Mosna and Vanossi, 1968; Boni *et al.*, 1971; Biancotti and Motta, 1988; Dallagiovanna *et al.*, 2012; Murialdo, Cabella and Arobba, 2019). Finally, the area emerges totally in the ***Tortonian*** (Biancotti and Motta, 1988).

The main formations in the study area will be presented below, starting from the more ancient and ending with the more recent.

Porfiroidi del Melogno fm.: Small-grained porphyroids deriving from the lamination, during the Alpine orogeny, of more or less tufaceous rhyolites, riodacites and trachytes. *Of the Upper Carboniferous? - From the Middle Permian?*(Boni *et al.*, 1971)

The formation derives from more or less tufaceous acidic volcanic rocks. There are relationships that are partly heteropic and partly overlapping with respect to the Gorra schists (*Scisti di Gorra* fm.). Due to these relations it is difficult to give an exact estimate of the maximum thickness reached by the formation (perhaps 700 m). The stratigraphic unit above is missing due to erosion. (Boni *et al.*, 1971)

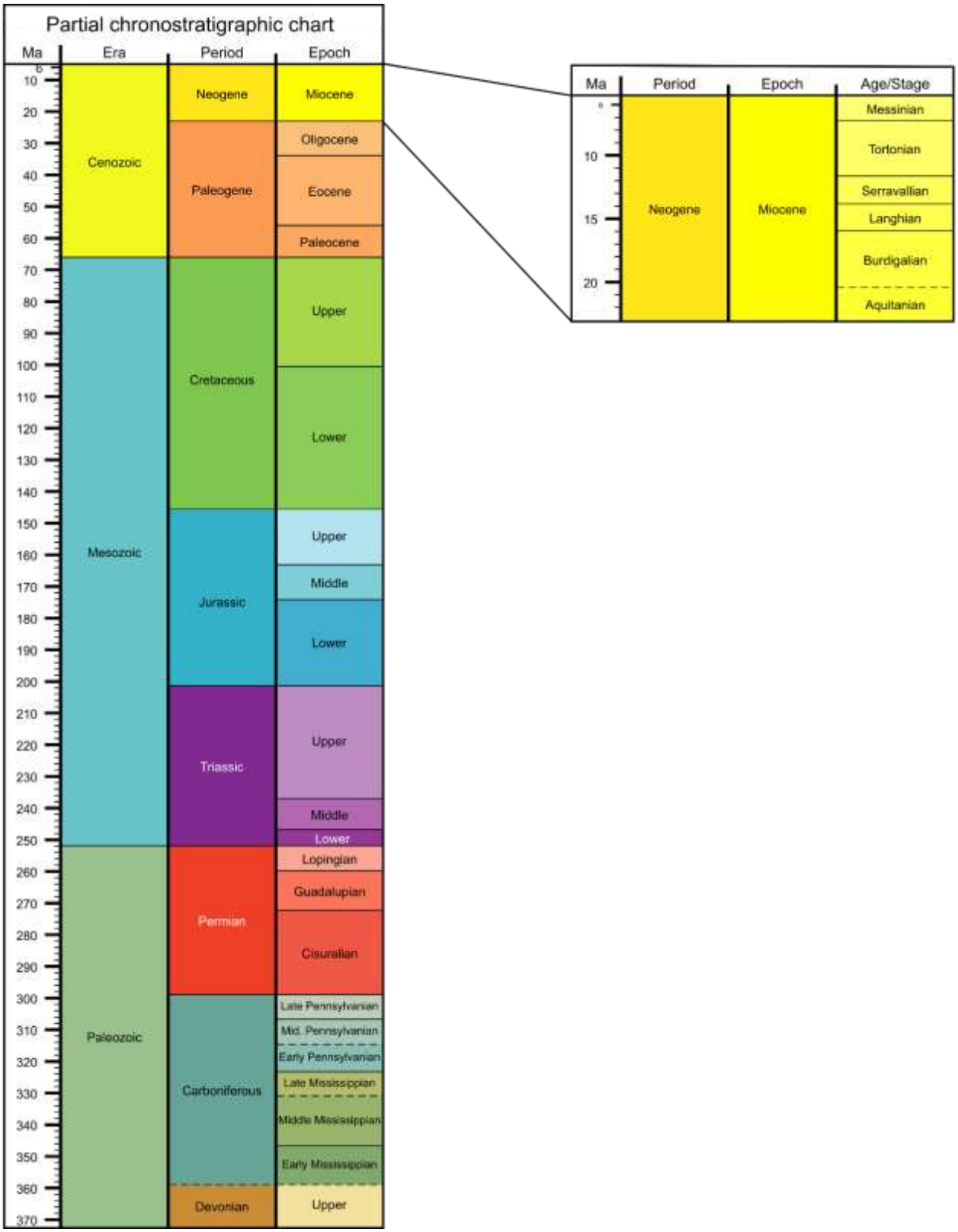

Figure 11 – Pre-Pliocene chronostratigraphic chart with focus on the Miocene Epoch. Pliocene, Pleistocene and Holocene are not reported here.

Formazione di Eze fm.: Andesite, effusive and hypabyssal; prasinic, chloritic-epidotic schists, deriving from lamination during the Alpine orogeny. *Permian? Carboniferous?* (Boni *et al.*, 1971)

The areal distribution of the rocks belonging to this formation is closely connected with that of the other permo-carboniferous rocks (Figure 10). There are mainly two facies of rocks: one more massive and one more schistose, both green or green-like in the most massive form and brown or green-reddish in the most weathered form. (Boni *et al.*, 1971)

Scisti di Gorra fm.: Quartz schists, quartz-sericite schists, chlorite, mica schists, gneissic schists. *Permian? Carboniferous?*(Boni *et al.*, 1971; Dallagiovanna *et al.*, 2011)

They derive, like the formations previously listed, from the lamination caused by the Alpine orogenesis, in this case on arenite-pelitic, tuffaceous-arenaceous and possibly lava materials. The relationships with the Melogno Porphyroids (*Porfiroidi del Melogno* fm.) and the Eze Formation (*Formazione di Eze* fm.) are difficult to interpret. Therefore, even the thicknesses are uncertain and can be considered to be between 200 m and 800 m. (Boni *et al.*, 1971; Dallagiovanna *et al.*, 2011)

Figure 12 - Legend of the geological map of the Finalese area. The geological formations are in alphabetical order.

Quarziti di Ponte di Nava fm.: Whitish and greenish quartzites, medium- to coarse- grained, sometimes schistose, with rare green and purple pelites to the top of the formation. *Lower Triassic*. (Boni *et al.*, 1971; Dallagiovanna *et al.*, 2011; Decarlis *et al.*, 2013)

The formation is rather homogeneous in all of the Briançonnais series. Only at roof level it has alternating quartz and pelitic layers, for up to 30 m. There is an erosional surface in the areas where the upper limit is represented by the Val Tanarello limestones formation (*Calcari di Val Tanarello* fm.). (Boni *et al.*, 1971)

Dolomie di San Pietro dei Monti fm.: Thick carbonate succession of more or less grey limestone dolomites, alternating with grey dolomitic limestone and limestone, sometimes with red and green pelitic interlayers. There are also micaceous, siliceous limestones and dolomites with flint nodules. In this level there are fossils of: *Dadocrinus gracilis* (Von Buch), *Tetractinella trigonella* (Schloth), *Meandrospira dinarica* (Kochansky-Devide and Pantic), Glomospira densa (Pantic), *Glomospirella grandis* (Salaj), *Diplopora uniserialis* (Pia) and *Diplopora annulata* (Schaf.). *Middle Triassic*. (Boni *et al.*, 1971; Dallagiovanna *et al.*, 2011; Decarlis *et al.*, 2013)

The formation is mainly composed of limestone in the lower part and dolomite in the upper part. Its outcrops are generally accompanied by those of the Ponte di Nava quartzite formation (*Quarziti di Ponte di Nava* fm.) and have an almost similar distribution. The thickness fluctuates around 200 m. The presence of fossils and so rare, additionally, facilitates the temporal classification. (Boni *et al.*, 1971; Dallagiovanna *et al.*, 2011)

Calcari della Val Tanarello fm.: Light, ceroid, well-stratified marble limestones and multicolour marbles. Locally, at the base, arenaceous limestones and conglomerates, while at the top, sometimes, rose and almond marbles. Very rare fragments of crinoids, belemnites, ammonites and aptychus. *Upper Jurassic*. (Boni *et al.*, 1971; Dallagiovanna *et al.*, 2011)

It is a very characteristic formation, although rather reduced in thickness and, also for this reason, not very extensive. The thickness is comprised between 10 and 80 meters and, everywhere, the formation is stratigraphically covered by the limestone schists of the Caprauna Formation (*Formazione di Caprauna* fm.). Between these two we can find a *hard-ground* delineating the transition to the Upper Cretaceous. (Boni *et al.*, 1971; Dallagiovanna *et al.*, 2011)

Formazione di Caprauna fm.: Calcareous and calcareous-arenaceous schists, or even phyllitic, dark grey, pale schistose limestones with rare reddish clay levels in the lower part. At times with nummulites, at times with Globotruncana. *Upper Cretaceous? Eocene?* (Boni *et al.*, 1971; Dallagiovanna *et al.*, 2011)

Its facies is more uniform, consisting of calcareous, clayey, and phyllitic schists, dark grey in colour, characterized by veins of quartz and calcite. The thickness is around 200 m. All the outcrops are located above the Jurassic limestones already examined above, with sometimes the *hard-ground*

in between. The upper limit of the formation is not known. (Boni *et al.*, 1971; Dallagiovanna *et al.*, 2011)

Complesso di base del Calcare di Finale Ligure fm.: The outcrops are rather limited in extent. These are arenaceous conglomerates and quarzitic coarse-grained sandstones, with some heterogeneous breccia beds. *Upper Oligocene? - Lower Miocene.* (Dallagiovanna *et al.*, 2011)

These facies are located at the stratigraphic base of the Limestone of Finale Ligure (*Calcare di Finale Ligure* fm.), separated from it by an erosional surface. In general, the basic complex consists mainly of marly facies and coarse clastic facies. (Boni *et al.*, 1971) In the study area mainly the former are present. The following fossils were recognized in this formation by A. Boni et al., (1971) in the study area: *Globoquadrina sellii* (Borsetti), *Globigerina ampliapertura* (Bolli), *Cibicides cushmani* (Nuttall), *Cibicides mexicanus* (Nuttall), *Cibicides perlucidus* (Nuttall), *Stilostomella nuttalli* (Cushman and Jarvis).

Calcare di Finale Ligure fm. (also known as "*Pietra di Finale*") (Figure 13): Bioclastic vacuolar limestones with corals and Codiaceae, white, pink or reddish, with interspersed sandstones in layers and lenses, massive in the upper part, well stratified in the lower part. (Boni, Mosna and Vanossi, 1968; Boni *et al.*, 1971; Dallagiovanna *et al.*, 2011) The fossiliferous component is very important and mainly constituted of: macrofauna with Echinoidea and Bivalvia (*Chlamys bollenensis* (May-Eym), *Chlamys macrotis* (Sow.), *Chlamys malvinae* (Dub.), etc.), Brachiopoda, Elasmobranchii, ... for the Monte Cucco member, at least. *Lower-? Middle Miocene?* (Boni *et al.*, 1971; Dallagiovanna *et al.*, 2011)

In 2019, a Mysticete fossil (*Eubalaena glacialis)* has been made available to the public of Finale Ligure (and exposed in Finalborgo, in the *Museo Archeologico del Finale*) and to researchers. It is the second marine mammal fossil find, the first being a small fragment of a rib, in the Verezzi member, possibly attributable to a Sirenia. (Murialdo, Cabella and Arobba, 2019)

This formation can be divided into five different members: Monte Cucco (Figure 13), Rocce dell'Orera, Verezzi, Torre di Bastia and the Poggio member.

Monte Cucco member is the hugest member and the member within which all three studied caves can be found. It consists of bioclastic limestones, with calcitic, coarse-grained cement. The inorganic fraction is slight, it is whitish and the stratification is not always recognizable. Arenaceous or conglomerate lenses can be found within. It can reach up to 200 m thick. (Boni *et al.*, 1971)

For an in-depth analysis of these plaques, see the excellent and detailed bibliography (Boni, Mosna and Vanossi, 1968; Murialdo, Cabella and Arobba, 2019)

Figure 13 - Calcare di Finale Ligure *fm. ("*Pietra di Finale*", Finale Ligure limestone) outcrop. Detail of the Monte Carmo member.*

Site description and previous studies

Three of the studied caves are located within the Finalese area: Arma degli Zerbi, Caverna delle Fate and Arma delle Manie. Of these three, the last two are the most studied and have generally been considered together, also for geographical reasons, in fact they are not far apart. All three, however, until now, have mostly been examined purely from an archaeological point of view.

Arma degli Zerbi

This cave is located 255 m a.s.l. and its entrance is NW oriented (Figure 14a), about 4.20 m wide and about 5.60 m high (Figure 14b) (Dodero, 2017; Negrino *et al.*, 2018). It consists of a single 22 m long tunnel, 5 m wide at its maximum point. Like the other caves, it belongs to a no longer active karst system. Towards the entrance it is possible to recognize the remains of a dry-stone wall, probably built by local farmers who used the cave as a stable for their cattle.

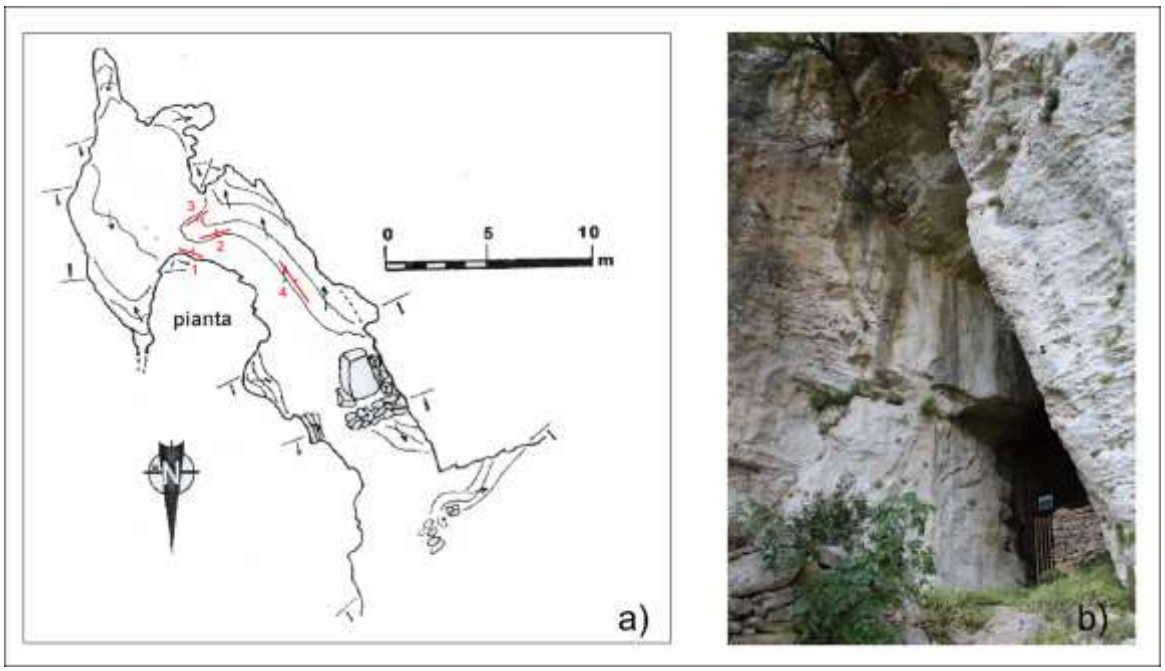

Figure 14 - a) Plan of Arma degli Zerbi (modified from Farinazzo (1999)*). b) The entrance to the cave.*

The first information regarding this cave dates back to 1884, when Arturo Issel and the Captain d'Albertis carried out the first investigation (Dodero, 2017). They studied the entrance closest part and found some fragments of *Ovis*'s horns, fragments of long ruminants bones and teeth of *Ursus*. Finding no artefacts there, they desisted from continuing their explorations (Dodero, 2017).

Father Amerano, another of the most distinguished scholars of that era, visited the cave in 1891 and found bones of *Ursus spelaeus*, as well as traces of human presence (fragments of charcoal, pottery, etc.). In any case, there are not many materials attesting to further exploration and studies of the deposits of this cave. Only in the nineties of the last century a collaboration between the *Museo Archeologico del Finale*, the *Soprintendenza Archeologia della Liguria* and a local high school did make it possible to conduct research on the remaining deposits (Farinazzo, 1999; Dodero, 2017). Unfortunately, a large part of the cave sediments had been removed during clandestine excavations and for the creation of terraces outside the cave, making the study of the stratigraphy very difficult (Dodero, 2017; Negrino *et al.*, 2018).

Previous studies, as mentioned above, have left little information about this cave. For now, the insights taken into consideration here will mainly be those of our archaeological collaborators. In concert with them, four stratigraphies, previously exposed by clandestine excavations, have been recognized (Figure 14a and Figure 15), but new ones will be presented in the results, only to facilitate the geological approach.

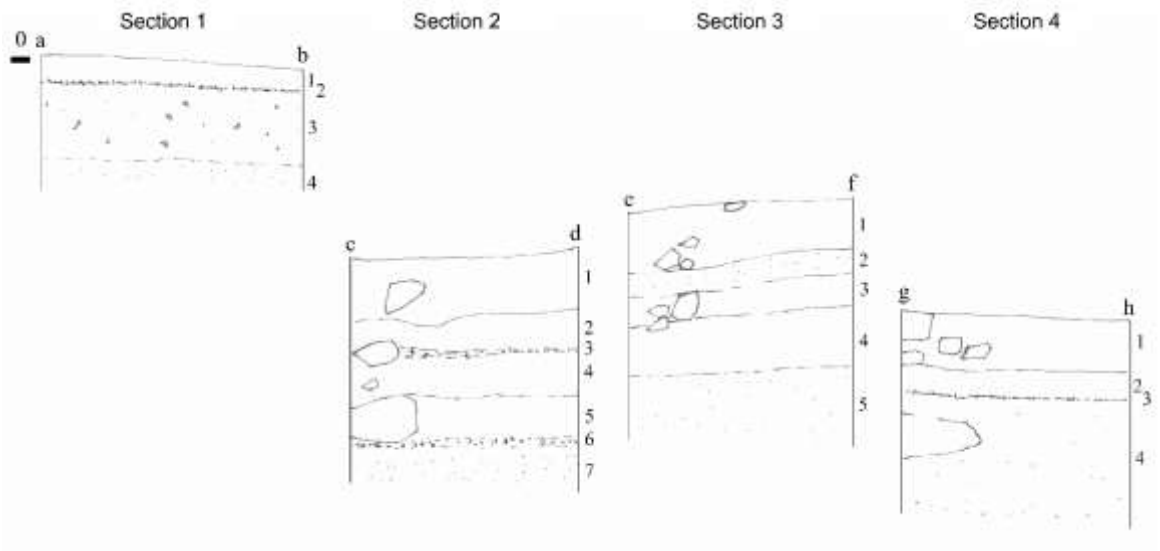

Figure 15 - The four sections as drawn by prof. Negrino.

Leaving out the archaeological context, which is not the aim of this thesis, it can be said that this cave's deposits cover a period of time ranging from the most recent phase of the Middle Palaeolithic to the Neolithic (Dodero, 2017; Negrino *et al.*, 2018). This was ascertained through the study of the archaeological remains found inside the cave. These assertions were later supported by the dating provided by the *Max Planck Institute* (Table 3).

Table 3 - Recognition of the nature of the material (thanks to prof. Arobba, Museo Archeologico del Finale) and dating of coals from the four studied sections of Arma degli Zerbi cave deposits.

Sample	**Material (charcoal)**	**^{14}C Age (yr BP)**	**Calibrated dating (95.4) (OxCal 4.3) (yr cal. BP)**
Sec. 1 – SU 1	*Quercus t. ilex/coccifera*	9008±48	10249-9935
Sec. 1 – SU 4	*Pinus t. pinea/pinaster*	14010±90	17355-16664
Sec. 2 – SU 7	*Pinus t. halepensis*	47070±720	>50000
Sec. 3 – SU 1	*Pinus t. sylvestris/mugo*	13870±50	17023-16554
Sec. 4 – SU 3	*Pinus sp.*	48900±970	>50000
Sec. 4 – SU 4	*Pinus t. sylvestris/mugo*	46980±1290	>50000

Caverna delle Fate

Caverna delle Fate was discovered by scholars, even though the locals already knew this cave well, in 1876 by Cap. D'Albertis (Isetti and de Lumley, 1962). The cave is located at 280 m a.s.l., opens to the SW and extends for 300 m (Bichet, 1987) (Figure 16). It consists of three rooms, connected by corridors. It is not very far from Arma delle Manie cave: in fact, they are only 500 m apart as the crow flies (Isetti and de Lumley, 1962). Already in 1962, Isetti & de Lumley (1962) report that the most important entrance, consisting of a large and luminous hall (Figure 17), must have constituted an important archaeological deposit, which had already disappeared then, probably to create or fertilize some agricultural terraces. Furthermore, in recent times, inside the cave, there was a sheepfold and the entrance was partially closed for this reason (Isetti and de Lumley, 1962).

D'Albertis led Issel and Perrando, in 1876, inside the cave, where they conducted some excavations, collecting a good amount of material (Isetti and de Lumley, 1962; De Pascale, 2008). Nevertheless, the first real excavations took place between 1887 and 1889, and they were directed by Padre Amerano (De Pascale, 2008; De Lumley and Giacobini, 2013a). These mainly involved the entrance hall and corridor 3, but all the rooms were explored (Psathi, 2003). During these, large quantities of bear bones were found, as well as archaeological material dating back to at least the Neolithic (Isetti and de Lumley, 1962; Bichet, 1987; Psathi, 2003). All the material found was preserved for a long time in museums, until, in the 1980s, bones belonging to some Neanderthal individuals were recognized among all the bones sampled (Giacobini *et al.*, 1984; Echassoux *et al.*, 1989; De Lumley and Giacobini, 2013b). This led to a new season of excavations and studies of cave deposits. A series of studies with different techniques has been undertaken along the years: anthropological (Arnaud, 2013; Giacobini et al., 1984, among others), archaeological (Echassoux *et al.*, 1989; Cauche, 2007), faunal (De Marchi, 2003; Psathi, 2003; Quiles & Monchot, 2004; Valensi & Psathi, 2004, …), palynological (Karatsori, 2003; Karatsori *et al.*, 2005), but also geological analyses (Bichet, 1987; Falguères, Yokoyama and Bibron, 1990).

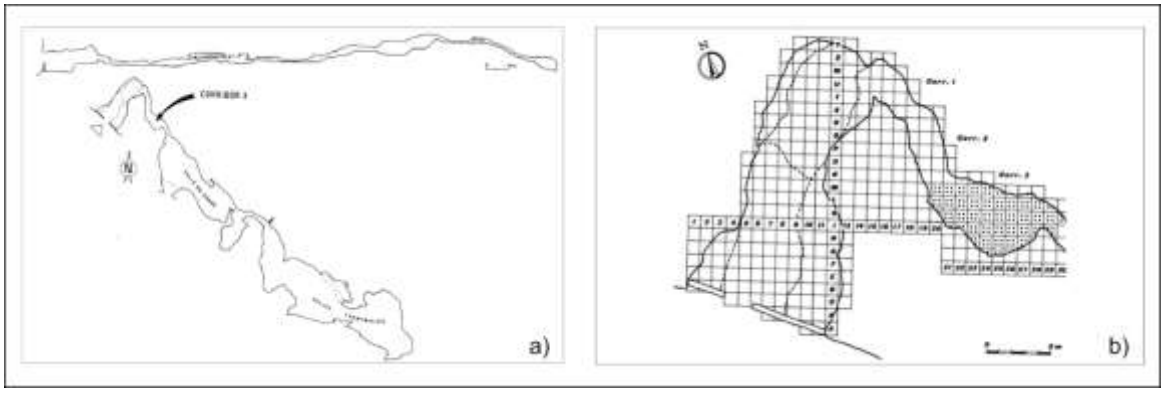

Figure 16 - a) Plan of the cave, with the arrow indicating the position of corridor 3 (from Bichet (1987)*). b) The detail of the first portion of the cave, including corridor 3, with the reference squares shown.*

As already mentioned, among the materials collected by Amerano in 1887 in corridor 3, in 1981 (Giacobini *et al.*, 1984) three Neandertal remains were recognized and then attributed to two individuals: one adult and a 8-10 year old boy (Giacobini *et al.*, 1984; Echassoux *et al.*, 1989). This discovery led to an Italian-French collaboration in order to reopen the excavations at the Caverna delle Fate (De Lumley and Giacobini, 2013b, 2013a). From this new series of excavations, other elements were found in place and very similar to those already described, making up sixteen elements, mostly teeth, of Neandertal origin that, still, can be attributed to a minimum of two individuals (Minimum Number of Individuals, MNI) (Arnaud, 2013; De Lumley and Giacobini, 2013a, 2013b). They have been attributed to what we refer to as the upper part of section A, in corridor 3 (De Lumley and Giacobini, 2013a, 2013b) (Figure 18, Figure 19a). These human remains have also been dated to a period comprised between 72 ka BP and 82 ka BP (Giacobini *et al.*, 1984; Echassoux *et al.*, 1989; Falguères, Yokoyama and Bibron, 1990) (Figure 19a).

Figure 17 - The entrance hall of Caverna delle Fate. a) Here it is possible to see the detail of the entrance, with the recent wall. b) The back of the entrance hall.

The archaeological context is not the subject of this thesis, but it could be useful in the subsequent paleoclimatic reconstruction. Since the first excavations, the lithic industry found was that of Mousterian type, in large quantities and with many elements in jasper (de Lumley *et al.*, 2008; Cauche, 2012). Furthermore, it was noted the alternation produced by the cave bear (*Ursus spelaeus*) and man, in different levels, but always with not entirely clear dynamics (Isetti and de Lumley, 1962; Echassoux *et al.*, 1989). Almost all the finds come from corridor 3 (Figure 18): it was already Amerano, in 1887 (Psathi, 2003), to start excavating in this portion of the cave, this also because the deposits in the entrance hall had all been removed. Only in later works (Echassoux *et al.*, 1989; de Lumley *et al.*, 2008) there are mentions of some Acheulean tools found in the portion of the cave between the entrance hall and the corridor. Finally, we are aware of the discovery of three hearths remains, with traces of burnt branches associated with them, but still in corridor 3 (Echassoux *et al.*, 1989).

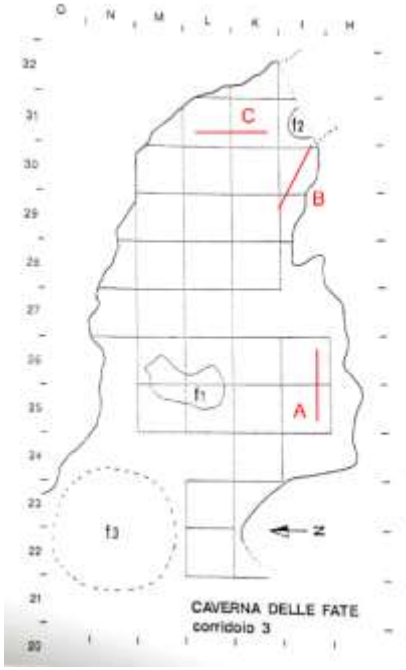

Figure 18 - Plan of corridor 3. f1-2-3: hearths. Sections A, B and C are also shown.

Psathi (2003) refers to a fauna with an "*archaic and endemic*" context, in a rather open forestry situation and a certain taxonomic richness. It is referred how the cave must have been occupied alternately by three distinct groups: cave bear, human groups and several carnivorous species (De Marchi, 2003; Psathi, 2003; Valensi and Psathi, 2004). Of these, the bear would seem to return cyclically and systematically in the deposits, while the other two groups - man and other carnivorous animals - have been identified for rare and short periods. This even though man is present seasonally, mainly for hunting reasons, and in particular in the second part of the year (Psathi, 2003; Valensi and Psathi, 2004). The main focus has mostly been that of the presence of *Ursus spelaeus*, given the large amount of bones found, which probably used the cave as a nursery (Quiles and Monchot, 2004). Psathi (2003) refers to the stratigraphy identified by saying that probably the lower part of section A is attributable to the Eemian (MIS 5e, Shackleton et al., 2003), while the general stratigraphy of Caverna delle Fate covers from the end of MIS 5 to the first part of MIS 3.

The pollen analysis (Karatsori, 2003; Karatsori *et al.*, 2005) focused exclusively on the upper part of what will be called here section A (using the Bichet nomenclature (1987), Figure 19a), due to the insufficiency of pollen in the other levels. From these studies four pollen zones were identified (Fat.1, Fat.2, Fat.3, Fat.4), delimited according to the nature of the infilling (alternation of speleothem or clayey levels, or sedimentary discontinuities), indicating time spans of unknown duration (Karatsori *et al.*, 2005). Starting from the downmost (Fat.1), *Pinus* is the dominant genre and a semi-closed to closed landscape, made up of mixed forest vegetation with conifers and deciduous trees, seems the most likely environment. This changed into a xerophilic and Mediterranean herbaceous vegetation (Cichorioideae, e.g.), indicating an opening of the landscape and a slight pluviometric deficit. Between the first two and the last two groups there is a sterile portion. In Fat. 3, ubiquitous herbaceous plants increase (Scrofulariaceae), deducing that a period of climatic instability, characterized by abrupt changes, must have taken place. It is suggested that perhaps it was a relatively warm period, with increasing dryness, perhaps a reflection of an interstadial phase. To end, Fat. 4 is evidenced by the expansion of *Quercus ilex/coccifera* type, then with a sudden transit to a closed landscape where

tree taxa increase in number. The climate would be temperate with a Mediterranean character, and a summer pluviometric deficit. (Karatsori, 2003; Karatsori *et al.*, 2005)

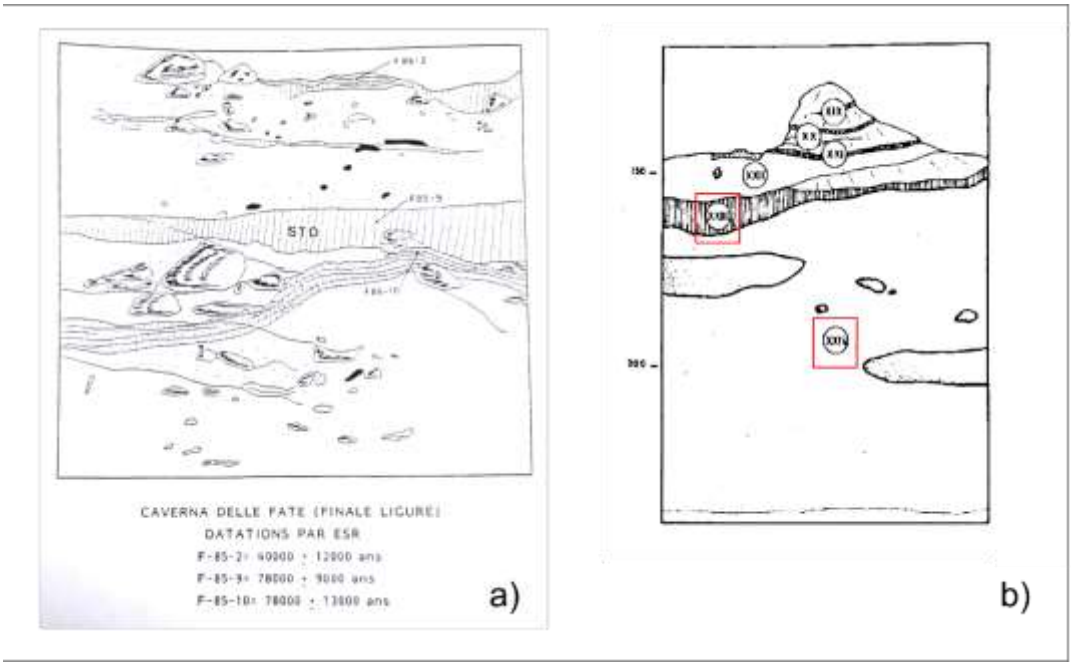

Figure 19 - a) Section A stratigraphy (Echassoux *et al.*, 1989). *b) Section B stratigraphy, in red the micromorphological samples position from* Bichet (1987). *Modified from* (Bichet, 1987).

On section C (Figure 20), analyses on magnetic minerals were also carried out (Bichet, 1987; Djerrab and Hedley, 2010). Given that only the first 50 cm of this section have been studied in this thesis and these fit perfectly into the so-called "*niveau 1*" (level 1) by Djerrab & Hedley (2010), only this one will be treated here. In the upper part of the infilling, minerals such as magnetite and maghemite were recognized, in very fine grains, formed by redox reactions of primary iron oxides under the effect of pedogenesis (Djerrab and Hedley, 2010). Bichet (1987) also adds that the homogeneity of the spectrum of heavy minerals underlines the invariability of the origin of the materials, throughout the detrital sedimentation of the filling.

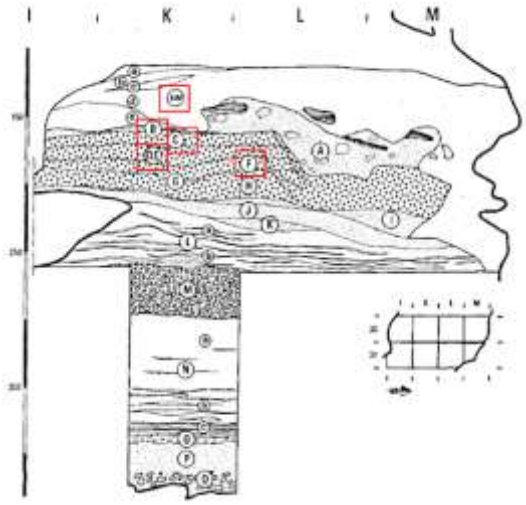

Figure 20 - Section C stratigraphy, modified from Bichet (1987). *In red micromorphological samples position in* (Bichet, 1987).

It is plain to see that there are many studies concerning these cave deposits, but only a few take into account the geological context. One above others is the one taken as reference point here: Bichet (1987). This because he deeply investigated many geological aspects and tried to apply, even if not systematically and not with the sufficient number of samples, the micromorphological technique. It will be useful to confront his data with those presented here forth.

In Bichet (1987), for the first time, corridor 3 is studied dividing its infillings into three sections: A, B and C (as depicted in Figure 19 and Figure 20), and here will be done the same.

One of the first aspects that Bichet (1987) underlines is the disparity, at the grain size level, between the active karst layers and those deposited afterward: the parameters values of the active karst layers (in section C) seem very unstable, while the levels that he indicates as "occupied" or of the evolved karst (section B and A) are more homogeneous.

Not considering the descriptions, following Brewer (1964) guidelines, Bichet (1987) affirms that, from the micromorphological observations, layer XXV (Levels 1 and 2 in our stratigraphy, Figure 42) would seem to present the characteristic traces of the periglacial action (such as vesicles and coatings) and, in some of its parts, thanks to the sedimentological parameters studied, also sedimentation by film runoff. This would explain the homogeneity of the layer, although no figures related to thaw were found. In the layer above, belonging to section B, but considered here as a continuation of section C, few probably Mousterian tools have been found. Furthermore, it can be observed that soil fragments, coming from the upper Manie Plateau, infiltrated down to this layer. Rare hydromorphic conditions have been recognised, but probably they are associated to biological activity.

Instead, the newformed phosphates identified, thanks to the OIL technique, in the XXIII layer of section B (Figure 19b), pointed to an high organic matter content of the original deposit. Thus, in contrast with the previous layer, all the characteristics described, such as the finer materials, the

biological activity and the absence of periglacial features, state for a climatic evolution towards less severe conditions but all the same cold.

Moving upward, a speleothem layer is found, indicating a biostatic period, soon followed by not so harsh conditions, but still cold, so much so that it is not possible to find any faunal trace. In this layer, it is common to find charcoal fragments and human tools. Other speleothem layers can be found, such as XVI, XV and XIV in section A (Figure 21). It is suggested the same origin and paleoenvironmental reconstruction for them, too.

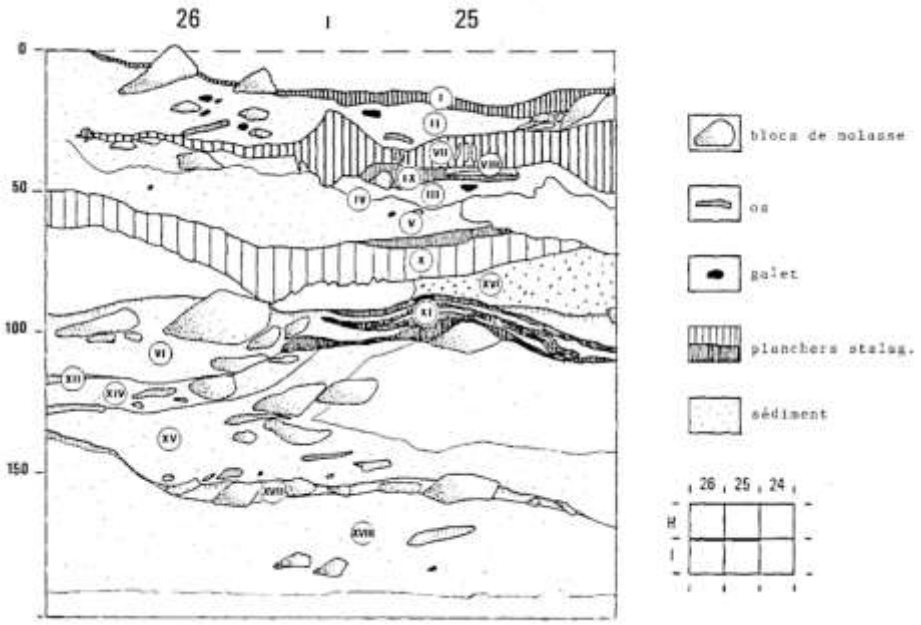

Figure 21 - Section A as drawn by (Bichet, 1987). *Here it is possible to see all layers' names.*

At the end of this cold period the formation of speleothem XIII (section A) can be positioned. Above this, probably, an erosion phase (lacuna) occurred. At level XII, XI, X, IX the climate would seem to re-establish with temperate and humid conditions. Two of these levels (XI and X) have been dated around 78 ka BP (Figure 19a) (Falguères, Yokoyama and Bibron, 1990). As for level VIII, the thickness is reduced and the soil apport is important, so much so that it could be interpreted as an index of climatic degradation (return to cold conditions). This situation worsens in the next level (VII), where it is also possible to notice a new phase of fragmentations and collapse of the Manie Plateau's soils. This must have affected also levels VI, V, III and II. This climatic degradation phase seems to end around 40 ka BP (Figure 19a) (Falguères, Yokoyama and Bibron, 1990) with the return

to more temperate and humid conditions, such as to allow the formation of the upper stalagmite level (I).

Arma delle Manie

The cave of Arma delle Manie (Figure 22) has always been known to the local population, but only at the beginning of the sixties of the last century it became a very important site for its archaeological finds.

Figure 22 - Arma delle Manie cave. a) The context of the cave. b) The entrance to the cave. Only the gated part has been studied. Arma delle Manie is one of the largest caves in western Liguria.

It is located 250 m a.s.l. and its entrance is SE oriented (Figure 22b). It is one of the largest caves in the whole western Liguria, extending for roughly 40 m^2, but only part of it is subjected to archaeological restrictions (Figure 22b, Figure 23). It developed from the contact between Permian schists (at the base) and Miocene limestone (above).

This cave, until the beginning of the first excavations, has always been used by peasants and farmers: the former removed the most superficial deposits to use them in the cultivated terraces of the area, the latter kept there their animals, using it as a stable (Psathi, 2003). In this way, a large amount of deposits and artefacts went lost (Psathi, 2003).

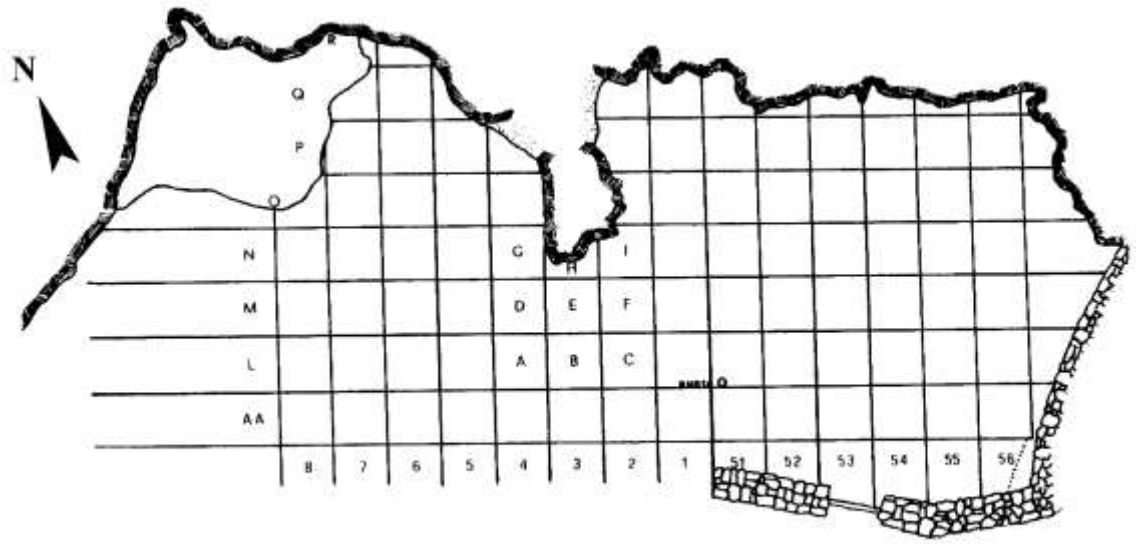

Figure 23 - Arma delle Manie cave studied area planimetry.

In this cave, the first excavations began thanks to the chance discovery of lithic industry (dating back to the Middle Palaeolithic), in 1962, by two visitors: Father Burlando and surveyor Ghianda (Arobba *et al.*, 1976; Leger, 2011). The first to conduct the excavations has been prof. Isetti, but, due to his premature departure, the assignment passed to Inspector Giuggiola (Arobba *et al.*, 1976). The first systematic excavation began in 1964 and continued for eight campaigns, until 1974 (Arobba *et al.*, 1976; Psathi, 2003). The excavations then continued in 1990 with a Franco-Italian team, resulting in different doctoral theses dealing with various disciplines (Psathi, 2003).

Arma delle Manie cave's deposits have been studied for long time and from different points of view. By presenting the results of the most recent works, divided (as much as possible) by discipline, in chronological order, we can mention the first stratigraphy presented in Arobba et al. (1976). In effect, the most recent works concerning the sedimentological context of the infillings of this cave date back to this first publication of the first excavations (Arobba *et al.*, 1976). On this occasion, a first sedimentological study and synthetic stratigraphy have been proposed (Arobba *et al.*, 1976; Psathi, 2003) (Figure 24). The stratigraphy was divided into seven layers, as shown in Figure 24, and these same layers are still addressed in all the successive works, and here too (even though they do not always coincide perfectly).

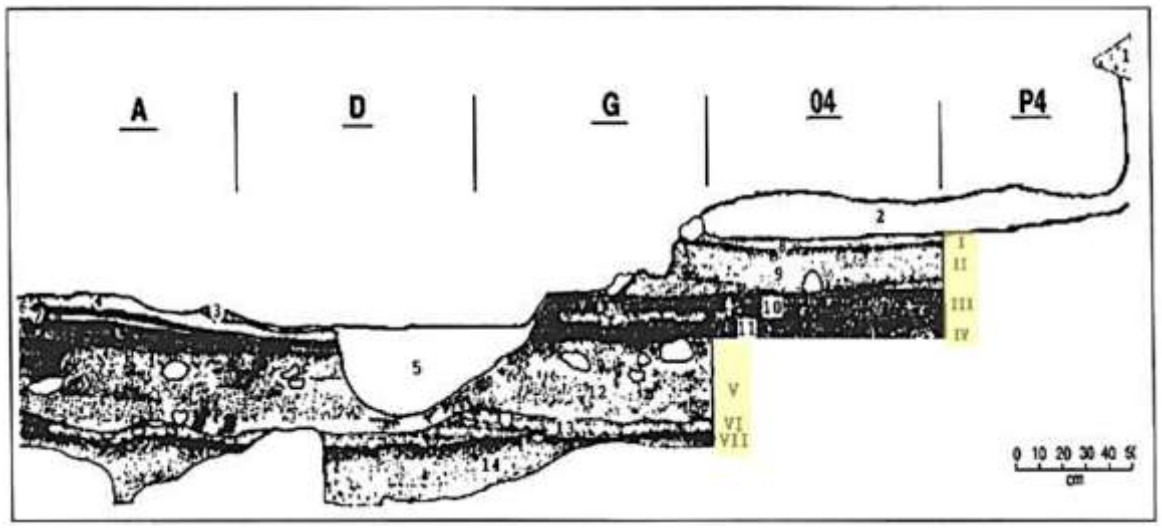

Figure 24 – Arma delle Manie's first stratigraphy. Modified from Arobba et al. (1976). *Highlighted in yellow the seven stratigraphic layers.*

In Arobba et al. (1976) was suggested that from layer VII to layer IV the clear signs associated to Würm II (ranging roughly from 75 kyr cal BP to 45 kyr cal BP, thus covering part of MIS 4 and MIS 3) are present, with cold peaks in layers VI and V. Layer VI, in particular, would seem to bear the signs of a humid condition then followed by dryer settings. An interphase between these two has also been suggested, in which a wetter and relatively more temperate climate then mutated into a windier and drier state. Instead, level V would demonstrate less wind action, but greater aridity. Layer IV shows climate-influenced levels interspersed with hearth remains, probably associated to the final phase of Würm II. Layers III and II, belonging to the Würm II-III interstadial (from 45 kyr cal BP to 30 kyr cal BP), display an increase in temperatures, humidity and a decrease in wind. Finally, from II to I, Würm III (from 30 kyr cal BP to 11 kyr cal BP, part of MIS 3, MIS 2 and the onset of MIS 1) starts and, with that, also cold conditions and wind strength.

The pollen sequence of Arma delle Manie (Arobba *et al.*, 1976; Karatsori *et al.*, 2005) describes the evolution of the plant paleoenvironment from the beginning of the Upper Pleistocene to the Holocene. To Karatsori et al. (2005), the vegetation is marked by the constant presence of meso-thermophilic and Mediterranean taxa, suggesting temperate climatic conditions, while Arobba et al. (1976) assert that the lower layer (VII, Figure 24) shows the traces of the dominance of the genera *Pinus* and *Corylus*, indicating a poorly tree-covered landscape. Karatsori et al. (2005) supposed that the persistence of the aforementioned taxa, during periods of climatic degradation, could be justified by the existence of sheltered areas which served as refuges. The open spaces are occupied by the Poaceae and the Asteraceae, including Asteroideae and *Artemisia*, while the dominance of

Cichorioideae is probably due to differential conservation. They identified nine pollen zones attributed to different phases, ranging from isotopic stage 5 to isotopic stage 3: layers VII to V at isotopic stage 5, layers IV to II at stage 4 and layer I at stage 3. A single zone has been linked to a stadial episode, reflecting a harsh climate, the others exhibiting characteristics typical of interstadial and / or interglacial periods.

From an archaeological point of view, only the levels from the Arobba et al. (1976) stratigraphy have been studied and on several occasions (Cauche *et al.*, 2004; Cauche, 2007, 2012; Leger, 2011). The lithic industry found in those seven layers is Mousterian, as expected, and in all those layers the presence of the *débitage levallois* has always been recognized, in different proportions and quantities depending on the layer. Furthermore, it is interesting to know that all the tools found seem to be manufactured from local raw materials, coming from geological formations in the areas surrounding the Manie cave (p. 31). From all these studies it was possible to propose a depositional period between MIS 5 and MIS 3. Additionally, the magnetic properties of these deposits have been tested (Djerrab and Camps, 2010) and all the parameters proved the presence of a high percentage of magnetic grains, mostly in the hearths layer and in the upper part of the infilling, in particular in layer IV (Figure 25).

The material investigated for archaeozoological analyses, also transferred on the same stratigraphy shown in Figure 24, considered both micromammals and macromammals (Abbassi and Brunet-Lecomte, 1997; Abbassi *et al.*, 1998; Psathi, 2003; Valensi and Psathi, 2004). The study of micromammals (Abbassi and Brunet-Lecomte, 1997; Abbassi *et al.*, 1998) has returned a very detailed reconstruction of what the environment must have been like and the changes it underwent during the deposition of the different layers. Starting from the lower one, VII, it is assumed a dominance in forest species and humid grasslands, with a cold and humid climate, with strong continental influences. This is followed by a drier period in level VI and then again more humid and continental in V. Levels IV and II show similar characteristics and are associated in turn with VI, thus more arid. There is a change again with level III, where the genus *Sicista* appears and with it the prairie species dominate, with a new cold and dry climate. Finally, with level I, humid temperate conditions are established.

From the studies on large mammals it is clear that the gatherings of fauna could mostly be the result of accumulation operated by human hunting (mainly the remains of *Cervus elaphus* L. are found), rather than a real occupation of the cave by fauna. Very different condition from that described for the Caverna delle Fate cave (Figure 26).

Again, the deposits are considered as a portrait of the period between the end of MIS 5 and the beginning of MIS 3.

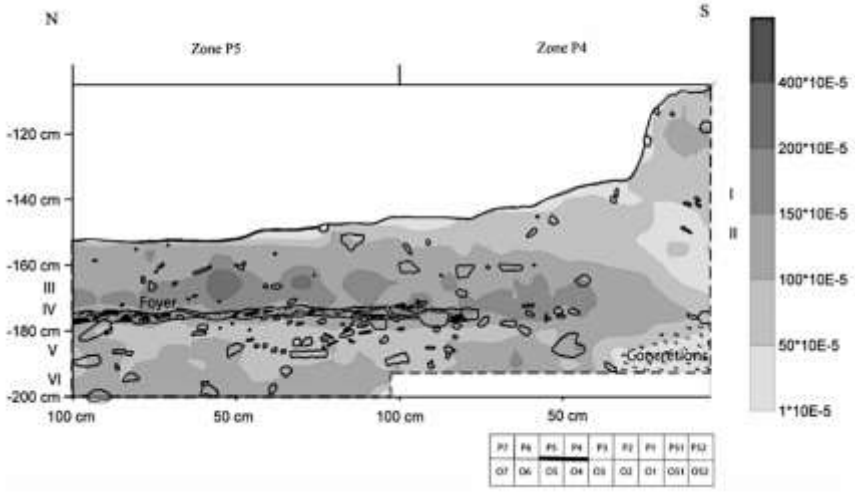

Figure 25 – Magnetic properties study of Arma delle Manie infillings, from Djerrab & Camps (2010).

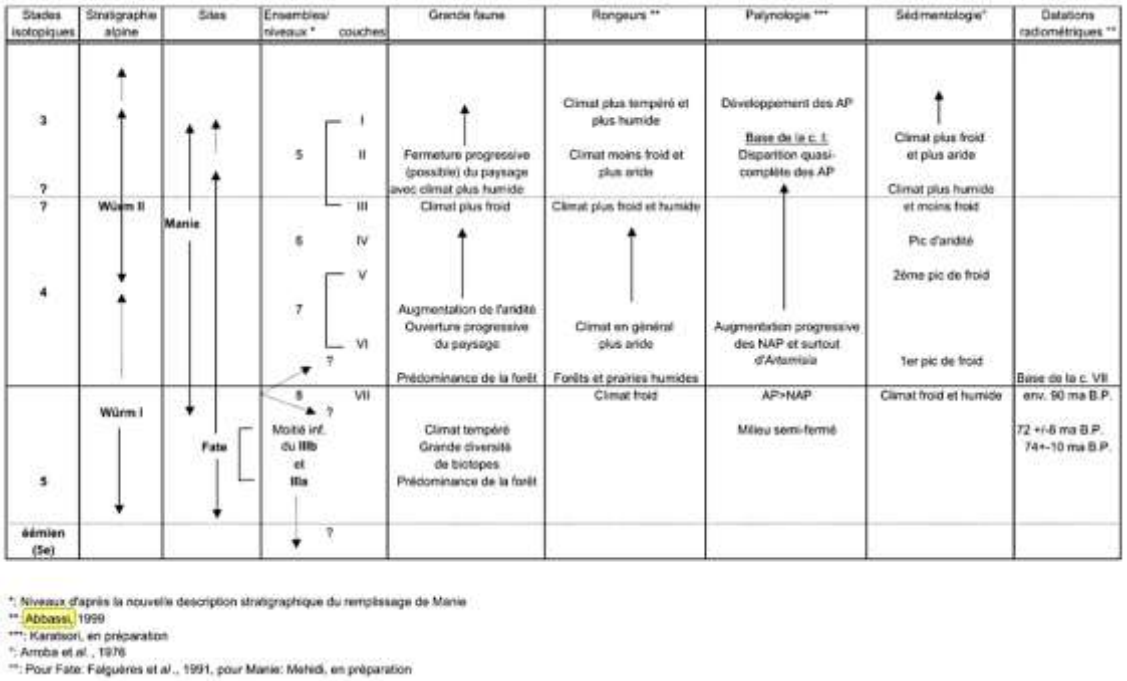

*: Niveaux d'après la nouvelle description stratigraphique du remplissage de Manie
**: Abbassi, 1999
***: Karatsori, en préparation
*: Arroba et al., 1976
**: Pour Fate: Falguères et al., 1991, pour Manie: Mehdi, en préparation

Figure 26 - Caverna delle Fate and Arma delle Manie infillings climatic and chronological evolution, based on multidisciplinary results. From Psathi (2003).

4. Materials and methods

It is now a consolidated practice in this field of study and, in particular, in these particular environments, to set up a recognised rigorous and detailed study approach. Also, it is very important to know and acknowledge the complexity of all the agents and variables acting on each site and to model a tailor-made method, changing, when needed, in time and space, even inside the same cave (Courty & Vallverdu, 2001; Goldberg & Sherwood, 2006; Woodward & Goldberg, 2001, and others).

Beside this statement, the materials and methods applied here fall right into the recognised routine of paleoenvironmental and palaeoclimatological reconstruction studies: what generally may change is the decision to apply or not a technique or an analysis considered as supporting to micromorphology.

This work mainly focuses on the use and importance of the micromorphological technique in these contexts, even though both micromorphology and sedimentary petrography principles and concepts have been used (as suggested by Courty et al., 1990; Courty & Vallverdu, 2001). Anyhow, there is no micromorphological study without a good field work, a good sampling and a sensible use of laboratory techniques.

4.1 Fieldwork and site stratigraphy

Most of the first PhD year was spent to collect and organize all the existing material about the four caves and plan their study. The first preparation required the identification of the sections and trenches already individuated and studied by our fellow archaeologists or by previous study groups, in such a way that our results could be easily compared, in a second time, with those already present. And then, also hypothesize where and why to sample inside the cave or in the specific section.

Field work has always followed this order:

- identification of the reference stratigraphy (Figure 27a);
- drawing, photographic record and description of the most significant sections' stratigraphy;
- sampling.

This approach has been applied to all the caves, except for Tana di Badalucco cave, where it was not possible to take bulk samples.

Drawing, photographic record and description of the stratigraphic section

The drawing process was carried out by reporting on a sheet the various constituents (geogenic, biogenic or anthropogenic) and the existing relationships between them, the most characteristic elements (whether it was a rock or a karst element, such as the presence of a flowstone, e.g.), and the limits of every stratigraphic unit recognized. During sampling, sample location was reported, too (Figure 27d).

For every site, an extensive photo recording has been produced. Not only the interior of the cave was portrayed, but also the surrounding area. In this way, every characteristic has been recorded and it was possible to see every single detail, once again, from different points of view. Every photograph was taken by a single-lens reflex camera (*Canon Reflex EOS 1300D*).

The description was conducted, always after having cleaned up the stratigraphic section (Figure 27b), pursuing the following scheme:

- Level thickness;
- Munsell colour (Figure 27c);
- Nature and appearance of the interface between levels;
- Sediment texture:
    - Fine fraction;
    - Support nature;
    - Clast morphology and lithology;
    - Anthropogenic and biogenic remains, material;
    - Sedimentary structure (if present).

It is considered necessary to dedicate a separate paragraph to sampling.

Figure 27 - Here are some of the different stages of field work. a) Recognition and study of the stratigraphic section. b) Cleaning of the section, in order to well expose the deposit. c) Description of the stratigraphy, in particular, Munsell colour recognition in this case. d) Notes on the position of the micromorphological samples.

4.2 Sampling

Two types of samples were taken from each cave (except for Tana di Badalucco): a disaggregated bulk sample for routine analysis (grain size and mineralogical analysis, for example) and a block sample for the creation of thin sections (for micromorphology).

In the first case, a sample weighting between 0,5 kg and 1 kg was taken from each level recognised, where it was possible. In some cases carbonates fully cemented the deposit making it difficult, where not impossible to sample it. It is the case of few levels in Caverna delle Fate cave and Arma delle Manie.

Undisturbed samples were collected by excavating around the desired location (Figure 28a) and covering it with plaster of Paris for every level, when possible and adequate, at the interface existing between levels when considered best (Figure 28b).

In Arma delle Manie cave, moreover, some charcoal fragments were taken for identification and subsequent dating. They were sampled by delicately digging around the larger fragments, successively placed in rigid containers and then in aluminium foil and rigid containers, always with a label on top to indicate their origin.

Figure 28 - Sampling. a) Block obtained from two levels by digging around the desired portion. b) Application of plaster jackets on undisturbed sample.

4.3 Laboratory analysis

The physical analysis were carried out in two different laboratories: one in the University of Genoa (Laboratory of sedimentology and marine geology, led by A. Demergasso) and another external to the university, Laboratorio regionale analisi terreni e produzioni vegetali (Regional Laboratories for Land and Plant Production Analysis, placed in Sarzana, La Spezia).

Figure 29 - Various steps of grain size determination procedure are shown. a) The samples are oven-dried. b) Subsequently sieved using different mesh sizes. c) Preparation of the fine fraction for the sedigraph (All pictures by me, except for the last one by Mr. Demergasso).

Grain size

All the samples were weighed and placed in oven overnight at 100 ° C (Figure 29a). Subsequently the samples were immersed in water for 30 minutes, in order to remove even the last pieces. The coarser part (> 63 µm) was divided from the finer one (Figure 29b). The latter was left to settle (Figure 29c) and then analysed by sedigraph. The coarse part was dried again in the oven and then dry sieved. Unlike what is applied during a standard procedure, at no time were the samples treated with HCl or H_2O_2, in this way neither carbonates nor the organic matter were dissolved. The reason that led to devise such a protocol lies in the fact that the deposits inside the cave are mostly composed of carbonates, but also the sediments coming from outside: most of the geological formations of the surrounding area are carbonates. Therefore, removing such a fraction would have undermined the meaning of the analyses themselves.

4.4 X-Ray Powder Diffraction (XRD)

The elemental composition of some samples was determined thanks to the use of X-ray Powder Diffraction, in The University of Genova laboratories and under Prof. Carbone direction. A Philips PW3710 diffractometer, equipped with a Cu-anode (CuKα radiation; current 20 mA, and voltage 40 kV) was used. The data were firstly elaborated with Philips X'pert High Score software, and then with Match!3 and QualX (Altomare *et al.*, 2008, 2015) software.

4.5 Radiocarbon dating

Two new sets of radiocarbon dating have been carried out in the wider context of a rediscovery and resumption of research work in at least two of the four caves investigated: Arma degli Zerbi and Arma delle Manie.

For Arma degli Zerbi six charcoal samples have been dated by the Max Planck Institute in Leipzig (lab Code R-EVA). For Arma delle Manie, instead, one charcoal sample has been dated by the University of Groningen and three by BETA Analytics.

In all cases, the calibration to calendar years was performed with software program OxCal, version 4.3 (Ramsey, 2009), and using calibration curve IntCal13 (Reimer *et al.*, 2013).

4.6 Micromorphological analysis

This thesis has as its main focus the micromorphological analysis of thin sections from the four caves deposits under study.

Micromorphology is "the study of undisturbed, oriented samples with the aid of microscopic and / or ultramicroscopic techniques, to determine the composition of the constituents and their spatial relationship, with the aim of deducing their genetic and chronological relationships" (Nicosia and Stoops, 2017).

The methodology used to sample has already been presented previously (page 57). The samples taken, wrapped with paper towels and film, on which the name of the sample and orientation were reported, were then sent to the Servizi per la Geologia laboratory (in Piombino, Livorno) to be prepared. The procedure, performed following Benyarku & Stoops (2005) guidelines, requires the samples to be dried, impregnated with epoxy resin and then cut and thinned, finally mounted on a slide and covered with a coverslip. At the end of this process the thin sections are ready to be studied.

As a first step, every single thin section has been scanned: thus every single microfacies or particular characteristic recognised could be drawn and be permanently available. This step also helped in examining macroscopically every single thin section.

The microscopic aspects have been detected thanks to the usage of a polarising petrological microscope under plane polarised light (PPL), crossed polarised light (XPL) and oblique incident light (OIL). All the pictures have been taken thanks to a camera fixed on a Leitz Laborlux 12 Pol microscope, with magnifications 2.5-50x.

Secondly, we proceeded with the description of every thin section, following Stoops' (2003) indications, with some supplements, where necessary, from Bullock (1985) and Macphail & Goldberg (2017). From this a table was developed and it has been modified, with additions and deletions throughout the period of the doctorate, as to be as complete as possible in describing and highlighting every aspect that would be important for the interpretation of the results (*Appendix A: Micromorphological description table*). Terms suggested by Stoops (2003) were adopted to describe fabric units sizes, whereas Bullock (1985) and Macphail & Goldberg (2017) tables and charts were used for estimations and numerical data. When referring to abundance (in the case of inorganic residues of biological origin, anthropogenic elements and pedofeatures) and frequency (for the quantification of voids, single mineral grains and compound mineral grains and rock fragments) the reference is Macphail & Goldberg (2017), with a single change: in abundance, when "rare" ("*a*") (Table 4) is used, we do not intend <2% but = 2%. We believe this is a clearer way to address

abundance, above all when also lower values from that same table are used (a * = 1%; a-1 = as single occurrence).

Frequency	**Abundance**
* - very few 0-5%	a-1 – single occurrence
f – few 5-15%	a* - 1%
ff – frequent 15-30%	**a – rare 2%**
fff – common 30-50%	aa – occasional 2-5%
ffff – dominant 50-70%	aaa – many 5-10%
fffff – very dominant >70%	aaaa – abundant 10-20%
	aaaaa – very abundant >20%

Table 4 - Frequency and abundance estimates from Macphail & Goldberg (2017). *In bold the change applied here.*

The last aspect, the interpretation of the results, has been addressed keeping as a cornerstone the indications of Stoops et al. (2010, 2018), Courty et al. (1990), Nicosia & Stoops (2017), Macphail & Goldberg (2017) and the vast existing bibliography about this technique applied to this line of research.

5. Results

Tana di Badalucco

Unfortunately, due to Covid-19 outbreak, for this cave it was not possible to conduct a proper excavation campaign and we were only able to study the already sampled thin sections. The result has been published (Sessa *et al.*, 2019) and can be considered as the first piece of the future work in this important site.

Field work and site stratigraphy

In the field, considering only the actually in place and not altered deposits, three main sections were identified. From the previous excavations, only few layers, probably not continuous, remain (Figure 30) and were sampled. They display very different characteristics and we consider them indicative of a very extended period of time, probably from the beginning of the last glaciation to the onset of the Holocene. The Munsell colours, as presented in Figure 30, were determined during field sampling. Starting from the oldest and more distant from the entrance layer:

Section in the inner part of the cave (Section 1, S. 1 in Figure 31):

- A1: The lower limit was not reached, the upper limit is 22 cm below the ground surface. Munsell colour: 7.5 YR 5/8, strong brown. The lower contact was not reached. It is composed of a rubified clayey silt, no clasts were recognised and no anthropogenic nor biogenic material was found.
- A2: from -22 cm to the ground surface. Munsell colour: 5 YR 5/8, yellowish red. The lower contact is wavy and clear. It is a rubified clayey silt, no clasts were found in it and neither anthropogenic or biogenic material.

Section in the middle part of the cave (section 2, S. 2 in Figure 31):

- B: The lower limit was not reached, the upper limit is 23 cm below the present-day ground surface. Munsell colour: 7.5 YR 6/4, light brown. It is silty, with pebble sized rock fragments, such as limestones and sandstones. The firsts are rounded and smooth, the latter are rough and subrounded. No anthropogenic or biogenic material was found.

- C: From -23 cm to -10 cm. Munsell colour: 10 YR 6/6, brownish yellow. The lower contact is smooth and clear. It is a loamy clay deposit, with granule and pebble sized clasts (mostly sandstones, in lesser amount carbonates). Sandstones are smooth and rounded, carbonates are undulating and subrounded. No anthropogenic or biogenic material.
- D: From -10 cm to the ground surface. Munsell colour: 10 YR 5/4, yellowish brown. Irregular and clear lower contact. It is a loamy deposit, with granule and pebble sized clasts. In this case limestone grains prevail over sandstone grains. No anthropogenic or biogenic material.

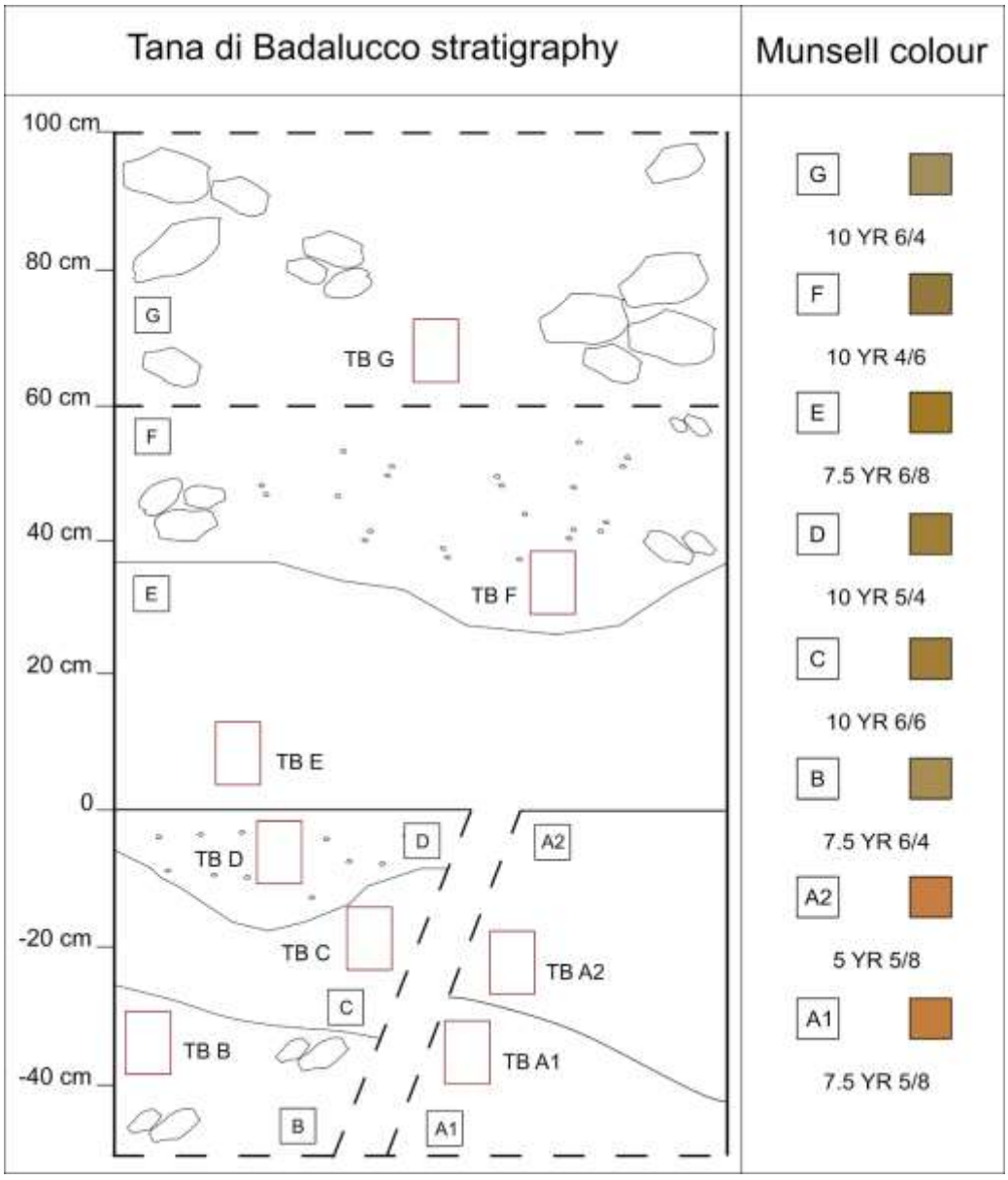

Figure 30 - Tana di Badalucco stratigraphy and Munsell colours, sample position and levels. the stratigraphy as presented here is to be intended as a synthesis of the different sections individuated in the field.

- E: From the ground surface up to +39 cm. Munsell colour: 7.5 YR 6/8, reddish yellow. The lower limit is not easily identifiable in the field. Firm silt, no clasts. No anthropogenic, nor biogenic material.
- F: From +39 cm to the upper end of the in place deposit (~65 cm). Munsell colour: 10 YR 4/6, dark yellowish brown. The lower limit is smooth and clear. Clay sediment, with pelite and limestone grains, tubular and undulating. Little bone fragments are present.

Entrance section (section 3, S. 3 in Figure 31):

- G: From +60 cm up to the ceiling. Munsell colour: 10 YR 6/4, light yellowish brown. The lower limit is abrupt and smooth. *Breccia* (a cemented deposit, Goldberg and Macphail, 2013) rich in angular and subangular, pebble sized, limestone clasts. Bone fragments are present.

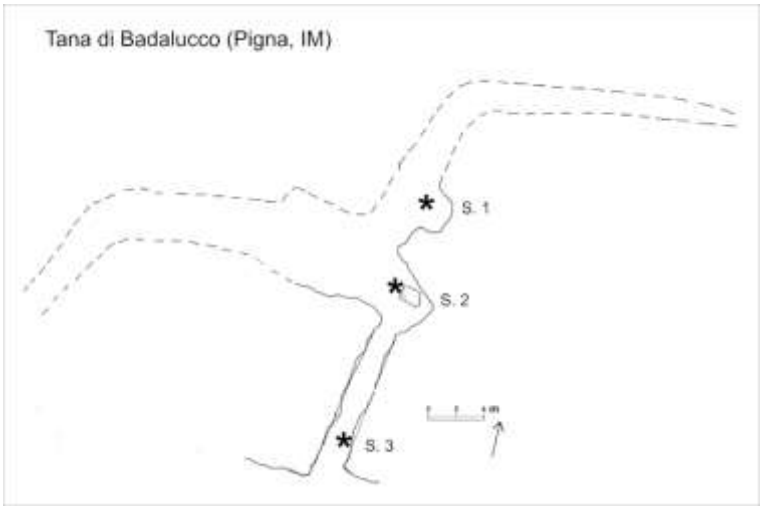

Figure 31 - Tana di Badalucco cave plan with sections indication.

Sampling

Only micromorphological samples were taken from the three sections studied, one per level, as shown in Figure 30 and Figure 32. Following the same order:

- Section 1:
    - TB A1: It was sampled at a depth of about 30-35 cm (Figure 30 deliberately shows a larger sample, and this also applies to all the others);
    - TB A2: It was sampled at a depth of about 20 cm.
- Section 2:
    - TB B: It was sampled 35-40 cm below the ground surface;
    - TB C: 20 cm below the ground surface;
    - TB D: Sampled at -5 cm;
    - TB E: Few centimetres above the ground surface (around 3 cm);
    - TB F: ~30 cm above the ground surface.
- Section 3:
    - TB G: It was sampled around 65-70 cm above the ground surface.

The samples were taken trying as much as possible to follow a regular, vertical order and trying to have a verification of all the salient features described in the field.

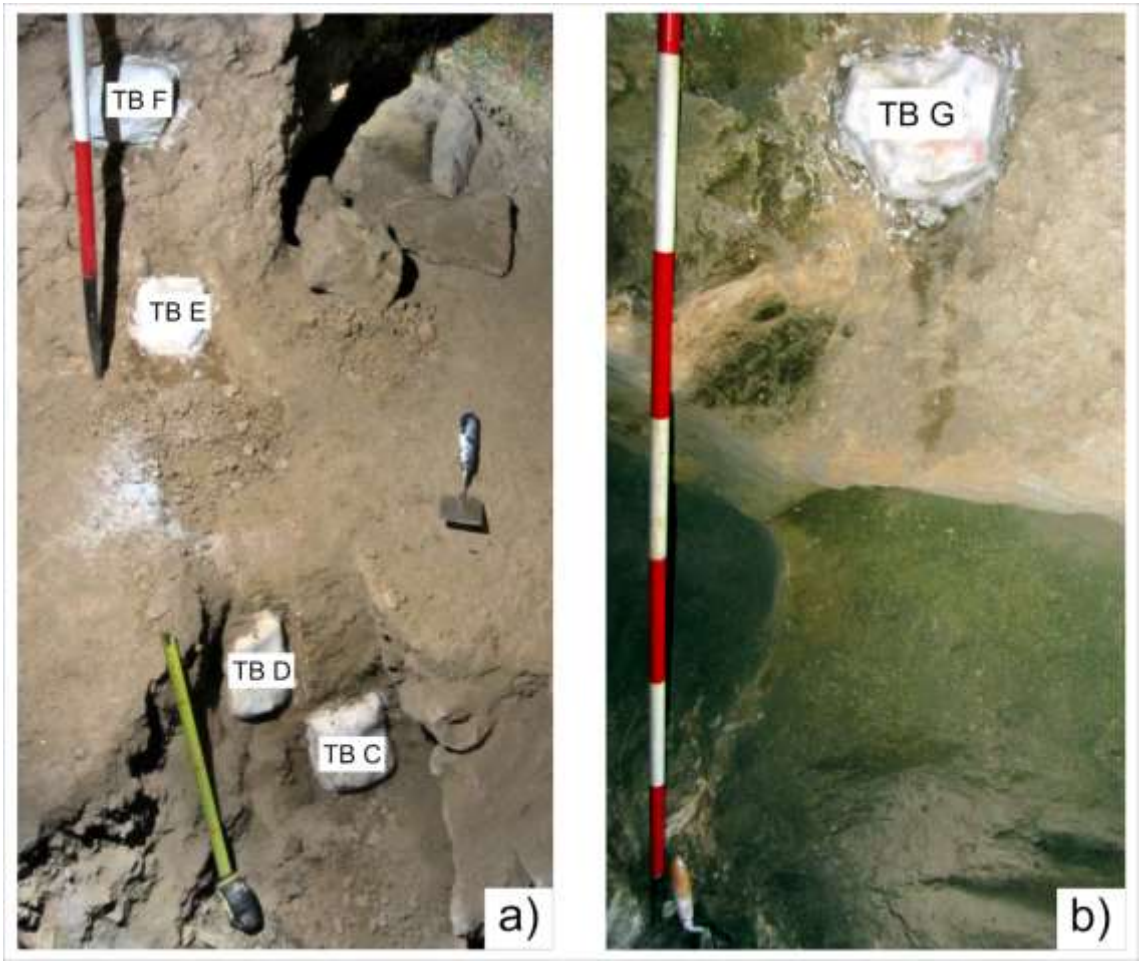

Figure 32 - Sampling of sections 2 and 3. a) Section 2 with four of the five samples taken. TB B was sampled before the photograph was taken, from beneath sample TB C. b) Sampling in section 3. It is evident how the sampled level is the only one still in place in this part of the cave.

Micromorphological analysis

The micromorphological analysis of Tana di Badalucco cave's deposits was conducted on eight thin sections, whose size is 90 x 60 mm (a quarter mammoth). Subsequently, after their interpretation, they were divided into four microfacies types (MFT) (Table 5) (Courty, 2001; Goldberg and Macphail, 2013), which will be deepened in the discussions. These are: 1. Quartz-rich, reddish clayey deposits MFT (QRC); 2. Occupation deposits MFT (OD); 3. Bioturbated clayey deposits MFT (BCD); 4. Manganese-rich, reddish clayey deposits (MRC).

Table 5 - Microfacies types (MFT) and simplified descriptions to highlight crucial aspects for interpretation of results for Tana di Badalucco cave deposits.

Str. lvl	TS	MFT	mF	Microstructure	Aggregates	Voids	C/f-related distribution	C/f-ratio	Coarse fraction					Fine fraction	B-fabric	Pedofeatures
									Bones	Burnt bones	Charcoal	Single mineral grains	Rock fragments			
TB G	TB G	Occupation deposits (OD)		Complex: Subangular blocky and granular	Subangular blocky peds, granules	Vughs, complex packing voids, planes, channels	Close fine enaulic and open porphyric	60\40	a	a*	a*	Quartz (ff), calcite (*)	Limestone (fff), greywacke (f)	Clay	Weakly developed random striated	Ferrous (a), phosphatic (a*)
TB F	TB F	Occupation deposits (OD)	2	Complex: subangular blocky and crumb	Subangular blocky peds, porous crumbs	Complex packing voids, planes, channels, vesicles, vughs	Open porphyric and single spaced enaulic	30\70	a	a	a	Quartz (f)	Limestone (f), greywacke (f)	Clay, carbonates	Weakly developed random striated	Ferrous (a*), phosphatic (a), excremental (aaaa)
		Bioturbated clayey deposit (BCD)	1	Subangular blocky	Subangular blocky peds, lenticular plates	Chambers, planes, channels, vughs	Open porphyric	20\80	a	a*	a	Quartz (f)	Limestone (f), greywacke (f)	Clay, carbonates	Weakly developed striated	Ferrous (a), calcitic (a), phosphatic (aaa), excremental (a*)
TB E	TB E	Mn-rich, reddish clayey deposit (MRC)		Complex: Subangular blocky and chamber	Subangular blocky peds	Chambers, planes, channels, vesicles, vughs	Open porphyric	20\80	-	-	-	Quartz (f), feldspar (*)	Limestone (*)	Clay	Weakly developed striated	Ferrous (a), manganese (aaa), calcitic (aa), clayey (aa), excremental (a)
TB D	TB D	Bioturbated clayey deposit (BCD)		Complex: Subangular blocky and crumb	Subangular blocky peds and porous crumbs	Planes, complex packing voids, channels, chambers, vughs, vesicles	Double spaced porphyric, locally single spaced coarse enaulic	30\70	a-1	-	-	Quartz (ff)	Limestone (*), greywacke (*), sandstone (*)	Clay	Weakly developed striated	Ferrous (a), calcitic (a*), clayey (a-1), phosphatic (a*), excremental (a*)
TB C	TB C	Bioturbated clayey deposit (BCD)		Complex: Subangular blocky and crumb	Subangular blocky peds and porous crumbs	Vughs, channels, planes, chambers	Single spaced porphyric	40\60	-	-	-	Quartz (ff)	Greywacke (*), limestone (*)	Clay	Granostriated	Ferrous (aaa), manganese (a*), calcitic (a), clayey (aaa), excremental (a)
TB B	TB B	Occupation deposits (OD)		Complex: subangular blocky and platy	Subangular blocky peds, lenticular plates, porous crumbs	Planes, vughs, chambers, channels, vesicles	Double spaced porphyric	40\60	a	a	-	Quartz (fff)	Greywacke (f), limestone (*)	Clay	Weakly developed granostriated	Ferrous (a), calcitic (a*), clayey (a), phosphatic (a), excremental (aa)

TB A2	TB A2	Quartz-rich, reddish clayey deposit (QRC)	Subangular blocky	Subangular blocky peds	Planes, channels, chambers, vughs	Single spaced porphyric	40\60	-	-	-	Quartz (fff), calcite (*)	N.r. (*)	Clay, iron	Granostriated	Ferrous (a), manganese (a*), calcitic (aa), clayey (aaaa), phosphatic (a*)
TB A1	TB A1	Quartz-rich, reddish clayey deposit (QRC)	Subangular blocky	Subangular blocky peds	Planes, channels, chambers, vughs, vesicles	Single spaced porphyric	40\60	-	-	-	Quartz (ff), Feldspar (*)	N. r. (f)	Clay, iron	Granostriated	Ferrous (a), manganese (a), calcitic (aa), clayey (aaaa)

Starting from the inner parts of the cave and the lowest levels of the deposit:

Section 1:

Thin section TB A1 (MFT: Quartz-rich, reddish clayey deposits MFT, QRC)

It is a vertical thin section, whose microstructure can be defined as a highly separated subangular blocky microstructure, with subangular blocky peds (2-3 cm). The porosity is represented by planes (very fine sand sized, v.f.s.; ±10% of the peds), channels (fine sand, f.s., ±10%), chambers (f.s., ±5%), vughs (v.f.s., ±5%) and vesicles (f.s., ±2%).

The groundmass has a coarse/fine ratio of 40/60, with the limit at 5µm, and a c/f-related distribution pattern as single spaced porphyric. Thus, the coarse material is composed of a mineral part, with angular grains of quartz (v.f.s., ±20% of the entire thin section area), and angular grains of feldspars (v.f.s., ±5%), both with no signs of weathering. Quartz can sometimes be found in same sized grains lenses; but also few tabular, not identifiable (due to weathering) rock fragments are present (medium sand, m.s., ±5%). The micromass is reddish brown, constituted of cloudy clay and iron with a granostriated b-fabric.

Different types of pedofeatures have been recognised. The pedofeatures constituted of oxides are typic ferrous nodules, around 100 µm in diameter, with no peculiar pattern identified (±2% of the total area), and typic manganese nodules, around 100 µm in diameter, no pattern found (±2%). The carbonatic ones are the micritic mammillate nodules, f.s., ±2% and the continuous micritic hypocoatings, about 50 µm thick, ±1%. Abundant clayey features are also present: dusty parallel microlaminated clay coatings with sharp extinction lines, in some cases showing signs of reworking, about 50 µm thick, ±10%.

Thin section TB A2 (Quartz-rich, reddish clayey deposits MFT, QRC)

Also in this case it is a vertical thin section. The microstructure is subangular blocky, with a single subangular blocky ped (5 cm in diameter). The voids can be divided in planes (v.f.s., ±10%), channels (f.s., ±5%), chambers (f.s., ±2%), and vughs (v.f.s., ±2%).

With a limit between coarse and fine fraction set at 5µm, the ratio is still 40/60 and the c/f-related distribution pattern is a single spaced porphyric. Angular quartz grains (f.s., ±30%) and subangular calcite grains (f.s., ±2%), highly altered, represent the single mineral grains recognised. The rock

fragments are few, all not identifiable (due to weathering) and tabular (f.s., ±2%). The micromass is brown, made of cloudy clay and iron, with granostriated b-fabric.

The pedofeatures comprehend: typic iron nodules, f.s., ±2%, some of which fragmented; manganese (hydr)oxides hypocoatings, v.f.s., ±1%; micritic hypocoatings, v.f.s., ±2%, concentrated in the upper half of the thin section; micritic mammillate nodules, f.s., ±1%, concentrated in the upper half of the thin section, as well; limpid parallel microlaminated clay coatings with sharp extinction lines, v.f.s., ±10%; limpid parallel microlaminated infillings with sharp extinction lines, f.s., ±5%, some are fragmented; cryptocrystalline typic apatite nodules, m.s., ±1%, showing low degree of alteration.

Section 2:

Thin section TB B (Occupation deposits MFT, OD)

Horizontal thin section, showing a complex microstructure: subangular blocky and platy microstructure denote its peculiar appearance. It has subangular blocky peds (5 mm), lenticular plates (0.5 mm) and porous crumbs (0.5 mm). Voids take the shape of planes (v.f.s., ±10%), vughs (v.f.s., ±5%), chambers (f.s., ±5%), channels (f.s., ±5%), and vesicles (v.f.s., ±2%).

The $c/f_{5\mu m}$ ratio is 40/60, while the c/f-related distribution pattern is double spaced porphyric. Two textural classes of quartz grains are present: one more angular and finer (silt size, s.s., ±10%), the other subangular and bigger (f.s. and m.s., ±10%). Tabular greywacke fragments (m.s., ±10%) -with their main axis perpendicular to the ground surface- are the dominant rock fragments, moderately weathered subangular fossiliferous limestone (f.s., ±5%) follow. Also Inorganic residues of biological origin have been recognised: moderately to highly altered bones (f.s., ±2%) can be seen in all thin section. Moderately to highly altered bones showing signs of burning (f.s., ±2%) have been identified and recorded as anthropogenic elements. Micromass is dark brown, made of cloudy clay with weakly expressed granostriated b-fabric.

Pedofeatures are typic ferrous nodules, f.s., ±2%; micritic hypocoatings, v.f.s., ±1%; clay depletion hypocoating, coarse sand size (c.s.), ±2%; cryptocrystalline apatite nodules, f.s., ±2%; subrounded excrements of large animals, sometimes clustered, f.s., ±2%.

Thin section TB C (Bioturbated clayey deposits MFT, BCD)

Vertical thin section. It is characterised by a complex microstructure: moderately separated subangular blocky and moderately separated crumb microstructure, with subangular blocky peds (pebble size), and porous crumbs (f.s.). Vughs (v.f.s., ± 10%), channels (v.f.s., ±5%), planes (s.s., ±5%) and chambers (f.s., ±5%) delineate the total porosity.

c/$f_{5\mu m}$ ratio is 40/60, with a single spaced porphyric c/f-related distribution pattern. Angular quartz grains (v.f.s.-s.s., ±20%) are the only kind of single mineral grains found. However, two types of rock fragments are distinguished: rounded micritic limestone, highly weathered (v.f.s., ±2%); tabular and subrounded greywacke, highly weathered (v.f.s.-s.s., ±2%). A brown micromass, composed of cloudy clay, with granostriated b-fabric is present.

Pedofeatures are: typic ferrous nodules, v.f.s., ±5%; manganese (hydr)oxides hypocoatings, dendritic sometimes (s.s., ±1%); micritic hypocoatings (s.s., ±2%); limpid nonlaminated clay coating with diffuse extinction lines, occasionally juxtaposed on Mn hypocoatings (v.f.s., ±2%), seemingly, limpid nonlaminated clay infilling with diffuse extinction lines, occasionally juxtaposed on Mn hypocoatings as well (v.f.s., ±2%); clay depletion hypocoating (c.s., ±2%); subrounded excrements of large animals, (m.s., ±2%).

Thin section TB D (Bioturbated clayey deposits MFT, BCD)

Vertical thin section with a complex microstructure: moderately separated subangular blocky and, contemporarily, moderately separated crumb. Subangular blocky peds (pebble size) and porous crumbs (very coarse sand, v.c.s.) are the aggregates present. Planes (v.f.s., ±10%), complex packing voids (f.s., ±5%), channels (f.s., ±5%), chambers (f.s., ±5%), vughs (v.f.s., ±2%) and vesicles (v.f.s., ±2%) describe the porosity.

The c/$f_{5\mu m}$ ratio this time is 30/70, and the c/f-related distribution pattern is double spaced porphyric, locally single spaced coarse enaulic. Only angular grains of quartz (s.s., ±20%) are present as single mineral grains. However, different types of rock fragments can be recognised: fossiliferous rounded limestone, highly altered (m.s., ±2%); tabular greywacke, highly to moderately weathered (m.s., ±2%); and highly weathered subangular sandstone (very coarse sand, v.c.s., one occurrence). One bone fragment is present (pebble size) at the top of the thin section. Micromass is brown, there is cloudy clay with weakly developed striated b-fabric. The pedofeatures are: typic ferrous nodules (v.f.s., ±2%); micritic hypocoating, found only in the spongy bone fragment voids (v.f.s., ±1%); clayey silt capping, nonlaminated, on a highly weathered sandstone grain (200 µm thick); cryptocrystalline apatite nodules (f.s., ±1%); subrounded excrements of large animals, (m.s., ±1%).

Thin section TB E (Manganese-rich, reddish clayey deposits, MRC)

Vertical thin section. The microstructure is complex and it is a combination of a moderately separated subangular blocky microstructure and chamber microstructure. The aggregates are subangular blocky peds, 2 cm in size. Chambers (c.s., ±10%), planes (f.s., ±5%), channels (f.s., ±5%), vesicles (f.s., ±5%) and vughs (f.s., ±2%) compose the porosity. Groundmass has a $c/f_{5\mu m}$ ratio of 20/80 and a c/f-related distribution pattern open porphyric. Quartz is present in subangular grains, moderately weathered (two size classes: s.s. and f.s., ±5%), but also subangular feldspar grains, moderately to highly weathered (v.f.s., 2%) can be recognised. Subangular limestone, highly weathered (m.s., ±1%) is the only type of rock fragments. The micromass is brown, cloudy clay with weakly developed random striated b-fabric. The pedofeatures present are typic ferrous nodules (v.f.s., 2%) and manganese (hydr)oxides hypocoatings, dendritic sometimes (v.f.s., ±5%); micritic hypocoatings (v.f.s., ±2%), but also dense and incomplete calcite infilling, with equigranular and xenotopic crystals, fractured (±1 cm, in the top left part of the thin section, ±2%); dusty clay coatings(v.f.s., ±2%) and infillings (f.s., ±1%), nonlaminated, diffuse or absence of extinction lines; subrounded excrements of large animals, (m.s., ±2%).

As regards unit F, thanks to the microscope analysis it was possible to recognize two different microfacies which have been indicated below with F1 and F2.

Thin section TB F1 (Bioturbated clayey deposits MFT, BCD)

Vertical thin section. Moderately separated subangular blocky microstructure. Subangular blocky peds (pebble size, p.s.) and, secondly, plates (c.s.). Chambers (f.s., but one is 1 cm in size, ±20%), planes (v.f.s., ±10%), channels (f.s., ±10%) and vughs (f.s., ±10%). The $c/f_{5\mu m}$ ratio is 20/80 in this case, and the c/f-related distribution pattern is open porphyric. Angular quartz grains (s.s., ±10%) are present. Subrounded limestone, highly weathered (m.s., ±10%) and subangular greywacke, moderately weathered (m.s. ±5%) constitute the totality of rock fragments. Fragments of bones are found bones (m.s., ±2%), and also burnt bone (m.s., ±1%) and charcoal fragments (f.s., ±2%). The micromass is dark brown, with cloudy clay and calcite as main components and with weakly developed striated. Pedofeatures are typic ferrous nodules (f.s., ±2%); micritic hypocoatings (v.f.s., ±2%); cryptocrystalline apatite nodules (v.f.s., ±5%); subrounded excrements of large animals, (m.s., ±1%).

Thin section TB F2 (Occupation deposits MFT, OD)

Vertical thin section. It has a complex microstructure: a combination of a moderately separated subangular blocky and moderately separated crumb microstructure. Subangular blocky peds (pebble size, p.s.) are the dominand aggregates, followed by porous crumbs (c.s.). The voids are: complex packing voids (c.s., ±10%), planes (v.f.s., ±5%), channels (f.s., ±5%), vesicles (f.s., ±5%) and vughs (f.s., ±5%). The groundmass has a $c/f_{5\mu m}$ ratio of 30/70 and an open porphyric and single spaced enaulic c/f-related distribution patterns. The Mineral fraction is represented by angular quartz grains (s.s., ±10%), and subrounded limestone, highly weathered (m.s., ±10%), and subangular greywacke, moderately weathered (m.s. ±5%). Bone (m.s., ±2%), burnt bone (m.s., ±2%) and charcoal fragments (f.s., ±2%) are present, and sometimes ashes (f.s., ±5%), too. The micromass is dark brown, constituted of cloudy clay and calcite, with weakly developed striated b-fabric. Pedofeatures are: typic ferrous nodules (f.s., ±1%); cryptocrystalline apatite nodules (v.f.s., ±2%); subrounded excrements of large animals, (m.s., ±10%).

Section 3:

Thin section TB G (Occupation deposits MFT, OD)

Vertical thin section. A complex microstructure was recognised: a combination of a moderately separated subangular blocky and of a moderately separated granular microstructure. Subangular blocky peds (cobble size, c.s.) and granules (c.s.-v.c.s.) constitute the aggregates. Vughs (m.s., ±10%), complex packing voids (c.s., ±5%), planes (v.f.s., ±5%) and channels (f.s., ±5%) constitute the voids.

The $c/f_{5\mu m}$ ratio is totally different from the previous ones and it is roughly 60/40, with a c/f-related distribution pattern that is a mixture of a close fine enaulic and of an open porphyric. Angular quartz grains (two size classes: f.s. and m.s., ±15%) and calcite grains (m.s., 2%) are the minerals identified. Angular and subangular fossiliferous limestone, highly weathered (cobble size, ±30%) and subangular greywacke, moderately weathered (m.s. ±5%) the rock fragments individuated. Also, bone (m.s., ±2%), burnt bone (f.s., ±1%) and charcoal fragments (f.s., ±1%) were found. The micromass is brown, with cloudy clay and weakly developed striated b-fabric. Only two kinds of pedofeatures were observed: typic ferrous nodules (f.s., ±2%) and cryptocrystalline apatite nodules (f.s., ±1%).

Arma degli Zerbi

On two occasions we had the opportunity to survey the cave called Arma degli Zerbi. On these occasions it was possible to propose a description, expand the photographic record and collect loose and micromorphological samples.

Fieldwork and site stratigraphy

For this cave it was possible to have more than one stratigraphic section of reference on field (as shown in Figure 14a). This is very useful when trying to understand the processes that led to the formation of the site, or to understand if different parts of the cave were affected by different phenomena or used in a different way, by fauna or man (Bar-Yosef *et al.*, 1992; Alperson and Hovers, 2005; Shahack-Gross *et al.*, 2008). This despite the many clandestine excavations that have taken place over time. The work presented here has been built on the previously excavated trenches.

The stratigraphic sections are four, and identified by numbers, as follows: 1, 2, 3 and 4.

Section 1

Unfortunately, section 1 (Figure 33) is so impregnated with carbonates that it was impossible to perform a real description and sampling. Therefore, only one sample was collected for laboratory analysis and one for micromorphological analysis. We still determined its colour, by means of the Munsell chart, as 7.5 YR 4/3, brown, and we noticed its brecciated nature. Its lower part is rich in big bone and charcoal fragments.

Section 2

Section 2 is located not far from section 1, but it is positioned, in its entirety, below the ground surface (Figure 33). It extends for 95 cm below the ground surface and it was divided into five levels based on its main features. From the top to the bottom these are:

Level 1: pale yellow (2.5Y 7/3). The level is 21 cm thick, with a smooth and clear limit, emphasised by the presence of little charcoal fragments (Figure 34). Matrix supported texture. Limestone cobbles

are present, subrounded and subangular in shape, moderately weathered. Clay loam. One tooth and one big charcoal fragment have been found (Figure 34).

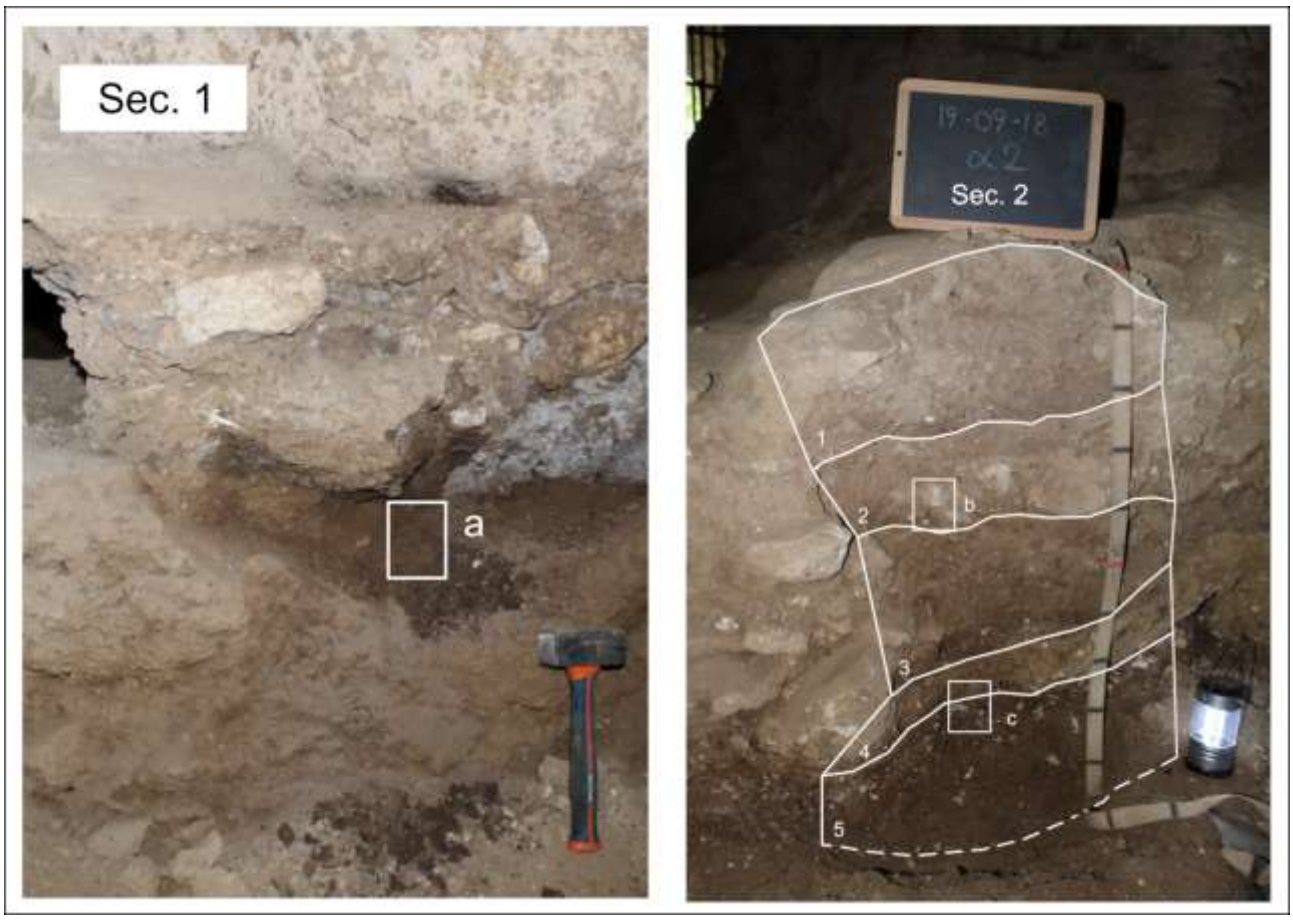

Figure 33 - Stratigraphic sections and division into levels of stratigraphies. White rectangles indicate the micromorphological samples taken.

Level 2: 2.5Y 7/2, light grey. From 21 cm to 40 cm. The lower limit is abrupt and smooth, delimited by cobbles and boulders. Also gravel and coarse sand are present. All of those are carbonates, subrounded and highly weathered. Matrix supported texture. Clay loam. Small charcoal fragments are present.

Level 3: 10YR 5/3, brown. From 40 cm to 60 cm. The lower limit is wavy and abrupt. Diminishes the limestone cobbles quantity. Clay loam and matrix supported texture. Rich in bone fragments. One carnivore jaw was found in this level.

Level 4: 10YR 5/4, yellowish brown. From 60 cm to 72 cm. The lower limit is wavy and abrupt. Subrounded limestone pebbles can be found, from moderately to highly weathered. Matrix supported and sandy clay loam texture. Few charcoal fragments.

Level 5: 10YR 4/4, dark yellowish brown. From 72 cm to 100 cm, even though the lower limit was not reached. Subrounded limestone cobbles are present, moderately weathered. Matrix supported, with a clay loam texture. Few big charcoal fragments.

Figure 34 - Section 2, level 1 in detail: in this figure it is easier to appreciate the clear limit, with little charcoal fragments, and, with two asterisks for clarity, one tooth and one big charcoal fragment in place.

Section 3

This section (Figure 35) is located in front of the previous one (Section 2) and only one metre separates them. This one, in particular, is NW oriented, thus towards the cave entrance.

Level 1: 10YR 7/3, very pale brown. From the ground surface to 36 cm below it. The lower limit is wavy and clear. Many limestone pebbles, subangular in shape. Sandy clay loam, matrix supported. Charcoal fragments have been found.

Level 2: 2.5Y 7/2, light grey. From 36 cm to 48 cm below the ground surface. Partly cemented. The lower limit is smooth and clear. Limestone cobbles and pebbles, subrounded. Clay loam, matrix supported.

Level 3: 2.5Y 7/4, pale yellow. From 48 cm to 58 cm. The lower limit is smooth and clear. There are fewer pebbles than on the upper level, moderately weathered and subrounded. Sandy clay loam, matrix supported.

Level 4: 2.5Y 5/4, light olive brown. From 58 cm to 70 cm. The lower limit is wavy and clear. Limestone pebbles are common, weathered and subrounded. Loam texture. Matrix supported, locally

clast supported. Few charcoal fragments are present and a *Levallois* lithic tool has been found (Figure 36).

Level 5: 2.5Y 5/3, light olive brown. From 70 cm to 120 cm, but the lower limit was not reached. The coarse fraction diminishes significantly, still is represented by limestone pebbles, moderately-highly weathered. Clay loam, matrix supported. Thin charcoal stratum at the top of the level.

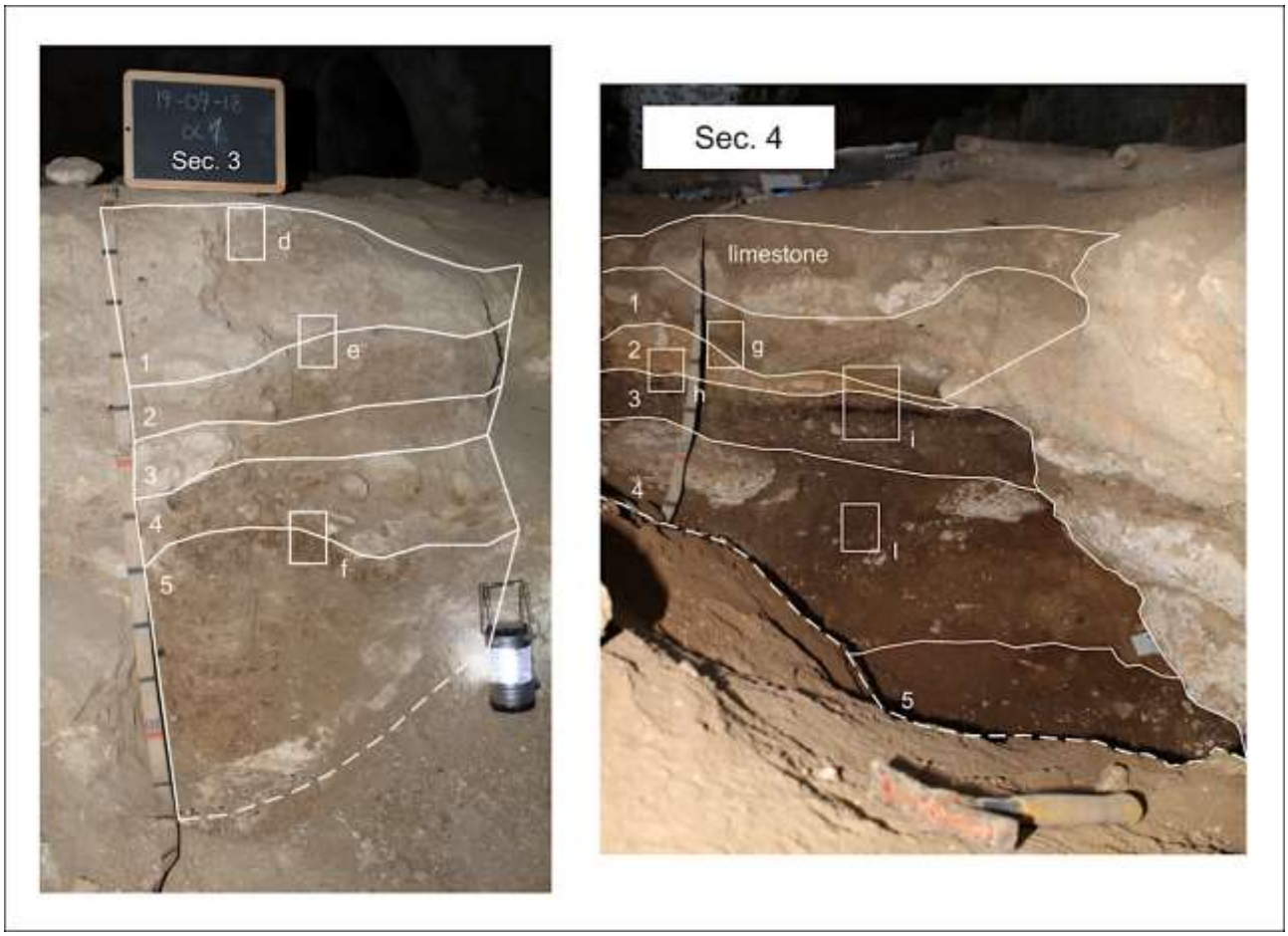

Figure 35 - Sections 3 and 4 with the micromorphological samples position.

Section 4

Section 4 (Figure 35) is the closest to the entrance to the cave. It is surmounted with an approximately 15 cm thick flowstone, with a wavy lower level. This was not recognized as an actual level.

Level 1: 2.5Y 7/2, light grey. From 15 cm to 25 cm below the present-day ground surface. The lower limit is wavy and abrupt. Limestone pebbles are present, subangular and moderately weathered. Clay loam, matrix supported. Presence of channels with a diameter of 2-3 mm.

Figure 36 - Section 3. At about 60 cm from the surface it is possible to see a lithic instrument in place.

Level 2: 2.5Y 8/4, pale yellow. From 25 cm to 33 cm below the ground surface. The lower limit is smooth and abrupt. Limestone cobbles are present in great quantity and are subangular and moderately weathered. Sandy loam, clast supported. Presence of channels with a diameter of 2-3 mm.

Level 3: 2.5 Y 5/3, light olive brown. From 33 cm to 45 cm. The lower limit is wavy and clear. Only small limestone pebbles and granules are present in the coarse fraction. Clay loam and matrix supported. A charcoal lens is present in the central part of the stratigraphy.

Level 4: 10YR 5/4, yellowish brown. From 45 cm to 90 cm. The lower limit is smooth and clear. Limestone cobbles are abundant, moderately to highly weathered, subrounded. Clay loam, matrix supported. Charcoal is present, but also chert and big bone fragments have been found.

Level 5: 10YR 4/4, dark yellowish brown. From 90 cm to 110 cm, although the lower limit was not reached. The coarse fraction, represented mainly by limestone cobbles, is abundant, also few silt rich lenses are present. Rare subrounded quartzite fragments are also present. Loam, matrix supported. Rare charcoal fragments, abundant bone fragments.

Sampling

Sampling was conducted on every level of all the stratigraphic sections presented above. This applies to loose samples for laboratory analysis and for those subjected to XRD analysis. The samples for the micromorphological analysis, on the other hand, had a different treatment. It was not possible to sample every single level and limit between them, but we still tried to have a picture as complete as possible of the processes that led to the formation of these deposits. This is especially true for sections 2 and 3, facing each other at very short distances. Recognizing the similarities and differences between them, levels and transitions between complementary levels were sampled. This made it

possible to sample in such a way as to cover all the variations of the stratigraphies. In the case of section 1, only three samples were taken: one sample for laboratory analyses, one for XRD and one for the micromorphological thin section. The micromorphological samples' position is already visible in Figure 33 and Figure 35, so it is their nomenclature.

Laboratory analysis

Grain size analysis was performed in part in University of Genova and in part in the Liguria region laboratories. The visualization of the results can be observed in Figure 38 and Figure 39.

Section 1

Section 1 is completely cemented and could not be analysed like the other samples, therefore it was treated with hydrochloric acid and only its fine component was considered. This proved to be largely (more than 50% of the total) composed of sand and then, in smaller quantities, of silt and clay. In this way determining a sandy loam texture (Figure 37).

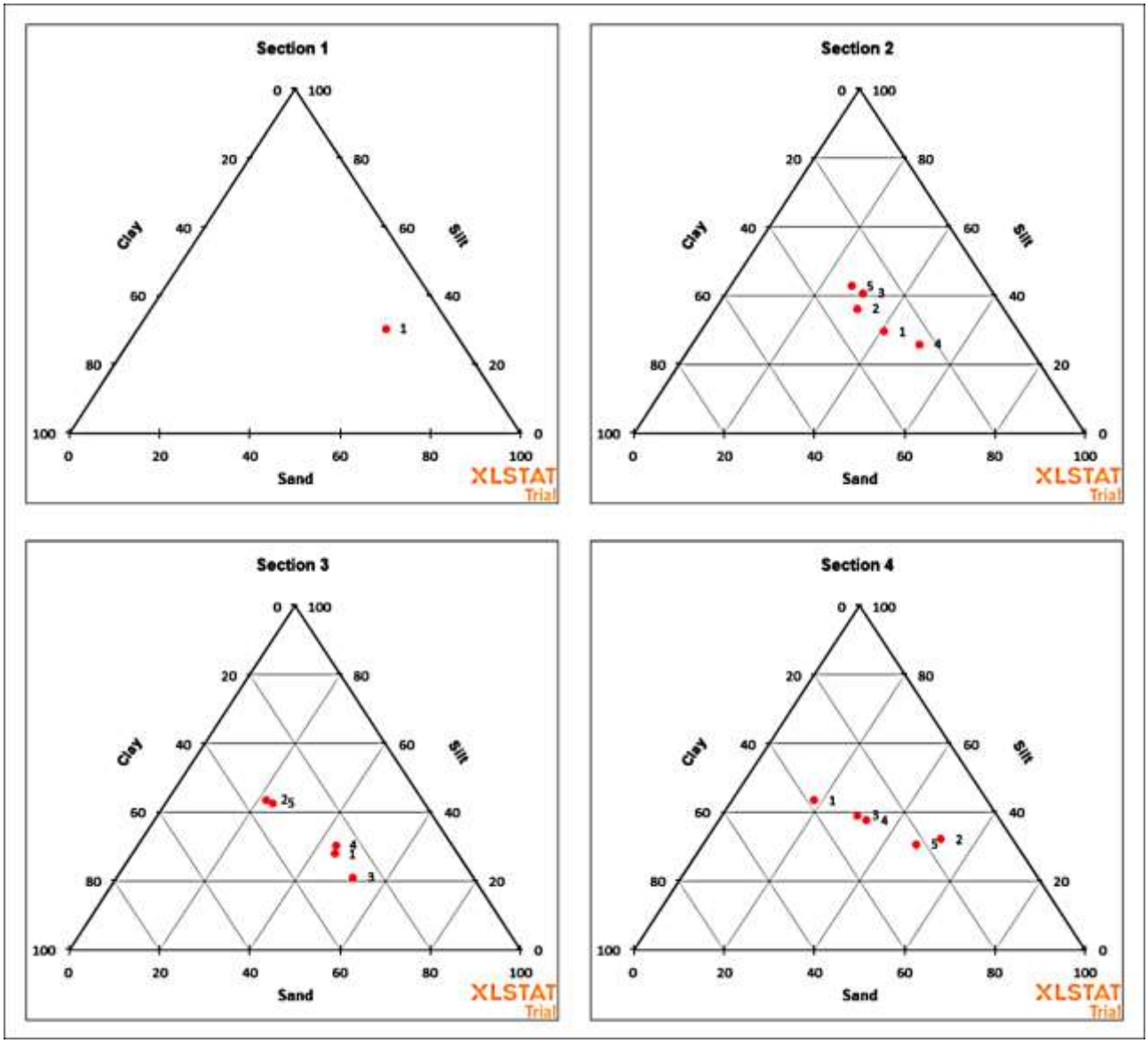

Figure 37 - Arma degli Zerbi cave fine earths' textures.

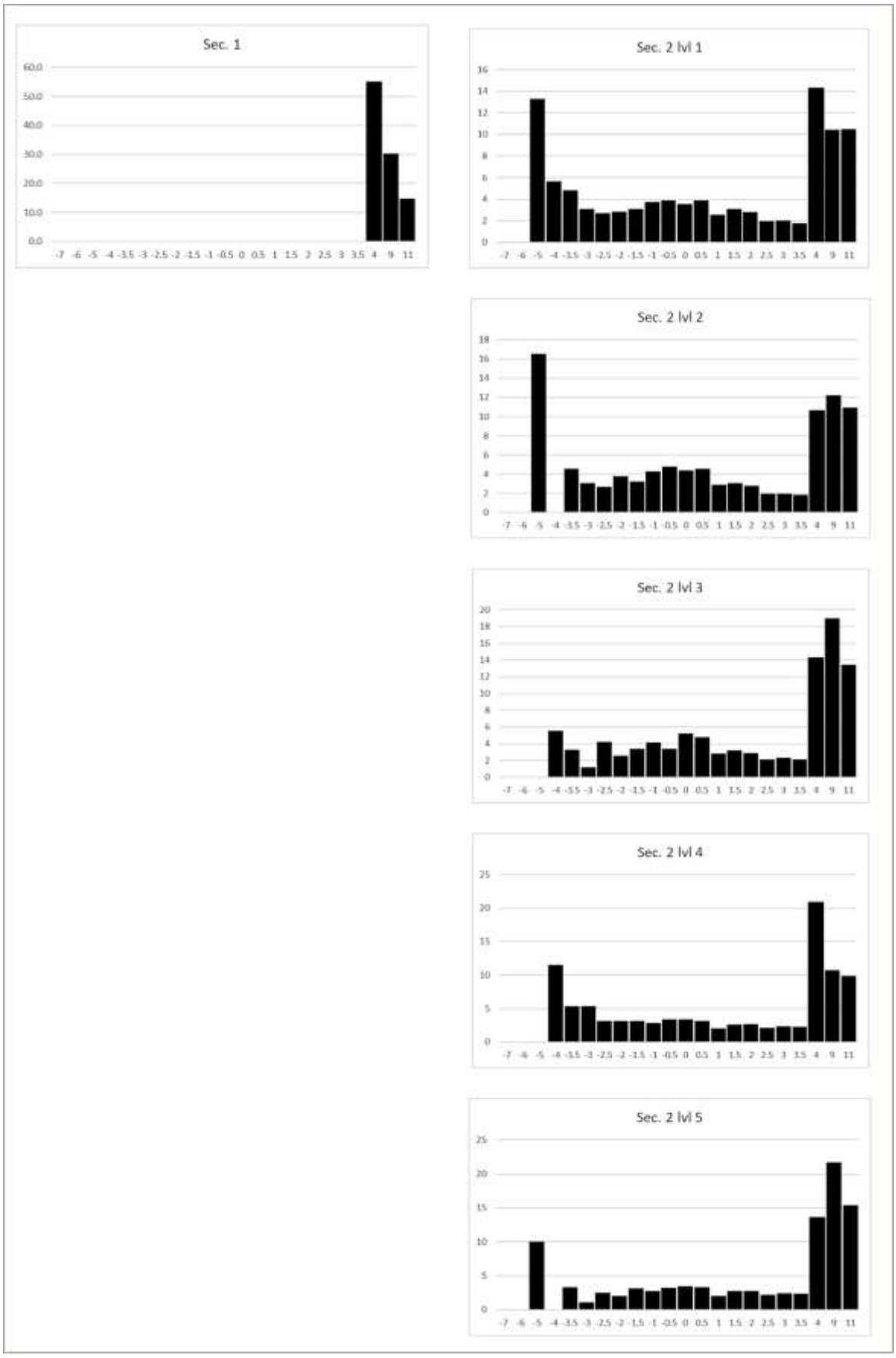

Figure 38 - Grain size analysis results (in %) for the first two sections of Arma degli Zerbi cave.

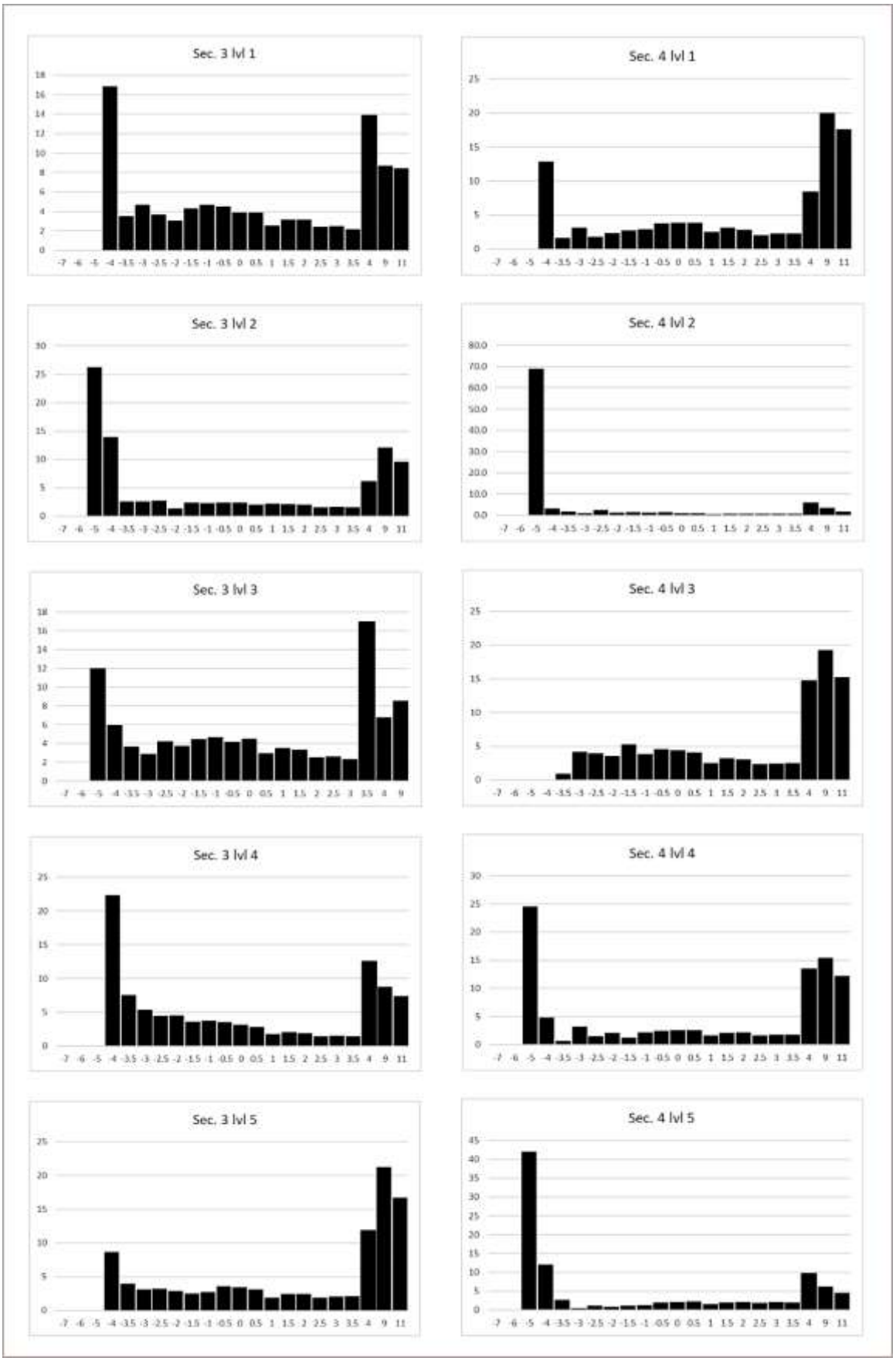

Figure 39 - Grain size analysis results (in %) for the last two sections of Arma degli Zerbi cave.

Section 2

The most represented granulometric classes within all levels are those of cobbles and pebbles (from -6 to -2 φ, Nichols, 2009) and those from very fine sands to clay. The classes with φ greater than 4 tend to be the best represented grain size classes for all levels. The class with phi equal to -5 is present only in three cases, but always with relatively high percentages: this is the case of levels 1, 2 and 5. The classes in the middle (granules and sand) are more or less steady in their relative quantities, with slightly higher percentages for the upper levels, i.e. 1, 2 and 3.

Textures have already been presented for each level in *Fieldwork and site stratigraphy* (from page 75).

Section 3

Cobbles are only present in level 2, while in all levels pebbles are present and in abundance. Fine earths are abundant too, albeit with different ratios. The very fine sand class is higher in levels 1 and 3, whereas in levels 2 and 5 (and in the latter, to a large extent) the silt is predominant. The appearance of the graphs is always analogous, with two peaks: one for the cobbles and pebbles fraction and one for the fine earths.

Section 4

Cobbles are present in more levels in this section. In fact, they represent one of the most represented classes in levels 2, 4 and 5. In level 1, instead, the class of the coarse fraction in greater quantity is that of pebbles. Level 3 shows a completely different distribution from that of all other levels, even from other stratigraphic sections, not having a large amount of coarse fraction. As far as the fine fraction is concerned, almost all the levels have a distribution similar to those already seen, except for levels 2 and 5, where it is present in low percentages. In levels 1, 3 and 4, the silts are predominant, but not too far from the very fine sand and clay classes. Only level 1 has a lower percentage of sands.

X-ray powder diffraction

The analyses conducted on the deposits of this cave have returned different results from those seen in other caves. The ratio between quartz and calcite is almost constant(Table 6, Figure 40), with some

values particularly positive in the case of level 5 of section 4 or in the higher levels of section 2, and negative in the case of levels 1 and 2 of section 3 and level 2 of section 4.

Plagioclase is present only in section 1, in the first three levels of section 3 and in levels 1 and 4 of section 4.

Muscovite can be found, in varying quantities, in all the levels studied, except for level 2 of section 4 (s.4 l.2).

In an approximately similar way, apatite can also be found in the entire deposit, sometimes only in trace amounts, but it is not found in s.1. Another peculiarity of this last mentioned section is represented by the last three minerals detected, i.e. serpentine, amphibole and chlorite, present only here.

Table 6 - Semi-quantitative XRD analysis results for Arma degli Zerbi cave deposits. All numbers shown are percentages. The abbreviations for minerals are those suggested by Whitney and Evans (2010).

Samples	**Qz**	**Cal**	**Pl**	**Ms+Ilt**	**Ap**	**Srp**	**Amp**	**Chl**
Sec. 1	42	30	8	10		7	traces	3
Sec. 2 lvl 1	54	40		2	4			
Sec. 2 lvl 2	52	45		traces	3			
Sec. 2 lvl 3	53	45		traces	2			
Sec. 2 lvl 4	48	44		4	4			
Sec. 2 lvl 5	46	45		4	5			
Sec. 3 lvl 1	35	47	15	3	traces			
Sec. 3 lvl 2	41	42	8	4	5			
Sec. 3 lvl 3	48	37	2	5	8			
Sec. 3 lvl 4	52	40		3	5			
Sec. 3 lvl 5	48	43		3	6			
Sec. 4 lvl 1	48	40	5	3	4			
Sec. 4 lvl 2	43	49			8			
Sec. 4 lvl 3	48	41		6	5			
Sec. 4 lvl 4	38	36	12	6	8			
Sec. 4 lvl 5	63	28		4	5			

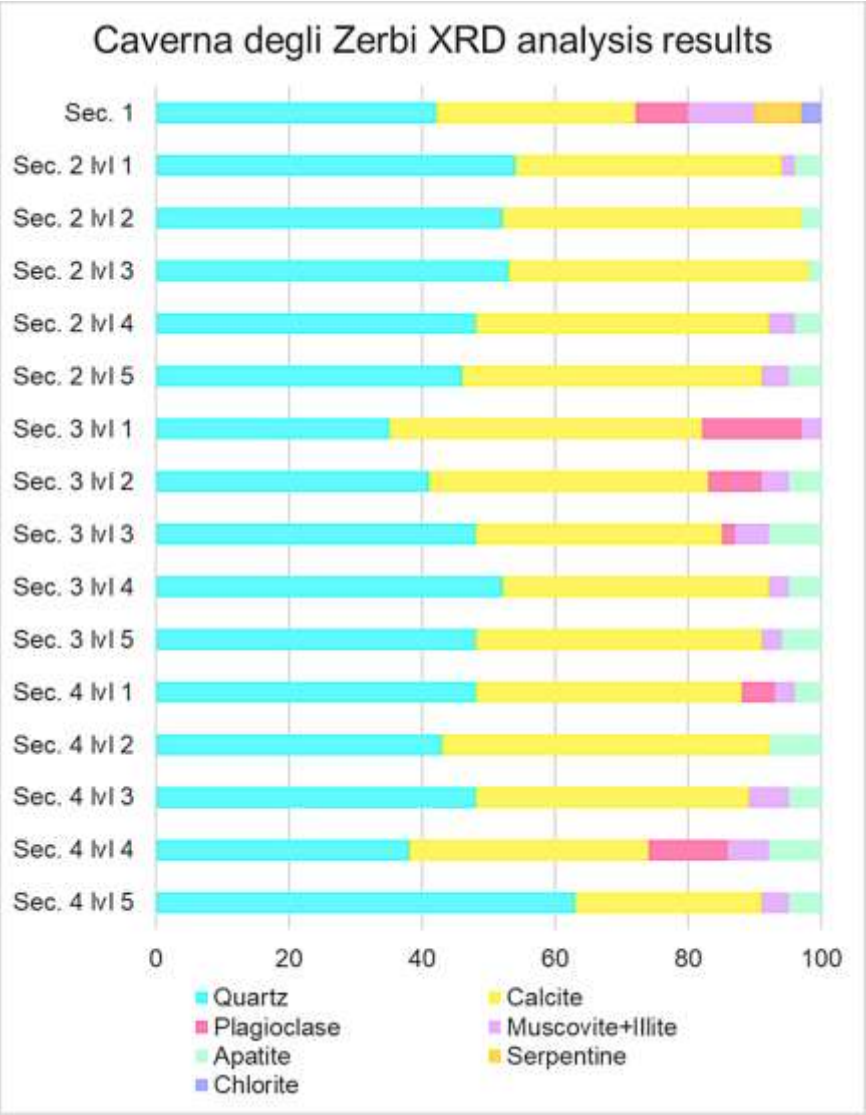

Figure 40 - XRD analysis results for Arma degli Zerbi. This is the graphical representation of Table 6.

Radiocarbon dating

As already mentioned in *Site description and previous studies*, the deposits of this cave have already been partially dated by the Max Planck Institute and the results have been reported in Table 3. However, in that table the samples names refer to the archaeological stratigraphy. To associate those results to the stratigraphic units described and used so far, they can be presented as follows:

- *Section 1* has not been divided into no more than one level in the geological stratigraphy, however, it can be said that the samples we have taken come exactly from the area located in the middle of the two datings (17355-16664 yr cal. BP and 10249-9935 yr cal. BP);
- *Section 2*, had a unique charcoal sampling in level 5, and unfortunately it proved to exceed the maximum limit for radiocarbon dating;
- Level 1 of *section 3* was dated 17023-16554 yr cal. BP;
- An attempt was made to date section 4 in two positions: at the height of carbon lens (level 3) and in the level below it (level 4). Both dates exceeded the maximum radiocarbon limit.

Micromorphological analysis

The micromorphological description follows the same order as already seen: in order of stratigraphic sections numbers, and from the top downward.

Descriptions can also be found in their synthetic way in the appendices (*Arma degli Zerbi*), divided by thin section or, if necessary, by microfacies (mF). After their description and their interpretation, they were divided into five microfacies types (MFT) (Courty, 2001; Goldberg and Macphail, 2013), which will be deepened in the discussions. These are: 1. Deposits rich in material of organic origin (MOO). 2. Sediments rich in charred material (CM). 3. Greyish and coarse deposit (GC). 4. Yellowish deposit (YD). 5. Cave wall deposit (CW).

Section 1:

Thin section* a *(MFT: Cave wall deposit, CW)

The microstructure was not detectable and neither the aggregates, due to carbonates cementation. The porosity is represented by channels (fine sand, f.s., ±10%), planes (v.f.s.; ±5%) and chambers (c.s., ±2%).

The ratio between coarse and fine fraction (put at 5µm) is 40/60, with a c/f-related distribution pattern single spaced porphyric. The coarse material has very few angular and subangular grains of quartz (v.f.s., ±2%), with no signs of weathering. Fossiliferous limestone rock fragments (pebble size, ±20%) are, instead, frequent. Bones (f.s., ±2%) and charcoal fragments (f.s., ±5%) are present. The micromass is greyish brown, a speckled mixture of clay and calcite, with a crystallitic b-fabric.

Different types of pedofeatures are present: typic ferrous nodules (v.f.s., ±1% of the total area); sparitic calcite coatings with palisade fabric (equigranular hypidiotopic) (m.s., ±50%); micritic nodules (f.s., ±5%); silt nonlaminated coatings with no extinction lines (m.s. in thickness, ±10%).

Section 2:

Thin section* b *(MFT: Greyish and coarse deposit, GC)

Weakly separated subangular blocky and crumb microstructure, with a platy overprint in the upper part, and with subangular blocky peds (v.c.s.) and porous crumbs (c.s.).

Table 7 - Microfacies types (MFT) and simplified descriptions to highlight crucial aspects for interpretation of results for Arma degli Zerbi cave deposits. ("n.d." for not detectable, f-1 for single occurrence)

Strat. lvl	TS	MFT	mF	Microstructure	Aggregates	Voids	C/f-related distribution	C/f-ratio	Coarse fraction				Fine fraction		B-fabric	Pedofeatures
									Bones	Burnt bones	Charcoal	Single mineral grains	Rock fragments	Fine fraction		
Sec.1	a	Cave wall deposits		n.d.	n.d.	Channels, planes, chambers	Single spaced porphyric	40\60	a	-	aaa	Quartz (*)	Limestone (ff)	Clay, carbonates	Crystallitic	Ferrous (a*), calcitic (aaaaa), clayey (aaaa)
Sec.2 lvl 2	b	Greyish and coarse deposit		Complex: subangular blocky and crumb microstructure	Subangular blocky peds and porous crumbs	Complex packing voids, planes, channels, chambers, vughs	Single spaced porphyric - single spaced equal enaulic	50\50	a*	a*	a	Quartz (f)	Limestone (fff), Quartzite (f), porphyroid (f-1)	Carbonates, clay, phosphates	Undifferentiated, crystallitic	Ferrous (a*), manganese (a), calcitic (aaa), clayey (a-2), phosphatic (a*), excremental (a)
Sec.2 lvl 4/5	c	Deposits rich in material of organic origin		Crumb microstructure	Porous crumbs	Complex packing voids, channels, vughs	Single spaced equal-coarse enaulic	40\60	aaa	aaa	a	Quartz (f), calcite (f)	Limestone (ff), quartzite (f)	Carbonates, clay, phosphates	Weakly developed crystallitic, undifferentiated	Ferrous (a), manganese (a*), calcitic (aaa), excremental (a*)
Sec.3 lvl 1	d	Deposits rich in material of organic origin	I	Subangular blocky	Subangular blocky peds	Channels, planes, chambers	Double spaced porphyric	30\70	aaa	a*	a	Quartz (f), microcline (*)	Limestone (ff), quartzite (*)	Carbonates, clay, phosphates	Undifferentiated, crystallitic	Ferrous (a*), calcitic (aaa), excremental (a-1)
		Sediments rich in charred material	II	Crumb microstructure	Porous crumbs	Compound packing voids, channels, planes	Single spaced coarse enaulic	30\70	aaa	a*	aaaa	Quartz (f)	Limestone (f), quartzite (*)	Carbonates, clay, phosphates	Weakly developed crystallitic	Ferrous (a*), calcitic (a*), excremental (a)
Sec.3 lvl 1/2	e	Deposits rich in material of organic origin		Complex: subangular blocky and crumb microstructure	Porous crumbs, subangular blocky peds	Complex packing voids, channels, vughs	Single spaced equal enaulic and double spaced porphyric	30\70	a*	a*	a	Quartz (f)	Limestone (ff), quartzite (f)	Carbonates, clay, phosphates	Undifferentiated, crystallitic	Ferrous (a*), calcitic (aa), phosphatic (a*)
Sec.3 lvl 4/5	f	Deposits rich in material of organic origin	I	Crumb microstructure	Porous crumbs	Complex packing voids, channels, vughs	Close coarse enaulic	20\80	a	a*	a	Quartz (f)	Limestone (f)	Carbonates, clay, phosphates	Undifferentiated, crystallitic	Ferrous (a*), manganese (a), calcitic (aaa), phosphatic (a*), excremental (a*)
		Sediments rich in charred material	II	Crumb microstructure	Porous crumbs	Compound packing voids, channels	Single spaced equal enaulic	40\60	a	a	a	Quartz (f), calcite (*)	Limestone (ff), quartzite (*), chert (*)	Carbonates, clay, phosphates	Weakly developed crystallitic	Ferrous (a), manganese (a*), calcitic (a*), phosphatic (a*), excremental (a*)

	g	Disturbed material	I	Subangular blocky	Suangular blocky peds	Channels, compound packing voids, planes	Close coarse enaulic	30\70	a*	a*	a*	Quartz (f)	Limestone (f), quartzite (*)	Carbonates, clay, phosphates	Undifferentiated, crystallitic	Ferrous (a*), manganese (a*), calcitic (a), clayey (a-1), excremental (a-5)
	g, i, h	Yellowish deposit	II	Crumb microstructure	Porous crumbs, subangular blocky peds	Complex packing voids, channels, planes	Single spaced equal enaulic and double spaced porphyric	50\50	a	-	a	Quartz (f)	Limestone (fff), quartzite (*)	Carbonates, clay	Crystallitic	Ferrous (a*), manganese (a*), calcitic (aaaa), clayey (aaaaa)
	i, l	Deposits rich in material of organic origin	III	Crumb microstructure	Porous crumbs, subangular blocky peds	Complex packing voids, channels, planes, chambers	Single spaced equal enaulic	30\70	a*	a*	a	Quartz (f), calcite (*)	Limestone (f), quartzite (*)	Carbonates, clay	Crystallitic	Ferrous (a*), manganese (a*), clayey (a*), phosphatic (a*), excremental (a*)
Sec.4																
	i, l	Sediments rich in charred material	IV	Granular microstructure	Granules	Complex packing voids, planes, channels	Single spaced equal enaulic	50\50	a	aaa	aaaaa	Quartz (f), microcline (f-1)	Limestone (ff)	Carbonates, organic matter, charred material, phosphates, clay	Undifferentiated, crystallitic	Ferrous (a*), calcitic (a)
	i, l	Deposits rich in material of organic origin	V	Crumb microstructure	Porous crumbs, subangular blocky peds	Complex packing voids, channels, planes, chambers	Double spaced equal enaulic, locally double spaced porphyric	30\70	a	a	a	Quartz (f), calcite (f)	Limestone (f), quartzite (*)	Carbonates, clay, phosphates	Crystallitic	Ferrous (a*), calcitic (aaa), clayey (a*), phosphatic (a*), excremental (a*)
	l	Deposits rich in material of organic origin		Crumb microstructure	Porous crumbs	Complex packing voids, channels, planes	Single spaced equal enaulic	30\70	a	a*	a*	Quartz (f)	Limestone (ff), quartzite (f)	Carbonates, clay, phosphates	Undifferentiated, crystallitic	Ferrous (a*), calcitic (aaa), phosphatic (a*), excremental (aaaa)

The porosity is divided in: complex packing voids (v.f.s., ±10%); planes (v.f.s.; ±5%); channels (s.s., ±5%); chambers (f.s., ±2%); regular vughs (s.s., ±2%).

The c/$f_{5\mu m}$ ratio is 50/50, with a c/f-related distribution pattern possessing traits both of a single spaced porphyric and of a single spaced equal enaulic. The mineral fraction is composed of subangular grains of quartz (f.s., ±5%), with no signs of weathering. Fossiliferous and non-fossiliferous subrounded limestone rock fragments (m.s., but with a fragment occupying all the lower part 6x2 cm, ±30%), quartzite subangular and subrounded rock fragments (m.s.; ±10%) and subrounded porphyroid rock fragment (v.c.s., one occurrence in the middle lower part of the thin section) are present. Highly weathered bones (f.s., ±1%) are the only inorganic residues of biological origin existing in this thin section. On the other hand, the anthropogenic elements are highly weathered burnt bones (f.s., ±1%) and charcoal fragments (f.s., ±2%).

The micromass is yellowish brown, a speckled mixture of calcite, clay and phosphates. This determines an undifferentiated and crystallitic b-fabric.

The pedofeatures identified are: typic ferrous nodules, no pattern found (s.s., ±1%), manganese (hydr)oxide hypocoatings (v.f.s., ±2%), two silty cappings on two quartz grains (v.c.s.), micritic (equigranular xenotopic) nodules (f.s., ±5%), cryptocrystalline typic apatite nodules (f.s., ±1%), subrounded excrements of large animals, (m.s., ±2%).

Thin section* c *(MFT: Deposits rich in material of organic origin, MOO)

Weakly separated crumb microstructure, with porous crumbs (m.s.). The voids recognised are: complex packing voids (s.s., ±20%); channels (s.s., ±10%); regular vughs (s.s., ±2%).

Diminishes the coarse fraction (c/$f_{5\mu m}$ ratio: 40/60) and the c/f-related distribution pattern becomes a single spaced equal-coarse enaulic.

Only two types of minerals are seen: subangular grains of quartz (f.s., ±10%), with no signs of weathering, and subangular grains of calcite (f.s., ±5%). The rock fragments are the fossiliferous subangular and subrounded limestone (m.s., but with a unique 3 cm fragment, ±20%) and the quartzite subangular and subrounded rock fragments (f.s.; ±5%). Then, moderately weathered bones (f.s., ±5%) and burnt bones (f.s., ±5%), and charcoal fragments (f.s., ±2%), bigger in size in the lower part of the thin section.

The micromass is yellowish brown, and it is a speckled mixture of calcite, clay and phosphates, with a weakly developed crystallitic - undifferentiated b-fabric.

The pedofeatures found are the typic ferrous nodules (s.s., ±2%); the manganese (hydr)oxide hypocoatings (s.s., ±1%); the micritic (equigranular xenotopic) nodules (s.s., ±5%); and the subrounded excrements of large animals, (f.s., ±1%).

Section 3:

***Thin section* d**

Two microfacies are present and will be described separately.

Microfacies I (MFT: Deposits rich in material of organic origin, MOO)

Weakly separated subangular blocky microstructure, with weakly developed pedality. Channels (f.s., ±5%), planes (s.s.; ±5%) and chambers (f.s., ±2%) to describe the porosity.

The coarse fraction diminishes again (c/$f_{5\mu m}$ ratio: 30/70) and the c/f-related distribution pattern is double spaced porphyric.

Subangular and angular grains of quartz (f.s., ±5%), with no signs of weathering and subangular grains of microcline (f.s., ±1%), with low signs of weathering can be observed for the single mineral class. The rock fragments are the fossiliferous and non-fossiliferous subrounded limestone rock fragments (v.c.s., but with fragments up to 2 cm in size, ±20%) and the quartzite subangular rock fragments (v.c.s.; ±2%).

The inorganic residues of biological origin present are just bones (f.s., ±5%). The anthropogenic elements are both burnt bones (f.s., ±1%) and charcoal fragments (m.s., ±2%).

The micromass is a speckled mixture of calcite, clay and phosphates giving it a brown grey colour and an undifferentiated-crystallitic b-fabric.

Also organic material not included in the groundmass is present, in the form of one brown burnt plant tissue residue, isotropic in XPL (c.s.).

Finally, pedofeatures are: typic ferrous nodules (s.s., ±1%); coatings with palisade fabric (equigranular hypidiotopic) (f.s.-m.s., ±5%), found on rock fragments and in contact with voids; micritic (equigranular xenotopic) nodules (f.s., ±1%); and subrounded excrement of large carnivore, (granule size, one occurrence).

Microfacies II (MFT: Sediments rich in charred material, CM)

In this microfacies the microstructure is Moderately separated crumb, with porous crumbs (f.s.) as only aggregates recognised. Compound packing voids (v.f.s., ±20%), channels (f.s., ±5%) and planes (f.s.; ±2%) define the porosity of the mF. The c/$f_{5\mu m}$ ratio stabilises around 30/70, even if the c/f-related distribution pattern is different (single spaced coarse enaulic).

Subangular grains of quartz (f.s., ±5%) are the only single mineral grains. Fossiliferous subrounded limestone rock fragments (c.s., ±10%) and quartzite subangular rock fragments (f.s.; ±2%) are reported. Other elements in the groundmass are: bones (v.f.s., ±5%), burnt bones (s.s., ±1%) and charcoal fragments (f.s., ±10%).

The micromass is generally light brown, but few crumbs show a reddened micromass. It is a speckled mixture of calcite, clay and phosphates and this leads to a weakly developed crystallitic b-fabric.

The pedofeatures are: typic ferrous nodules (s.s., ±1%); dusty clay laminated coatings with diffuse extinction lines (f.s., ±1%) and only found on rock fragments; micritic (equigranular xenotopic) nodules (f.s., ±1%); subrounded excrement of large animals, (c.s., ±2%).

Thin section* e *(MFT: Deposits rich in material of organic origin, MOO)

A complex microstructure can be describes as moderately separated crumb and subangular blocky, with porous crumbs (v.f.s.) and subangular blocky peds (f.s.). Complex packing voids (f.s., ±10%), channels (f.s., ±5%) and vughs (v.f.s., ±5%) constitute the porosity.

The c/$f_{5\mu m}$ ratio is stable at 30/70 and the c/f-related distribution pattern is single spaced equal enaulic and double spaced porphyric. The coarse material is composed of a mineral part: subangular grains of quartz (v.f.s., ±10%), fossiliferous and speleothem subangular limestone rock fragments (c.s., but up to 3 cm, ±20%), and quartzite subangular and subrounded rock fragments (v.f.s.; ±5%); but also of bones (f.s., ±1%), burnt bones (f.s., ±1%) and charcoal fragments (v.f.s.-f.s., ±2%).

The micromass is yellowish grey and very light brown, being a speckled mixture of calcite, clay and phosphates, and having a crystallitic - undifferentiated b-fabric.

The pedofeatures identified are: typic ferrous nodules (v.f.s., ±1%); micritic (equigranular xenotopic) nodules (f.s., ±2%); equigranular xenotopic calcitic infillings (f.s., ±1%); and cryptocrystalline typic apatite nodules (f.s., ±1%).

***Thin section* f**

Two microfacies are present and will be described separately.

Microfacies I (MFT: Deposits rich in material of organic origin, MOO)

Microstructure and porosity are described by a moderately separated crumb microstructure, with porous crumbs (v.c.s.), and by complex packing voids (f.s., ±10%), channels (s.s., ±5%), and vughs (f.s., ±5%).

There is an increase in the fine fraction relative quantity ($c/f_{5\mu m}$ ratio: 20/80) contributing to a close coarse enaulic c/f-related distribution pattern.

The mineral fraction is constituted of subangular grains of quartz (f.s., ±5%) and fossiliferous rounded limestone rock fragments (m.s., ±5%). The inorganic residues of biological origin seen are bones (f.s., ±2%), while the anthropogenic elements: are burnt bones (v.f.s., ±1%) and charcoal fragments (f.s., ±2%). The micromass is yellowish grey, and a speckled mixture of calcite, clay and phosphates. The b-fabric is crystallitic and locally undifferentiated.

Pedofeatures are: typic ferrous nodules (f.s., ±1%); manganese (hydr)oxide hypocoatings (s.s., ±2%), along the outlines of the aggregates; micritic (equigranular xenotopic) nodules (m.s., ±5%); cryptocrystalline typic apatite nodules (f.s., ±1%).

Microfacies II (MFT: Sediments rich in charred material, CM)

Moderately separated crumb microstructure, with porous crumbs (c.s.); compound packing voids (v.f.s., ±20%) and channels (m.s., ±5%) as porosity.

The coarse fraction is increases ($c/f_{5\mu m}$ ratio: 40/60) and the c/f-related distribution pattern becomes single spaced equal enaulic. Subangular grains of quartz (f.s., ±10%) and calcite (f.s., ±1%) are the single minerals present. Fossiliferous subrounded limestone (v.c.s., ±20%), subangular quartzite (m.s.; ±2%) and subangular chert (m.s., ±1%) rock fragments are found. Bones (m.s., ±2%), burnt bones (m.s., ±2%) and charcoal fragments (m.s., ±2%) compose the groundmass, too.

The micromass is brown, a speckled mixture of clay, calcite and phosphates, with a weakly developed crystallitic b-fabric.

Pedofeatures are: typic ferrous nodules (m.s., ±1%); manganese (hydr)oxide hypocoatings (s.s., ±1%), also here along the outlines of the aggregates; micritic (equigranular xenotopic) nodules (f.s.,

±1%); cryptocrystalline typic apatite nodules (f.s., ±1%); subrounded excrement of large animals, (c.s., one occurrence).

Section 4:

For section 4, a different approach to description will be used: the same levels have been sampled more than once, thus we will proceed following the order of the microfacies recognized (as presented in Figure 41).

Microfacies I (present only in thin section g) (MFT: 1. Deposits rich in material of organic origin, MOO)

Weakly separated subangular blocky microstructure, with weakly developed pedality, and subangular blocky peds (c.s.). Channels (f.s., ±10%), complex packing voids (v.f.s., ±5%) and planes (s.s.; ±5%) to describe the porosity.

The $c/f_{5\mu m}$ ratio is evaluated as 30/70, with a c/f-related distribution pattern close coarse enaulic.

The component of the coarse material are subangular and angular grains of quartz (f.s., ±5%); subangular grains of calcite (f.s., ±2%); fossiliferous subrounded limestone rock fragments (m.s., ±10%); quartzite subangular and subrounded rock fragments (f.s.; ±2%) for the mineral fraction. The inorganic residues of biological origin found are bones (f.s., ±1%), and the anthropogenic elements are burnt bones (v.f.s., ±1%) and charcoal fragments (f.s., ±1%).

The micromass is brown grey, a speckled mixture of calcite, clay and phosphates, with an undifferentiated-crystallitic b-fabric.

Pedofeatures are: typic ferrous nodules (v.f.s., ±1%); manganese (hydr)oxide hypocoatings (f.s., ±1%); micritic (equigranular xenotopic) nodules (f.s., ±2%); compound parallel layered typic clay coatings (m.s., one occurrence), fragmented; subrounded excrement of large animals, (granule size, five occurrences).

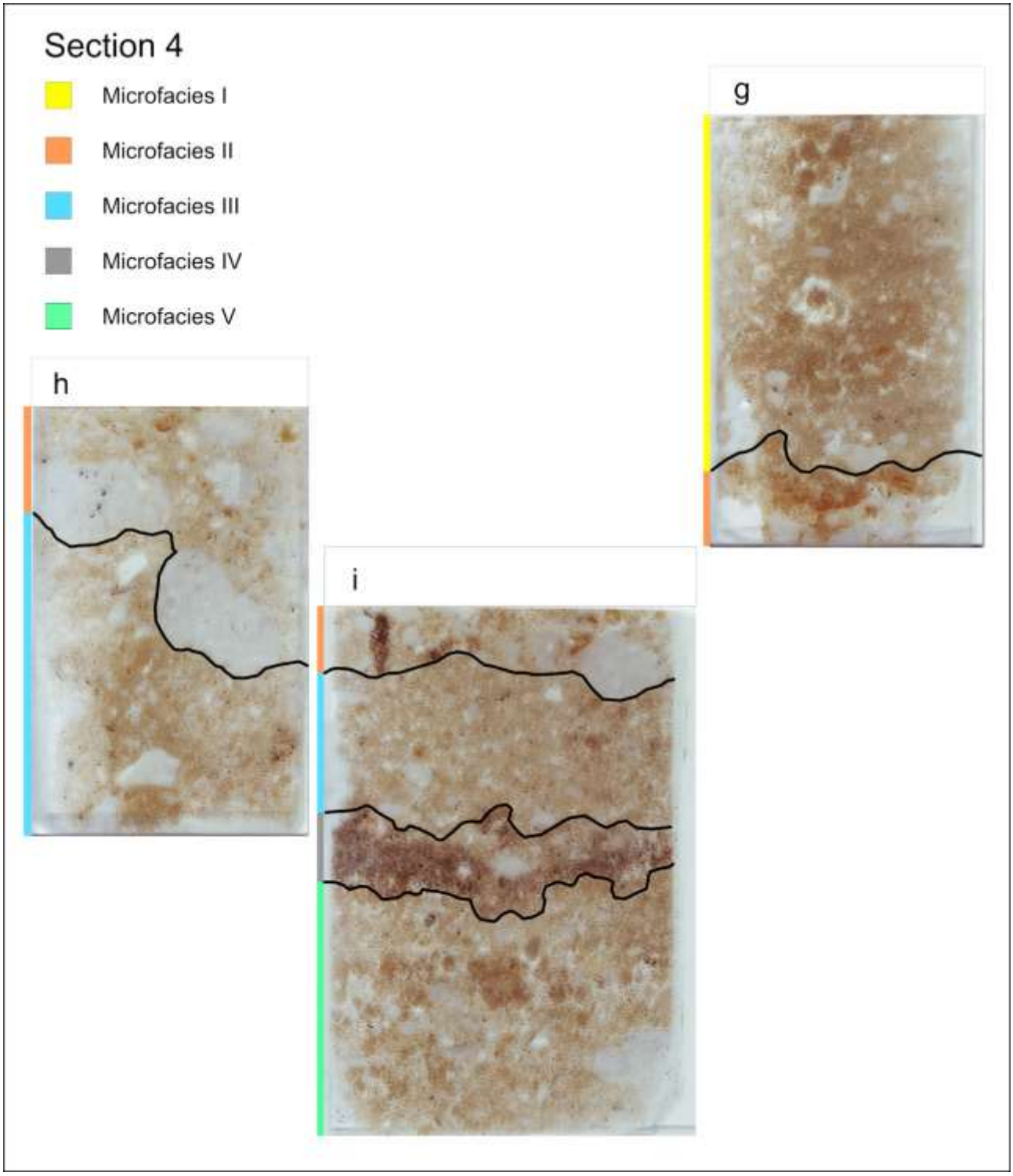

Figure 41 - Section 4 microfacies presentation. Only the L *thin section is excluded from this figure. Thin sections' position are meant only to convey the relative relations between them.*

Microfacies II (in thin sections g, i, h*) (MFT: Yellowish deposit, YD)*

Moderately separated crumb microstructure, with porous crumbs (f.s.) and subangular blocky peds (fine gravel size). The porosity is described by complex packing voids (v.f.s., ±20%), channels (s.s., ±5%) and planes (s.s.; ±2%).

The $c/f_{5\mu m}$ ratio is 50/50 again, with a c/f-related distribution pattern single spaced equal enaulic and double spaced porphyric.

The mineral fraction is constituted of subangular grains of quartz (v.f.s., ±10%), fossiliferous subrounded limestone rock fragments (f.s. but up to cobble size, above all at the limit between mF II and mF III, ±30%) and quartzite subangular and subrounded rock fragments (f.s.; ±2%). Bones (v.f.s., ±2%) and charcoal fragments (f.s., ±2%) are present in the groundmass.

Micromass is light brown grey, and a cloudy mixture of calcite and clay, with a crystallitic b-fabric.

Pedofeatures are: typic ferrous nodules (f.s., ±1%); manganese (hydr)oxide hypocoatings (s.s., ±1%); micritic (equigranular xenotopic) nodules (v.f.s., ±10%); equigranular hypidiotopic calcite coatings (f.s., ±5%); compound parallel layered typic clay coatings (granule size, ±20%), fragmented; dense incomplete compound parallel layered clay infillings (granule size, ±5%), fragmented.

Microfacies III (thin section* i *and* l*) (MFT: Deposits rich in material of organic origin, MOO)

Moderately-weakly separated crumb microstructure, with porous crumbs (f.s.) and subangular blocky peds (v.c.s.). The porosity is represented by complex packing voids (f.s., ±20%), channels (v.f.s., ±5%), planes (s.s.; ±2%) and chambers (f.s., ±1%).

The $c/f_{5\mu m}$ ratio is roughly 30/70 and the c/f-related distribution pattern is single spaced equal enaulic.

The components of the coarse material are subangular and angular grains of quartz (f.s., ±10%), subangular grains of calcite (f.s., ±1%), fossiliferous subrounded limestone (c.s., ±10%) and quartzite (f.s.; ±1%) rock fragments, but also bones (f.s., ±1%), burnt bones (f.s., ±1%), and charcoal fragments (f.s., ±2%), of which one fragment is embedded in a brownish aggregate.

The micromass is brown grey, a speckled mixture of calcite and clay, with a weakly developed crystallitic b-fabric.

Pedofeatures are: typic ferrous nodules (f.s., ±1%); manganese (hydr)oxide hypocoatings (f.s., ±1%); micritic (equigranular xenotopic) nodules (f.s., ±2%); compound parallel layered typic clay

coatings (m.s., ±1%), fragmented; cryptocrystalline typic apatite nodules (v.f.s., ±1%); subrounded excrement of large animals, (m.s., ±1%).

Microfacies IV (thin section i) (MFT: Sediments rich in charred material, CM)

The microstructure is moderately separated granular, with granules (m.s.) as aggregates. Voids can be complex packing voids (v.f.s., ±30%), planes (s.s.; ±2%) and chambers (f.s., ±1%).

The $c/f_{5\mu m}$ ratio is 50/50, with a single spaced equal enaulic c/f-related distribution pattern.

Subangular and angular grains of quartz (v.f.s., ±10%), together with subangular grains of microcline (f.s., one occurrence) are present. Fossiliferous subrounded limestone rock fragments (f.s., ±20%) are the only rock class identified. Bones (v.f.s., ±2%), burnt bones (v.f.s., ±5%) and charcoal fragments (f.s., ±20%) are reported.

Micromass is dark brown and a dotted-opaque mixture of calcite, organic matter, charcoal, phosphates and clay, producing an undifferentiated-crystallitic b-fabric.

Pedofeatures are: typic ferrous nodules (f.s., ±1%) and micritic (equigranular xenotopic) nodules (s.s., ±2%).

Microfacies V (thin section i) (MFT: 1. Deposits rich in material of organic origin, MOO)

Highly separated crumb and subangular microstructure, with porous crumbs (v.f.s.) and subangular blocky peds (m.s., but also gravel size). Complex packing voids (s.s., ±30%), planes (s.s., ±5%), channels (s.s., ±2%) and chambers (f.s., ±1%) compose the porosity.

The $c/f_{5\mu m}$ ratio returns to 30/70 and the c/f-related distribution pattern is double spaced equal enaulic, locally double spaced porphyric.

The mineral fraction sees the presence of subangular and angular grains of quartz (m.s., ±10%) and subangular grains of calcite (m.s., ±5%). Fossiliferous subangular limestone rock fragments (v.c.s., ±10%) is flanked by quartzite subangular rock fragments (m.s.; ±1%). Bones (f.s., ±2%), burnt bones (v.f.s., ±2%) and charcoal fragments (v.f.s., ±2%) are, as well, components of the groundmass.

The micromass is brown, darker in the subangular peds and beige in the crumbs. It is a speckled mixture of calcite, clay and phosphates in the crumbs, clay and calcite in the blocky peds. In general it has a weakly developed crystallitic b-fabric.

Pedofeatures are: typic ferrous nodules (f.s., ±1%); micritic (equigranular xenotopic) nodules (f.s., ±5%); typic impure clay nonlaminated coatings (v.f.s., ±1%), fragmented; cryptocrystalline typic apatite coatings (v.f.s., ±1%); subrounded excrement of large animals, (f.s., ±1%).

Thin section* l *(MFT: Deposits rich in material of organic origin, MOO)

It shows a highly separated crumb microstructure, with porous crumbs (f.s.). Complex packing voids (v.f.s., ±30%), channels (s.s., ±10%) and planes (s.s., ±5%) are the porosity types recognised.

The $c/f_{5\mu m}$ ratio is 30/70, with a single spaced equal enaulic c/f-related distribution pattern.

The coarse material is composed of subangular grains of quartz (f.s., ±5%), fossiliferous subangular limestone rock fragments (c.s., up to cobble size, ±20%), quartzite subangular rock fragments (m.s.; ±5%), bones (m.s., ±2%), burnt bones (f.s., ±1%) and charcoal fragments (f.s., ±1%).

The micromass is a yellowish brown, and a speckled mixture of calcite, clay and phosphates, expressing a crystallitic-undifferentiated b-fabric.

Pedofeatures are: typic ferrous nodules (v.f.s., ±1%); micritic (equigranular xenotopic) nodules (f.s., ±2%); micritic (equigranular xenotopic) hypocoatings (f.s., ±5%); cryptocrystalline typic apatite nodules (f.s., ±1%); subrounded excrement of large animals, (m.s., ±10%).

Caverna delle Fate

As already mentioned (in *Site description and previous studies*), also in the case of Caverna delle Fate cave it was difficult to find the original, and not reworked, deposits. This problem had already been addressed in the past by other scholars, who found that the only sediments suitable for a detailed study were those in corridor 3 (Giacobini *et al.*, 1984; Bichet, 1987; Echassoux *et al.*, 1989; Falguères, Yokoyama and Bibron, 1990; Psathi, 2003; Valensi and Psathi, 2004; Karatsori *et al.*, 2005; Valensi, 2009). In this portion of the cave, rather far from the entrance actually, three stratigraphic sections have been recognized and studied. The work presented here has been based on these (Figure 42).

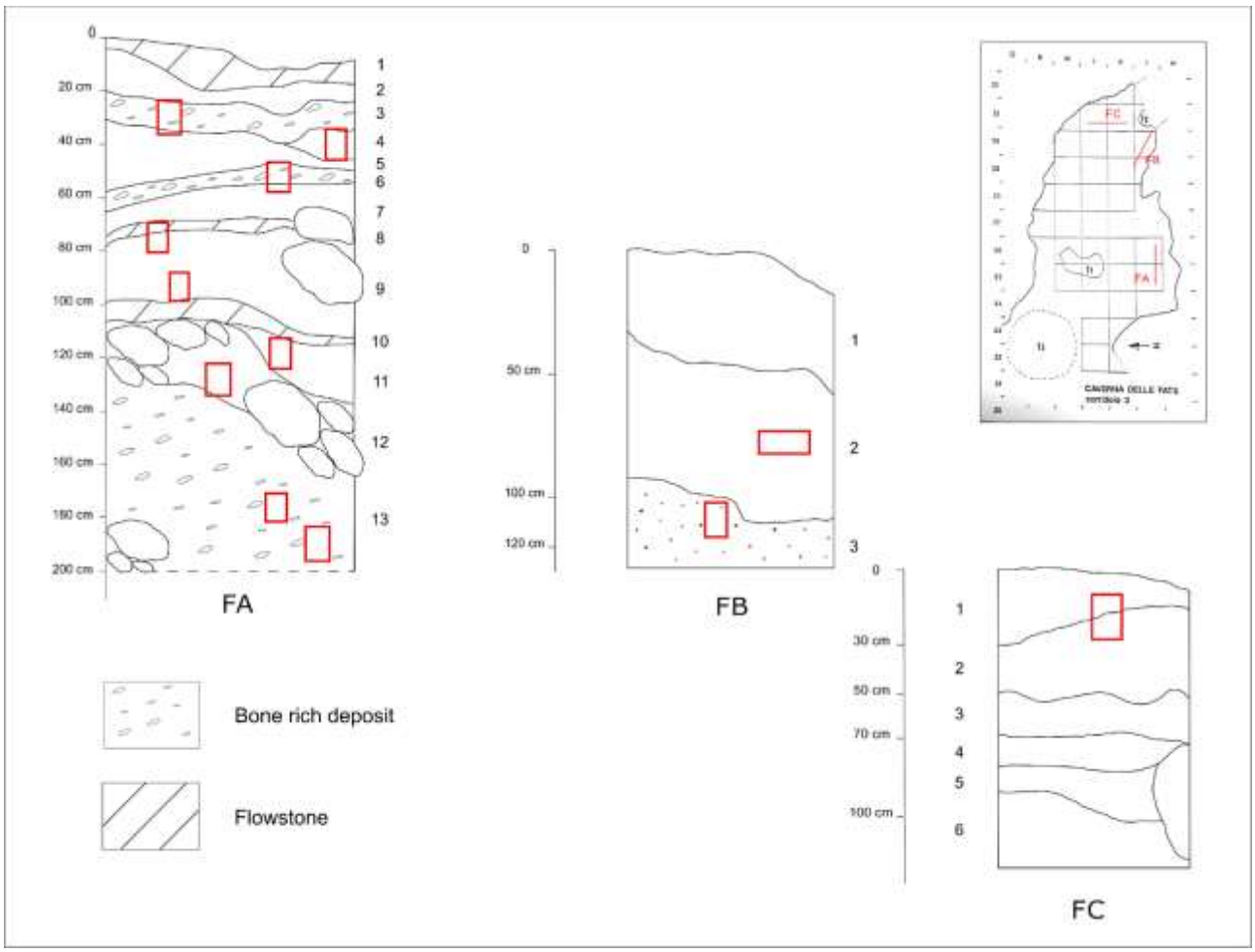

Figure 42 - Caverna delle Fate stratigraphy. At the top right it is also possible to see the exact location of the three stratigraphies in corridor 3. The micromorphological samples are indicated with a red rectangle.

Fieldwork and site stratigraphy

In this case, the stratigraphies taken as a reference are those indicated by previous works (Bichet, 1987 predominantly). Unfortunately, not all the stratigraphies have been considered in their entirety since they are intensely cemented by carbonates or too old for the purposes of this thesis: the deposits cementation is an important problem for section (F) A and (F) B, while section (F)C deposits are dated before MIS5e (Bichet, 1987).

The 0 of section C coincides with the ground surface, but it varies for the other two sections. For section B, the base of a drapery speleothem was chosen as 0, while for section A it was opted for the top of a flowstone, which is also its highest point.

Section FA

The FA section is heavily impregnated with carbonates, and levels 1, 8 and 10 are actually flowstones, therefore they have not been described. The same also applies to the more cemented levels (2, 3, 5, 7, 10).

Level 3: Reddish yellow (7.5 YR 6/8). From 20 cm to 35 cm. The lower limit is wavy and clear. It is a matrix supported level, even though cobbles and pebbles are common. The texture il silty loam. Big and little bone fragments can be seen in the field.

*Level 4:*Brownish yellow (10 YR 6/8). From 35 cm to 45 cm. The lower limit is wavy and abrupt. This level is actually a sediment lens with a high quantity of coarse fraction. Despite this, it is matrix supported. Silty loam texture.

Level 6: Brown (7.5 YR 4/4). From 58 cm to 65 cm. The lower limit is smooth and clear. The quantity of calcitic coarse fraction (mainly cobbles and pebbles) is still high, but, all the same, matrix supported. Silty loam texture. Whole bones of likely medium-sized animals can be easily observed.

Level 9: Very pale brown (10 YR 7/4). From 80 cm to 100 cm. The lower limit is smooth and clear. The coarse fraction is mainly concentrated in the upper part, where pebbles are common and few boulders could be noticed. In any case, it is still matrix supported, with a silty loam texture. It is moderately impregnated by carbonates.

Level 11: Light yellowish brown (10 YR 6/4). From 110 cm circa to 140 cm. The lower limit is irregular and clear. The coarse fraction diminishes considerably. It is matrix supported and the texture is silty loam.

Level 12: Yellowish red (5YR 5/6). From 110 cm to 160 cm (at its maximum). The lower limit is irregular and clear. Frequent calcitic boulders are present, but no other coarse fraction classes. There is a silty loam texture and it is matrix supported.

Level 13: Brown (7.5 YR 4/4). From 120 cm to 200 cm circa. The lower limit is the ground surface. It is matrix supported and the texture is silty loam. Bones are common.

Section FB

The FB section is almost entirely cemented by carbonates or composed of speleothems and this has made its description and sampling difficult. Only level 3 allowed to deepen the study of the section characteristics.

Level 3: Strong brown (7.5 YR 5/6). From 97 cm to 103 cm. The lower limit is the present-day ground surface. Matrix supported. Calcitic pebbles are common. The fine earths texture is silty loam. Little charcoal fragments (2 mm) have been observed.

Section FC

Only the two upper levels have been considered (level 1 and level 2).

Level 1: Yellow (10 YR 7/8). 25 cm thick. The lower limit is wavy and abrupt. Calcite nodules are present (2 mm in diameter circa). Matrix supported. The fine fraction is predominant and it shows a silty loam texture.

Level 2 (Figure 43): Reddish yellow (7.5 YR 6/6). From 25 cm to 50 cm below the present-day ground surface. The lower limit is smooth and abrupt. Small calcite nodules (2 mm), secondary calcite crystals (4 cm) and loamy lenses with wavy/turbulent lamination are the sedimentary structures present.

Figure 43 - Section FC and its peculiar appearance. The perspective changes level 1 lower limit position.

Sampling

Sampling was conducted for three types of analyses: a small sample of loose sediment for XRD analysis, a sample of about 1 kg for grain size analysis, and finally, a sampling for micromorphology. All this was performed only where it was possible, given the advanced stage of carbonates cementation.

Samples subjected to X-ray powder diffraction have been: FA 3, FA 4, FA 9 (two different samples for the upper and lower part of the level), FA 11, FA 12, FA 13 (two different samples, due to the level thickness), FB and FC.

Samples subjected to grain size analysis have been: FA 3, FA 4, FA 9 (two different samples for the upper and lower part of the level), FA 11, FA 12, FA 13 (two different samples, due to the level thickness), FB and FC.

The micromorphological sampling location is portrayed in Figure 42 and the sample take the name from the level of origin. Thus, they are FA 3, FA 4, FA 6, FA 9a, FA 9b, FA 11, FA 12, FA 13a and FA 13b for section FA. For section FB, four samples were taken, but they will be considered here only as FB2 (the three samples from level 2) and FB3 (the semi-mammoth from level 3). Only one

sample comes from the third stratigraphic section and it takes its name: FC, and it is a semi-mammoth. All the other thin sections listed above, with, obviously the exception of FB3 and FC, are quarter mammoth.

Laboratory analysis

Although the large amount of coarse material present was already evident in the field, the particle size analysis confirmed this consideration. In particular, it can be said that a rather characteristic trend is observed for the coarser classes. Starting from the lowest level (FC, Figure 44), we can see how this is almost exclusively composed of fine earths, then, passing to level FB 3 (Figure 44), the coarse material increases, but only in this portion of the cave. In fact, from the levels positioned at the same height in FA (FA 13a + b, Figure 45), the coarse fraction is almost absent. Moving upwards, along the stratigraphic section FA, it can be seen that almost all the lower levels (at least up to FA 11) do not show elements with phi > -1, with the exception of few boulders in levels 13 and 12. In the latter, boulders are very common. In level 11 the coarse fraction increases, in particular that of pebbles, there is a decrease in 9b and, finally, increases and remains more or less constant.

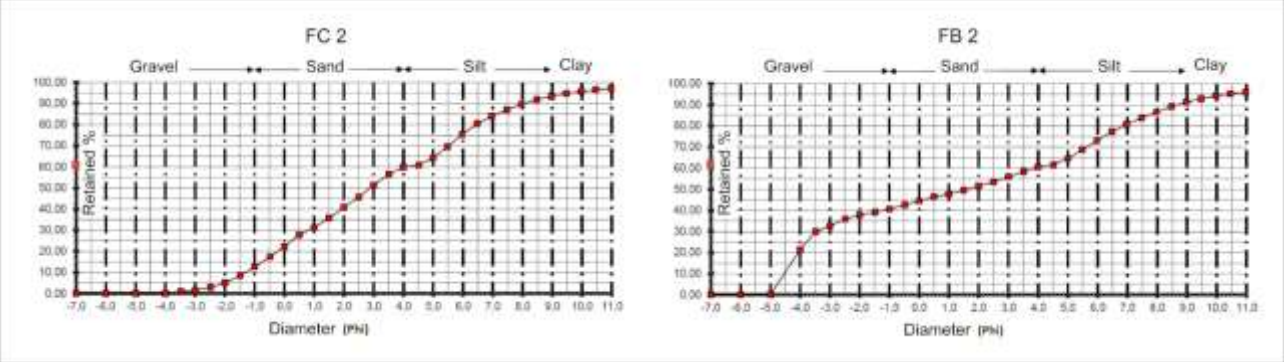

Figure 44 - Grain size analysis results (in %) of section FB and FC of Caverna delle Fate cave.

As for the fine earths, however, silt is always dominant, arriving at constituting even more than 45% of the total sample in level 12. The reciprocal relationships between sand, silt and clay are quite constant (as can be seen in the Figure 46) and making all the samples fall into the silty loam texture class.

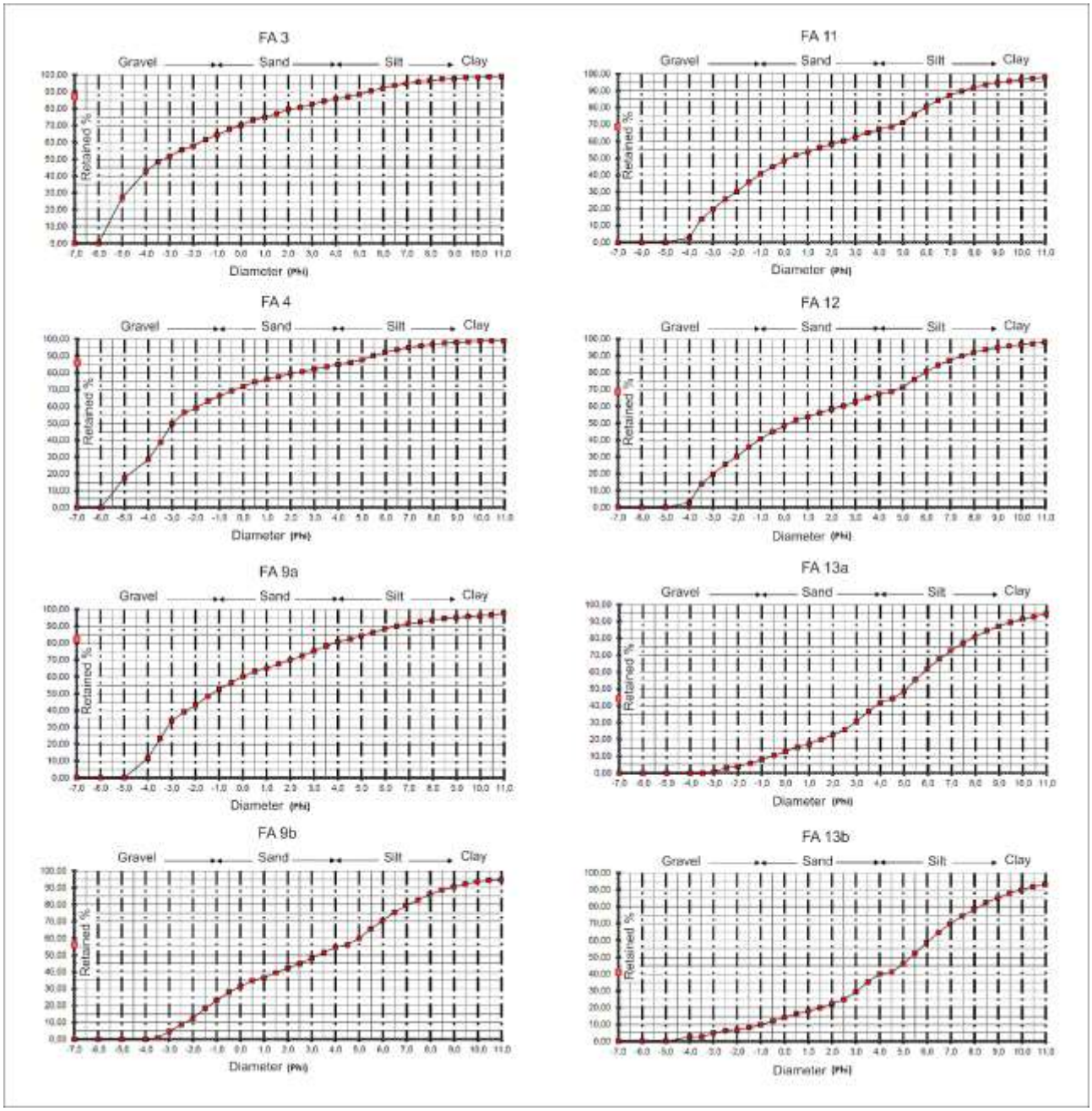

Figure 45 - Grain size analysis results (in %) for section FA of Caverna delle Fate cave.

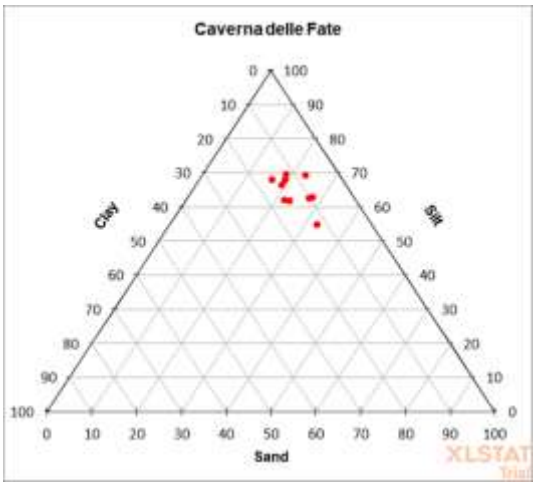

Figure 46 - Caverna delle Fate cave fine earths' textures.

X-ray powder diffraction

The results of the XRD analysis (Figure 47) permitted the identification of four minerals as main components of the deposits: quartz, calcite, illite and muscovite) and hydroxyapatite (a variety of apatite).

It can be noted that, in all samples, quartz is always present and in very high quantities, in some cases it is almost the only mineral present in the sample analysed. Illite is also always present, albeit in smaller quantities, only FA 4 is an exception.

Calcite is not always present, in fact in FA 12, FA 13a, FA13 b and FC it has not been found, but when it occurs, it is always in considerable quantities. Finally, hydroxyapatite was also found, but only in four samples: FA 4, FA 9a, FA 9b and FA 11.

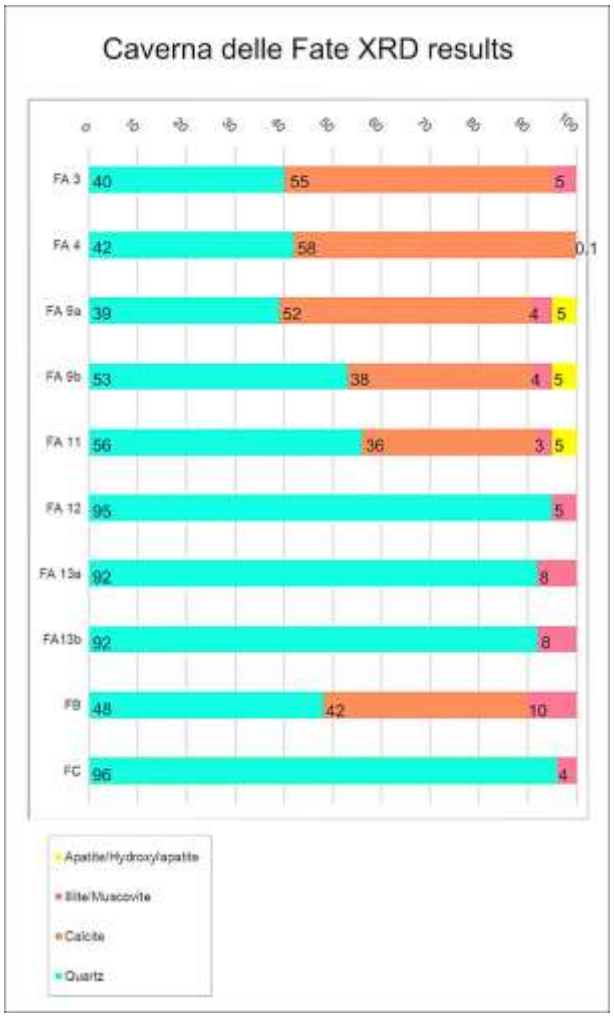

Figure 47 - XRD analysis results for Caverna delle Fate deposits. All data are in percentages.

Radiocarbon dating

It had been planned to perform a new series of dating on these deposits, but, given the state of the deposits, we had to turn to institutions and universities outside the Italian borders. Given the arrival of Covid-19, it was not possible to continue with this program.

Micromorphological analysis

Descriptions are given below and in the appendices (*Caverna delle Fate*), divided by thin section or, where necessary, by microfacies. After their description and their interpretation, they were divided into six microfacies types (MFT) (Courty, 2001; Goldberg and Macphail, 2013), which will be deepened in the discussions. These are: 1. Strongly cemented deposits (SC); 2. Partly cemented

deposits (PC); 3. Reddish brown deposits (RB); 4. Cave wall deposits (CW); 5. Pale yellow deposit (PY); 6. Laminated silt (LS).

Section FA

Thin section* FA 3 *(MFT: Strongly cemented deposits, SC)

Moderately separated crumb microstructure, with porous crumbs (granule size) and subangular blocky peds (fine gravel). The porosity is represented by complex packing voids (f.s., ±20%), channels (v.f.s., ±5%), vughs (v.f.s., ±5%) and planes (s.s., ±2%).

The ratio between coarse and fine fraction (at 5µm) is of 30/70, with a c/f-related distribution pattern single spaced coarse enaulic.

In particular, the coarse material is composed of a mineral part, corresponding to angular and subangular grains of quartz (f.s., ±5%), angular grains of calcite (f.s., ±2%) and subangular grains of muscovite (v.f.s., ±1%); while the rock fragments are: fossiliferous and speleothem subangular limestone rock fragments (c.s., up to cobble size, ±10%) and quartzite subangular rock fragments (c.s.; ±2%). Also inorganic residues of biological origin are present, as bone fragments (m.s., ±5%). Furthermore, burnt bones (f.s., ±1%) and charcoal fragments (f.s., ±5%) constitute the anthropogenic elements.

The micromass is grey-brown, and a speckled mixture of calcite, clay and phosphates for the porous crumbs, while it is reddish brown, and a cloudy mixture of clay and iron for the subangular blocky peds. It has a crystallitic, locally undifferentiated, b-fabric.

The recognised pedofeatures are: typic ferrous nodules (f.s., ±1%); dendritic manganese hypocoatings (f.s., ±1%); calcite coatings, with palisade fabric, having meniscus between the fabric elements (m.s., ±30%); micritic (equigranular xenotopic) nodules (m.s., ±5%); micritic (equigranular xenotopic) hypocoatings (s.s., ±10%); phosphatic rims on rocks and bones (cryptocrystalline apatite hypocoatings (v.f.s., ±1%)); cryptocrystalline typic apatite nodules (f.s., ±2%); subrounded excrement of large animals (among them are carnivores), (v.c.s., ±5%).

Table 8 - Microfacies types (MFT) and simplified descriptions to highlight crucial aspects for interpretation of results for Caverna delle Fate cave deposits.

Strat. lvl	***TS***	***MFT***	***mF***	***Microstructure***	***Aggregates***	***Voids***	***C/f-related distribution***	***C/f-ratio***	***Coarse fraction***				***Fine fraction***	***B-fabric***	***Pedofeatures***
									Bones	***Burnt bones***	***Charcoal***	***Single mineral grains*** / ***Rock fragments***			
FA 3	FA 3	Strongly cemented deposits		Crumb	Porous crumbs, subangular blocky peds	Complex packing voids, channels, vughs, planes	Single spaced coarse enaulic	30\70	aaa	a*	aaa	Quartz (f), calcite (*), mica (*) / Limestone (f), quartzite (*)	Carbonates, clay, phosphates	Crystallitic, undifferentiated	Ferrous (a*), manganese (a*), calcitic (aaaaa), phosphatic (aa), excremental (aaa)
FA 4	FA 4	Strongly cemented deposits		Crumb	Porous crumbs, subangular blocky peds	Complex packing voids, channels, vughs, planes	Single spaced coarse enaulic	30\70	aaa	a*	aaa	Quartz (f), calcite (*) / Limestone (f), quartzite (*)	Carbonates, clay, phosphates, iron	Crystallitic, undifferentiated \ granostriated	Ferrous (a*), manganese (a), calcitic (aaaaa), phosphatic (a), excremental (aaa)
FA 6	FA 6	Strongly cemented deposits		Complex: subangular blocky and crumb	Porous crumbs, subangular blocky peds	Complex packing voids, planes, channels, chambers, vughs,	Double spaced porphyric, close coarse enaulic	30\70	aaa	-	a-1	Quartz (f), calcite (*) / Limestone (f), quartzite (*), sandstone (f-1)	Carbonates, clay, phosphates	Weakly developed crystallitic	Ferrous (a*), manganese (a*), calcitic (aaaaa), phosphatic (a*), excremental (a)
FA 9	FA 9a	Strongly cemented deposits		Crumb	Porous crumbs, subangular blocky peds	Complex packing voids, channels, vughs, planes	Close coarse enaulic	40\60	aaa	-	a-2	Quartz (f), calcite (*) / Limestone (f), quartzite (*)	Carbonates, clay, phosphates, iron	Crystallitic, undifferentiated \ porostriated	Ferrous (a*), manganese (aa), calcitic (aaaaa), clayey (a), phosphatic (a), excremental (aaa)
FA 9	FA 9b	Partly cemented deposits		Complex: subangular blocky and crumb	Porous crumbs, subangular blocky peds, granules	Complex packing voids, channels, planes, chambers, vughs	Single spaced porphyric and single spaced coarse enaulic	40\60	aaa	-	a-2	Quartz (f), calcite (*), feldspars (*) / Limestone (f), quartzite (f)	Carbonates, clay, phosphates	Crystallitic, undifferentiated \ porostriated	Ferrous (a*), manganese (aaa), calcitic (aaa), clayey (a-1), phosphatic (a), excremental (a*)

FA 11	FA 11	Partly cemented deposits	Complex: angular blocky and granular	Angular blocky peds, granules	Complex packing voids, channels, planes, vughs	Single spaced porphyric and single spaced equal enaulic	30\70	a	-	a*	Quartz (f), calcite (f), feldspars (*)	Limestone (f), quartzite (*)	Carbonates, clay, phosphates, iron	Crystallitic, undifferentiated \ porostriated	Ferrous (a), manganese (aa), calcitic (aaaaa), clayey (a*), phosphatic (a*), excremental (a)
FA 12	FA 12	Reddish brown deposits	Subangular blocky	Subangular blocky peds	Planes, chambers, channels, vughs	Single spaced porphyric	40\60	a	a*	a	Quartz (f), calcite (f), feldspars (*)	Limestone (f), quartzite (*), sandstone (f-2)	Clay, phosphates, iron	Undifferentiated \ porostriated	Ferrous (a*), manganese (aaa), calcitic (a), clayey (a-1), phosphatic (a), excremental (a)
FA 13	FA 13a (+ upper part 13b)	Reddish brown deposits	Subangular blocky	Subangular blocky peds	Planes, chambers, channels	Close porphyric	40\60	aaa	a*	a	Quartz (ff), calcite (*), mica (*)	Limestone (f), quartzite (f)	Clay, phosphates, mica, iron	Undifferentiated \ porostriated	Ferrous (a*), manganese (aaa), clayey (a*), phosphatic (a), excremental (aaa)
FA 13	FA 13b	Reddish brown deposits	Subangular blocky	Subangular blocky peds	Planes, chambers, channels, vughs	Close porphyric, locally single spaced	40\60	a*	-	a*	Quartz (ff)	Quartzite (f), mudrock (*)	Clay, phosphates	Undifferentiated \ porostriated	Ferrous (a*), manganese (a), calcitic (a), clayey (aaa), phosphatic (a*), excremental (aaa)
FB 2	FB 2	Cave wall deposits	Subangular blocky	Subangular blocky peds	Planes, chambers, channels, vughs	Open porphyric	20\80	aaa	-	a	Quartz (ff)	Limestone (*), quartzite (*)	Clay, phosphates	Undifferentiated \ porostriated	Ferrous (a*), manganese (a), calcitic (aaaaa), clayey (a-1), phosphatic (a*), excremental (a)
FB 3	FB 3	Reddish brown deposits	Complex: spongy and crumb	Porous crumbs, subangular blocky peds	Channels, vughs, planes, chambers	Single spaced porphyric	30\70	a	-	a	Quartz (ff), mica (*)	Quartzite (f)	Clay, phosphates, iron	Granostriated, undifferentiated	Ferrous (a*), manganese (aaa), calcitic (aaa), clayey (aaaa), phosphatic (a-1), excremental (aaa)

FC 1	FC	Pale yellow deposits	1	Subangular blocky	Subangular blocky peds	Compound packing voids, planes, chambers, channels	Single spaced porphyric	40\60	a*	-	-	Quartz (f)	Quartzite (f)	Clay, carbonates, phosphates	Undifferentiated	Ferrous (a*), manganese (a*), calcitic (a), clayey (aaaa), phosphatic (a), excremental (aaaaa)
FC 2		Laminated silt	2	Angular blocky	Angular blocky peds	Planes, chambers, channels, vughs	Close porphyric	60/40	-	-	-	Quartz (ffff), mica (*)	-	Clay, mica, iron	Unistrial	Ferrous (a*), calcitic (a-1), phosphatic (aa), excremental (a)

Thin section* FA 4 *(MFT: Strongly cemented deposits, SC)

Moderately separated crumb microstructure, with porous crumbs (fine gravel) and subangular blocky peds (granules). The porosity takes the shape of complex packing voids (m.s., ±10%), channels (v.f.s., ±5%), vughs (f.s., ±2%) and planes (s.s., ±2%).

The c/$f_{5\mu m}$ ratio is roughly 30/70, and the c/f-related distribution pattern is a single spaced coarse enaulic.

The single minerals in the thin section are angular and subangular grains of quartz (m.s., ±5%) and angular grains of calcite (m.s., ±2%). Fossiliferous subrounded and subangular limestone rock fragments (granule size, ±5%) and quartzite subrounded rock fragments (g.s.; ±2%) are the only two kinds of rock fragments present. Bones (m.s., ±5%) and one animal tooth (m.s.) are also part of the groundmass. As some anthropogenic elements, like burnt bones (v.f.s., ±1%) and charcoal fragments (f.s., ±5%).

The micromass is light brown, and a cloudy mixture of calcite, clay and phosphates for the porous crumbs; whereas it is reddish brown, and a cloudy mixture of clay and iron for the subangular blocky peds. There are also two different b-fabric appearances: crystallitic, locally undifferentiated, b-fabric for the porous crumbs, and weakly developed granostriated for the subangular blocky peds.

The pedofeatures are: typic ferrous nodules (m.s., ±1%); dendritic manganese hypocoatings (f.s., ±1%); typic manganese nodules (m.s., ±1%); calcite coatings, with palisade fabric, forming braces between the fabric elements (f.s., ±40%); phosphatic rims on rocks and bones (cryptocrystalline apatite coatings) (f.s., ±1%); cryptocrystalline typic apatite nodules (f.s., ±1%); subrounded excrement of large animals, (v.c.s., ±5%).

Thin section* FA 6 *(MFT: Strongly cemented deposits, SC)

The microstructure can be defined as complex, thus as weakly separated subangular blocky microstructure and crumb microstructure, with subangular blocky peds (cobble size) and porous crumbs (v.c.s.). Complex packing voids (m.s., ±5%), planes (f.s., ±5%), channels (v.f.s., ±5%), chambers (m.s., ±2%) and vughs (s.s., ±2%) best describe the porosity of this thin section (t.s.).

The c/$f_{5\mu m}$ ratio is 30/70, and the c/f-related distribution pattern is both double spaced porphyric and close coarse enaulic.

Angular and subangular grains of quartz (from s.s. to pebble size, ±10%), angular grains of calcite (f.s., ±2%) and very few not identifiable grains (v.f.s., ±1%) are the single minerals present. The rock fragments, instead, are: fossiliferous subangular limestone (granule size, ±5%), quartzite subangular (v.c.s.; ±1%) and angular sandstone (pebble s.; one occurrence). Bone fragments (granule s., ±2%), not showing signs of burning, and charcoal fragments (v.c.s., one occurrence) are other elements of the groundmass.

The micromass is dark greyish brown, and a cloudy mixture of calcite, clay and phosphates. The b-fabric is weakly developed crystallitic.

Pedofeatures are: typic ferrous nodules (f.s., ±1%); dendritic manganese hypocoatings (f.s., ±1%); calcite coatings, with palisade fabric, forming a meniscus between the fabric elements (m.s., ±20%); micritic (equigranular xenotopic) hypocoatings (m.s., ±5%); calcite geodic nodules (m.s., ±2%); cryptocrystalline apatite coatings, unsorted and nonlaminated (f.s., ±1%); subrounded excrement of large animals, (m.s., ±2%).

Thin section* FA 9a *(MFT: Strongly cemented deposits, SC)

It has a weakly separated crumb microstructure, with porous crumbs (granules) and subangular blocky peds (granules). The voids present are: complex packing voids (m.s., ±10%), channels (v.f.s., ±5%), vughs (f.s., ±2%) and planes (v.s., ±2%).

The proportion between coarse and fine fraction increases (c/f5$_{\mu m}$ ratio: 40/60), while the c/f-related distribution pattern becomes close coarse enaulic.

The minerals are subrounded and subangular grains of quartz (from v.f.s. to pebble s., ±10%) and angular grains of calcite (m.s., ±2%). Fossiliferous subangular limestone (granule size, but one fragment is 3 cm, ±5%) and quartzite subrounded (g.s.; ±2%) represent the rock fragments identified. Bones (m.s., ±2%), one fragmented tooth (c.s., one occurrence) and only two charcoal fragments (v.c.s., two occurrences) are the last groundmass elements described.

The micromass is light brown, and a cloudy mixture of calcite, clay and phosphates, for what concerns the porous crumbs; it is reddish brown, and a cloudy mixture of clay and iron for the subangular blocky peds foreseen. The b-fabric is crystallitic, locally undifferentiated, in the case of the porous crumbs, and weakly developed porostriated, for the subangular blocky peds.

Finally, the pedofeatures are: typic ferrous nodules (s.s., ±1%); dendritic manganese hypocoatings (f.s., ±2%); typic manganese nodules (f.s., ±1%); calcite coatings, with palisade fabric, forming braces between the fabric elements (f.s., ±20%); limpid parallel microlaminated clay coatings, with sharp extinction lines (f.s., ±1%); limpid parallel microlaminated clay infillings, with sharp extinction lines (f.s., ±1%); cryptocrystalline typic apatite nodules (f.s., ±2%); subrounded excrement of large animals, some of which presumably carnivores (c.s., ±5%).

Thin section* FA 9b *(MFT: Partly cemented deposits, PC)

The microstructure is complex, having characteristics proper of a weakly separated subangular blocky and of a weakly separated crumb microstructure. The aggregates recognised are subangular and angular blocky peds (granules size), porous crumbs (granules size) and granules (granules size). The porosity sees the presence of complex packing voids (m.s., ±10%), channels (m.s., ±5%), planes (m.s., ±5%), chambers (c.s., ±2%) and vughs (f.s., ±2%).

The $c/f_{5\mu m}$ ratio is stable around 40/60, while the c/f-related distribution pattern is single spaced porphyric and single spaced coarse enaulic.

Subrounded and subangular grains of quartz (f.s., ±5%), angular grains of calcite (m.s., ±2%) and rounded grains of feldspars (m.s., ±1%) make up the total of the single minerals present. Fossiliferous rounded limestone rock fragments (pebble size, ±10%) and quartzite rounded rock fragments (g.s.; ±5%) are the recurring rock fragments. Bones (m.s., ±2%) and charcoal fragments (m.s., two occurrences) are part of the groundmass.

The micromass is greyish brown, and a cloudy mixture of calcite, clay and phosphates. Some aggregates, in particular some of the subangular blocky peds, instead, show a reddish brown micromass, which is also a cloudy mixture of clay and iron. The birefringence, in turn, is crystallitic, locally undifferentiated, for the majority of the aggregates, but weakly developed porostriated for some of the subangular blocky peds.

Pedofeatures are: typic ferrous nodules (c.s., ±1%); dendritic manganese hypocoatings (v.f.s., ±1%); typic manganese nodules (f.s., ±5%); equigranular hypidiotopic sutured micritic nodules (f.s., ±2%); micritic (equigranular xenotopic) hypocoatings (s.s., ±5%); limpid parallel microlaminated clay coatings, with sharp extinction lines (v.c.s., one occurrence); cryptocrystalline typic apatite nodules (f.s., ±1%) and coatings (v.f.s., ±1%); subrounded excrement of large animals, some of carnivores (c.s., ±1%, but one big element, 1 cm).

Thin section* FA 11 *(MFT: Partly cemented deposits, PC)

The microstructure is still complex, but this time it is better described as a moderately separated angular blocky and a moderately separated granular microstructure, with angular blocky peds (pebble size) and granules (m.s.) as aggregates. Complex packing voids (v.f.s., ±10%), channels (m.s., ±10%); planes (c.s., ±10%) and vughs (v.f.s., ±2%) complete the porosity description.

The groundmass sees a $c/f_{5\mu m}$ ratio returning to 30/70 and a c/f-related distribution pattern that has the characteristics of a single spaced porphyric and of a single spaced equal enaulic.

The coarse material is made of subrounded-subangular grains of quartz (m.s. but up to granule size, ±10%), angular grains of calcite (v.c.s., ±5%) and subangular grains of feldspars (m.s., ±1%). It also has fossiliferous rounded limestone rock fragments (v.c.s. but up to pebble size, ±10%) and quartzite rounded rock fragments (v.c.s.; ±1%). Then, bones (f.s., ±2%) and charcoal fragments (m.s., ±1%).

Micromass is generally greyish brown, and a cloudy mixture of calcite, clay and phosphates but few of the granules show a more reddish brown micromass, composed of clay and iron. The b-fabric is crystallitic and locally undifferentiated in the first case, and weakly developed porostriated for certain granules.

Pedofeatures described are: typic ferrous nodules (f.s., ±2%); dendritic manganese hypocoatings (v.f.s., ±1%) and nodules (m.s., ±2%); micritic (equigranular xenotopic) hypocoatings (v.c.s., ±20%); sparitic coatings with palisade fabric (f.s., ±5%), in contact with the micritic hypocoatings; equigranular xenotopic mosaic-like calcite infillings (m.s., ±1%); Fe-stained nonlaminated clay coating with few quartz fragments (of different sizes), underneath few of the micritic hypocoatings (c.s., ±1%); cryptocrystalline typic apatite coatings (v.f.s., ±1%) (reactions rims on rock fragments); subrounded excrement of large animals, some of which carnivores (f.s., ±2%).

Thin section* FA 12 *(MFT: Reddish brown deposits, RB)

The microstructure is a highly separated subangular blocky microstructure, with subangular blocky peds (cobble size). The porosity is composed of planes (c.s., ±10%), chambers (v.c.s., ±5%), channels (f.s., ±2%), and vughs (v.f.s., ±2%).

The c/$f_{5\mu m}$ ratio is again 40/60 and the c/f-related distribution pattern is single spaced porphyric.

The quartz is subrounded and subangular (s.s.-c.s., ±10%), calcite is angular (c.s., ±5%), and also feldspars grains are present in angular shape (f.s., ±1%). Fossiliferous rounded limestone and speleothem rock fragments (v.c.s.-pebble size, ±5%) are with quartzite rounded rock fragments (pebble s.; ±2%) and sandstone angular rock fragments (v.c.s.; two occurrences) the only rock species present. Inorganic residues of biological origin are only represented by bones (m.s.-granule size, ±2%). Whereas anthropogenic elements are burnt bones (f.s., ±1%) and charcoal fragments (f.s., ±2%), even if fragmented.

The micromass is brown and cloudy, composed of clay and phosphates. It has a weakly developed porostriated, locally undifferentiated, b-fabric. Still, few aggregates in the groundmass are reddish brown, iron- and clay-rich, with porostriated b-fabric.

Pedofeatures are: typic ferrous nodules (f.s., ±1%); dendritic manganese hypocoatings (m.s., ±5%) and typic nodules (f.s., ±2%); micritic (equigranular xenotopic sutured) nodules (f.s., ±2%), mainly in the inferior part; fragmented compound layered clay coating (c.s., one occurrence); cryptocrystalline typic apatite coatings (f.s., ±2%) (reactions rims on mineral grains and rock fragments); subrounded excrement of large animals (m.s., ±2%).

Thin section* FA 13a *and the upper part of* FA13b *(MFT: Reddish brown deposits, RB)

The pedality in this case decreases and there is a weakly separated subangular blocky microstructure, with subangular blocky peds (cobble size). Planes (f.s., ±10%, many perpendicular to the ground surface), chambers (m.s., ±5%) and channels (f.s., ±5%) compose the porosity.

The c/$f_{5\mu m}$ ratio is 40/60 and the c/f-related distribution pattern is close porphyric.

The major mineral is quartz (v.f.s., ±20%), with angular shape, followed by calcite (v.c.s., ±2%), also angular, and flakes-like grains of muscovite (s.s., ±1%). Fossiliferous subangular and subrounded limestone rock fragments (granule s., ±5%) are flanked by quartzite subangular and subrounded rock fragments (c.s.; ±5%). Inorganic residues of biological origin are only bones (f.s., ±5%). The anthropogenic elements are burnt bones (f.s., ±1%), charcoal fragments (m.s., ±2%) and one burnt aggregate (granule s.).

The micromass is brown, cloudy, and made of clay, phosphates and mica. The b-fabric is weakly developed porostriated, locally undifferentiated. Few aggregates in the groundmass are reddish brown, iron- and clay-rich, with porostriated b-fabric.

Pedofeatures are: typic ferrous nodules (v.f.s., ±1%); dendritic manganese (hydr)oxide hypocoatings (m.s., ±5%), mostly in the inferior part and sometimes associated to bones; nonlaminated dusty and limpid clay infillings (f.s., ±2%); cryptocrystalline typic apatite coatings (f.s., ±2%) (reactions rims on mineral grains and rock fragments); subrounded excrement of large animals (f.s.-granule s., ±5%).

Thin section* FA 13b *(MFT: Reddish brown deposits, RB)

It shows a weakly separated subangular blocky microstructure, with subangular blocky peds (pebble size). It has planes (f.s., ±10%), chambers (c.s., ±5%), channels (f.s., ±5%) and vughs (f.s., ±5%).

The c/$f_{5\mu m}$ ratio is still 40/60, and the c/f-related distribution pattern is close porphyric, locally single spaced.

Only angular grains of quartz (f.s., ±20%) are present as single minerals. Limestone is absent, but there are quartzite subrounded rock fragments (c.s.; ±5%) and mudrock subrounded rock fragments (c.s., ±1%). The inorganic residues of biological origin are bones (f.s., ±1%), and the anthropogenic elements are the charcoal fragments (v.f.s., ±1%).

Micromass is reddish brown, cloudy, and composed of clay and little of phosphates. The b-fabric is weakly developed porostriated, locally undifferentiated.

Pedofeatures are: typic ferrous nodules (v.f.s., ±1%); dendritic manganese (hydr)oxide hypocoatings (m.s., ±2%); parallel compound layered clay and silt coatings (c.s. but up to v.c.s., ±5%), mainly along a straight line and partly fragmented; cryptocrystalline typic apatite coatings (v.f.s., ±1%); subrounded excrement of large animals (m.s., ±5%).

Section FB

Thin section* FB 2 *(MFT: Cave wall deposits, CW)

There is a weakly separated subangular blocky microstructure, with subangular blocky peds (pebble size). The voids are planes (f.s., ±10%), chambers (c.s., ±5%), channels (f.s., ±5%) and vughs (f.s., ±5%).

The $c/f_{5\mu m}$ ratio changes completely and becomes 20/80, so does the c/f-related distribution pattern, becoming open porphyric.

Angular grains of quartz (f.s., ±10%) but in small quantity. Fossiliferous subangular and subrounded limestone rock fragments (f.s., ±1%) and quartzite subangular and subrounded rock fragments (f.s.; ±1%) are also present. The inorganic residues of biological origin are only bone fragments but they rise in number (c.s. but two fragments are cobble size, ±5%). Charcoal fragments are also existing (v.f.s., ±1%).

The micromass is brown, cloudy, and composed of clay and a little of phosphates. It has a weakly developed porostriated, locally undifferentiated, b-fabric. Some portions along the calcite coatings show a light brown micromass and a weakly developed crystallitic b-fabric.

Pedofeatures are: typic ferrous nodules (v.f.s., ±1%); dendritic manganese (hydr)oxide hypocoatings (v.f.s., ±2%); compound layered equigranular xenotopic calcitic coatings (c.s., ±20%), beneath the other carbonate pedofeatures classes; compound layered equigranular hypidiotopic calcitic coatings (c.s., ±10%), between the other two carbonate pedofeatures classes described; equigranular idiotopic calcitic coatings (c.s., ±20%), usually above the other two carbonate pedofeatures classes; silt capping, nonlaminated (v.c.s., one occurrence); cryptocrystalline typic apatite nodules (v.f.s., ±1%); subrounded excrement of large animals (m.s., ±2%).

Thin section* FB3 *(MFT: Reddish brown deposits, RB)

The microstructure is complex, having both the characteristics of a spongy and of a weakly separated crumb microstructure. The aggregates are subangular blocky peds (cobble size, weakly developed pedality) and crumbs (v.c.s., weakly developed pedality). Channels (m.s., ±10%), vughs (f.s., ±10%), planes (f.s., ±5%) and chambers (m.s., ±5%) compose the porosity.

The $c/f_{5\mu m}$ ratio is 30/70, while the c/f-related distribution pattern is single spaced porphyric.

Angular grains of quartz (v.f.s., ±20%) and angular grains of muscovite (s.s., ±1%) can be recognised. Quartzite subangular and subrounded rock fragments (c.s.; ±5%) is the only rock species present. Bones (c.s., ±2%) and charcoal fragments (c.s., ±2%) can also be found.

The micromass is brown, slightly reddish brown, cloudy, and composed of clay and phosphates. The birefringence is weakly developed granostriated, locally undifferentiated. Few aggregates in the groundmass are reddish, iron- and clay-rich, with striated b-fabric.

Pedofeatures are: typic ferrous nodules (f.s., ±1%); dendritic manganese (hydr)oxide hypocoatings (s.s., ±1%) and typic nodules (f.s., ±2%); sparitic coatings (c.s., ±5%) and infillings (c.s., ±2%) with palisade fabric (equigranular hypidiotopic); nonlaminated limpid clay coatings with diffuse extinction lines (v.f.s., ±10%); a unique cryptocrystalline typic apatite infilling (m.s.) cuts the thin section in half; subrounded excrement of large animals (c.s., ±5%).

Section FC

Thin section FC

Two microfacies are present and actually represent level 1 and level 2 of the FC stratigraphic section. They will be described separately.

Microfacies 1 (MFT: Pale yellow deposit, PY)

Moderately separated subangular blocky microstructure, with subangular blocky peds (cobble size). The porosity is composed of compound packing voids (v.c.s., ±10%), planes (m.s., ±10%), chambers (c.s., ±5%) and channels (m.s., ±5%).

The $c/f_{5\mu m}$ ratio is 40/60, with a c/f-related distribution pattern single spaced porphyric.

Angular and subangular grains of quartz (f.s., ±10%) and quartzite, subangular and subrounded, rock fragments (c.s.; ±2%) were identified. To these are added only bones (f.s., ±1%).

The micromass is greenish yellow, cloudy, composed of clay, calcite and phosphates, and it has an undifferentiated b-fabric.

Pedofeatures are: typic ferrous nodules (v.f.s., ±1%); dendritic manganese (hydr)oxide hypocoatings (m.s., ±1%); typic micritic (equigranular xenotopic) nodules (c.s., ±2%), isotropic in XPL; clay and silt coatings, compound layered, the laminae are parallel and extinction lines are absent (pebble s., ±10%), can be found only in the lower part of the mF; cryptocrystalline typic apatite nodules, mammillate (c.s., ±2%); subrounded excrement of large animals (v.c.s., ±20%).

Microfacies 2 (MFT: Laminated silt, LS)

Moderately separated angular blocky microstructure, with angular blocky peds (cobble size). There are planes (v.c.s., ±10%), chambers (c.s., ±5%), channels (v.f.s., ±2%) and vughs (s.s., ±2%).

The ratio between coarse and fine fraction is 60/40, and the c/f-related distribution pattern is close porphyric.

Angular and subangular grains of quartz (s.s., ±60%) are dominant, while flake-like grains of muscovite (s.s., ±2%) are very few. No other elements compose the groundmass.

The micromass is reddish brown, speckled, composed of clay, mica and iron, its b-fabric is unistrial.

Pedofeatures are: typic ferrous nodules (s.s., ±1%), only in the finer layers; only one typic micritic (equigranular xenotopic) nodule (pebble s.), isotropic in XPL; cryptocrystalline typic apatite nodules (f.s., ±2%); crescent apatite coating (c.s., ±1%); subrounded excrements (c.s., ±2%), predominantly in the upper part of the mF.

Arma delle Manie

Arma delle Manie is a very bright open cave (almost a shelter). As in other cases, only some portions of the deposits are in place after previous excavation campaigns and the intervention of local people. In this case it was possible to focus only on a single stratigraphic section which, in part, coincides with most of the studies already conducted here.

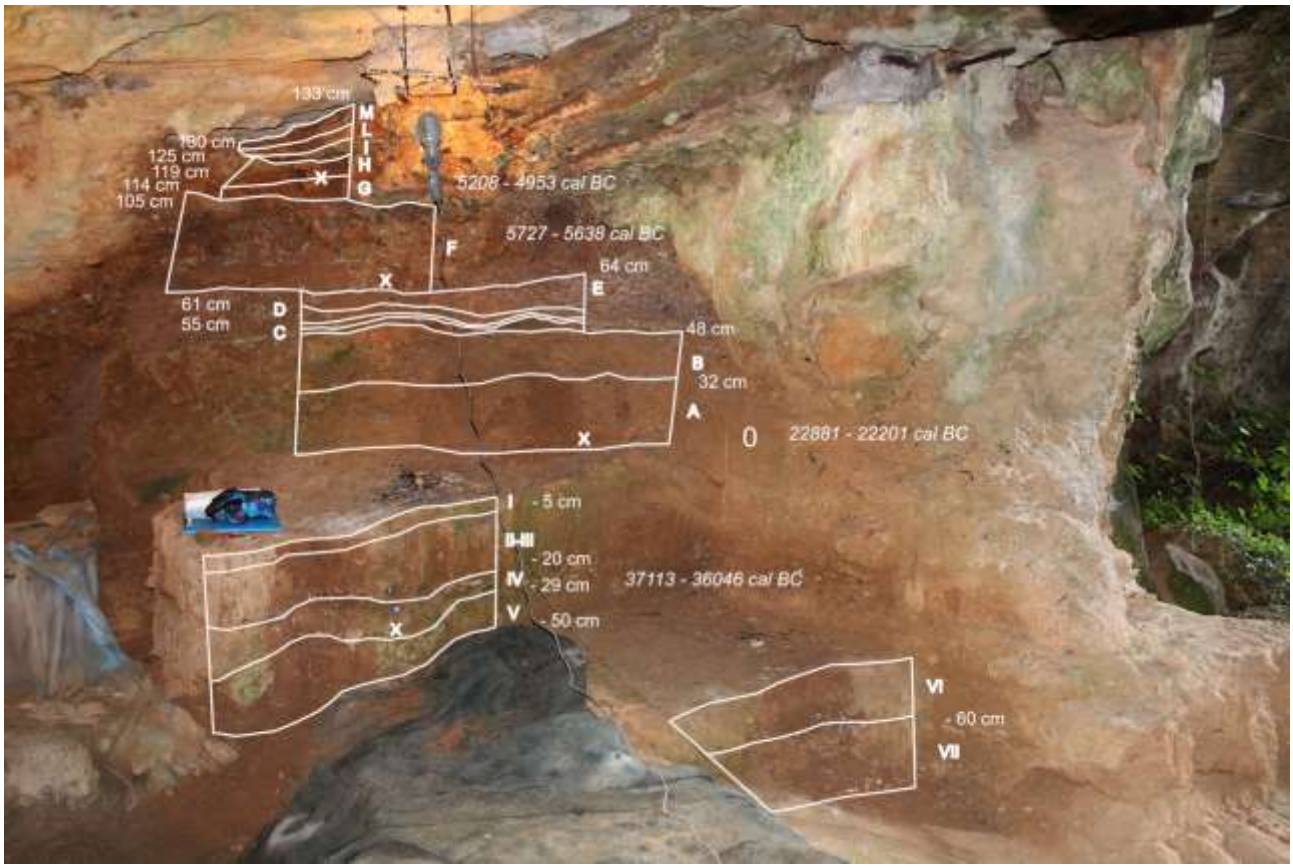

Figure 48 - Arma delle Manie cave stratigraphic section. Crosses indicate the sampling points for radiocarbon dating. In several positions the perspective creates optical illusions that could impact on depths of the levels.

Fieldwork and site stratigraphy

For this stratigraphic section the zero coincide with the highest point of level I of 1970s' stratigraphy (Figure 24). This was decided also to underline how in this work we concentrated on the study of more recent sediments. The lower level studied, in this case, is that of level VI. Previous studies stopped only in correspondence of a speleothem identified as the lower limit of level VII that we never reached.

Level M: From +133 cm to +130 cm. Not described as too perturbed by modern influences (remains of brick and concrete used to set up the excavation grid in the 1970s).

Level L: reddish brown (2.5 YR 5/4). From +130 cm to +125 cm. The lower limit is wavy and abrupt. It is matrix supported and partly cemented by carbonates. Few pebbles are present and the texture is silty loam. Occasional charcoal fragments and centimetric bones.

Level i (to distinguish it from the first level below zero): Brown (7.5 YR 5/4). From +125 cm to +119 cm. The lower limit is smooth and clear. It is matrix supported and cemented. In the middle part a thin flowstone is present. Very few cobbles are present. The texture is silty loam. Charcoal fragments are more and larger, big bone fragments are still present.

Level H: reddish yellow (5 YR 6/6). From +119 cm to +114 cm. The lower limit is smooth and abrupt. It is matrix supported, the coarse fraction is almost absent and the texture is silty loam. Occasional charcoal fragments at the base of the level.

Level G: Reddish yellow (5 YR 6/8). From +114 cm to +105 cm. The lower limit is wavy and abrupt. It is matrix supported. The coarse fraction has frequent pebble size limestone fragments. The texture is silty loam.

Between G and F a thick (~5 cm) flowstone is present.

Level F: Strong brown (7.5 YR 4/6). From +105 cm to +64 cm. The lower limit is smooth and clear. It is matrix supported, almost clast supported. Limestone (mainly) and schists (few) cobbles size are dominant in this level. The texture of fine material is still silty loam. Many centimetre sized charcoal fragments and big long bones are abundant.

Level E: From +64 cm to + 61 cm. It is constituted only of pebbles. The lower limit is smooth and abrupt.

Level D: Dark reddish brown (2.5 YR 2.5/3). From +61 cm to +55 cm. The lower limit is marked by the presence of a flowstone (indicated also in Figure 48) on the northern part, where this is not present, it is wavy and abrupt (Figure 49). It is matrix supported, even if the coarse fraction is an important component. The texture is silty loamy. Many charcoal and bone fragments are present. It is partly cemented.

Figure 49 - The peculiarity of the limit between level D (upper part) and level C (lower part).

Level C: Strong brown (7.5 YR 5/6). From +55 cm to + 48 cm. The lower limit is smooth and abrupt. Matrix

supported, but many cobbles are present. Partly cemented. The texture is silty loam. Charcoal and bone fragments are present.

Level B: Strong brown (7.5 YR 5/8). From +48 cm to + 32 cm. The lower limit is smooth and clear. It is matrix supported. The coarse fraction is not frequent, but calcitic granules and pebbles are present. Silty loam texture. Charcoal fragments are present. Insect nests (or what remains of them) can be observed in the field.

Level A: reddish yellow (7.5 YR 6/8). From +32 cm to 0. The lower limit is smooth and clear. The coarse fraction is absent. Silty loam. Bioturbation (insect nests) and charcoal fragments.

Level I: Reddish yellow (7.5 YR 7/6). From 0 to -5 cm. The lower limit is smooth and clear. The coarse fraction is scarce and mainly composed of quarzitic pebbles, the texture is silty loam. Small charcoal fragments.

Level II: Reddish brown (5 YR 4/3). From -5 cm to -12 cm. The lower limit is smooth and clear. It is matrix supported. The coarse fraction is almost absent, but when present are limestone pebbles. The texture is silty loam. In the lower part, there are clasts positioned along a line. Big bones fragments are present.

Level III: Reddish brown (5 YR 4/4). From -12 cm to -20 cm. The lower limit is smooth and clear. It is matrix supported, the coarse fraction is even less than in the level before, but still in the form of limestone pebbles. The texture is silty loam. Bone and charcoal fragments are present in small quantities.

Level IV: Yellowish brown (10 YR 5/8). From -20 cm to -29 cm. The lower limit is wavy and clear, outlined by angular and subangular limestone cobbles, disposed along a line. The rest of the level can be described as matrix supported, with a very low quantity of limestone or quarzitic coarse fraction (granules-pebbles). The texture is silty loam. Fragments of bones and charcoal are present. Among these a wild boar (*Sus scrofa*) jaw was found.

Level V: Yellowish red (5 YR 4/6). From -29 cm to -50 cm. The lower limit is smooth and clear. It is matrix supported, with little or no coarse fraction and with a silty loam texture. Few charcoal and bone fragments can be found.

Level VI: Strong brown (7.5 YR 5/6). From -50 cm to -60 cm. The lower limit is smooth and clear. The coarse fraction is nearly not present. Matrix supported, and silty loam. Few charcoal fragments.

Sampling

The sampling was conducted in order to have samples for grain size, XRD and micromorphological analysis. All samples are named after the level they come from.

Thus, the loose samples taken for grain size analysis are (in order from the uppermost): AM L, AM H, AM G, AM F, AM D, AM C, AM B, AM A, AM II, AM III, AM IV, AM V-VI.

For XRD analysis are: AM I, AM H, AM G, AM F, AM D, AM C, AM B, AM A, AM II, AM III, AM IV, AM V-VI.

The thin sections obtained for the micromorphological analysis are: AM GH (semi-mammoth), AM E, AM CD, AM B, AM A (semi-mammoth), AM II, AM III, AM IV, AM V, AM VI. Where it is not specified it is assumed they are quarter mammoth.

Levels V and VI have always been sampled together for bulk samples, in order to obtain the weight required.

Laboratory analysis

In general, in this cave, the amount of coarse material is limited to certain levels and, where we did not sampled in specific points, we can only deduce it from the field study (this applies to the coarse material found line-arranged, i.e. level II and V).

From the data analysis it can be seen that in the higher levels pebbles and cobbles are present more frequently, but in any case in limited quantities if compared to the fine fraction. This applies up to level F. Already on the field it was realized how it is almost clast supported, thus it is not surprising to find a peak of cobbles here. It is interesting to see how also in D the coarse component is present, but with a very poorly sorted aspect. Instead, from C the situation drastically returns to that already seen for F.

The second part of the stratigraphic section, on the other hand, has a slightly more homogeneous trend. Level A is an exception: here the coarse component is almost absent. The rest of the levels are almost entirely composed of silt, with some reduced presence of pebbles.

All levels show the same texture (as already happened in Caverna delle Fate): silty loam.

In any case, it is necessary to mention that part of the analysed elements are bone remains, charcoal fragments or other non-geogenic material. This is because we have chosen not to remove the organic matter and carbonates.

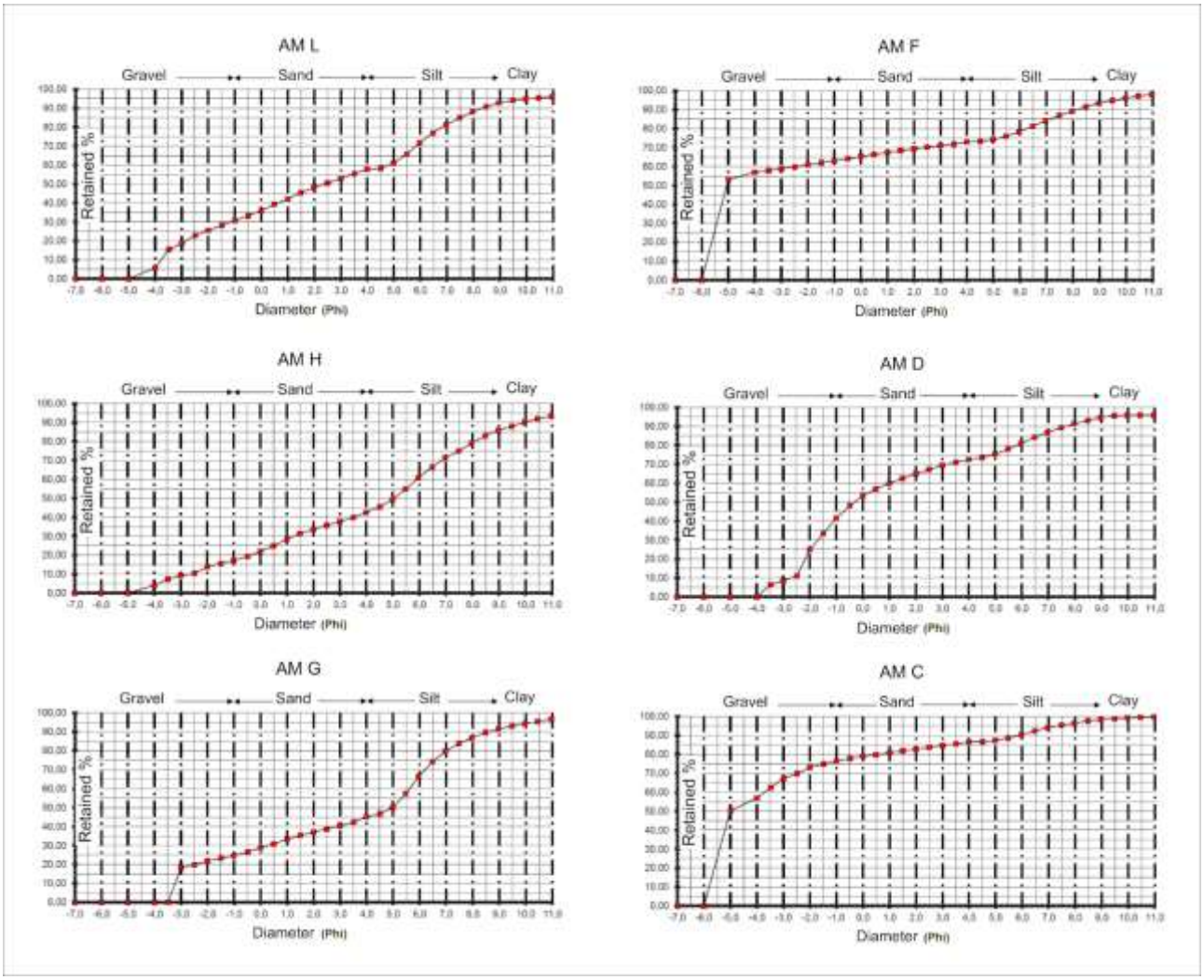

Figure 50 - Grain size analysis results for the first half of the samples from Arma delle Manie cave.

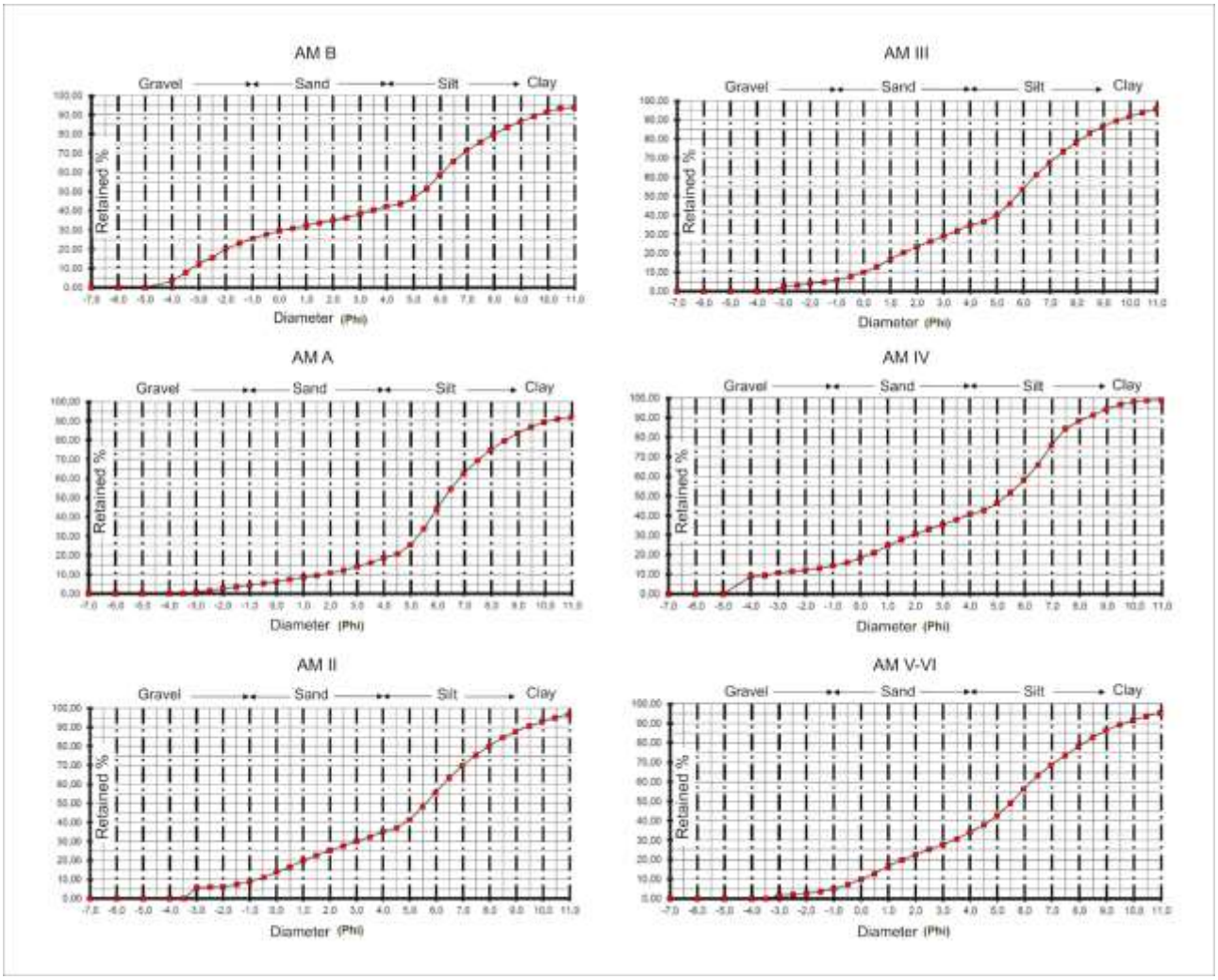

Figure 51 - Grain size analysis results for the second part of the samples from Arma delle Manie cave.

X-ray powder diffraction

The mineralogical analyses permitted to ascertain how quartz is present in all levels, in rather different relative quantities (Figure 52 and Table 9). Unlike Caverna delle Fate deposits, the presence of well-diversified classes based on the proportion of one mineral or another is not noted. Quartz is the dominant mineral in the first three and in the last three levels of the stratigraphy. Calcite is also present in all levels and in variable quantities, sometimes surpassing quartz in relative quantities (as

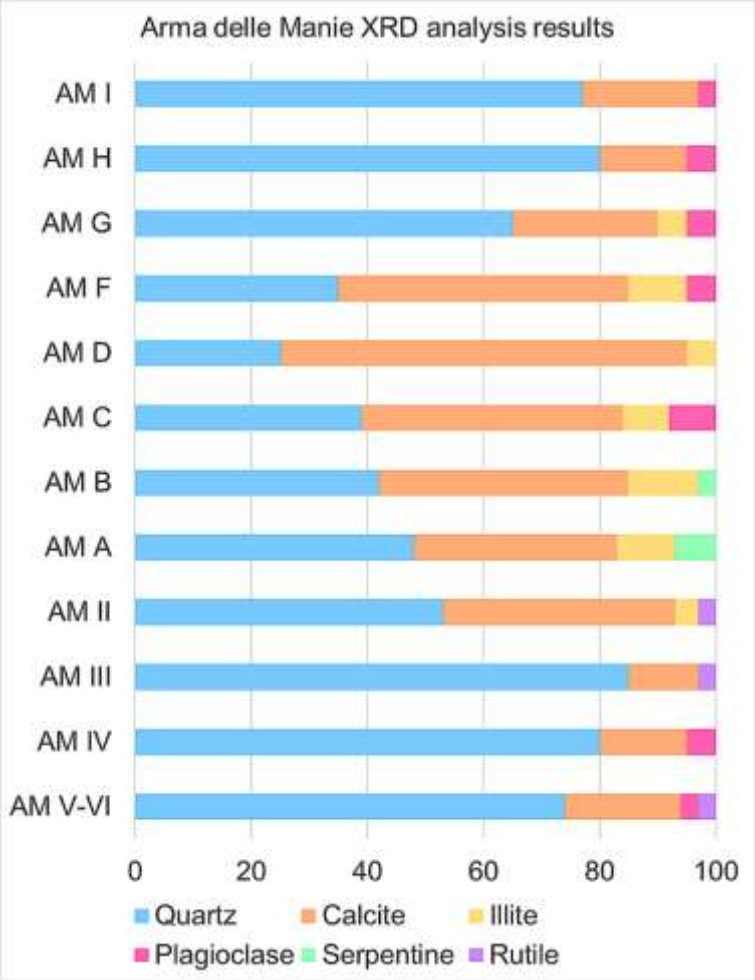

Figure 52 - XRD analysis results. This is the graphical representation of Table 9.

in the cases of F, D, C and B). Some mineral species accompany these two in smaller quantities: illite, plagioclase, serpentine and rutile. Illite is mainly concentrated in the central levels, especially in B (12%). Plagioclase is found in many levels, but always with percentages around 3% or 5%, except for C where the percentage is 8%. The serpentine is present only in three levels: A, B, and with 0.1%, in H. Finally, rutile is found only in the lower part of the stratigraphy, always with a 3% (levels II, III and V-VI).

Table 9 - Semi-quantitative XRD analysis results for Arma delle Manie cave deposits. All numbers shown are percentages.

Samples	Quartz	Calcite	Illite	Plagioclase	Serpentine	Rutile
AM I	77	20		3		
AM H	80	15		5	0.1	
AM G	65	25	5	5		
AM F	35	50	10	5		
AM D	25	70	5			
AM C	39	45	8	8		
AM B	42	43	12		3	
AM A	48	35	10		7	
AM II	53	40	4			3
AM III	85	12				3
AM IV	80	15		5		
AM V-VI	74	20		3		3

Radiocarbon dating

For this cave it was possible to perform four new ^{14}C datings starting from the charcoal fragments sampled in four different levels, as indicated by crosses in Figure 48. Furthermore, these fragments were examined by prof. Arobba (from Museo Archaeologico del Finale), who was able to determine its nature. Starting from the top, we thus have *Quercus t. caducifolia* from level GH, *Fagus sylvatica* from level F, Coniferae from level A and Angiospermae from level IV. Datings results are given in Table 10.

Table 10 - Radiocarbon datings for Arma delle Manie deposits.

Samples	^{14}C age (yr BP)	Calendar calibration (95.4% probability)	Laboratory reference n.
AM GH	6120 ± 40	5208 - 4953 cal BC (7157 - 6902 cal BP)	Beta-579345
AM F	6790 ± 30	5727 – 5638 cal BC	AM F
AM A	20350 ± 90	22881 - 22201 cal BC (24830 - 24150 cal BP)	Beta-579346
AM IV	34050 ± 220	37113 - 36046 cal BC (39062 - 37995 cal BP)	Beta-579344

Micromorphological analysis

Descriptions are given below and in the appendices (*Arma delle Manie*), divided by thin section or, where necessary, by microfacies. After their description and their interpretation, they were divided into four microfacies types (MFT) (Courty, 2001; Goldberg and Macphail, 2013), which will be deepened in the discussion. These are: 1. Reddish brown deposit MFT (RB) (thin section GH); 2. Dark, cemented deposit MFT (DC) (thin sections E and C); 3. Reworked loess MFT (RL) (thin sections B and A); 4. Brown clay MFT (CC) (thin sections II, III, IV, V and VI).

Table 11 - Microfacies types (MFT) and simplified descriptions to highlight crucial aspects for interpretation of results for Arma delle Manie cave deposits. ("n.r." for not recognisable).

Strat. lvl	TS	MFT	mF	Microstructure	Aggregates	Voids	C/f-related distribution	C/f-ratio	Coarse fraction					Fine fraction	B-fabric	Pedofeatures
									Bones	Burnt bones	Charcoal	Single mineral grains	Rock fragments			
AM G - AM H	GH	Reddish brown deposits	1	Angular blocky	Angular blocky peds	Planes, chambers, channels	Close porphyric, open porphyric	50\50	-	-	a-2	Quartz (fff)	-	Clay, quartz	Stipple speckled	Calcitic (aa)
			2	Subngular blocky	Subngular blocky peds	Planes, channels	Single spaced porphyric	30\70	-	-	aaa	Quartz (ff)	-	Clay	Stipple speckled	Manganese (a*), calcitic (a)
			3	Equal enaulic	Porous crumbs	Complex packing voids, channels	Single spaced equal enaulic	60\40	-	-	a-2	Quartz (ffff)	Quartzite (*)	Clay, iron	Stipple speckled	Manganese (a*), calcitic (aaa), excremental (a*)
			4	Subngular blocky	Subngular blocky peds	Complex packing voids, planes, channels, chambers	Open porphyric	20\80	-	-	a*	Quartz (f)	-	Clay, iron	Stipple speckled	Manganese (a*), clayey (aa)
AM E	E	Dark, cemented deposit		Subngular blocky	Subngular blocky peds, porous crumbs	Planes, vughs, channels	Double spaced porphyric	50\50	aaaaa	aaa	aaaa	Quartz (f)	Limestone (f)	Clay, charcoal, carbonates	Undifferentiated, crystallitic	Ferrous (a), manganese (a*), calcitic (aaa), clayey (aa)
AM C	C			Complex: crumb and granular	Porous crumbs, granules	Complex packing voids, channels	Single spaced coarse enaulic	40\60	aaa	a	aaaa	Quartz (f)	Limestone (ff), schist (f-1)	Clay, carbonates, charcoal	Stipple speckled, undifferentiated	Ferrous (a*), calcitic (aaaaa), clayey (aa)
AM B	B	Reworked loess		Complex: crumb and granular	Porous crumbs, granules	Complex packing voids, chambers, vughs, planes, channels	Close coarse enaulic	40/60	a*	-	a-2	Quartz (ff), mica (*)	Limestone (f)	Clay, carbonates	Crystallitic	Ferrous (a*), manganese (a*), calcitic (aaaa), clayey (aaa)
AM A	A			Platy	Plates, subangular blocky peds	Planes, vughs, chambers, channels	Double spaced porphyric	30\70	aaaa	-	a*	Quartz (f), mica (*)	Limestone (f), quartzite (f), schist (*)	Clay, carbonates	Weakly developed crystallitic	Ferrous (a*), calcitic (aaaa), clayey (a*)

AM II	AM II		Platy	Plates, subangular blocky peds	Planes, chambers, vesicles, channels, vughs	Double spaced porphyric	40\60	aaa	a	a*	Quartz (ff), mica (*)	Limestone (f), quartzite (*)	Clay	Weakly developed porostriated	Ferrous (a*), manganese (a*), clayey (a*)
AM III	AM III		Platy	Plates	Planes, channels, chambers, vughs, vesicles	Single spaced porphyric	40\60	a*	a*	a*	Quartz (ff)	Limestone (*), quartzite (*), schist (*)	Clay	Weakly developed cross-striated	Ferrous (a*), manganese (a*), clayey (a*)
AM IV	AM IV	Brown clay	Complex: platy, subangular blocky	Plates, subangular blocky peds	Planes, channels, chambers, vesicles	Double spaced porphyric	30\70	a	aaa	a	Quartz (f)	Limestone (f), schist (*)	Clay	Weakly developed porostriated	Ferrous (a), manganese (a*)
AM V	AM V		Complex: platy, subangular blocky	Plates, subangular blocky peds	Planes, vesicles, channels, chambers	Double spaced porphyric	30\70	aaa	a*	aaa	Quartz (f), calcite (*)	Limestone (f), quartzite (*), n.r. (*)	Clay	Weakly developed porostriated	Ferrous (a*), manganese (a*), clayey (a*)
AM VI	AM VI		Prismatic	Prismatic peds	Planes, chambers, channels, vughs	Single spaced porphyric	40\60	a	a	a	Quartz (f), calcite (*), plagioclase (*)	Limestone (ff), quartzite (*), n.r. (*)	Clay	Weakly developed granostriated	Ferrous (a*), calcitic (a*), clayey (a*)

Thin section* GH *(MFT: Reddish brown deposit MFT, RB)

Vertical semi-mammoth thin section. In this case four microfacies were recognised: the first coincides with level H in the stratigraphy, the rest of them belong to level G (Figure 53). They will be described separately.

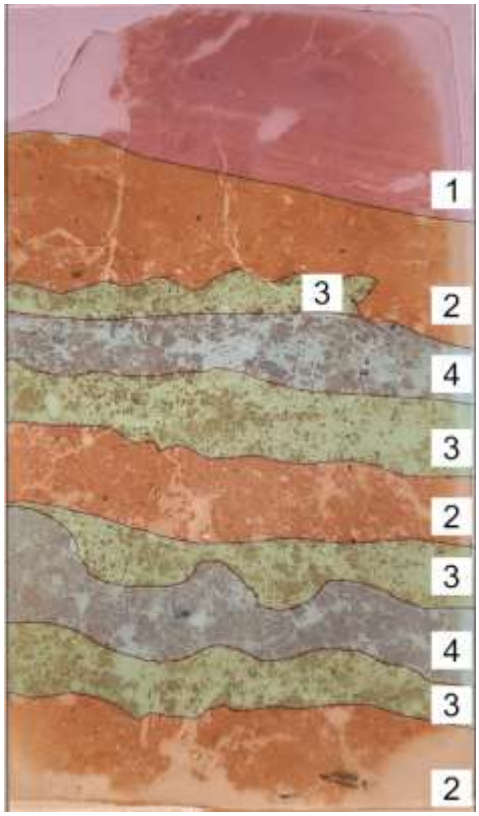

Figure 53 - Thin section GH from Arma delle Manie cave, with all mF numbers, as used in the description. The original aspect of GH is in figure.

Microfacies 1

It possesses a moderately separated angular blocky microstructure, with angular blocky peds (pebble size). The porosity is described by the presence of planes (c.s., ±5%), chambers (v.c.s., ±5%) and channels (m.s., ±2%).

The $c/f_{5\mu m}$ ratio is around 50/50, with a c/f-related distribution pattern varying (it depends on the lamina) between close porphyric and open porphyric. Only angular grains of quartz (s.s., ±40%) are present in the mineral coarse fraction, while the anthropogenic elements are represented by charcoal fragments (c.s., two occurrences) in the coarser laminae.

The micromass is reddish brown, speckled, and composed of clay and quartz. The b-fabric is stipple speckled.

The pedofeatures found are calcitic coatings (v.c.s., ±1%) and infillings (v.c.s., ±2%) with palisade fabric (equigranular hypidiotopic both of them).

Microfacies 2

The microstructure is weakly separated subangular blocky, with subangular blocky peds (granule size). Only two types of voids are present: planes (f.s., ±10%) and channels (m.s., ±5%).

The ratio between coarse and fine fraction is ($c/f_{5\mu m}$ ratio) 30/70, with a c/f-related distribution pattern single spaced porphyric.

Also here angular grains of quartz (f.s., ±20%) are the only mineral components. Charcoal fragments (c.s., ±5%) can be identified in the groundmass.

The micromass is reddish brown, cloudy, composed of clay, with a stipple speckled b-fabric.

Pedofeatures are manganese (hydr)oxide typic nodules (f.s., ±1%) and fragmented calcitic coatings with palisade fabric (equigranular hypidiotopic) (v.c.s., ±2%).

Microfacies 3

The microstructure changes, becoming a single spaced equal enaulic, with porous crumbs (v.c.s.). Complex packing voids (m.s., ±10%) and channels (s.s., ±2%) describe the porosity.

The $c/f_{5\mu m}$ ratio increases up to 60/40 and the c/f-related distribution pattern changes with it, becoming a single spaced equal enaulic.

The mineral fraction is composed of subangular grains of quartz (v.c.s., ±50%) and quartzite, subangular and tabular, rock fragments (v.c.s.; ±1%). Two charcoal fragments (v.c.s.) complete the groundmass.

The micromass is reddish brown, speckled opaque, and composed of clay and iron, contributing to a weakly developed stipple speckled b-fabric.

Pedofeatures are: manganese (hydr)oxide dendritic hypocoatings (m.s., ±1%); fragmented calcitic coatings with palisade fabric (equigranular hypidiotopic) (v.c.s., ±5%); mammillate excrements (v.c.s., ±1%).

Microfacies 4

The microstructure returns to moderately separated subangular blocky microstructure, with subangular blocky peds (granule size). Complex packing voids (f.s., ±5%), planes (f.s., ±2%), channels (v.f.s., ±2%) and chambers (f.s., ±2%) are the voids present.

The coarse fraction diminishes extremely as the $c/f_{5\mu m}$ ratio becomes 20/80, and the c/f-related distribution pattern becomes open porphyric.

Angular grains of quartz (s.s., ±10%) are the only mineral elements found. Charcoal fragments (f.s., 1%) are the unique anthropic elements.

The micromass is reddish brown, speckled opaque, composed of clay and iron, with a weakly developed stipple speckled b-fabric.

Pedofeatures are: manganese (hydr)oxide digitate nodules (f.s., ±1%); one parallel laminated micropan (moving towards the surface: silt, impure clay, dusty clay laminae), on the contact between the last mF 4 and the last mF 3 (1 mm thick x 15 mm long); fragmented limpid, and sometimes dusty, clay parallel laminated coating (m.s., ±2%).

Thin section* AM E *(MFT: Dark, cemented deposit MFT, DC)

Weakly separated subangular blocky microstructure, with subangular blocky peds (pebble size) and porous crumbs (granule size). The porosity is represented by planes (v.f.s., ±10%), complex packing voids (m.s., ±5%), vughs (f.s., ±5%) and channels (s.s., ±5%).

The $c/f_{5\mu m}$ ratio is 50/50, but the c/f-related distribution pattern is double spaced porphyric.

The mineral elements are subangular grains of quartz (f.s., ±2%) and limestone subrounded rock fragments (f.s.; ±10%). There are three kinds of inorganic residues of biological origin: bones (cobble size, ±30%), teeth (cobble size, two occurrences) and one hair (3 mm long), in the uppermost part of the thin section. Also abundant anthropogenic elements are present, and are charcoal fragments (v.c.s., ±10%) and burnt aggregates (v.c.s., ±5%).

Two different micromasses are found: one dark brown, cloudy, composed of clay and charcoal, with an undifferentiated b-fabric; the other one is brown, cloudy, composed of clay and carbonates, with crystallitic b-fabric.

The pedofeatures are: typic ferrous nodules (m.s., ±2%); dendritic manganese (hydr)oxide hypocoatings (f.s., ±1%); equigranular xenotopic calcitic coatings (s.s., ±2%) and infillings (f.s., ±5%); limpid nonlaminated clay coatings with no extinction lines (f.s., ±1%), and when a calcite coating is also present, the clay coating is found between the ped and the $CaCO_3$ coating, often are fragmented; limpid nonlaminated clay infillings with no extinction lines (f.s., ±2%), also often fragmented.

Thin section* AM CD *(MFT: Dark, cemented deposit MFT, DC)

The micromass is complex, with characteristics proper of a weakly separated crumb and of a weakly separated granular microstructure, with porous crumbs (granule size) and granules (granule size). Complex packing voids (m.s., ±10%) and channels (f.s., ±5%) constitute the porosity.

The $c/f_{5\mu m}$ ratio is 40/60 and the c/f-related distribution pattern is single spaced coarse enaulic.

Different elements compose the mineral fraction: subangular grains of quartz (s.s., ±5%), but also limestone subangular rock fragments (c.s.; ±20%) and a unique schist subangular rock fragments (c.s.). Then, there are the inorganic residues of biological origin, such as bones (m.s., ±5%) and the anthropogenic elements, such as charcoal fragments (c.s., but one element is pebble size, ±10%), burnt bones (m.s., ±10%), burnt aggregates (granule s., ±2%) and one supposed lithic artefact remain (granule s.), in the upper part of the thin section.

The micromass is dark brown, cloudy, composed of clay, calcite and charcoal, with a stipple speckled, undifferentiated at traits, b-fabric.

Pedofeatures are: typic ferrous nodules (f.s., ±1%); calcitic coatings, equigranular xenotopic (f.s., ±20%); limpid parallel laminated, alternating yellowish and reddish laminae, clay coatings with diffuse extinction lines (f.s., ±5%), observed on voids, aggregates and mineral grains.

Thin section* AM B *(MFT: Reworked loess MFT, RL)

It has a complex microstructure, with the characteristics of a weakly separated crumb microstructure and of a weakly separated granular microstructure, with porous crumbs (granule size) and granules (granule size). Complex packing voids (f.s., ±10%), chambers (v.c.s., ±10%), vughs (v.f.s., ±5%), planes (f.s., ±5%) and channels (f.s., ±2%) portray the porosity.

The $c/f_{5\mu m}$ ratio is 40/60, with a close coarse enaulic c/f-related distribution pattern.

The signel minerals are subangular grains of quartz (s.s., ±20%) and flake-like grains of mica (s.s., ±5%). Limestone (speleothem) subangular rock fragments (c.s.; ±10%) are also identified. Bones (f.s., ±1%), one shell (c.s.) and two charcoal fragments (f.s.) are also part of the groundmass.

The micromass is yellowish grey, cloudy, composed of clay and carbonates, and with a weakly developed crystallitic b-fabric.

Pedofeatures are: typic ferrous nodules (f.s., ±1%); manganese (hydr)oxide hypocoatings (s.s., ±1%); calcitic infillings, equigranular xenotopic (s.s., ±10%); limpid and dusty clay coatings,

nonlaminated, with diffuse extinction lines (s.s., ±5%), if in presence of calcite infillings, underneath them.

Thin section* AM A *(MFT: Reworked loess MFT, RL)

For the first time in this stratigraphy the weakly separated platy microstructure appears, with plates (pebble size) and subangular blocky peds (pebble size). The porosity is defined by planes (v.f.s., ±10%), vughs (f.s., ±10%), chambers (v.c.s., ±5%) and channels (f.s., ±2%).

The groundmass has a $c/f_{5\mu m}$ ratio of 30/70, and a double spaced porphyric c/f-related distribution pattern. The single minerals are the subangular and angular grains of quartz (f.s., ±10%) and the flake-like grains of mica (s.s., ±1%). Limestone (fossiliferous and speleothem) rock fragments are subangular, subrounded and tabular (granule s.; ±10%), and some of them seem oriented with their main axis perpendicular to the ground; quartzite is subrounded and subangular (v.c.s.; ±5%), and also subrounded and subangular schist rock fragments can be distinguished (v.c.s.; ±2%). The inorganic residues of biological origin present are bones (f.s., ±10%) and one single shell (c.s.). The anthropogenic elements are only charcoal fragments (f.s., ±1%).

The micromass is yellowish grey, cloudy, composed of clay and carbonates, with a weakly developed crystallitic b-fabric.

Pedofeatures are: typic ferrous nodules (f.s., ±1%); micritic (equigranular xenotopic) nodules (granule s., ±5%); calcitic dense incomplete infillings, equigranular xenotopic (granule-pebble size, ±5%); dusty parallel microlaminated clay coatings with diffuse extinction (s.s., ±1%).

Thin section* AM II *(MFT: Brown clay MFT, CC)

The microstructure is moderately-weakly separated platy, given by the presence of plates (pebble size) and subangular blocky peds (granule size), but als by the porosity, that is composed of planes (v.f.s., ±10%), chambers (v.c.s., ±10%), vesicles (c.s., ±2%), channels (c.s., ±2%) and vughs (c.s., ±2%).

The $c/f_{5\mu m}$ ratio is 40/60 and the c/f-related distribution pattern is double spaced porphyric.

The mineral fraction is constituted of subangular and angular grains of quartz (s.s., ±20%), angular grains of mica (s.s., ±10%), limestone (both fossiliferous and speleothem) subangular rock

fragments (c.s.; ±5%), whose some elements seem oriented with their main axis perpendicular to the ground, and quartzite subrounded rock fragments (v.c.s.; ±1%). Bones fragments (c.s. with one big fragment 23 mm long, ±5%) and one hair (1 mm long; one occurrence), in the middle part of the thin section, are the members of the inorganic elements of biological origin found. For what concerns the anthropogenic elements, charcoal fragments (c.s., ±1%) and burnt bones (m.s., ±2%) were identified.

The micromass is brown, speckled, composed of clay, and with weakly developed porostriated b-fabric.

Pedofeatures are: typic ferrous nodules (m.s., ±1%); typic manganese (hydr)oxide nodules (f.s., ±1%); clay coarsening from dusty clay parallel lamination, to chaotically disposed silt sized quartz, dense incomplete infilling (granule size, one occurrence in the lower part of the t.s.); limpid parallel microlaminated clay coatings with diffuse extinction lines (s.s., ±1%), mainly in the lower part of the t.s..

Thin section* AM III *(MFT: Brown clay MFT, CC)

The microstructure is rather homogenous, being a moderately separated platy microstructure, with plates (pebble size). The porosity takes the shapes of planes (v.f.s., ±10%), channels (c.s., ±5%), some of which oblong, chambers (c.s., ±10%), vughs (f.s., ±2%) and vesicles (f.s., ±2%).

The groundmass is characterised for having a $c/f_{5\mu m}$ ratio around 40/60 and a c/f-related distribution pattern single spaced porphyric.

Its coarse material is made of subangular and angular grains of quartz (s.s., ±20%), limestone, mainly fossiliferous, subrounded rock fragments (v.c.s.; ±2%), schist subangular-tabular rock fragments (v.c.s.; ±2%) and quartzite subrounded rock fragments (c.s.; ±1%). Furthermore, there are of bones (f.s., ±1%), charcoal fragments (f.s., ±1%) and burnt bones (v.f.s., ±1%).

The micromass is brown, cloudy, composed of clay, and with a weakly developed cross-striated b-fabric.

Pedofeatures are: typic ferrous nodules (f.s., ±1%); manganese (hydr)oxide hypocoatings (s.s., ±1%); clay coarsening, from dusty clay parallel lamination, to chaotically disposed silt sized quartz, dense incomplete infilling (v.c.s., ±1%).

Thin section* AM IV *(MFT: Brown clay MFT, CC)

Moderately separated platy and weakly separated subangular blocky microstructure, with plates (v.c.s.) and subangular blocky peds (granule s.). Different types of voids are present: planes (f.s., ±10%), channels (f.s., ±5%), chambers (c.s., ±5%) and vesicles (f.s., ±2%).

Groundmass has a $c/f_{5\mu m}$ ratio around 30/70 and a subsequent double spaced porphyric c/f-related distribution pattern.

Subangular grains of quartz (m.s., ±10%), limestone (fossiliferous) subangular rock fragments (v.c.s.; ±5%) and schist subangular-tabular rock fragments (v.c.s.; ±2%) are present. Also, in the groundmass can be found bones (m.s., ±2%), charcoal fragments (v.c.s., ±5%) and burnt bones (c.s., ±5%), and one big fragment can be calcined.

The micromass is brown, cloudy, composed of clay, with weakly developed porostriated b-fabric.

The thin section shows the presence of these pedofeatures: typic ferrous nodules (c.s., ±2%) and manganese (hydr)oxide nodules (s.s., ±1%).

Thin section* AM V *(MFT: Brown clay MFT, CC)

Moderately separated platy and weakly separated subangular blocky microstructure, with plates (granule size) and subangular blocky peds (pebble size). Planes (f.s., ±10%), vesicles (m.s., ±10%), channels (f.s., ±5%) and chambers (c.s., ±2%) define the porosity.

The $c/f_{5\mu m}$ ratio is 30/70, and the c/f-related distribution pattern can be identified as double spaced porphyric.

The constituents of the coarse material are subangular grains of quartz (f.s., ±10%); subangular grains of calcite (f.s., ±2%); fossiliferous limestone, subangular, subrounded and tabular, rock fragments (granule s.; ±10%); quartzite subangular rock fragments (granule s.; ±2%); and very few not recognisable subangular-tabular rock fragments (granule s.; ±2%). Few tabular limestone fragments are disposed on a line, as already observed in the field. In addition, bones (m.s., ±5%), charcoal fragments (v.c.s., ±2%) and burnt bones (m.s., ±1%) are also present.

The micromass is reddish brown, cloudy, composed of clay, with weakly developed porostriated b-fabric.

Pedofeatures are: typic ferrous nodules (m.s., ±1%); manganese (hydr)oxide quasicoatings (s.s., ±1%); limpid parallel microlaminated clay coatings with sharp extinction lines (s.s., ±1%).

Thin section* AM VI *(MFT: Brown clay MFT, CC)

This is the only case where a weakly-moderately separated prismatic microstructure can be observed. Only one type of aggregates is present: prismatic peds (pebble size). The porosity is given by planes (f.s., ±10%), chambers (v.c.s., ±5%), channels (f.s., ±2%) and vughs (f.s., ±2%).

The $c/f_{5\mu m}$ ratio changes into 40/60 and the c/f-related distribution pattern becomes single spaced porphyric.

Subangular and subrounded grains of quartz (m.s., ±10%), angular grains of calcite (f.s., ±2%) and subangular and subrounded grains of plagioclase (f.s., ±2%) are the single minerals present. The rock fragments are represented by: limestone, fossiliferous and speleothem, subangular, subrounded and tabular (granule s.; ±20%); subrounded quartzite (granule s.; ±2%); not recognisable subrounded rock fragments (v.c.s.; ±1%). In all cases, all the mineral elements are positioned with their main axis (if present) perpendicular to the ground surface. In the groundmass can also be found: bones (f.s., ±2%), charcoal fragments (f.s., ±2%) and burnt bones (f.s., ±2%).

The micromass is reddish brown, cloudy, composed of clay, with weakly developed granostriated b-fabric.

The pedofeatures are: typic ferrous nodules (f.s., ±1%); micritic (equigranular xenotopic) nodules (f.s., ±1%); dusty parallel microlaminated clay coatings with sharp extinction lines (s.s., ±1%); two loose continuous infilling of granule size peds, not dissimilar from the rest of the thin section.

6. Discussion and conclusions

Tana di Badalucco

Discussion

Unfortunately, the preliminary field analyses did not allow an immediate confirmation of the relationships between the different units. This is partly attributable to the absence of a continuous deposit, also due to previous removals and rearrangements, as already anticipated. Having said that, in any case, it is possible to propose an almost relative chronology, also suggested by the interpretations suggested, which will be presented below. Although the exact relationship between the lower levels of section 2 and the levels of section 3 is not entirely clear, we are nevertheless convinced that the latter are more ancient, especially given the climatic situation they depict. Then, section 2 is able to guarantee a more or less continuous reflection of a certain time interval and to represent it very well, showing how sensitive to the environmental changes that have occurred in this area these deposits are. Finally, section 1, unfortunately represented by only one unit, is considered with some certainty as the most recent of the entire stratigraphy that has been studied, at least so far. It is absolutely certain that further investigations are necessary and how these will require the use of absolute dating.

Some of the data, previous results and discussions that will be presented here have already been published in Sessa *et al.* (2019).

As anticipated in the results (page 63), the micromorphological analysis permitted the division of the Tana di Badalucco deposits into four different microfacies types (MFT), based on their peculiar features and the interpretation of the results (Table 5). These are:

1. Quartz-rich, reddish clayey deposits MFT (QRC);
2. Occupation deposits MFT (OD);
3. Bioturbated clayey deposits MFT (BCD);
4. Manganese-rich, reddish clayey deposits (MRC).

Quartz-rich, reddish clayey deposits MFT (QRC)

One of the most important aspects of this MFT is the presence of a large amount of coarse material (Figure 54a-b), almost exclusively in its lithic form: quartz is frequent, flanked by other minerals of different nature (such as feldspar and calcite), and rock fragments not recognizable under the petrographic microscope (due to the high degree of alteration). Given the particular nature, texture and appearance of the silt and sand sized components, it is assumed that they had a loessic origin (Goldberg *et al.*, 2001; Stoops, Langohr and Van Ranst, 2020). They could belong to a previous loessic deposit, perhaps located towards the entrance of the cave, which, following a reworking, was transported and deposited in the most internal investigated part of the cave.

Traces of water presence (the most probable agent of transport in this environment) and its influence on the deposits has not been directly recognized: no sedimentary figures visible to the naked eye were distinguished in the field. Nevertheless, clayey, ferrous, manganese-rich pedofeatures and rubefaction of the micromass were found through micromorphological analysis (Figure 54c-f). All these features point to hydromorphic conditions, which allowed the displacement of the clay in suspension and the mobilization of iron and manganese (Stoops, 2003; Kamel, 2019). These conditions are certainly more recent, being in contact with the voids, and indicate a particularly humid period in the cave and in the surrounding area. As is known, loess is an indication of an arid and cold period, with almost total absence of vegetation cover (Rousseau *et al.*, 2018), and these conditions occurred before the humid ones. Probably the change was sudden, so much so as to lead to a complete dismantling of the sedimentary structures and other elements (Sessa *et al.*, 2019). No signs of frost action are recognisable in field nor in thin section, and this supports the humid phase hypothesis.

Small fragments of bones, excrements and apatite nodules have been recognized in the upper unit (Figure 54g-h) and this suggests a weak, yet existing, animal or human presence (Brönnimann, Ismail-Meyer, *et al.*, 2017; Brönnimann, Pümpin, *et al.*, 2017; Karkanas, 2017; Villagran *et al.*, 2017; Karkanas and Goldberg, 2018). In fact, the apatite nodules are attributable to the alteration of phosphates, which may have been present either as further bone fragments or as excrements (Karkanas *et al.*, 2000; Karkanas and Goldberg, 2018). Unfortunately, the subsequent and current climatic and environmental conditions did not allow the survival of more important or more extensive traces. We are not able to quantify how much actual organic or inorganic matter of organic origin was previously present, but what exists allows us to assert that this cave has been occupied for a certain

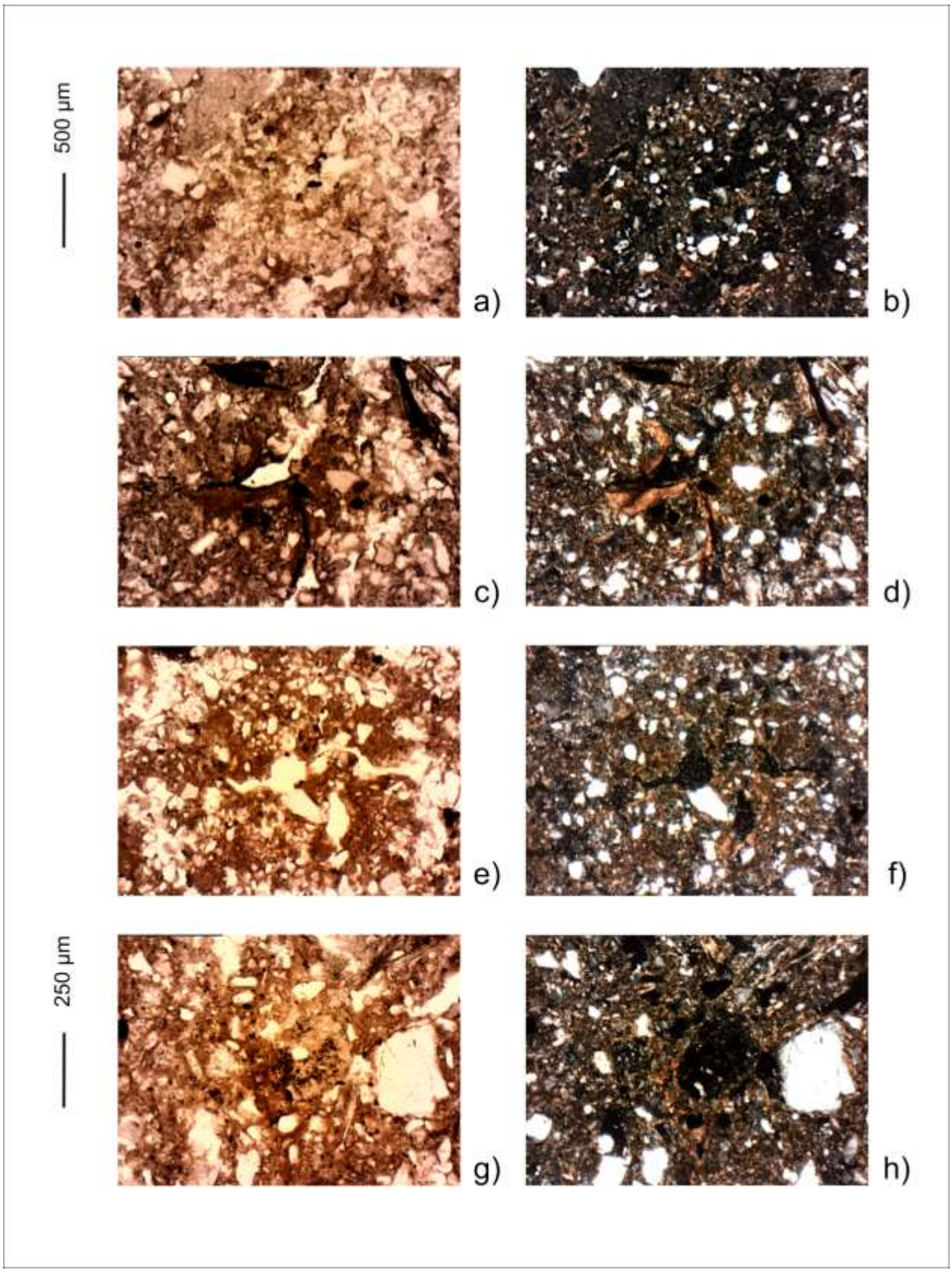

Figure 54 - Arid and then humid temperate MFT. a-b) In this microphotograph it is possible to note the large amount of coarse material of this MFT, the presence of small clay pedofeatures and the granostriated b-fabric. (Always PPL and XPL) c-d) Parallel microlaminated clay coatings with traces of manganese. e-f) Dusty parallel microlaminated clay coatings in contact with the voids. g-h) In the centre a small coprolite is present, recognizable thanks to the characteristic yellowish aspect in PPL and isotropic in XPL, typical of phosphates.

period of time and that some traces are still present and recognizable, albeit only under the microscope.

In the case of this MFT, the two units that compose it belong to the same section and are in contact with each other. As can be seen from the descriptions (pages 63 and 235), many points coincide, but not all. TB A2, for example, has small fragments of bones and phosphatic pedofeatures, which have allowed us to evaluate an animal influence on these deposits. Given all that has been said so far, it is possible to assume that these levels could be broadly traced back to MIS 5, in particular to the last interglacial.

Occupation deposits MFT (OD)

The second MFT has the peculiarity that none of the microfacies that compose it are in contact with each other. What actually binds these three microfacies together is that they have shared similar climatic conditions, processes and anthropogenic influences. Among these, the effect of frost, well represented by microstructures is very important. Although they are all categorised as complex, and are all in part well represented by the subangular blocky microstructure, they also show characteristics of a platy (TB B) (Figure 55a-b), crumb (TB F2), or granular microstructure (TB G). All the latter are known to be associated with cold conditions (Van Vliet-Lanoe, Fox and Gubin, 2004; Van Vliet-Lanoë and Fox, 2018), but obviously it is not a sufficient element in itself to reach this conclusion. These are accompanied by: the particular types of voids found, such as vughs and vesicles (Figure 55c-d) (Van Vliet-Lanoë, Coutard and Pissart, 1984; Van Vliet-Lanoë and Fox, 2018); the particular orientation of some large fragments of rock, which are perpendicular to the ground (Van Vliet-Lanoë and Fox, 2018); while in the higher level (TB G) the rock fragments can be interpreted as *éboulis*, i.e. bedrock fragments from roof collapse, (Mentzer, 2018), usually attributed to cryoclastic events (Courty and Vallverdu, 2001; Goldberg and Macphail, 2013).

Evenly distributed in the micromass, there are also elements of undoubtedly human origin (Canti, 2017a, 2017b; Canti and Brochier, 2017; Villagran *et al.*, 2017): bones showing signs of burning (Figure 55e-f), charcoal (Figure 55g-h) and ashes are present, even if not in very large quantities. The material does not have an arrangement or structure to affirm without any doubt that they are found in place (Karkanas *et al.*, 2007; Karkanas and Goldberg, 2010; Shahack-Gross *et al.*, 2014). Probably they have undergone reworking, in this way the fact that the quantities are limited, the fragments broken and there are no typical hearth structures would be explained (Miller *et al.*, 2010; Mallol, Mentzer and Miller, 2017; Whitau *et al.*, 2018).

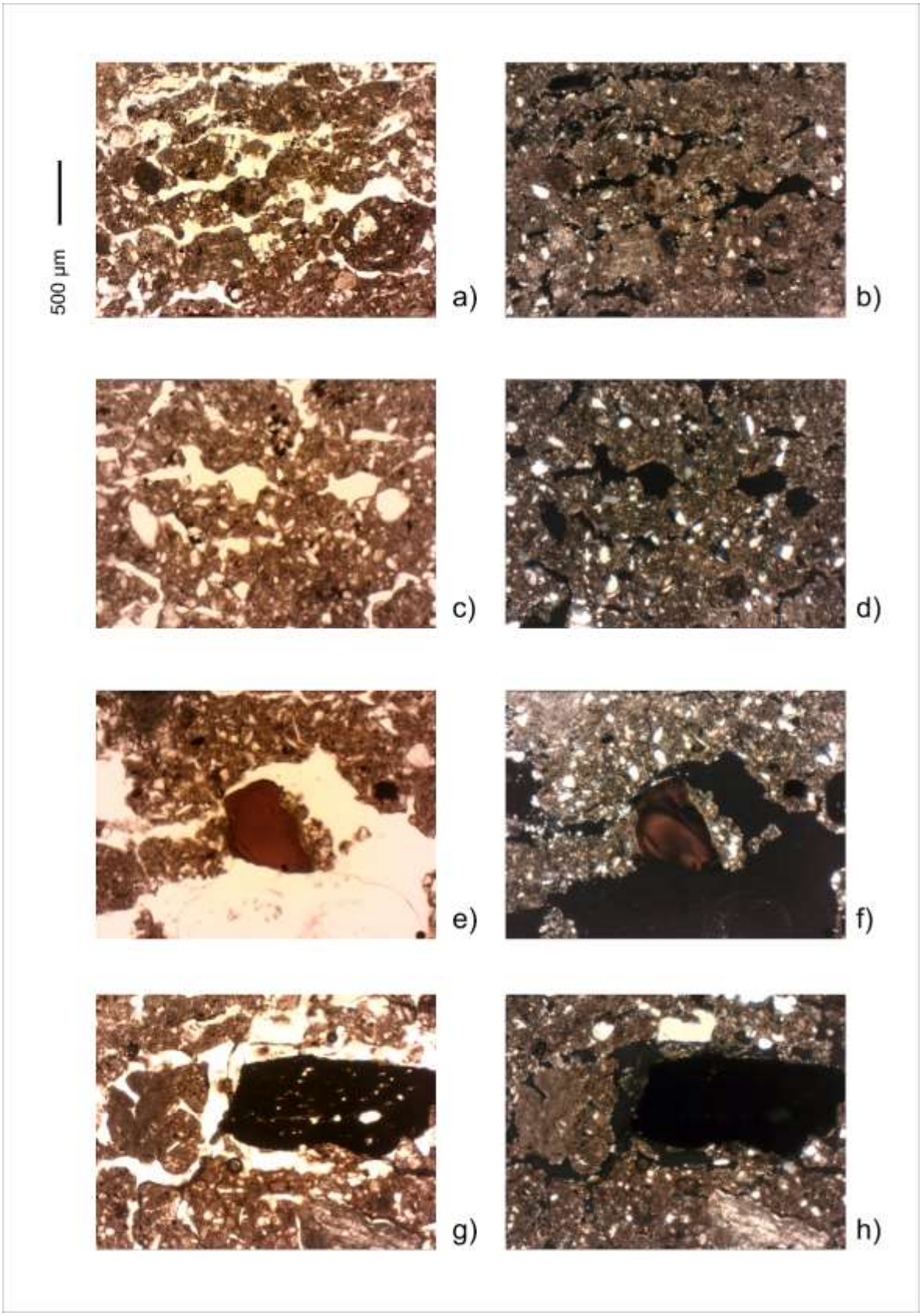

Figure 55 – Microphotograph from the Cold and human influence MFT. a-b) In this microphotograph it is possible to notice the well-developed platy microstructure of t.s. B, in PPL and XPL. c-d) Vesicles, like those clearly visible in the centre, are one of the distinctive features of a deposits influenced by frost action. Thin section G, PPL and XPL. e-f) A bone fragment, bearing the clear signs of burning, marks is placed in the centre of thin section B, PPL and XPL. g-h) A large fragment of charcoal from section F. PPL and XPL.

However, being quite concentrated, the transport probably did not have to be long and over long distances. Unfortunately, the removal of most of the original sediments does not allow an unequivocal confirmation of these statements. Yet, it can probably be assumed that human influence was exerted on these levels in a period of time perhaps preceding or penecontemporaneous to their complete deposition. The agent perhaps responsible for this is once again water, maybe in the form of a fluviokarst stream. In support of this, there are some pedofeatures and the nature and appearance of the mineral fraction considered above. Starting from the latter: fragments of greywacke, a type of rock present in the formations located around this cave, are present, and, in addition, the shape of these fragments, platy rounded (although still tabular in shape) (Goldberg and Macphail, 2013), not so well sorted, but not particularly rough, suggest fluvial transport, even if over short distances (Folk, 1980; Bosellini, Mutti and Ricci Lucchi, 1989). Finally, the ferrous, the rich in manganese and the depletion pedofeatures are all linked to water passage and saturation (Kühn *et al.*, 2018; Marcelino, Schaefer and Stoops, 2018).

As already mentioned, although the modelling agents of these levels were presumably the same, the exact deposition period of the studied sediments cannot be said with equal confidence. It is known that in part they come from areas of the cave occupied by man, whose deposits were then partly transported, from inside and from outside this same cave. After being deposited, they were affected by frost action and only afterwards there was the creation of figures associated to a new moment of humidity (perhaps brief seasonal thaw events). The conditions described above do not differ much from those recognized in other similar caves, also in Liguria, in the period of the Last Glaciation (Courty and Vallverdu, 2001; Rellini *et al.*, 2013), perhaps with a cold peak reached in unit TB G.

Bioturbated clayey deposits MFT (BCD)

Also in this MFT the signs left by the cryoturbation are the most important and exhibit themselves through the microstructure (complex and partly subangular blocky, but then also crumb and granular) (Figure 56a-b), the aggregates, the peculiar types of voids and the pedofeatures (above all the single capping identified in the thin section TB D, an unequivocal sign of freezing and thawing) (Figure 56c-d) (Van Vliet-Lanoë and Fox, 2018; Rodríguez-Ochoa *et al.*, 2019). In this case, however, these same microstructures, aggregates and voids are not exclusively attributable to these conditions. Their appearance is partly influenced by bioturbation (Aldeias *et al.*, 2014) (Figure 56a-b), which is also visible to the naked eye. These traces, as much as the anthropogenic ones, have the peculiarity of

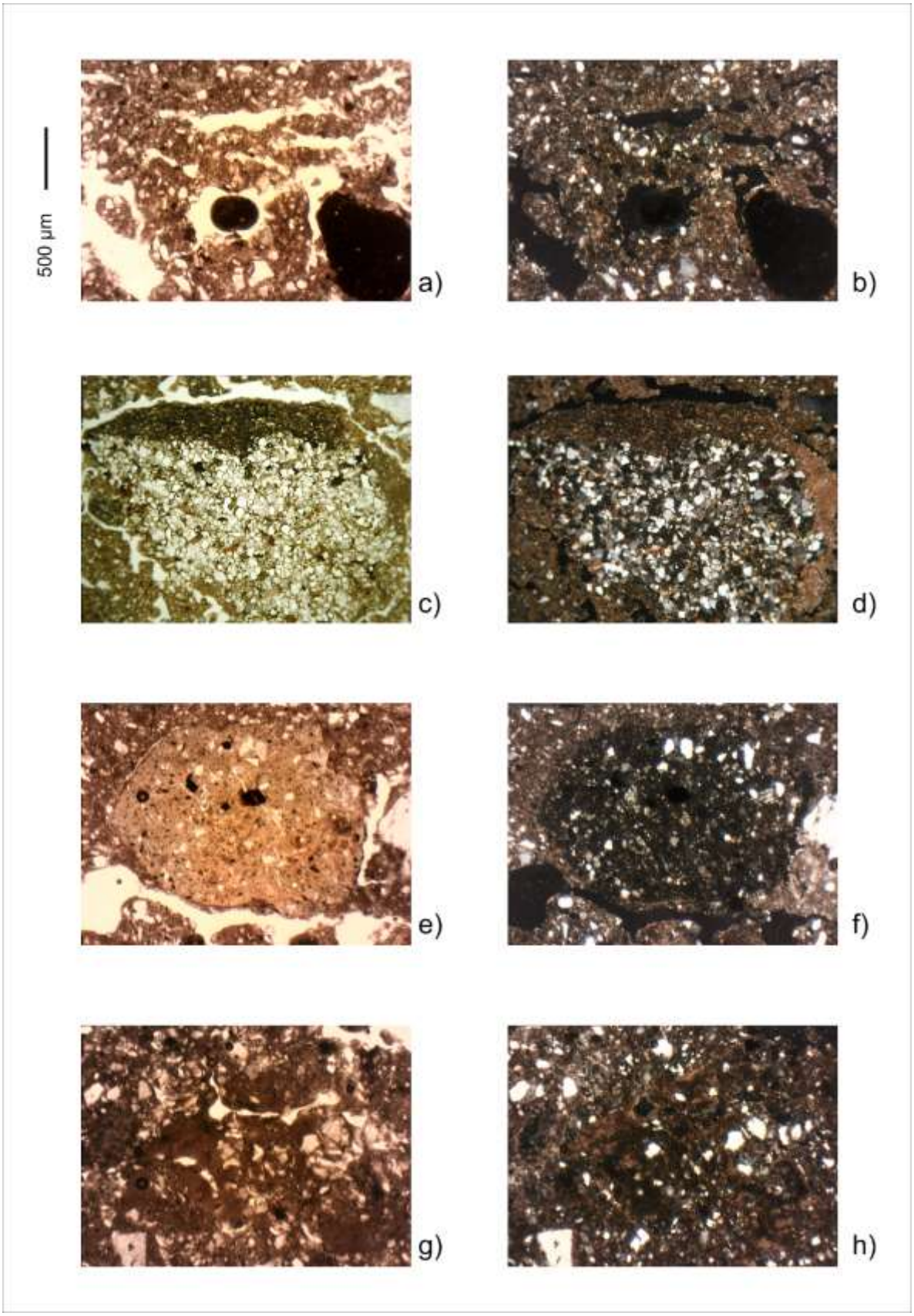

Figure 56 - Microphotograph from the Cold and bioturbation MFT. a-b) In this microphotograph it is possible to notice the platy microstructure (partly reworked by bioturbation) of t.s. F. PPL and XPL. c-d) In t.s. D a single silt capping was observed on a weathered rock fragment. e-f) A coprolite with quartz grains inside of it is easily discernible thanks to its yellowish colour in PPL and isotropic behaviour in XPL. g-h) Nonlaminar clay infillings, probably result of water passage. PPL and XPL.

influencing the original appearance of the sediments and masking possible important information that will be thus lost (Aldeias *et al.*, 2014). Generally these are attributable to insects, rodents or other small animals burrowing into the ground (Aldeias *et al.*, 2016; Sessa, Bona and Angiolini, 2021). Not knowing exactly where the original ground surface was collocated before the recent excavations began, it is not easy to propose an exact moment of biological interference on the sediments. However, the fact that they are located on different levels, even distant from each other, suggests that their activity occurred at different times. Other signs left by biological action are bone fragments, excrements (attributable to animals of larger size than the aforementioned, maybe *Ursus spelaeus*, Ricci, 2011) (Figure 56e-f) and also phosphate pedofeatures, generally linked to decay and diagenesis processes acting on organic remains or of organic origin (Karkanas *et al.*, 2000; Braillard, Guélat and Rentzel, 2004; Rellini *et al.*, 2013; Brönnimann, Ismail-Meyer, *et al.*, 2017; Brönnimann, Pümpin, *et al.*, 2017; Karkanas, 2017; Karkanas and Goldberg, 2018). Finally, there are also signs of periods of water passage or saturation, possibly still associated with seasonal thaw events (Vandenberghe *et al.*, 1998) (Figure 56g-h). Unfortunately, it is not possible to know whether the biological activity had particular reasons to manifest itself predominantly here rather than elsewhere. Instead, it is probable that the anthropogenic material recognized in TB F1 is actually deriving from the microfacies above and due to a reworking (possibly further evidence of the recognized biological activity) and it was transported there.

Also in this case, the absence of absolute dating makes it very difficult to give an exact temporal context to the deposits. However, the signs of cold are so evident and so well developed to indicate a different situation from the current one, attributable to the last glaciation.

Manganese-rich, reddish clayey deposits (MRC)

Although it is a level located in the upper part of the stratigraphy (unit E), it shows characteristics and conditions of formation totally different from the previous ones, more common to find under the ground surface. The frequent signs of freezing and thawing are completely absent here, as for AH MFT, but unlike that case, in this situation the coarse mineral fraction is in much smaller quantities. In greater quantities than in other MFTs are pedofeatures rich in clay, iron and manganese oxides (Figure 57a-d), indicating, together with the rubefaction, hydromorphic conditions (Stoops, 2003; Kühn *et al.*, 2018; Marcelino, Schaefer and Stoops, 2018). A long period of water saturation must have particularly influenced the E unit and this is proven also by the presence of carbonates pedofeatures, in the form of infillings, which usually point to vadose conditions (Alonso-Zarza and Tanner, 2010b; Durand *et al.*, 2018) (Figure 57a-b and e-f).

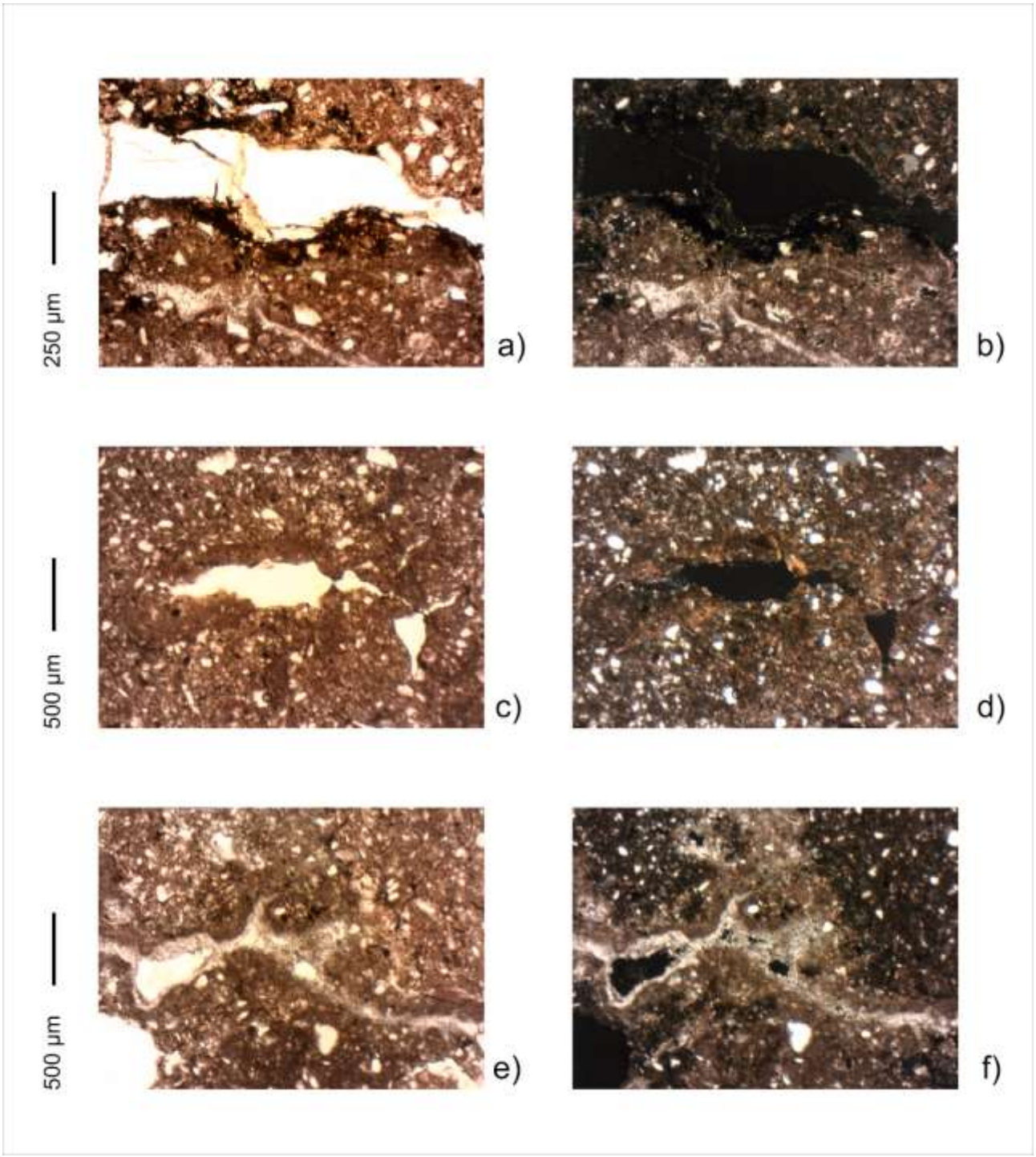

Figure 57 - Microphotograph from the Humid temperate MFT. a-b)Typical signs of humidity are visible, such as manganese-rich pedofeatures. Inside the aggregate it is also possible to notice a calcite infilling, another sign linked to humidity. PPL and XPL. c-d) Another pedofeature, but this time a dusty clay coating. PPL and XPL. e-f) In this case it is possible to see two different pedofeatures, one on top of the other: a calcite hypocoating and, in contact with the void, a partial infilling of calcite. PPL and XPL.

This, together with the fact that there are no signs of frost, unequivocally point to a rather humid and temperate climatic stage. Since samples considered more recent than this (such as TB F, for example) show new signs of frost action, it can be assumed that the period in which this climatic amelioration can be placed is that of an interstadial, i.e. a short period of thermal amelioration

during a glaciation (Anderson, Goudie and Parker, 2013), unfortunately it is difficult to assert exactly which one.

Conclusions

The Tana di Badalucco cave is unquestionably a very important site and shows all the characteristics necessary to conduct investigations on the climate changes occurring in this area over the last 120 kyr years: temporal resolution and environmental sensitivity (Woodward and Goldberg, 2001). Unfortunately, for reasons beyond our control, it was not possible to conduct a more thorough investigation of his deposits. Despite this, the site has provided important insights into the climate and environmental changes since the last interglacial, perhaps even earlier. Another difficulty encountered was that due to the removal of a large amount of material during previous excavation campaigns, especially the clandestine ones. In any case, we know that in this area, probably from MIS 5 to LGM, the climate was very rigid with very low temperatures, so much so as to lead to the formation of figures linked to freeze and thaw. During this whole period, this karst cavity, has seen the passage of animals, more or less big in size (bioturbation and excrements), and of man. Unfortunately the remains are not many and perhaps not even in place, but they are still an important testimony in support of the hypotheses that see this valley as a strategic passage for humans to and from France to Italy (Chiarenza, 2007). We have the confirmation, thanks also to this study, that it was not a stable climatic stage, but on the contrary, we found the signs of an interstadial during which the water was free and not in the form of ice, thus allowing the dislocation of clay, manganese and iron. Finally, a cold peak occurred, deduced by the shape, position and orientation of some rock fragments, that had been recognized as *éboulis*. The period of its dismantling can be supposed to have happen around the Last Glacial Maximum. All these hypotheses will be confirmed by new samplings and absolute dating.

Arma degli Zerbi

Discussion

It is evident how this cave was a favourite destination for animals. Perhaps they have used it as a hibernation den for a long time (as cave bears usually do) (Fosse *et al.*, 2004), alternating with humans, so much so that sometimes it is difficult to say where the traces left by one end and where those left by the other begin. What remains after these occupations are the signs of the presence of a large quantity of bones, carcasses, excrements and organic matter (Karkanas *et al.*, 2000; Braillard, Guélat and Rentzel, 2004; Goldberg and Macphail, 2013). Following the post-depositional processes that took place on all the deposits, only a part of the original materials are recognizable, the rest of it has been totally altered and, as happens in these cases, remains, in the deposits, exclusively in the form of phosphatic minerals (Karkanas and Goldberg, 2018). Cave deposits are particular environments that allow the preservation of these elements and the results of these reactions, thus keeping track of the various events (bio- and geochemical) that have occurred over time (Woodward and Goldberg, 2001; Karkanas and Goldberg, 2017).

These are the focal information coming from this site, although some signs also give us the opportunity to hypothesize the paleoclimatic change that has taken place in the background.

It should be emphasized how the lack of datings beyond ~17 kyr BP makes it difficult to give a reliable chronological context to the deposits studied. On this regard, future research will be needed.

As anticipated in the results (page 87), the micromorphological analysis permitted the division of the Arma degli Zerbi deposits into five different microfacies types (MFT), based on their peculiar features and the interpretation of the results. These are:

- Deposits rich in material of organic origin (MOO): c, d mF I, e, f mF I, section 4 mF I, section 4 mF III, section 4 mF V, l;
- Sediments rich in charred material (CM): d mF II, f mF II, section 4 mF IV;
- Greyish and coarse deposit MFT (GC): b;
- Yellowish deposit MFT (YD): section 4 mF II;
- Cave wall deposit MFT (CW): a.

We believe that the oldest deposits of the cave could be those belonging to section 4 level 5 and to the lower part of level 4 (s.4 l.5, s.4 l.4 lower part) (Figure 63.1), where the coarse material appearance (sub-rounded pebbles and cobbles) and the presence of silty sediment lenses suggest a previous state of fluvial-karst transport and sedimentation (Bosellini, Mutti and Ricci Lucchi, 1989; Nichols, 2009), subsequently deeply diagenised. These post-depositional processes are mainly represented by the diagenesis of large amount of bones and excrements, probably attributable to an animal occupation of the cave (in this case, also s.2 l.5 and s.3 l.5 lower parts and s.4 l.4 upper part are to be considered) (Figure 63.2). Part of these was recognized in the field and in t.s. (t.s. l, MOO MFT) (Figure 58a-b), while part of it was completely removed during the development of this phenomenon. The result is found in the form of apatite in the XRD analysis results. Percentage values similar to those found here are also present in Braillard, Guélat and Rentzel (2004), where phosphatization and reworking of sediments is attributed to the presence of hibernating cave bear. This could also have happened here, where a large quantity of bones of this species has been found (although the exact stratigraphic provenance is not known) (Farinazzo, 1999; Dodero, 2017). The fact that sedimentary structures, possibly having water as depositional agent, are not recognizable in other parts of the cave (almost, with the exception of s.4 l.2, as we shall see), leads us to suppose an earlier relatively humid period, perhaps before the beginning of the last glacial period (MIS 5?).

In the upper part of s.2 l.5 and in s.3 l.5 (Figure 63.3), there are fragments of charcoal and burnt bones, visible both to the naked eye and in thin section (lower part of the t.s. c and t.s. f mF II, CM MFT) (Figure 58c-f). However, these elements do not seem to be in their primary depositional location, given the total absence of combustion features (Morley *et al.*, 2019). These elements testify to a sporadic frequentation by man and the contemporaneous or successive reworking of the sediments (Miller *et al.*, 2010; Morley *et al.*, 2019). Throughout the cave, the levels of phosphates are very high, as already mentioned, and also in this case it is possible to assume that part of the deposit has been altered or has undergone partial dissolution.

Different portions of the cave seem to show a simultaneous increase in the amount of coarse material: pebbles, cobbles and boulders suddenly seem to represent a level shared by almost the entire cave. Section 2 sees an accumulation of coarse material mainly towards the westernmost part of the cave (left in the figure), section 3 in the lower part of level 4 and section 4 in the upper part of l.4 (Figure 64.4). All the coarse material is constituted of limestone, in particular of *Calcare di Finale* fm., easy to recognize even in the field, thanks to its great amount of fossils. It would not seem to have been transported from outside the cave, also given its size. Therefore we are persuaded that it may derive from the cave ceiling and it can be considered *éboulis* (roof spall) and

thus associated with cycles of freezing and thawing that led to its fracturing (Goldberg and Sherwood, 2006; Mentzer, 2018). Unfortunately, the material is too altered to be able to state it with complete certainty, but if so, this deposit could be traced back to the beginning of the last glacial period and roughly with MIS 4.

Subsequently, the pattern of alternation between animal and human occupation seems to repeat. First, having episodes with traces left by animals, in s.2 l.4 and l.3 (part of t.s. c and t.s. f mF I, MOO MFT) (Figure 59g-h), and s.4 l.3 (t.s. section 4 mF V, MOO MFT) (Figure 58g-h), in the first phase (Figure 64.5); in the second phase there are similar traces in correspondence with s.3 l.2 and l.3 (t.s. e, MOO MFT) and s.4 l.3 (mF III, MOO MFT) (Figure 64.6) (Figure 59a-b and c-d, respectively). These two phases seem to be separated only by a subtle level of man activity, recognizable in s.3 l.4 / 3 and s.4 l.3 (mF IV, CM MFT) (Figure 59e-f).

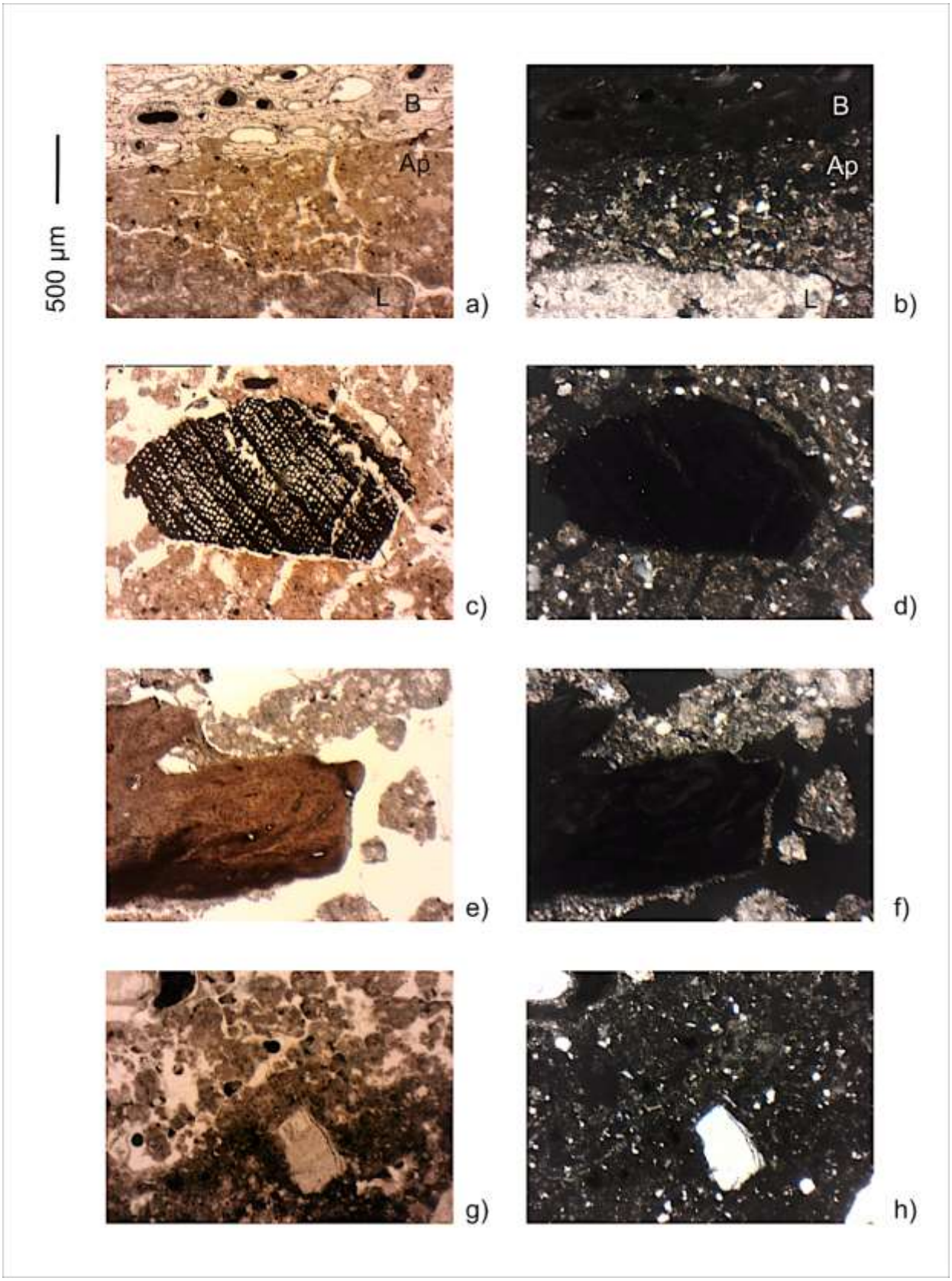

Figure 58 - a-b) Microphotographs of t.s. l. It is possible to see, above, a fragment of bone, surrounded by apatite (more easily appreciated in XPL) and below a fragment of slightly altered limestone. It is interesting to see how the influence of apatite decreases as we approach the carbonate rock. Thin section l, PPL and XPL. c-d) In t.s. c, especially towards its lower part, there are numerous fragments of charcoal, an example in microphotograph. CM MFT. PPL and XPL. e-f) Also belonging to the CM MFT, a large fragment of bone bearing burn marks. T.s. f mF II. PPL and XPL. g-h) At the bottom right, there is a part of a larger coprolite. MOO MFT, t.s. section 4 mF V. PPL and XPL.

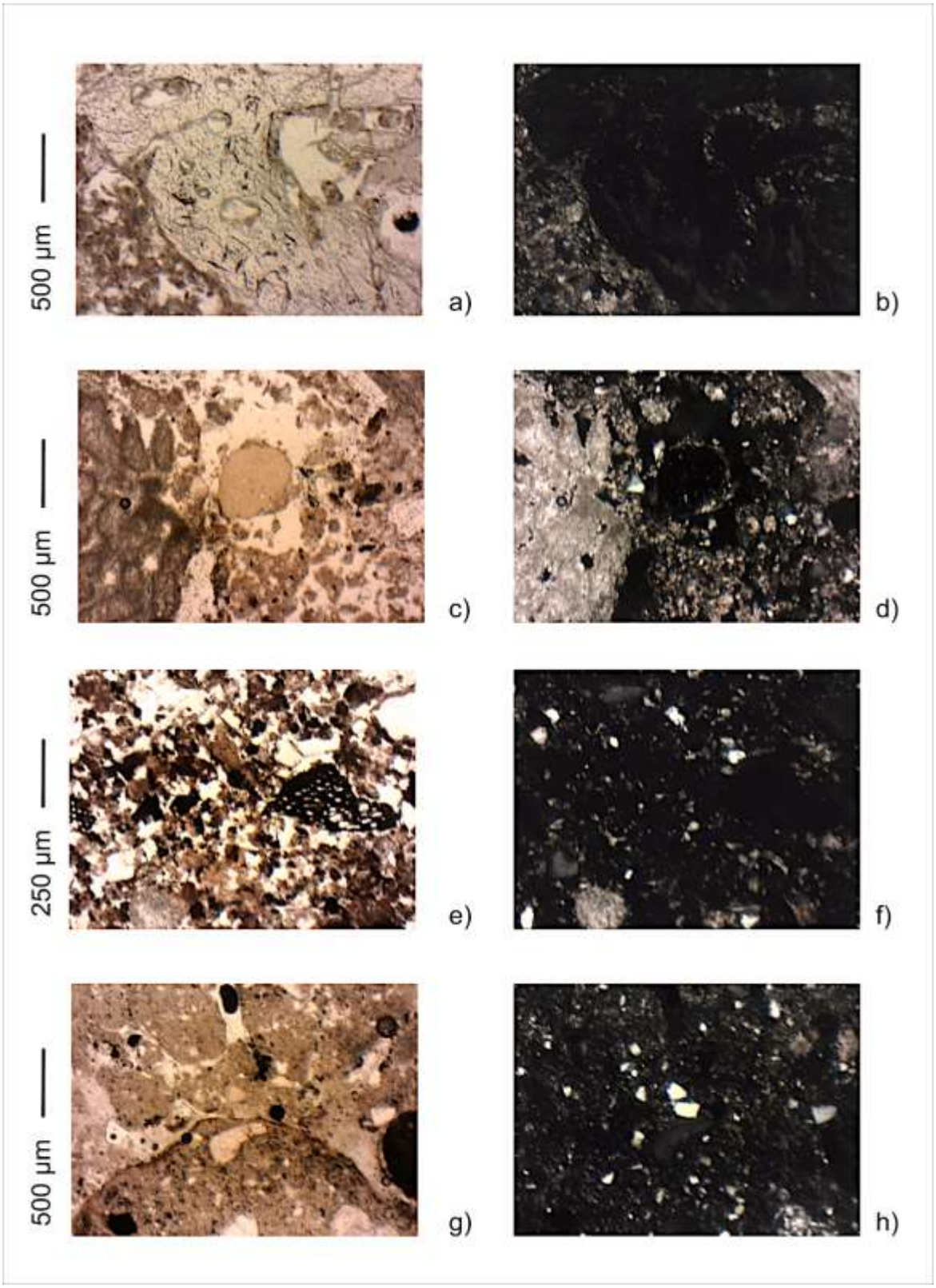

Figure 59 - a-b) Thin section e (MOO MFT), belonging to the second phase of animal occupation. In the microphotograph one of the many large fragments of bones is present. PPL and XPL. c-d) Microfacies III of section 4, also of the second phase of animal occupation and MOO MFT. In this case, it is possible to see, in the centre, an apatite nodule, probably the result of bones and animal excrement alteration. On the left there is a fragment of limestone from the "Calcare di Finale" formation, recognizable thanks to the presence of coral fossils. PPL and XPL. e-f) In the microphotograph it is possible to appreciate more aspects of the mF IV: the moderately separated granular microstructure, the presence of charcoal, perhaps organic matter and probably other burned material, as well as fragments of limestone and quartz grains. PPL and XPL. g-h) In the lower part there is a carnivore excrement with the typical yellowish-greyish colour and a little bone fragment in its upper part. In the upper part, the porous crumbs aggregates can be seen. The b-fabric is crystallitic-undifferentiated, maybe due to the high phosphates content. PPL and XPL.

Animal occupation was already recognized in the field, where a carnivore jaw and a tooth were found, as well as a certain amount of bones, especially in section 2, where the apatite percentage seem lower. In the thin sections, this is further confirmed by the presence of excrements, bone fragments and apatite nodules (often the by-products of bone diagenesis) (Karkanas and Goldberg, 2018) and it was also possible to see excremental pedofeatures slowly becoming part of the micromass. As for the traces left by man, in section 3 a lithic tool was found, while in section 4 what could be considered as a combustion substrate is present. These appear as those described in Aldeias *et al.* (2016) and Mallol, Mentzer and Miller (2017), who show how this blackish layer could possibly represent what was once the surface underneath a hearth, perhaps a surface already rich in organic matter. It is difficult to place chronologically these sediments.

Above these levels there are traces of different, but perhaps related, processes. The most particular aspects are those in s.4 l.2 (mF II, YD MFT) (Figure 65.7). As already mentioned, beyond this, only one other level shows sedimentary structures, although in this case they are clearly reworked. These are dusty clay coatings (lenses of silty clay) (Figure 60a-d), deposited in an almost stagnant water (Nichols, 2009). Considering this, we can hypothesize that there was an episode of great water availability, perhaps in a quite humid environment (Nichols, 2009). Thanks to the micromorphological analysis, it was possible to notice that these are not in their original position, but have been slightly reworked. In fact, they do not appear to be too far from their original position, no fragments are seen at important distances from their supposed origin, and the fractures are not so much. This suggests a successive low energy transport. However, mixed with these pedofeatures fragments, strongly unsorted limestone fragments are also found. Since it also appears to be a sediment moving almost on a flat surface, everything would suggest solifluction (Ciccacci, 2015). This process is generally associated with frost (taking the name of gelifluction, in this case) (Ciccacci, 2015), but we don't have enough evidences to state it with absolute certainty. The sediments seem to originate from outside the cave and then be transported in, where clay coatings were already present. This level propagates further towards the cave entrance following section 4 open trench.

At the same time or shortly after, in the innermost part of the cave (s.2 l.3 / 2 and s.3 l.2 / 1) (Figure 65.7), a new ceiling collapse took place. The modality and the material seem to be the same, what changes is that this time the limestone fragments are smaller (cobbles mainly), perhaps indicating a second cold episode (Goldberg and Macphail, 2013; Mentzer, 2018), possibly indicating the beginning of the LGM. Again, without exact dating, it's hard to tell.

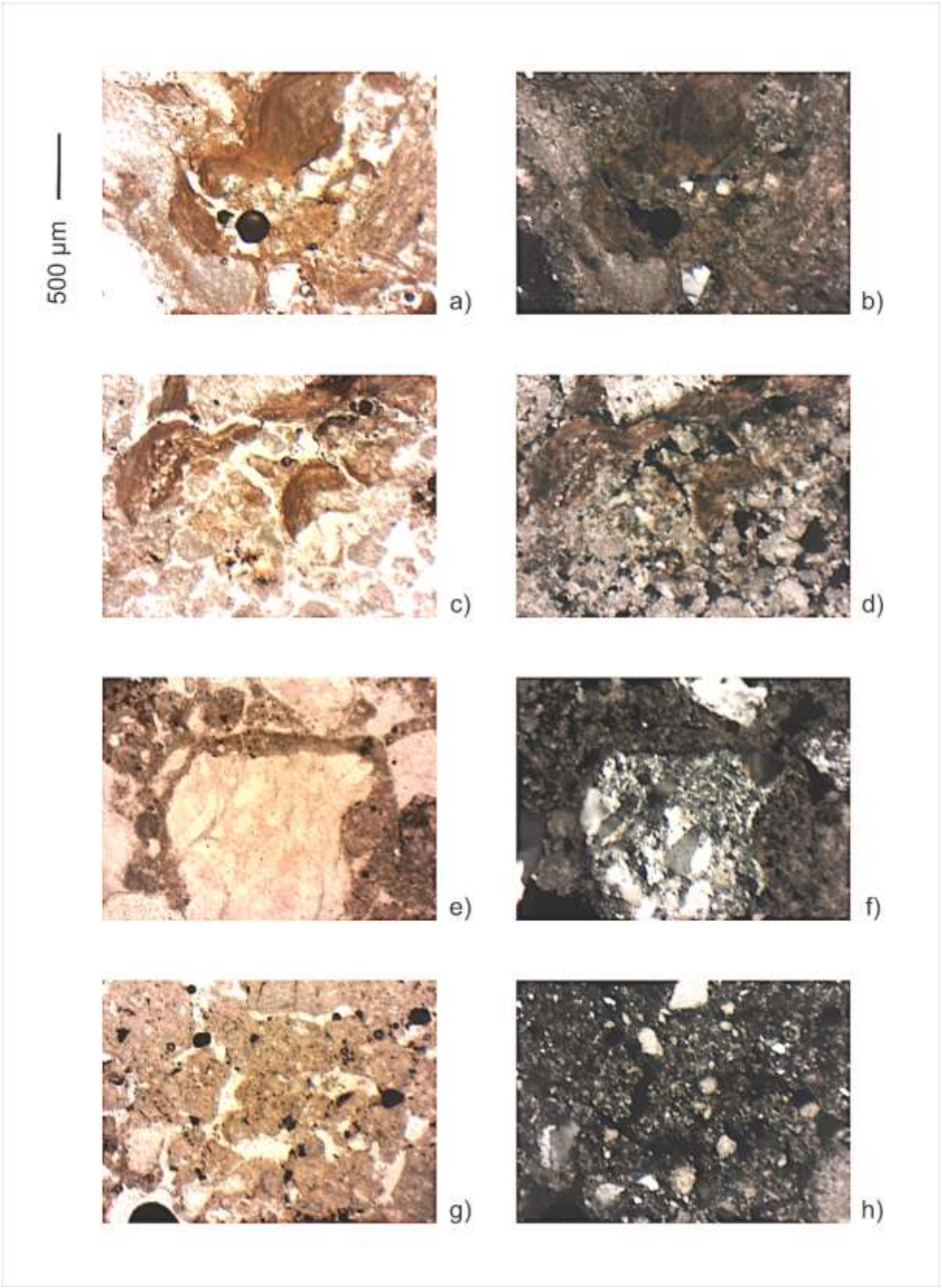

Figure 60 - a-d) In the first four microphotographs it is possible to notice the clayey pedofeatures from section 4 mF II (YD MFT). It is evident that they are fractured and not in equilibrium with the current surface. These are surrounded by limestone fragments of different sizes. PPL and XPL. e-f) In t.s. b it is possible to note the presence of a silt capping placed above a rock fragment. It is also possible to state that it is silt capping as the deposition of the material above shows a sedimentation different from that of the surrounding aggregates. The presence of such a figure implies the action of frost. PPL, XPL. g-h) Porous crumbs aggregates are present and it is possible to notice the platy overprint present in this t.s. (b, GC MFT). PPL, XPL.

From the micromorphology we have evidences confirming the presence of a cold climatic episode (t.s. b, GC MFT). There are silt cappings (Figure 60e-f), generally associated with frequent cycles of freezing and thawing, and a platy overprint that suggests the evolving of the same phenomenon (van Vliet and Langohr, 1981; Vliet-Lanoë, 2010) (Figure 60g-h).

Around 17 kyr BP, there are again the distinguishable signs of a predominantly human occupation of the cave. In effect, the marks left by man in the concerned levels (s.1 lower part, s.2 l.2 and l.1, s.3 l.1, s.4 l.1, Figure 65.8) are accompanied by those left by animals, always inhabiting this cavity and leaving great amounts of phosphatic sources behind them. We have many traces of charcoal and burnt bones (even of considerable size), but also fauna remains (which we do not know if related to hunting). Charcoals fragments are not in place, or, in any case, no combustion feature was found associated with them. In s.3 l.1 (t.s. d mF II, CM MFT) aggregates showing reddening were however observed (Figure 62a-b), imaginably linked to burning events (Courty, Goldberg and Macphail, 1990; Miller *et al.*, 2010; Shahack-Gross *et al.*, 2014; Rellini *et al.*, 2020), and always accompanied by the presence of burnt bones and charcoals (Figure 62a-d). In section 1 it was possible to see large fragments of bone and charcoal, all brecciated together, although the cementation was probably posterior (Figure 61).

Figure 61 - Section 1, but viewed from the south facing side. The large amount of bones and charcoals present in the lower portion is evident.

The cementation of the lower part of section 1 is similar to that of the upper part (Figure 65.9), perhaps of minor impact. It is evident in the thin section (t.s. a, CW MFT) how this part of the cave was affected by water dripping, if not vadose conditions (Alonso-Zarza and Tanner, 2010b, 2010a). Many consecutive layers of calcite crystals have been deposited (Figure 62e-h), sometimes with euhedral habit. These are the clear signs of a large-scale climate change towards milder and more humid conditions, arising between two dates: that of ~17 kyr BP and that of ~10 kyr BP. More or less exactly at the beginning of the Holocene (Anderson, Goudie and Parker, 2013). The large flowstone at the top of section 4 could also date back to this particularly wet period, but only further investigation would clarify this.

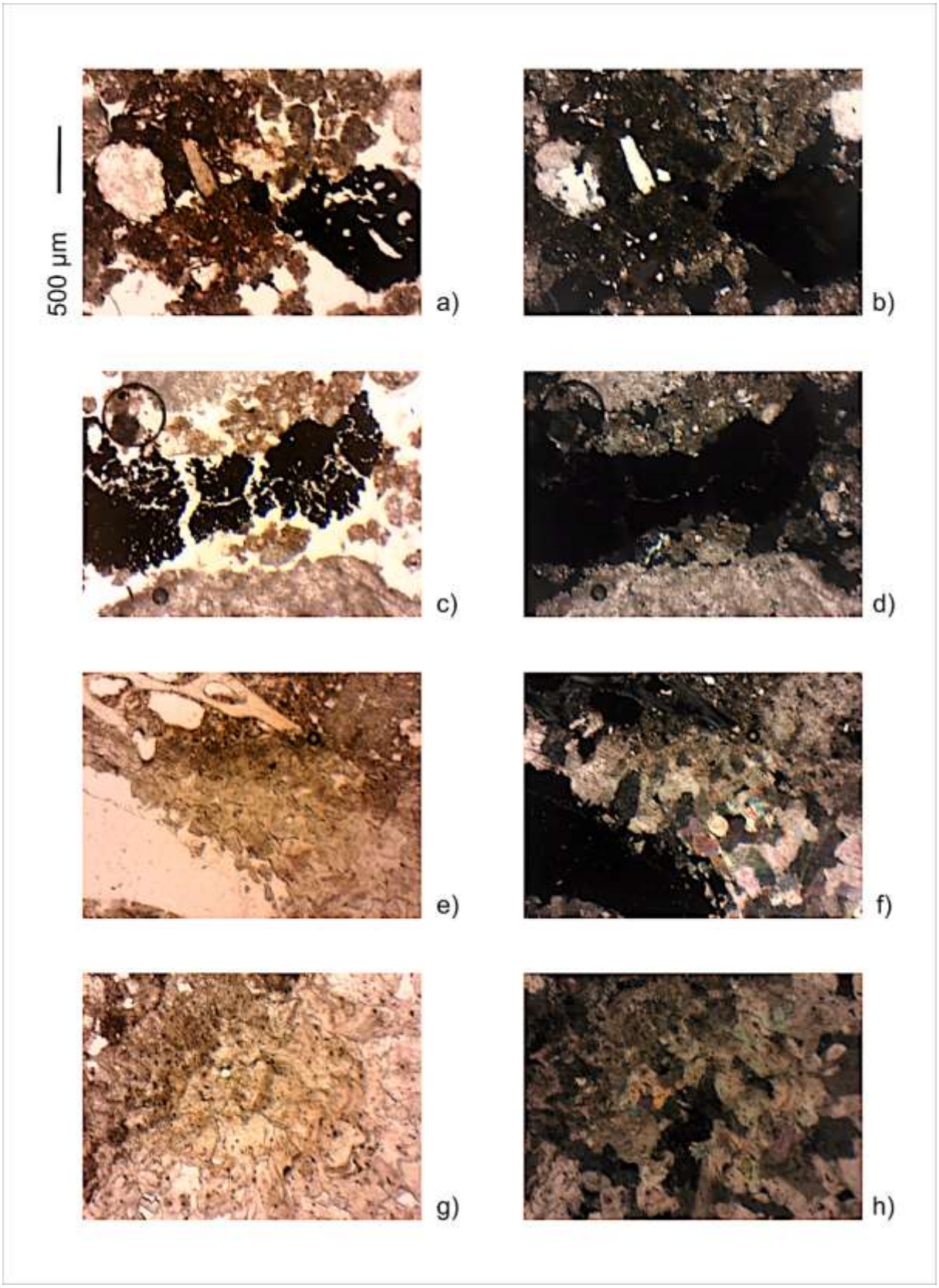

Figure 62 - a-b) On the right an aggregate in t.s. d mF II (CM MFT) showing signs of reddening (although in the microphotograph it is not very evident), while on the left there is a small fragment of charcoal. PPL, XPL. c-d) Still from the same t.s., a large fragment of charcoal and, further down, a fragment of fossiliferous limestone. PPL, XPL. e-f) From the t.s. a (CW MFT). It is possible to see multiple levels of carbonate deposition. In this case, the calcite began to settle on top of an aggregate rich in bone fragments. PPL, XPL. g-h) From the same t.s.. Different levels, with different development of mineral habit, of calcite. PPL, XPL.

Finally, we are convinced that t.s. d mF I could represent nothing more than the reworking of deposits in recent times (with mainly animal occupation features, MOO MFT), also having traces of present-day trampling (Miller *et al.*, 2010).

Conclusions

The cave of Arma degli Zerbi shows a strong animal presence, represented by deposits rich in bones, excrements, products of the diagenesis of these and reworking. Most of these are found towards the cave walls, as if to indicate a preference for more sheltered areas. These same important signs, unfortunately, cancel or overwrite others, making it difficult to clearly and safely read these deposits.

The traces left by the animals are present in practically every section and level of the stratigraphy studied, while the certain signs of a human occupation are more limited: only three episodes have been recognized, giving the impression to occur within a pattern that repeats itself over time.

Alongside these, however, there are also indications of the climate fluctuations occurring outside the cave: wet events around MIS 5 (Figure 63.1) and perhaps the traces left by an Interglacial in MIS 3 (Figure 65.7), cold events perhaps at the beginning of the Last Glaciation and at the beginning of the LGM (Figure 64.4 and Figure 65.7), and finally the establishment of humid phases with the Holocene (Figure 65.9).

Figure 63 - The figure (the first of three) shows the deposits of the Arma degli Zerbi cave considered, divided by the relative chronology proposed. From the oldest to the most recent levels.

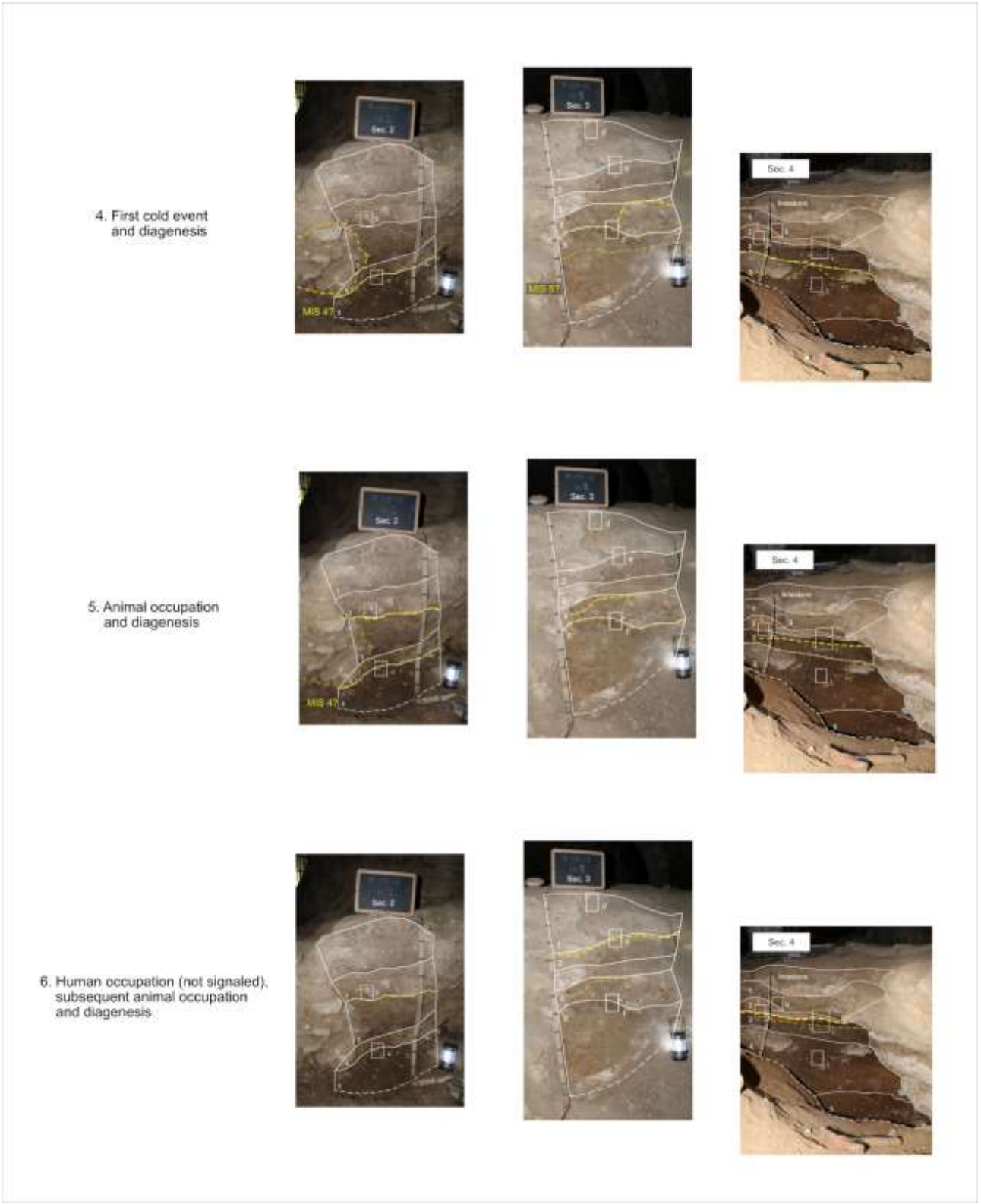

Figure 64 - The figure (the second of three) shows the deposits of the Arma degli Zerbi cave considered, divided by the relative chronology proposed. From the oldest to the most recent levels. "Not signalled" is to be considered as not indicated in the figure.

Figure 65 - The figure (the last of three) shows the deposits of the Arma degli Zerbi cave considered, divided by the relative chronology proposed. From the oldest to the most recent levels.

Caverna delle Fate

Discussion

The Caverna delle Fate cave is certainly a very complex environment and, although only the deposits of corridor 3 have been studied in depth, it has allowed us to have satisfactory results. The sediments present in this area of the cave cover a period of time which is assumed to extend between the end of MIS 5 and the end of MIS 3 (Psathi, 2003). Unfortunately, the absence of new datings is very noticeable, especially when trying to give a paleoclimatic interpretation of the infillings. This also because in such a limited space, well represented by the three stratigraphic sections, the climatic conditions of the past would seem to vary drastically and we cannot be so sure of this happening also in a limited amount of time. In any case, gaps due to erosion are certainly present, but, they are presumed not to cover too long periods of time.

As anticipated in the results (page 106), the micromorphological analysis permitted the division of the Caverna delle Fate deposits into six different microfacies types (MFT), based on their peculiar features and the interpretation of the results. These are:

1. Strongly cemented deposits (SC): FA 3, FA 4, FA 6, FA 9a;
2. Partly cemented deposits (PC): FA 9b, FA 11;
3. Reddish brown deposits (RB): FA 12, FA 13a, FA13b, FB 3;
4. Cave wall deposits (CW): FB 2.
5. Pale yellow deposit (PY): FC 1.
6. Laminated silt (LS): FC 2.

Thus, going in chronological order and starting from the oldest deposits studied - therefore starting from the lower part of the FC section - it is possible to observe when the cave was still an active karst, as already mentioned by Bichet (1987). This aspect can be easily understood in the field and, later, it was also confirmed in thin section. Recognized sedimentary structures indicate a good amount of water availability, but with rather low deposition energy (Folk, 1980; Nichols, 2009). Although these aspects are quite clear, both in the field and in the thin sections, previous authors (Bichet, 1987) have interpreted these same signs as characteristic of periglacial conditions,

finding vesicles and coatings to support this thesis. On this aspect we do not agree, neither in the description of the features themselves. What this author described as coatings are actually silty clay laminae (Figure 66c), typical of a sedimentary environment, pointing to an increasing energy dispersion of the flow runoff (Nichols, 2009; Goldberg and Macphail, 2013; Stoops, Langohr and Van Ranst, 2020). The grain size, the XRD and the micromorphological analysis tell us how these are deposition laminae rich in quartz silt and cyclically fining up to become clayey. Therefore, it can be said that the deposition occurred during a rather humid period, characterized by seasonal alternations, but always wet and relatively warm (Nichols, 2009; Goldberg and Macphail, 2013). Like other authors before us (Bichet, 1987; Amandola, 1995), we feel quite confident in confirming that the deposition took place around the last interglacial (MIS5e). From the study of the thin section it was also possible to distinguish traces of desiccation in level 2, perhaps indicative of when the cave became a passive karst and, anyway, indicative of a relatively dry period (Laminated silt MFT, LS).

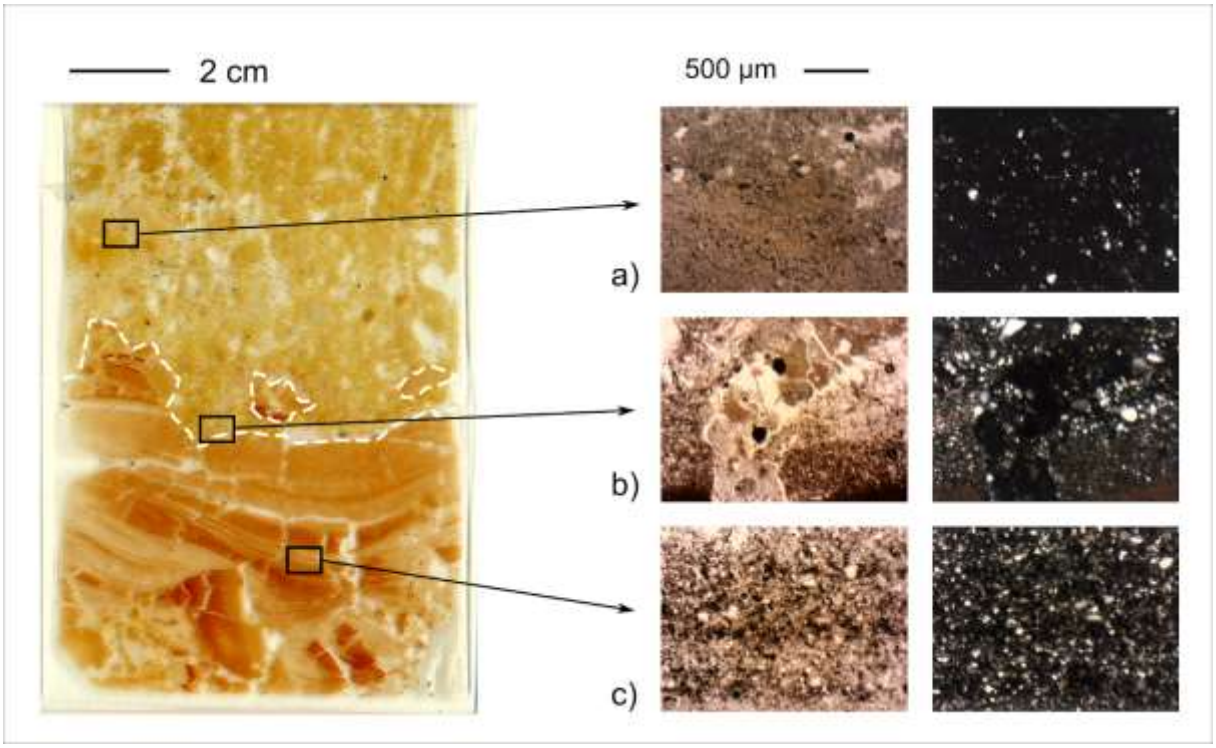

Figure 66 - Already from the FC thin section it is possible to notice the transition between level 1 and 2. The limits and fragments belonging to level 2 within level 1 are marked with a white dashed line. A) Level 1 is characterized by the presence of coprolites, one of which is also quite large, partly visible in the microphotograph. PPL, XPL. b) In the microphotograph it is possible to see the visible signs of the erosion that occurred at the contact between the two levels. In this case the different silt laminae are fragmented and mixed with aggregates from the top. PPL, XPL. c) In this case, the different silt laminae are shown. PPL, XPL.

The transition between level 2 and level 1 of the FC section appears sharp, with fragments of the respective two levels (totally different from each other) mixed together (Figure 66, Figure 66b), indicating a probably important erosional event that changed completely the cave environment. The very fact that immediately after a drying event an erosion occurs, suggests conditions of rhexistasy (Erhart, 1955; Moncel *et al.*, 2015), probably associated to the onset of the early episodes of the Last Glaciation. If the previously recognized sediments had pure geogenic characteristics, now we see an important contribution of biogenic elements: the large quantity of phosphates - detectable in the general appearance of the micromass and aggregates -, the advanced state of alteration given by the organic matter diagenesis, together with the presence of excrements (Figure 66a), confirm this fact (Karkanas *et al.*, 2000; Bergadà, Villaverde and Román, 2013; Brönnimann, Pümpin, *et al.*, 2017; Karkanas and Goldberg, 2018). The advanced state of alteration of the various elements, however, cannot occur if not in the presence of humidity (Pale yellow deposit MFT, PY) (Rellini *et al.*, 2013; McAdams *et al.*, 2020).

Unfortunately, it is not possible to recognize the exact contact and the consequent relationship between the highest levels of FC and the lowest levels of FB and FA, but the change is distinct.

Another aspect addressed by Bichet (1987) is that of the comparison between the granulometry analysis results obtained from the three different stratigraphic sections. He asserts that the grain size of FC compared to that of FA and FB is very different, and that the latter's (both FA's and FB's) is very homogeneous. We conducted the same analysis, still not using any acid or hydrogen peroxide, and, together with the field study, we have come to the conclusion (plain to see in Figure 44 and Figure 45) that it is not the case. Some of these same analysis helped in better understanding the processes at the base of the creation of these deposits, as they will be presented later.

It is interesting to see how the lower levels of FB and FA (FB 3, FA 13, FA 12) fall within the same MFT: strongly cemented deposits microfacies type. This is not only supported by micromorphological analysis, that still was indispensable in the final interpretation of the data, but also by grain size and XRD analysis. As already mentioned in the results section (*X-ray powder diffraction*), these are the only decalcified levels among those investigated (FB3 was not examined, though). This phenomenon can be explained by two different, yet linked, processes: waterlogging and diagenesis (Courty, Goldberg and Macphail, 1990; Mallol, Cabanes and Baena, 2010; McAdams *et al.*, 2020). In the thin sections many phosphatic pedofeatures are reaction rims, found along carbonatic minerals and rock fragments (Figure 67a), picture of the strong weathering, culminating in the complete dissolution of the rest of the carbonatic materials and micromass (Mallol, Cabanes and Baena, 2010). Beside this, waterlogging, or at least water saturation of these levels, left behind characteristic elements, such as manganese (Figure 67b-c), iron and clayey

pedofeatures (Figure 68a). In one case, one clayey pedofeature (in FA 13b) and a peculiar phosphatic coating (in FB 3) also indicate two previously exposed surfaces (Goldberg, 2000; Goldberg, Berna and Chazan, 2015) (Figure 68b-c).

The FB 3 grain size analysis results are not present, but they are for the FA levels section and they show almost homogenous results: the coarse fraction seems missing in all of them. Despite this, we know from field survey of the presence of limestone boulders marking a separation between FA 12 and FA 11. At this contact we see many differences: granulometric, mineral and the pedofeatures occurrence. All these aspects, together with the presence of limestone boulders, would seem to point towards a total change in the cave environment. What until then had been a karst no longer active (it is no longer active since FC 2, we assume), but still influenced by groundwater, becomes arid. Consequently, the whole cave must readjust according to this new balance of moisture. It is known that cave ceiling breakdown events can occur in these situations, due to drying of the sediments (Gillieson, 1996). In support of this thesis there are figures linked to water saturation and, beyond this limit, only signs of water dripping, pointing towards a vadose situation (Gillieson, 1996; Alonso-Zarza and Tanner, 2010a; Armenteros, 2010).

The total great amount of phosphates in these deposits also suggests a great input of organic matter since the very beginning of the deposition (Karkanas *et al.*, 2000; Goldberg, Berna and Chazan, 2015). In all this, however, the thin section sampled from FB 3 shows slightly different aspects from those of the other members of this MFT (e.g. microstructure and some pedofeatures), but despite this we are convinced that they are still the product of very similar conditions, i.e. moderate and wet environments (Nejman *et al.*, 2017, 2018). There is only one exception: the presence of carbonate pedofeatures. Nevertheless, these appear to be the outcome of subsequent water dripping events, affecting also other levels in the cave.

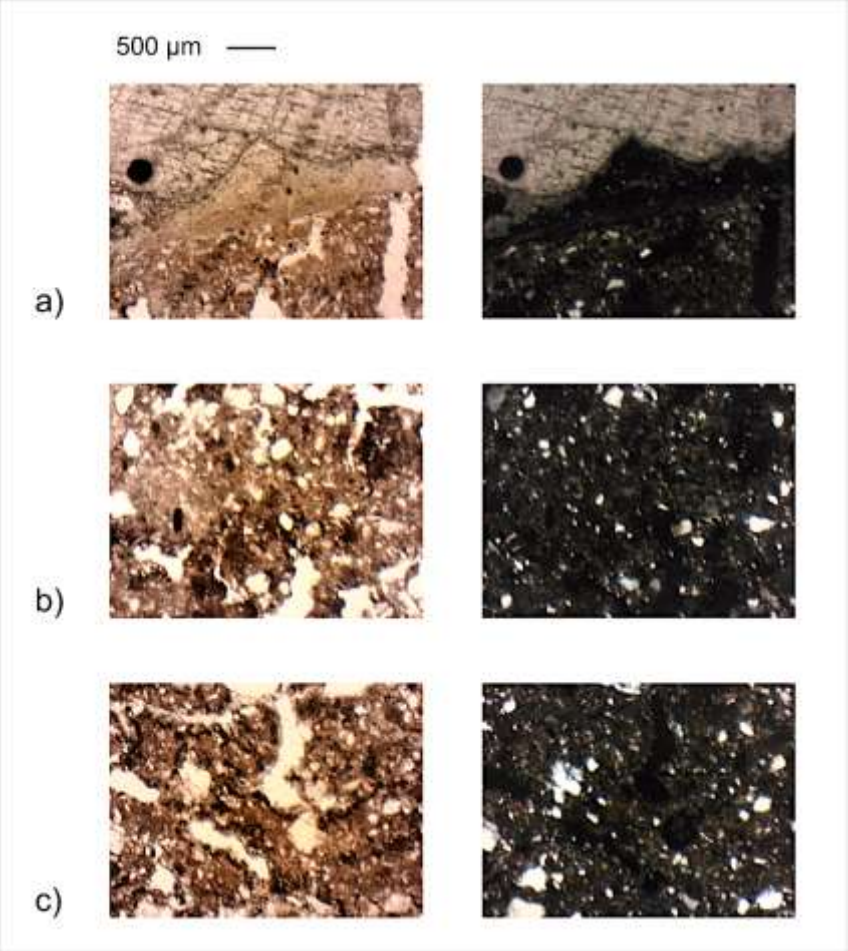

Figure 67 - a) In the first microphotograph it is possible to see a reaction rim on a big grain of calcite. T.s. FA 12. PPL, XPL. b) Mn hypocoatings in t.s. FA 13a. PPL, XPL. c) Mn hypocoatings in t.s. FB 3. PPL, XPL.

A very interesting aspect of this cave is the recurrence of reddish rounded or subangular aggregates, found in different levels of the FB and FA section (Figure 69). These were already recognised and studied in the previous bibliography (Bichet, 1987), where they were interpreted as small aggregates deriving from the soils above the cave. This origin is particularly evident in the FB3 thin section, where there is a sufficiently large aggregate to allow a more detailed observation. This permitted to find many aspects similar to those described by Rellini *et al.* (2015) in soils developed on the Manie Plateau, the typical *terra rossa* soils. These fragments are found in many levels, but have been recognized only in thin section. The infiltration of soil fragments is not uncommon and can be attributed to different agents (water transport, simple gravity, erosion, even earthquakes) (Gillieson, 1996; Courty and Vallverdu, 2001). In this case, we can merely see how their presence in these deposits confirms their relative dating: undoubtedly FB and FA stratigraphic sections can be dated to times subsequent to the last Interglacial, to which the genesis of these soils is located (Rellini, 2007; Rellini *et al.*, 2015).

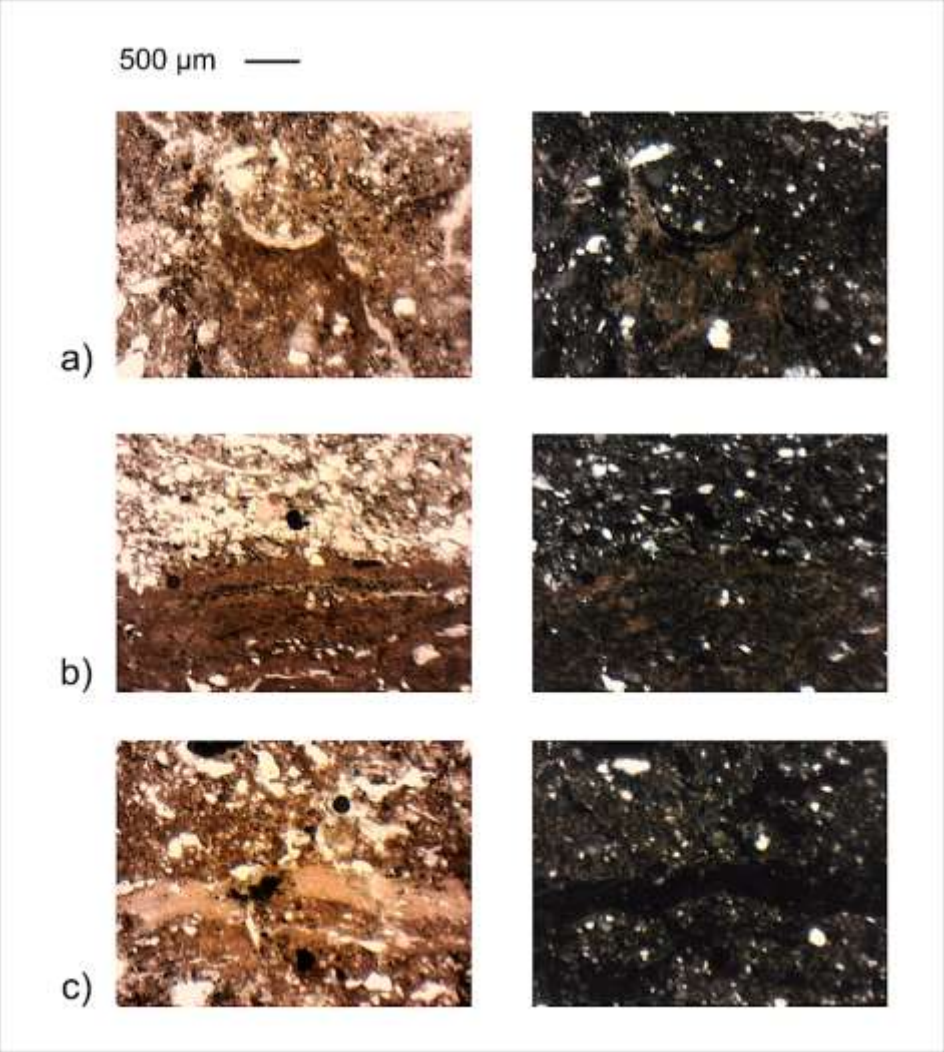

Figure 68 - a) Microphotograph of one of the different clay pedofeatures present. In particular t.s. FB 3. PPL, XPL. b) Part of the thick clay coating in FA 13b indicating a previously exposed surface. PPL, XPL. c) Only part of the cryptocrystalline phosphatic coating present in t.s. FB 3, always indicating a previously exposed surface. PPL, XPL.

Finally, in this MFT there are different signs of animal and human presence, in different absolute and relative quantities. Taking into consideration the fact that presumably, given the post-depositional processes identified, most of these traces have been lost, it is not possible to distinguish with unquestionable certainty when the cave was occupied by fauna or by man, maybe these two overlapped, in time and space (Morley *et al.*, 2019). Traces such as bones or coprolites (even with bone remains inside them) are always found in the samples, and so are small fragments of charcoal. The latter, along with burnt bones and even aggregates bearing traces of burning, on the other hand, are particularly concentrated in the thin section FA 13a (Figure 70). We know from previous works (Echassoux *et al.*, 1989; Psathi, 2003) that three hearths had been found, but we do not know at what depth. By crossing these two pieces of information, we can thus assume that "*foyer 1*" was at the same level as our level 13 (approximately around 20 cm from the present-day ground surface).

From all that has been asserted so far, it can therefore be assumed that the deposition and diagenesis of this level mainly took place during the substages of MIS 5, from MIS 5d to MIS 5a, but probably before the start of MIS 4.

A separate discussion must be made for level FB 2 (MFT Cave wall deposits, CW). There are many aspects, highlighted by the micromorphological analysis, delivering a portrait of, probably, different periods. It is a level placed below the cave wall and along a preferential passageway for the supersaturated carbonate waters, as confirmed by the drapery speleothem above. The oldest elements in this MFT are the aggregates encapsulated within the calcitic palisade fabric (Figure 71b). These aggregates show the same characteristics as those from the previous levels (levels 12 and 13 of FA, in particular), and few not yet described or found elsewhere. A striking example is the presence of an aggregate exhibiting a silt capping (with few sand size quartz fragments in it) (Figure 71c), that in no other sample it was possible to observe, this also counts for few big bone fragments (Figure 71d). This would appear to be the last incomplete information after the removal of large amounts of deposit. Thus, the picture we obtain is that of a certain erosion of older deposits and of cold conditions (silty sand capping, (Gillieson, 1996; Van Vliet-Lanoë and Fox, 2018). The deposition of calcitic secondary crystals would seem to have acted as a seal on aggregates, in fact, there are almost no signs of influence exerted by carbonates on them. Only in few and limited areas a slight calcitic impregnation determines a slight transition to a weakly developed crystallitic b-fabric, in the others calcite does not seem to impact the elements appearance (Figure 71b). The genesis of these calcitic features is more recent and probably attributable to more than one event, given also the different layers and the different development of the crystals involved (Alonso-Zarza and Tanner, 2010a).

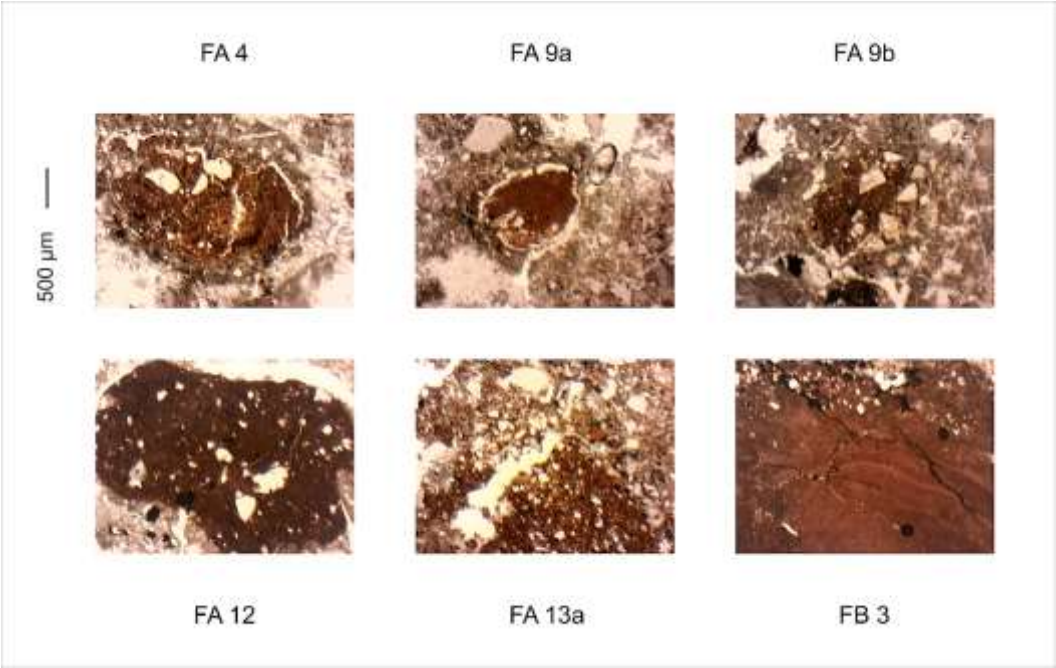

Figure 69 - Some examples of terra rossa *fragments. The names of the thin section of origin are reported.*

It is interesting to note how the crystals always grow in the opposite direction with respect to the aggregates, as these could be used as surfaces of growth, and always towards the water passageways. This can be interpreted as a seasonal carbonate deposition, with water more or less available and more or less saturated in carbonates (Alonso-Zarza and Tanner, 2010a, 2010b). The presence of big bones probably attributable to big mammals was already verified by Psathi (2003) and Valensi and Psathi (2004) that hypothised *U. spelaeus* exploiting this cave as nursery and/or den for short periods of time.

Unfortunately, it is not possible to assign an exact temporal frame to this layer formation and diagenesis: its development can only be placed after the previous MFT's levels sedimentation and before the carbonates rich levels deposition (thus before level 11 accumulation).

The net limit existing between FA 12 and FA 11 is also partly attributable to an erosional event, as it is easy to understand from the outline of the latter. Also the French authors recognised the presence of a lacuna somewhere in the middle of FA stratigraphy (Bichet, 1987). In fact, it is not possible to exclude that part of the aggregates recognized in FB 2 came from a level previously placed at this height. Nevertheless, levels FA 11 and the lower part of FA 9 (divided by a flowstone, identified as FA 10) have many aspects in common, so much so that they both fall within the same MFT (Partly cemented deposit, PC) (Figure 72).

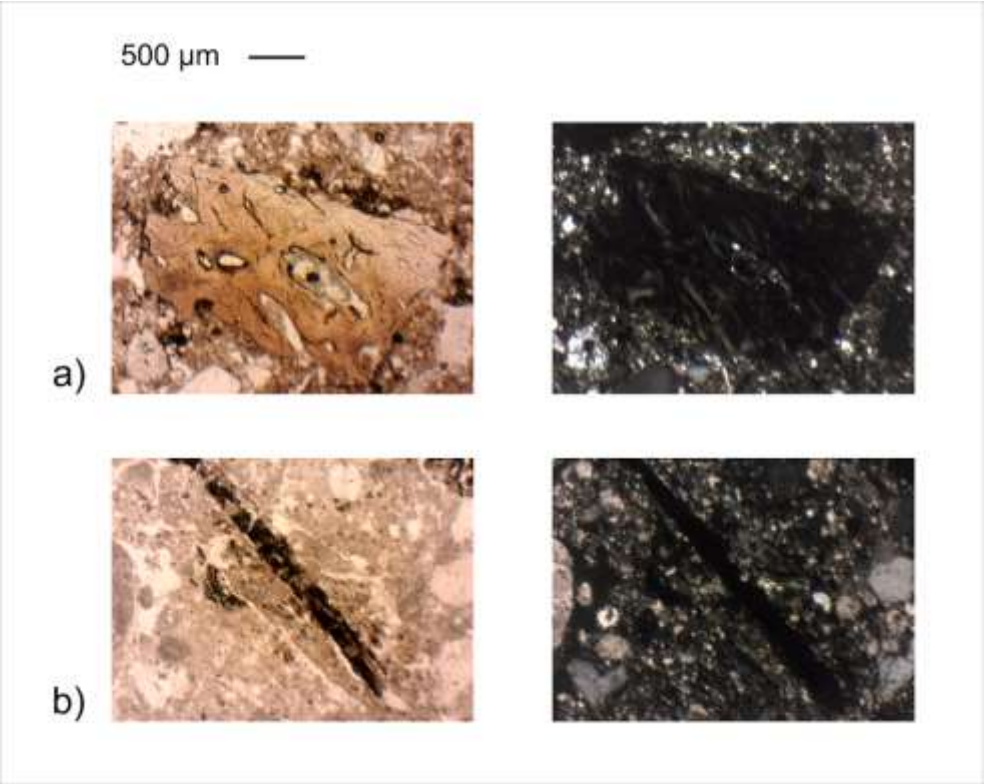

Figure 70 – Microphotographs of t.s. FA 13a showing two examples of the anthropogenic material found in this thin section. PPL, XPL. a) A bone fragment showing signs of burning. b) One thin charcoal fragment. PPL, XPL.

These common aspects include the mineral components (detected by the XRD analysis) and some characteristics identified by the micromorphological analysis: microstructure, traits of the micromass, pedofeatures. The microstructure - with those types of aggregates, voids and their arrangement -, the micromass nature and the b-fabric seem to point to cold conditions (Van Vliet-Lanoë and Fox, 2018) (Figure 72b-c). Anyhow these aspects would appear to be weakly developed or, at least, partially overprinted by the subsequent deposition of carbonates (Courty, Goldberg and Macphail, 1990; Karkanas, 2002; Barta, 2011) (Figure 72c).

From these layers, calcite starts to be an important part of the micromass (Figure 47). It is interesting to note how, in the case of these two levels, the ratio between $CaCO_3$ and quartz is very similar (Figure 47). From this point a certain degree of cementation starts to take place (as showed by the pedofeatures). FA 11 demonstrates a higher carbonates content than FA 9b, probably attributable to the successive deposition of the flowstone FA 10, enough to lead to the almost complete replacement of hydroxyapatite in favour of calcite in a big bone fragment seen in thin section (Nielsen-Marsh and Hedges, 2000) (Figure 72d). This bone fragment presents many planes perpendicular to the surface, perhaps indicative of the increase in volume caused by calcite deposition (Alonso-Zarza and Tanner, 2010a, 2010b), or, given its preferential orientation, to cold conditions (Van Vliet-Lanoë and Fox, 2018), or even both the situations. Anyway, in general, this

high calcitic content, in the micromass and in the pedofeatures, is probably due to repetitive humid events in vadose conditions (Sancho *et al.*, 2004), alternating with colder ones.

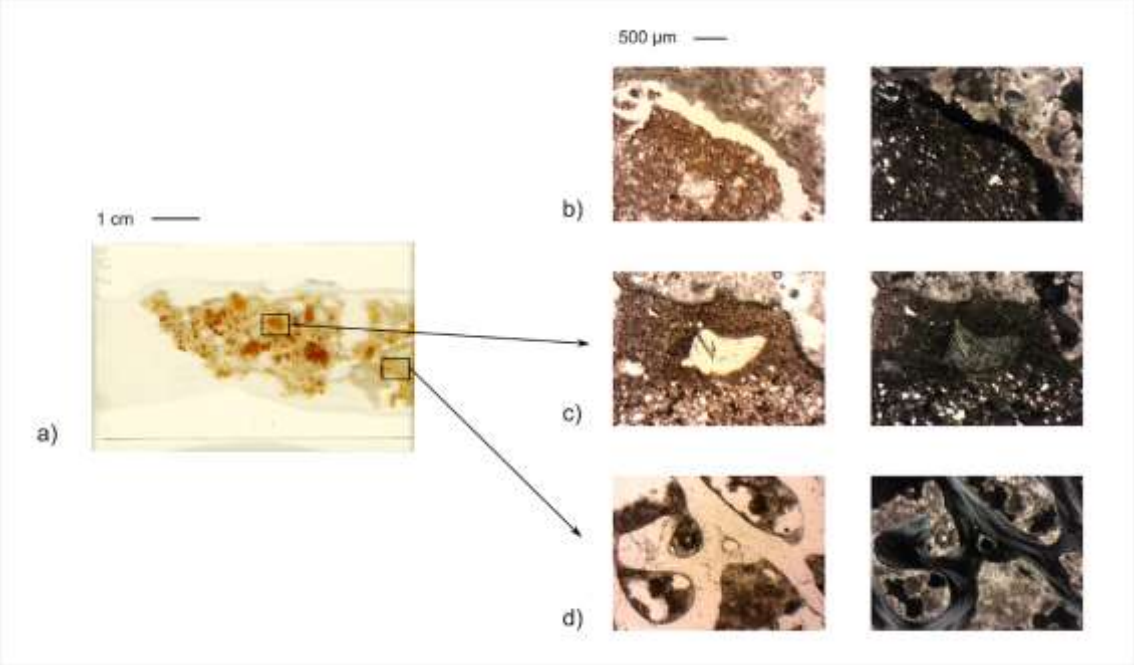

Figure 71 - Level FB 2. a) This is one of the thin sections from this level. b) The microphotograph shows the aggregates surrounded, but in this case, not touched, by the calcitic palisade fabric. PPL, XPL. c) Only part of the silt capping from FB 2, with the detail of the sand size quartz grain. PPL, XPL. d) Particular of a bone fragment in this level. PPL, XPL.

As for the speleothem present between these two levels (and for those present in the following ones, FA 8 and FA 1) we agree with Bichet (1987), who proposed, for its deposition, the onset of a biostasy phase and less rigid climatic conditions, although, for short periods of time (as already supposed, in simmilar contexts by Quinif, 2006). Furthermore, these three speleothems have also been dated. In particular, FA 10 has been dated to about 78 ka BP (Echassoux *et al.*, 1989), therefore in a period that more or less coincides with the beginning of MIS 4.

The levels from the upper part of FA seem to share the same characteristics and origin, falling under a unique MFT, recognised thanks to micromorphology: strongly cemented deposit (SC). The amount of coarse material (pebble and cobble size) increases, while the ratio of quartz to calcite decreases (remaining stable around 40% / 55%). The quantity of carbonates, as fine and coarse material, and as components of the pedofeatures in thin section, is very high. They begin to be part of the micromass, where they are partially masked by phosphates (giving the characteristic crystallitic-undifferentiated b-fabric appearance to the thin sections) (Karkanas and Goldberg, 2018). Also the mineral components of coarse fraction are mostly calcitic, as well as pedofeatures. In these, they take the particular aspect of menisci connecting the aggregates to each other (Alonso-

Zarza and Tanner, 2010a) (Figure 73c). The aggregates are all porous crumbs, rather similar in all the thin sections, which, together with characteristics such as the peculiar voids and the microstructure in general, indicate cold conditions influencing these deposits (Van Vliet-Lanoë, Coutard and Pissart, 1984; Van Vliet-Lanoë and Fox, 2018) (Figure 73a-b). We are convinced that the typical outlines of ice lensing have been modified by the deposition of secondary carbonates: during the crystallization of secondary calcite minerals' increase in volume seems to have affected the general appearance and spatial arrangement of the aggregates, repositioning them. This new repositioning, however, does not seem to have completely obliterated the evidences left by freezing and thawing. Beside this, similarly the clayey pedofeatures (in FA 9a) can be correlated to frost action: Van Vliet-Lanoë and Fox (2018) assert that also the occurrence of clay coatings, in deeper parts of the freeze and thaw affected deposits, can be attributed to fast percolation of particles after melting. Phosphates are also present in good quantities. This is evident in the b-fabric, in the pedofeatures and in the coarse fraction, where they exhibit different aspects.

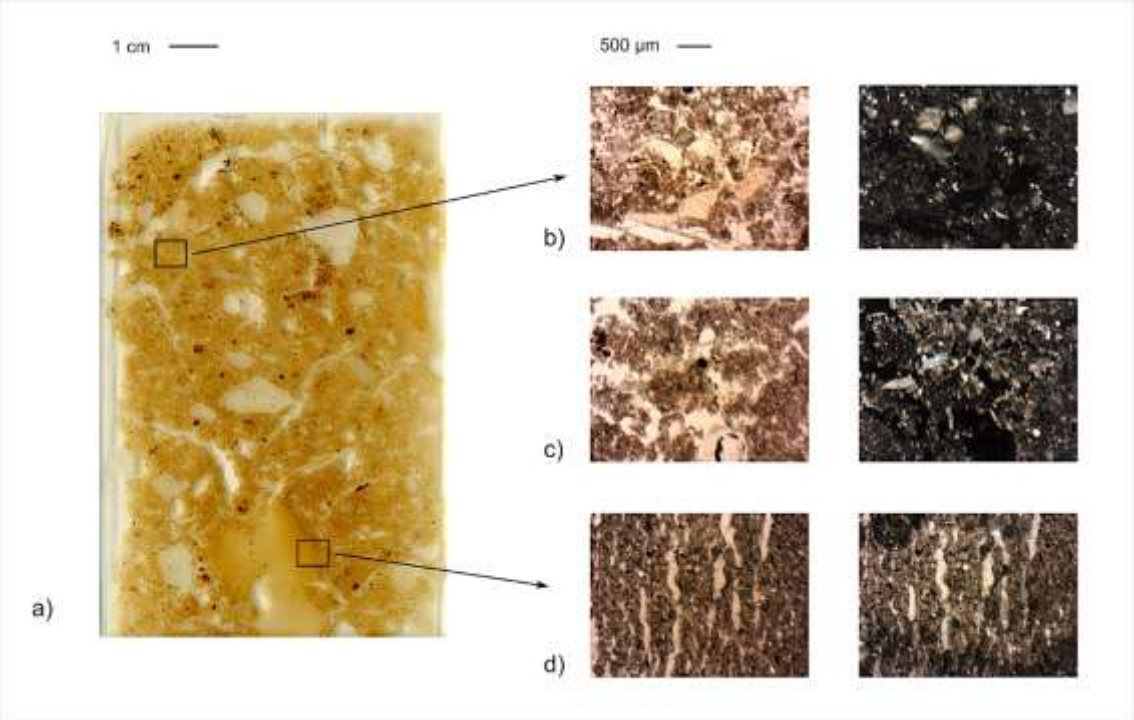

Figure 72 - PC MFT. A) Thin section FA 11. B) Microphotograph showing a portion of t.s. FA 11 with moderately separated granular microstructure. PPL, XPL. C) From t.s. FA 9b, porous crumbs with a platy overprint and calcitic pedofeatures. PPL, XPL. D) A small part of the big bone completely replaced by calcite. In microphotograph are evident the calcitic veins. PPL, XPL.

Some of these are traces left directly by animals or man (coprolites, bones) (Figure 73d-e), others are the by-product of strong alterations undergone by these deposits (Karkanas *et al.*, 2000; Karkanas and Goldberg, 2017, 2018; Villagran *et al.*, 2017) (Figure 73d). Therefore, the meteoric

water is not the only one responsible for diagenesis results. Reactions rims can be found as well here, but the outcome is not analogous to that seen in the lower part of this stratigraphic section. In this case, carbonates are too many to be removed, this thanks to the continuous input from percolation (responsible, here too, for the transport of small fragments of what Bullock (1985) called pedorelicts, i.e. soil relics, of *terra rossa*).

These levels lie between two datings, of which the lowest would always be around 78 ka BP, while the highest would be around 40 ka BP, with a further date (probably FA 8) still around 78 ka BP. Therefore the deposition of this part of the deposits should have taken place between the beginning of MIS 4 and the middle of MIS 3. The signs of cold conditions would thus seem justified. Unfortunately, we are not able to temporally place the deposition of such large quantities of calcium carbonate, in fact this could be even much more subsequent to the sedimentation of the cave deposits studied.

In conclusion, in almost all the stratigraphic units studied, fragments of bones, more or less burnt, of charcoal and excrements were found. Burnt material fragments start appearing from the lower levels of FB and FA, not before. Previously (Bichet, 1987) it had been hypothesized that it was only from these that we could speak of proper archaeological levels and on this we do agree. Unfortunately, it has not been possible to find or theorise with absolute certainty of the primary origin of these elements. The same is true for animal inputs which, however, begin to show from the highest level of FC, thus before man started to occupy this cave. Also in this case, it was not possible to recognize traces of den (however very difficult to recognize in general, (Fosse *et al.*, 2004)). Therefore it is not possible to give an exhaustive answer to the age-old question about the respective behaviour between animals and man that led them to occupy this cave almost simultaneously (Issel, 1908). These two probably used this place sporadically as a shelter for short periods of time.

Furthermore, in the past (Karatsori, 2003; Karatsori *et al.*, 2005) it was hypothesized that very dry episodes had occurred, such as to allow the development of a Mediterranean vegetation outside this cave. From the results we have presented here, we are not so sure. On the other hand, in fact, we believe that a certain amount of humidity has always been present, not only during the deposition of secondary calcite, but also during the developing of other elements recognised during micromorphological analysis (Fe, Mn and clay pedofeatures, but also weathering), that require a certain and prolonged presence of water to develop (Stoops, 2003; Kühn *et al.*, 2018; Marcelino, Schaefer and Stoops, 2018).

Conclusions

The Caverna delle Fate cave is characterized by the presence of very ancient deposits (probably, at least as regards the levels studied here, from MIS 5e to the middle of MIS 3). Unfortunately, a large part of these has been removed and only some parts, heavily calcified, are still present in place. By studying these portions it was possible to propose a partial paleoclimatic reconstruction of the surrounding area and to hypothesize the processes that led to the formation of these deposits, as well as the history of the cave itself.

In MIS 5e, it was still an active karst (MFT LS), but it consequently dried and became an important destination for hibernating animals, in rather humid conditions, not yet influenced by cold temperatures (MFT PY). During the MIS 5 substages, the cave must have behaved like an intermittently saturated zone (MFT RB). So much so as to have large portions of the FA and FB sections decalcified and rich in manganese and iron pedofeatures. All this, always in conditions that are assumed to be mostly temperate (MFT RB), perhaps also with seasonal fluctuations in water supply (MFT CW).

Arriving to a drastic division between the lower and upper part of the FA stratigraphic section, indicating a release from groundwater influence, substituting it with a greater impact of cold and rainwater (probably posterior) (MFT PC). Signs of both cold and vadose conditions would seem to intensify as proceeding upward in FA (MFT SC). All this reaching the top of the section, where a flowstone, interpreted as a sign of biostasy and dated to about 40 ka BP, can be found.

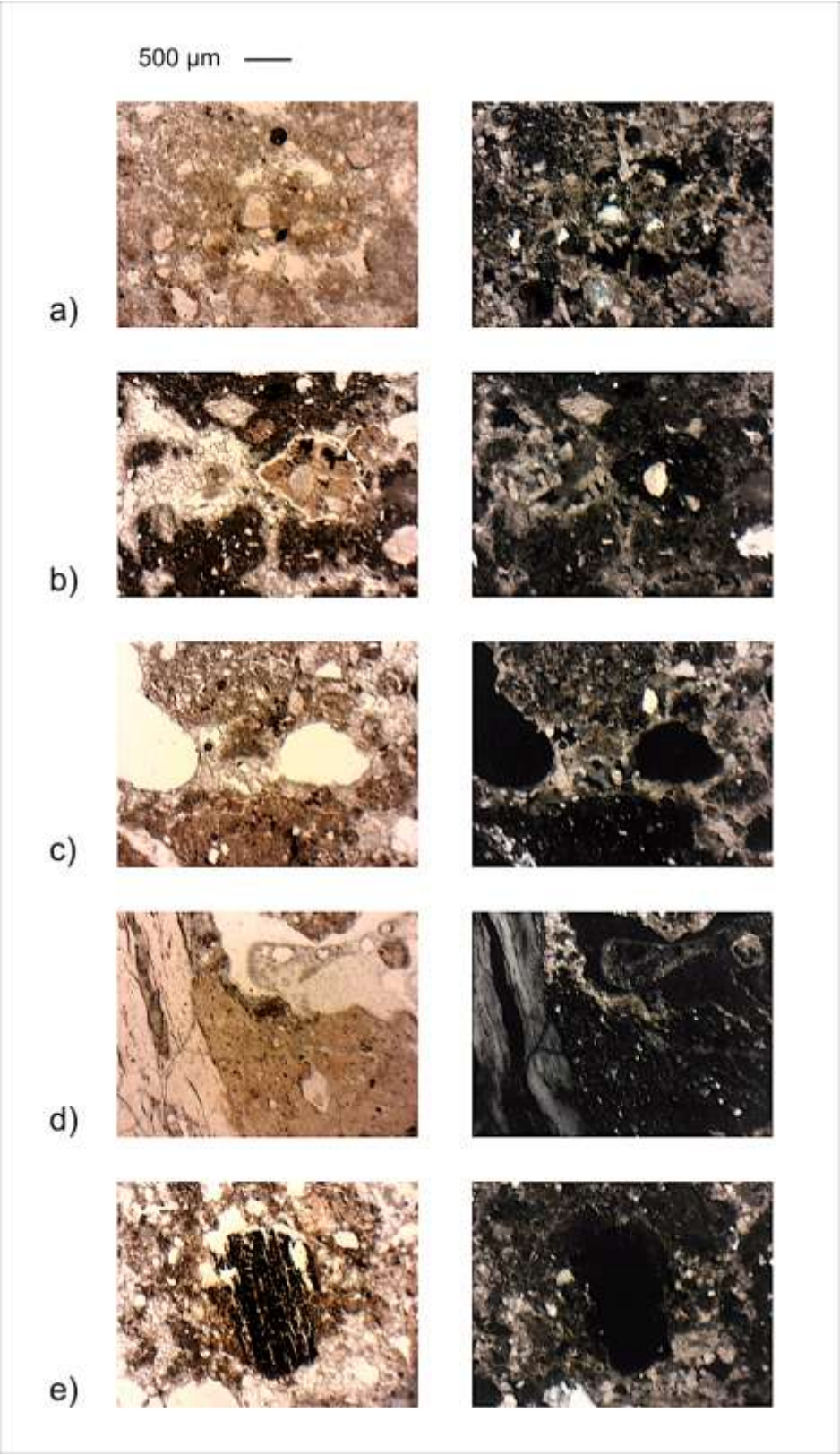

Figure 73 – Microphotographs from SC MFT. A) Porous crumbs aggregates surrounded by carbonates. It is possible to discern a vague platy overprint (t.s. FA 9a). PPL, XPL. B) In t.s. FA 6 it is possible to see the peculiar aggregates' arrangement, the great presence of carbonatic pedofeatures and a single coprolite. PPL, XPL. c) Porous crumbs and calcitic meniscus in t.s. 3. PPL, XPL. D) Part of a bone fragment on the left and the phosphatic material on the right. T.s. 4. PPL, XPL. E) Little charcoal fragment in t.s. 4. PPL, XPL.

Arma delle Manie

Discussion

Thanks to the study of the deposits of this cave we have a detailed picture of the climatic situation from MIS 4, given the dating of level VII speleothem, to MIS 1, given the new series of radiometric datings performed recently. This was possible also thanks to the peculiar appearance of this cave, more resembling a rockshelter rather than a cave.

In fact, it is evident how these deposits have been more subject to the action of the atmosphere and the weathering processes deriving from it, such as freezing and thawing, for example, and not to the usual wetter conditions encountered in caves, as considered by (Goldberg and Macphail, 2013). There was a real "direct contact" with the climatic conditions occurring outside the cavity, leaving less space for biological, chemical and biochemical activities, more typical of almost closed environments. Geochemical activity, for example, is less likely to be encountered in rockshelters and from this derives a different type of post-depositional processes and protection of the elements deposited there (Woodward and Goldberg, 2001; Goldberg and Macphail, 2013). Furthermore, since there is such a large opening to the outside, the contribution of sediments (but not only) from and towards the exterior is different (Woodward and Goldberg, 2001; Goldberg and Macphail, 2013). According to Woodward and Goldberg (2001) it is normal, in fact, in these cases and in particular in the Mediterranean area, to find more reddish deposits, as is actually our case.

As anticipated in the results (page 127, 75), the micromorphological analysis permitted the division of the Arma delle Manie deposits into four different microfacies types (MFT), based on their peculiar features and the interpretation of the results. These are:

- Reddish brown deposit MFT (RB) (thin section GH);
- Dark, cemented deposit MFT (DC) (thin sections E and C);
- Reworked loess MFT (RL) (thin sections B and A);
- Brown clay MFT (CC) (thin sections from AM II to AM VI).

Thus, starting from the lowest and oldest level studied (level VI), we find, thanks to the micromorphological analysis, evidences of freeze and thaw cycles (hence the *Brown clay* MFT, that extends up to level II), occurring for long times, so much so that a prismatic microstructure is present (Figure 74b-c) and the bigger elements of the coarse fraction show a prevailing orientation perpendicular to the ground surface (Van Vliet-Lanoë, Coutard and Pissart, 1984; Van Vliet-Lanoë

and Fox, 2018). This is also made possible thanks to the silty loam texture, that facilitates the expression of these signs (Van Vliet-Lanoë, Coutard and Pissart, 1984). Another aspect that is highlighted is that of the presence of water, indispensable for the development of these particular aggregates (Van Vliet-Lanoë, Coutard and Pissart, 1984). This would seem to disagree with the zooarchaeological evidences presented in the past that required a predominantly dry environment (Abbassi *et al.*, 1998; Psathi, 2003). From the XRD analysis, it was also possible to note the presence of minerals that are not commonly encountered in a cave context: in addition to the habitual presence of quartz and calcite, plagioclase and rutile are also present. The latter two are probably deriving from the bedrock, but are generally either not detected or altered by post-depositional processes, which obviously must not have taken place here, perhaps precisely because of the cavity characteristics we mentioned earlier. Limited traces of burning are present (Figure 74c), indicating the presence of man in the cave, imaginably for reduced periods of time (Goldberg, 2000). Traces of animal origin have also been found, but mostly as passage features and probably linked to present-day mesofauna (Todisco and Bhiry, 2008).

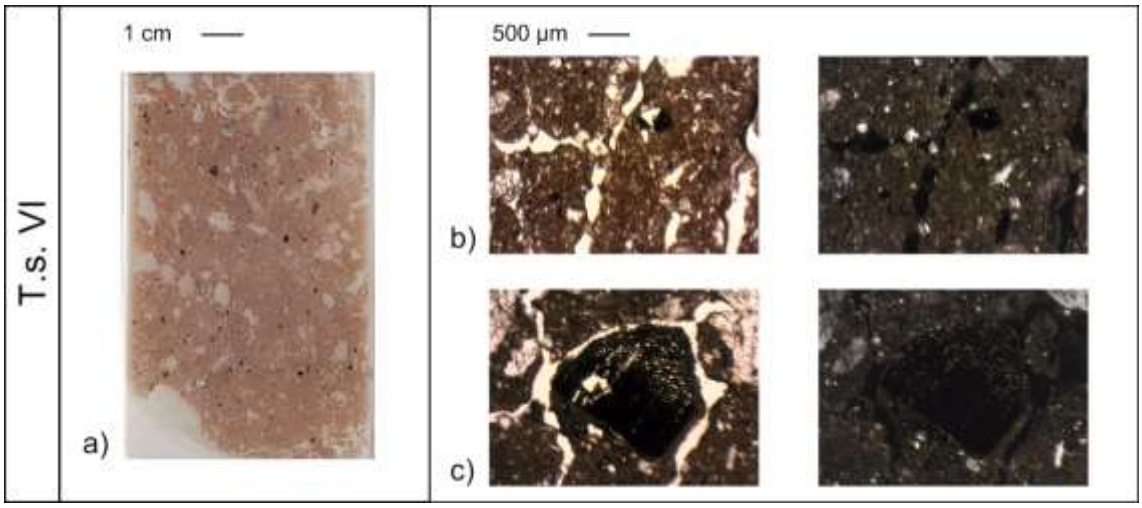

Figure 74 - Thin section VI scan (a) and microphotographs. B) It is possible to see the prismatic microstructure. PPL, XPL. C) It is still possible to appreciate the prismatic microstructure and the presence of a little charcoal fragment. PPL, XPL.

From level V upwards, the situation becomes more homogeneous, with only a few variations. Unlike the previous level, the aggregates and the microstructure turn into plates and platy respectively (Figure 75a and Figure 75d), perhaps due to the distance from the water source and/or to the slower infiltration of frost (Van Vliet-Lanoë, Coutard and Pissart, 1984). These figures are also less pronounced in levels V and IV (Figure 75d), indicating a period with less rigid temperatures, determining less freeze and thaw cycles (Van Vliet-Lanoë, Coutard and Pissart, 1984). The relative quantity of coarse fraction is generally low, although two levels composed of

coarse clasts were noticed in levels V and II. In particular, in level V with limestone cobbles and boulders, in level II mainly with limestone pebbles and cobbles. Given the surrounding conditions and the angular-tabular appearance of these, it is believed that it is to be considered *éboulis* coming from the cave ceiling (Woodward and Goldberg, 2001; Goldberg and Sherwood, 2006). Furthermore, the fact that in Level II the fragments are smaller would seem to indicate colder conditions that have lasted long enough to allow for greater fragmentation (Courty, Goldberg and Macphail, 1990). Only in another case we see the rough elements oriented vertically: we had witnessed this phenomenon in the case of level VI and it is also present in level II.

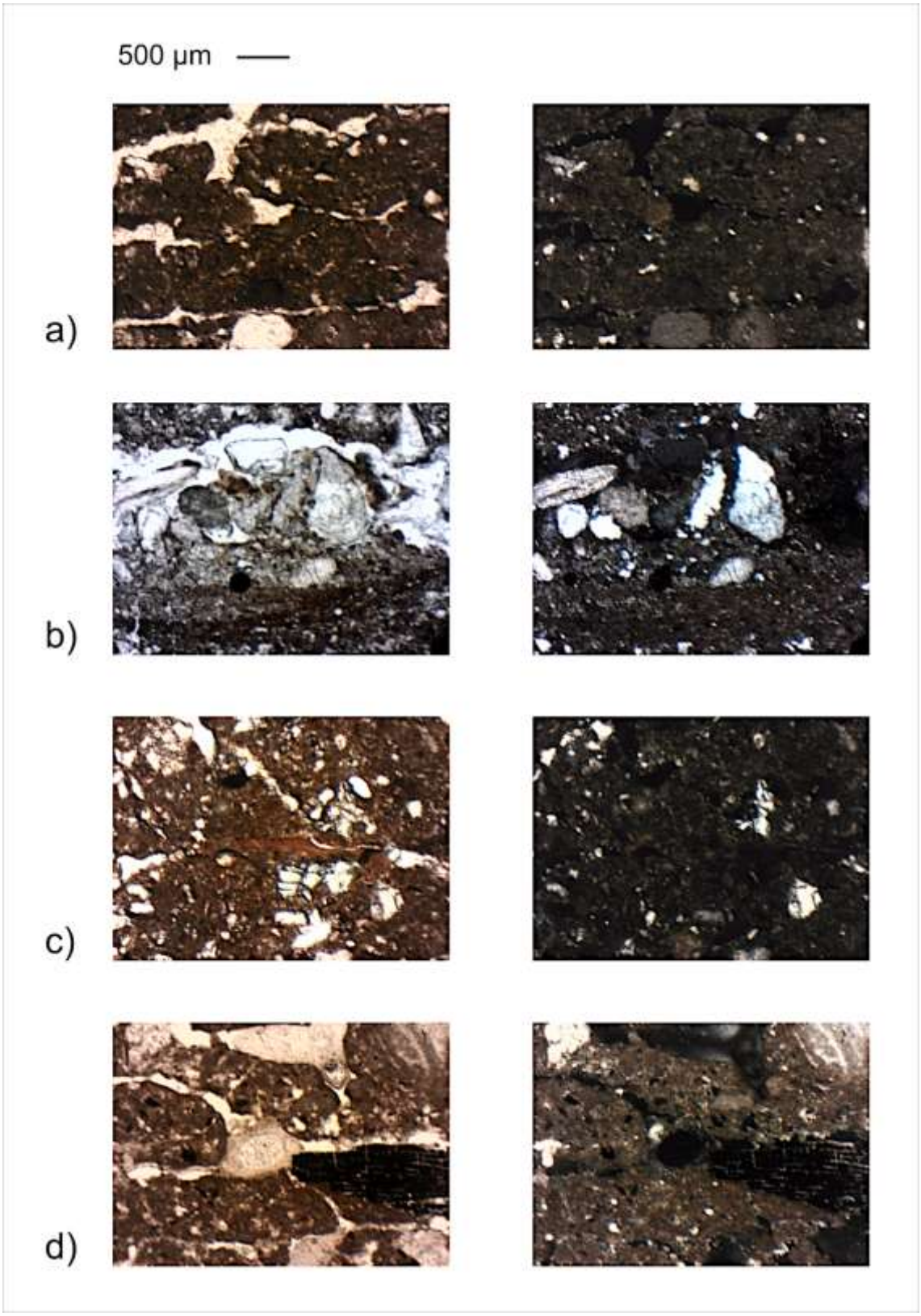

Figure 75 - Microphotographs from the BC MFT. A) The well-developed platy microstructure in t.s. III. PPL, XPL. B) In t.s. II few coarsening up infillings are present. PPL, XPL. C) Pure clay coatings in t.s. V. PPL, XPL. D) A less developed platy microstructure in t.s. IV and, on the right, a charcoal fragment. PPL, XPL.

This phenomenon is due to the pressure exerted by ice growth (Pissart, 1970; Van Vliet-Lanoë and Fox, 2018), therefore still linked to frost action. A further aspect that would seem linked to freezing conditions, would appear to be the presence of a particular type of pedofeature, such as coarsening up infillings (levels II and III) (Figure 75b). These are very similar to those described by Vallverdú-Poch and Courty (2012), associated with the presence of cryogenic modifications. Furthermore, it would seem that, concomitantly with levels V and II, short intervals with less rigid temperatures could have occurred, leading to the formation of silt size limpid clay coatings (Kühn *et al.*, 2018; Stoops, Marcelino and Mees, 2018b) (Figure 75c).

The animal presence in these levels, at least for this part of the cave, does not seem very important (few bone remains and no signs of excrements). As for human occupation, we have traces that are irrefutable (burned bones, charcoal fragments, Figure 75d) but not sufficient to establish the exact location of any hearths or to know for how long they remained in the cave (Morley *et al.*, 2019). In this regard, the previous works (Mehidi, 2005; Cauche, 2007; Djerrab and Camps, 2010) speak of a level with hearths regarding level IV, so it cannot be excluded that much of the material has already been removed.

Furthermore, the studies conducted so far on these infillings had given a chronological constraint different from that thanks to ^{14}C dating. Mehidi (2005) himself asserted that the most acceptable dates among those he had obtained were those of level VII (not reached here) between 60 and 46 kyr BP, while for this thesis level IV was dated to about 38 kyr BP, and level A (placed just above the levels considered so far) is set at around 24 kyr BP. This to underline how the chronological context may be different from that considered in the previous works. Other discrepancies were also noted. In fact, Arobba *et al.* (1976) asserts that in levels VI and V there were two peaks of cold, and between V and IV there must have been a temperate interphase; for Karatsori (2003) and Karatsori *et al.* (2005) the Mediterranean vegetation would seem to be already present (therefore dry and temperate climate); for Abbassi *et al.* (1998) and Psathi (2003) there would have been dry conditions in level VI (but also in IV and II), humid and continental conditions in level V. In addition to realising how difficult it was to reconcile all these data, we are sure that the conditions were actually humid (a certain availability of water is needed for the development of cryogenic figures) (Van Vliet-Lanoë and Fox, 2018) and extremely cold (temperatures around -5 °C are required for the development of these characteristics) (Van Vliet-Lanoe, Fox and Gubin, 2004), with less rigid short periods in levels V, IV and II.

Level I, as well as level A, would seem to have transitional characteristics between the lower and higher stratigraphy part. Unfortunately it was not possible to sample it, given its small size.

As just mentioned, level A presents transitional characteristics between the *BC* MFT (*Brown clay*) and the *RL* MFT (*Reworked loess*, to which it belongs). As it is easy to guess from the name assigned to this last MFT, there are the typical characters left by the action of frost, together with the presence of that particular aeolian sediment called loess. Level A shows a platy microstructure (Figure 76b-c), vertically oriented coarse elements and pedofeatures such as the dusty clay coatings, all typical of cold conditions, such as those already seen for the lower levels (Pissart, 1970; Van Vliet-Lanoë, Coutard and Pissart, 1984; Van Vliet-Lanoë, 2013; Van Vliet-Lanoë and Fox, 2018). Instead, what makes it a loessic deposit is the colour (reddish yellow, 7.5 YR 6/8), the great preponderance of silt size particles, the particular mineralogy that composes it and, finally, the porous aspect (such as to allow insects dug their nests there) (Pye, 1984; Cremaschi and Van Vliet-Lanoë, 1990; Bertran *et al.*, 2016; Krajcarz *et al.*, 2016; Rousseau *et al.*, 2018). In any case, we know that this loess is not a primary loess (Pye, 1984), consequently it could be either a weathered or reworked one, but we are unable to determine this for now. This particular type of deposit indicates cold and dry conditions, with low vegetation cover (Rousseau *et al.*, 2018), and has often been linked to the Last Glacial Maximum, a particularly cold climate peak occurred during MIS 2 (Svendsen *et al.*, 2004; Baumgartner *et al.*, 2014), whose culmination, in Liguria, seems to have taken place between 24 kyr BP and 22 kyr BP (Rellini *et al.*, 2013). The dates seem to coincide, and so do all the other characteristics. Loess tends to be associated with particularly dry periods (Cremaschi and Van Vliet-Lanoë, 1990; Zanchetta *et al.*, 2014) and, in fact, the evidence of freezing and thawing is subsequent, settling on the sediments already in place. Therefore it is possible to hypothesize cold and arid conditions were followed by new cold and moister conditions. Level B would also seem of loessic nature, although more coarse material is present (Figure 76e). In this case, there is no longer a platy microstructure, but crumb and granular, similarly often associated to freezing conditions, as well as dusty clay coatings (Van Vliet-Lanoë and Fox, 2018). Another element that levels A and B share, with very little margin of variation, is that of the results of the XRD analysis. Although the presence of almost all mineral species is easily predictable in contexts such as the one just described (quartz, calcite and even illite), serpentine is the only one whose origins should be investigated deeper. This would also help in better understand and confirm the nature and sedimentation agent of the two stratigraphic units.

Unfortunately, previous studies have always stopped at level I. This due to the fact that those deposits were believed dating back to the Holocene (Arobba *et al.*, 1976), but now we know that it is not the case. We are convinced that the deposition of these two units could be traced back to the LGM onset and culmination: an extremely cold period, certainly arid for a certain interval of time (such as to allow the transport of aeolian sediment), but with more humid phases, that left

behind traces of freeze and thaw. During the deposition of these two levels there would seem to be no traces of human or animal occupation of the cave: perhaps more sheltered places were preferred, or perhaps these traces were present in other areas of the cave and then removed.

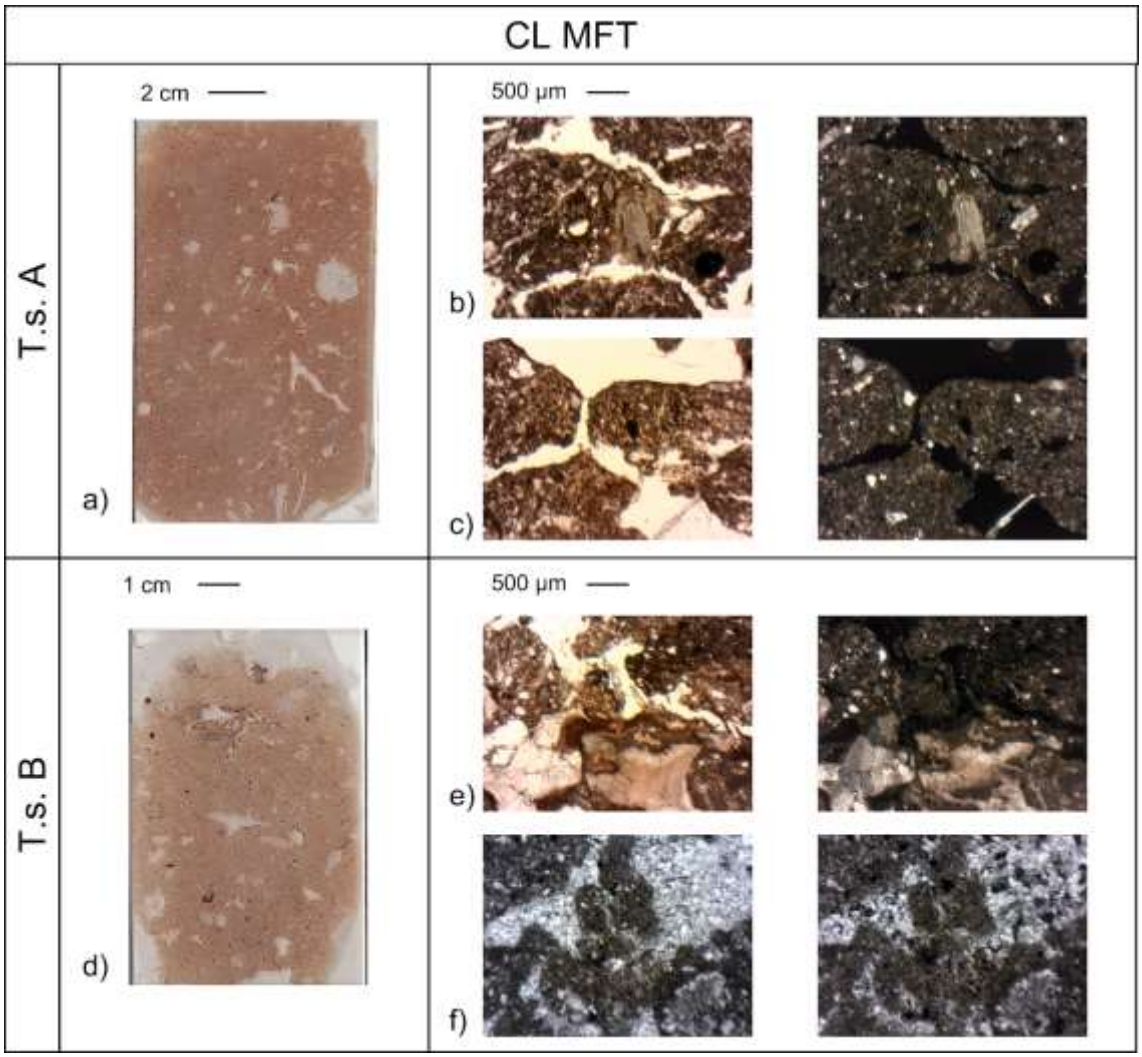

Figure 76 - CL MFT scanned thin sections and microphotographs. B)In this microphotograph the platy microstructure and a little rock fragment showing the peculiar vertical orientation are displayed. PPL, XPL. C)Another microphotograph to present the platy microstructure of the t.s. PPL, XPL. e) One dusty clay coating is presented here. It is also possible to see two sand size rock fragments. PPL, XPL. F) The upper part of t.s. B exhibits a certain degree of cementation. PPL, XPL.

As already occurred in the case of A, also level B presents some transitional characters with the upper MFT (*Dark, cemented deposit* MFT, *DC*). Already from the XRD results it was possible to glimpse an increase in the quantity of calcite which, in thin section, took on the appearance of partial cementation (Figure 76f). Probably a character linked to the onset of wetter conditions and increasing rainfalls (Alonso-Zarza and Tanner, 2010a, 2010b; Ford and Williams, 2013), typical of the arrival of the Holocene. Character that will be emphasised in the following levels.

The transition to this new phase is also underlined by the large amount of coarse material, found in these quantities for the first time. This is mainly belonging to the cobble class in levels C and F, in the case of D there is an increase from the coarse sand up to the pebble class. For D and E, bones and charcoals would appear to be the major accountable (Figure 77b and e), however. This is to further underline the reason for the name of the MFT. Already in the filed it was clear how the main aspects of these units were certainly the dark colour, the degree of cementation and the large presence of biogenic and anthropogenic sediments. In thin section these sediments end up composing almost half of the deposit, thus influencing the other characteristics. This happens for example in the case of aggregates, where, in thin section CD, are dark, with almost undifferentiated b-fabric and with the appearance of granules or crumbs, characteristics that could all be attributed to the presence of a certain amount of organic matter and charcoal (Goldberg *et al.*, 2009; Simões, Carvalho and Tente, 2020). Or as in t.s. E, where the aggregates seem to show traces of burning (McAdams *et al.*, 2020; Rellini *et al.*, 2020). Then hair and one flint fragments are also present. These are the aspects that most influence deposits, but not the only ones worth noticing. In fact, there are traces such as carbonate, ferrous and manganese pedofeatures, and clay coatings, which give precise indications on the climatic condition of the period. The carbonates were probably the first to form, leading to cementation of the deposits. Nevertheless, it is not possible to rule out that there could have been several deposition cycles, even at different times. In the t.s. E it has been seen that these lie beneath the clayey pedofeatures, thus giving a relative chronology between the two (Stoops, 2003). Generally, carbonate cementation is associated with a significant increase in humidity (Alonso-Zarza and Tanner, 2010a) (Figure 77f). So do clay coatings, especially when they are in pure form (Courty, Goldberg and Macphail, 1990). A particular type of clay coatings are those found in the t.s. CD, where they turn from reddish to yellowish moving towards the void (Figure 77c). According to (Courty, Goldberg and Macphail, 1990), they may be associated to clay illuviation, perhaps from the soils above, with a change also in the iron oxidation, responsible for the colouring. These would be the sign of temperate climatic conditions (Courty, Goldberg and Macphail, 1990). Finally, the FeMn pedofeatures, almost always ubiquitous, seem to be present in greater quantities in these units and perhaps highlight the establishment, for not so long periods, of slight hydromorphic conditions (Cremaschi *et al.*, 1990; Stoops, 2003; Stoops, Langohr and Van Ranst, 2020). All these aspects, together with the dating of the F level at about 7.8 kyr BP, would seem to concur in placing these stratigraphic units between the beginning of the Holocene and the end of the Holocene Climatic Optimum (HCO). The HCO has occurred from around 9 kyr BP to 5.5 kyr BP, with a maximum peak at around 8 kyr BP. It is evident how, during this improvement in climatic conditions, human and fauna, occupied the cave, perhaps for longer periods of time, or maybe just more often. Furthermore, the charcoal dated in level F is that of

beech (*Fagus sylvatica*), expanding rapidly in eastern Liguria in this same period (between about 7 kyr BP and 6 kyr BP) (Branch, 2013). This is attributed to increased water availability during summer, absence of winter frost and, to some degree, to human influence (Branch, 2013).

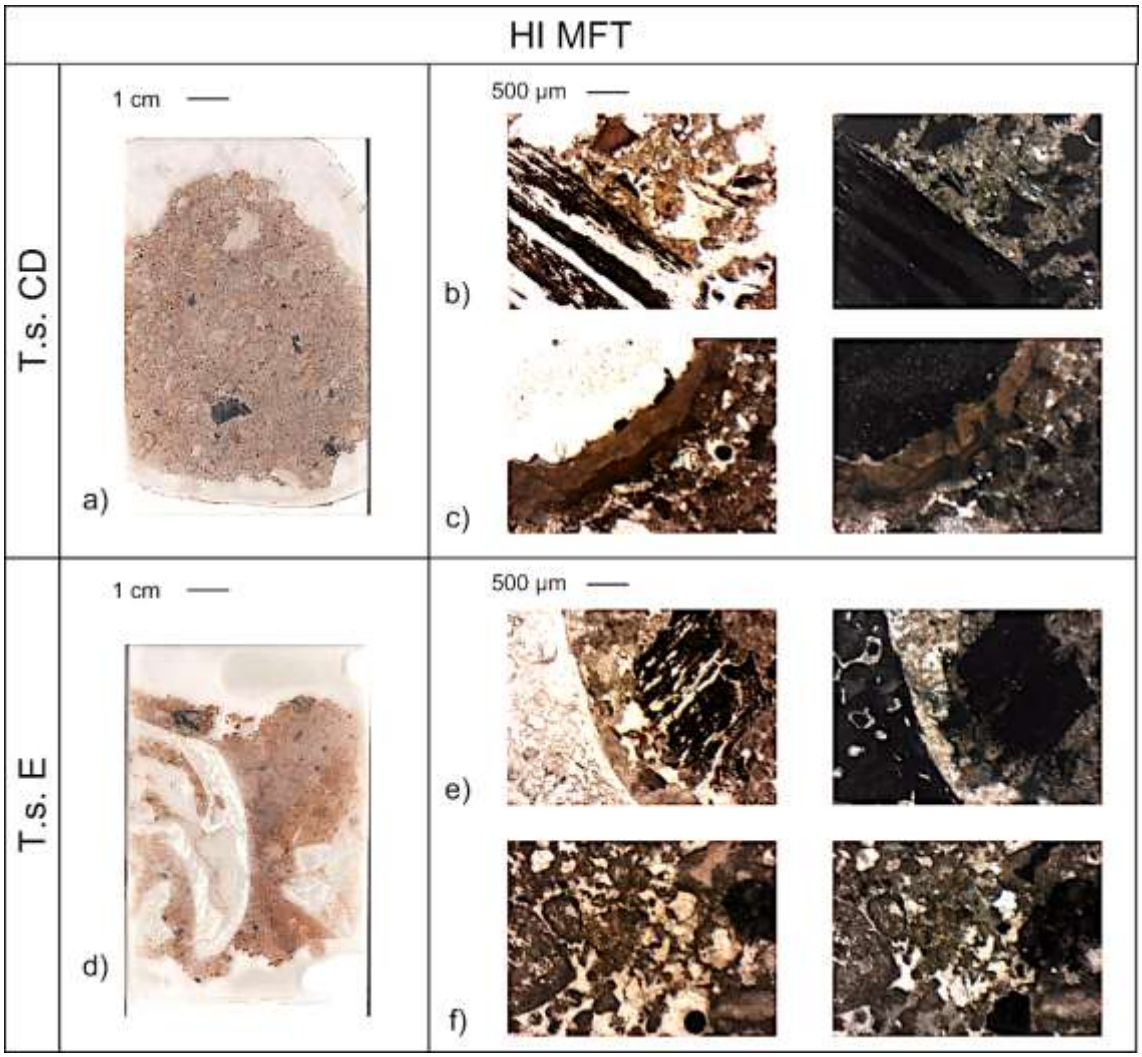

Figure 77 - DC MFT scanned thin sections and microphotographs. A) Thin section CD scan. The aggregates and part of the coarse fraction are recognisable to the naked eye. B) Part of a big charcoal and one little burnt bone fragment. It is also possible to see the presence of porous crumbs. PPL, XPL. C) The dual colour (yellowish and reddish) of few clayey pedofeatures present in t.s. CD. PPL, XPL. D) Thin section E scan. On the left some big bone fragments, on the right part of a jaw and carnivore teeth. E) On the left, part of a big bone fragment, on the right one big charcoal fragment. PPL, XPL. F) Evidence of cementation of this MFT. PPL, XPL.

In reality, we would have expected to see more marked aspects testifying the passage from the Pleistocene to the Holocene, but perhaps these have been masked by the influence exerted by human and biological activity (Angelucci and Zilhão, 2009; Fabio Scarciglia *et al.*, 2009; Herries and Fisher, 2010). Climate change, from what we know, has been fast and has had a great impact on the environment: suddenly the system found itself in a different climatic context and had to retrieve a certain balance (Macklin, Johnstone and Lewin, 2005). If in the sediments from levels

C to F we see a large amount of signs of humidity, increase in rainfalls and the establishment of more temperate conditions, in the levels positioned even higher (from G upward), we see different sedimentation cycles (identified in thin section GH as different microfacies, Figure 78) linked to the transport - by water - of silty and sandy particles, at different energy regimes (Nichols, 2009). The water that until that moment had been stored in the form of ice, started to move seaward, causing sometimes also periodic river flooding, as testified in diverse European areas (Macklin, Johnstone and Lewin, 2005; Roberts, 2014; Campo, Amorosi and Vaiani, 2017). In any case, given the time period (7 kyr BP circa), a vague human intervention by means of clearance of the area cannot be excluded (Branch, 2013). In this same period, in different areas of Liguria, similar phenomena are witnessed (Cruise *et al.*, 2009; Branch *et al.*, 2014).

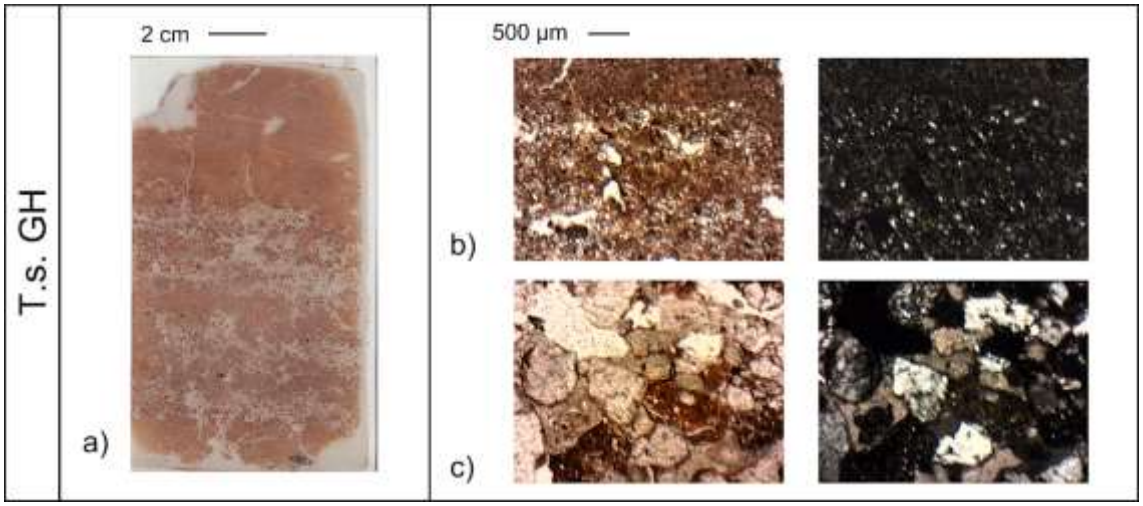

Figure 78 – Thin section GH scan and microphotographs. B) Silty laminae from mF 1. PPL, XPL. C) Single spaced equal enaulic microstructure of mF3. PPL, XPL.

Conclusions

From the deposits from the Arma delle Manie cave, it was possible to obtain a rather clear picture of the climatic changes that took place over a period of time ranging from about 46 kyr BP up to after 7 kyr BP.

In this period of time, the unique physical characteristics of the cavern allowed some aspects to show themselves in the deposits in an unequivocal way: the large opening of the cavity allowed the sediments to be subjected to many and intense events of freezing and thawing, for example. This was certainly the case of the lower levels, from level VI to level II (BC MFT), and also

influencing level A. Always linked to a cold period, but this time more arid, are the levels of loess (reworked or weathered) of levels A and B (RL MFT), dated to about 24 kyr BP, therefore placeable during the LGM. The transition to a more humid and temperate context is well represented on the field: numerous pedofeatures from levels C to F thin sections testify it, in fact (DC MFT). In this case, however, these aspects are masked by a strong human and animal activity that would seem to overprint climatic and environmental traces. The stratigraphic section would seem to end by portraying what must have happened on the landscape at the beginning of the Holocene: outside the cave there is an environment trying to find a balance with the new climatic conditions and -maybe-, at the same time, man begins to exert his strong influence, shaping the landscape (RB MFT).

7. Comparison between the study sites and general conclusions

The results obtained from the study of the deposits of these four caves gives a rather complete paleoclimatic reconstruction and it is significant how some data converge on certain particular conditions (Table 12). In fact, the deposits of these four caves show a good temporal resolution and environmental sensitivity. This can be appreciated, above all, by seeing how long the time span covered by these infillings is. The sedimentation rate varies between the different caves and also within them, but the stratigraphies always seem to be complete. This in combination with the great climatic changes that have occurred inside and outside the study sites and remained fixed in their infillings. It is evident that it was possible to have a good resolution also from this point of view: the sediments were very sensitive to climatic conditions and have kept their evidences for all this time. Obviously some cave deposits have shown a higher sensitivity and resolution than others, but the fact of having data available from more than one site at the same time has allowed to reach greater detail, but not only. We often talk about how certain local factors can influence the data obtained from the study of cave infills and therefore weaken the proposed reconstructions (Courty and Vallverdu, 2001; Woodward and Goldberg, 2001; Goldberg and Sherwood, 2006). Thanks to the study of multiple sites and teamwork with scholars from different disciplines, we are convinced that these components have been limited as much as possible. Proof of this is the fact that in all sites (even distant from each other) some conditions are mirrored, thus strengthening the results obtained.

We have seen how the deposits from inside the caves are a set of sediments with different origins: in all the caves we have found geogenic, biogenic and anthropogenic sediments. Knowing how to recognize them has also helped us to give a more solid reconstruction of the events that have taken place. It was also possible to distinguish elements coming from within the investigated karst system or from outside of it, as well as to distinguish between primary or secondary elements and how the post-depositional processes took place. In each cave the relationships and ratios between these classes are different, making each one unique in its kind and therefore requiring a tailor-made investigation system (White, 2007). Similarly, we are convinced of what Goldberg and Macphail (2013) already stated: "site formation processes are case-specific".

The most ancient deposits seem to be those of the caves of Caverna delle Fate, Tana di Badalucco and perhaps also Arma degli Zerbi, probably dating back to MIS 5. Unfortunately there is no way, at the present time, to be sure of this statement, since it was not possible to perform systematic dating on the entire extension of the infillings. Anyway, all three of these caves share

the presence of sedimentary structures or signs indicating the presence and influence exerted by water. An example of this is the Caverna delle Fate cave (CdF from now on), still in its active karst state, showing a well-stratified deposit of silt and clay, followed by humid conditions, showing only partial release from the influence of water. At the Tana di Badalucco cave (TdB) the silt-rich deposits show the presence of clayey pedofeatures and in Arma degli Zerbi (AdZ) there are lenses of silty material, probably of fluvio-karst origin. Therefore we know that temperate and humid conditions must have been present throughout western Liguria. This was already suggested in previous works, on these and other sites in this area (Valensi and Psathi, 2004; Kaniewski, Renault-Miskovsky and de Lumley, 2005; Onoratini *et al.*, 2012; Moussous, Valensi and Simon, 2014; Defleur and Desclaux, 2019; Brugal *et al.*, 2020). They state the presence of similar conditions, although, with the transition to MIS 4, they infer the occurrence of greater storminess and runoff (Bardají *et al.*, 2009), situations not particularly evident in our deposits.

These conditions seem to change radically with the onset of the Last Glaciation (MIS 4). This, at least, as far as TdB is concerned. Here the signs left by the new extremely low temperatures become evident. Meanwhile, in AdZ there are indications of *éboulis*, of human and animal occupation, together with the ever-present diagenesis of human and biological remains. In the CdF there are signs of much lower temperatures, but at the same time vadose conditions are still present. It is evident that in the case of these caves, it is not possible to consider particularly arid conditions, as are those usually thought for MIS 4 (Margari *et al.*, 2009; Biltekin *et al.*, 2019; Guido *et al.*, 2020): the signs left by humidity are many and very evident, but this aspect was already found for western Liguria (Kaniewski, Renault-Miskovsky and de Lumley, 2004, 2005; Kaniewski *et al.*, 2005). Still, we are very much in agreement when it is stated that the climate change was sudden and drastic towards colder conditions.

The transition from MIS 4 to MIS 3 is not particularly evident from what was observed in the deposits studied. Throughout the MIS 3 we note the presence, in all four caves, of cold conditions, with the exception of AdZ, where the signs left by frost action are not evident, perhaps due to the action exerted by the animals on the deposits. In all the sites we are witnessing the occupation of man and animals. In the case of man, we are convinced that it was only for short periods of time. The traces left are mainly in the form of microcharcoals, burnt bones and possibly lithic industry in the case of humans, coprolites and bones in the case of animals.

As we know, MIS 3 is characterized by being a very unstable period from a climatic point of view (Anderson, Goudie and Parker, 2013; Badino *et al.*, 2020). One aspect that all the caves share is the witnessing of a short period of climatic improvement around 40 kyr BP. In TdB there are no longer the signs of frost action, but, instead, signs of wetter conditions and less rigid temperatures

emerge. In AdZ a level characterized by the deposition of laminated silt and clays, in an environment rich in low energy water, occur. CdF sees the formation of a flowstone and perhaps a period of intense carbonate cementation. At AdM we do not see such a drastic improvement, but milder temperatures have led to a less developed platy microstructure. Traces of this short climatic improvement are also found in other sites, in fact. At Riparo Mochi and Riparo Bombrini, for what concerns western Liguria, the pollen studied testifies the development, around that period (~40 kyr BP), of more temperate and humid conditions (Berto, Santaniello and Grimaldi, 2019; Holt *et al.*, 2019). Similar conditions are also discovered in other sites: a climatic improvement is witnessed for the northern hemisphere in general (Anderson, Goudie and Parker, 2013), but, for example, also for Denmark and Spain (Houmark-Nielsen, 1994; Kehl *et al.*, 2018).

The climatic conditions soon return to being cold, but nonetheless humid, for a certain period of time, probably until the end of MIS 3. Signs of aridity, more indicative of MIS 2 (Moreno *et al.*, 2012), can only be seen in AdM, where there is the deposition of two levels of loess and there are almost no signs of moistness. In the meantime, however, signs of humidity are probably still present in more protected areas, such as TdB and AdZ. In the latter two cases, we observe the sediments resulting from the collapse of the cave ceiling, due to the action of freezing and thawing. And, again, also due to this phenomenon, in the three caves (AdM, TdB, AdZ), signs of frost action are present.

MIS 2, like MIS 4, is relatively brief. This is followed by MIS 1, which sees a complete change in the climate and the environment (Royer *et al.*, 2016; Šolcová *et al.*, 2020). The climatic situation is rapidly improving towards today's conditions. This change is sudden and brings with it the rapid melting of glaciers and ice (Davis, Menounos and Osborn, 2009), as well as a new vast availability of water. The rains and floods become more frequent and severe (Roberts, 2014), leading to more intense water dripping and flooding in caves (Zhornyak *et al.*, 2011). The brecciated deposits of the TdB, AdZ and AdM caves date all back to this exact period. They display an important human influence in the case of AdZ and AdM, up to the highest levels of AdM, where only the influence exerted by the deposition of laminated sediments, more or less coarse, persists, attesting the establishment of new temperate conditions.

To conclude, micromorphology proved to be very useful in recognizing features that would have been totally lost to the naked eye. An example of this was the recognition of the typical features linked to frost action that were not noticed in the field, as happened, for example, at the cave of Arma delle Manie. Furthermore, it is quite evident from the chapters dedicated to each cave's discussion of the results, how much this technique has influenced the final framework.

Table 12 - Summary and simplified table of the results obtained within this thesis for all four caves.

<table>
<tr><th>Kyr BP</th><th>MIS</th><th>TdB</th><th>AdZ</th><th>CdF</th><th>AdM</th></tr>
<tr><td>7</td><td rowspan="6">MIS 1</td><td rowspan="4"></td><td rowspan="2"></td><td rowspan="9"></td><td>Humid and temperate</td></tr>
<tr><td>8</td><td rowspan="5">Important human influence and cementation . Humid and temperate conditions</td></tr>
<tr><td>9</td></tr>
<tr><td>10</td><td rowspan="3">Humid and temperate conditions</td></tr>
<tr><td>11</td></tr>
<tr><td>11.7</td></tr>
<tr><td>15</td><td rowspan="2">MIS 2</td><td rowspan="2">II cold ep. - human occupation</td><td rowspan="2">Loess deposition and cold conditions</td></tr>
<tr><td>20</td><td rowspan="2">Cold and human influence</td></tr>
<tr><td>25</td><td rowspan="5">MIS 3</td><td rowspan="5">Human occupation - humid conditions and erosion</td><td>Cold conditions and human influence</td></tr>
<tr><td>30</td><td rowspan="4">Frost action, animal and human occupation. Signs of short climatic amelioration in the middle.</td><td rowspan="2">Around 38 : less rigid conditions</td></tr>
<tr><td>35</td></tr>
<tr><td>40</td><td>Humid event</td><td>Cold and humid, human influence</td></tr>
<tr><td>50</td><td rowspan="2">Cold and subsequent intense humid events</td><td rowspan="4"></td></tr>
<tr><td>60</td></tr>
<tr><td>70</td><td>MIS 4</td><td>Human occupation - I cold ep. - animal occupation</td><td>Cold conditions and vadose situation</td></tr>
<tr><td>80</td><td rowspan="3">MIS 5a-d</td><td rowspan="3">Arid and then humid and temperate</td><td rowspan="3">Fluvio-karstic deposit and animal occupation</td><td rowspan="3">Intermittently saturated zone, temperate conditions. Animal and human influence</td></tr>
<tr><td>90</td></tr>
<tr><td>100</td></tr>
<tr><td>120</td><td>MIS 5e</td><td></td><td></td><td>Active karst</td><td></td></tr>
</table>

Figure index

Figure 1 - International Stratigraphic Chart as released by the International Commission on Stratigraphy in 2020. The red square indicates the restricted temporal extension of the Quaternary period.....8

Figure 2 - "Ideal variation of temperature with time, and stage numbers". From Emiliani (1955). The original (and ideal) Marine Isotope Stages (MIS) as proposed by Emiliani and Arrhenius. .10

Figure 3 - The reciprocal relationships existing between geochronological and climatostratigraphic units as they are known today. Figure realized with TS-Creator (2020). 11

Figure 4 – From (Rasmussen et al., 2014). Here it is possible to see the correlation between temperatures and stable isotopes of the last 123 kyr (here reported as ka b2k, i.e. thousand of years before 2000 AD) as obtained from Greenland ice core studies (and from the GRIP, GISP2 and NGRIP projects, in red, green and blue respectively). All recognized events are differentiated by colour (white or grey), such as the last interglacial (Eemian) and the various stadials and interstadials.....14

Figure 5 - Global mean sea level compared with paleoclimate proxies and human evolution and industry since 140 kyr BP. From Benjamin et al. (2017). a) Global mean sea-level curve, with its uncertainty (from Waelbroeck et al. (2002)). b) Variation in oxygen isotopes indicating paleoclimatic variations for the SE Mediterranean basin. c) Paleoclimatic proxy for the northern hemisphere from the NGRIP project (North Greenland Ice Core Project members, 2004; Kindler et al., 2014). d) Variation of stable oxygen isotopes for the benthic composition (Lisiecki and Stern, 2016). Brown dashed shading indicates periods of sapropel deposition (Rohling, Marino and Grant, 2015).....16

Figure 6 - Permafrost extension 20 kyr BP, related to the northern European ice sheets and the active networks of ice wedges. In Van Vliet-Lanoë and Hallegouët (2001). 18

Figure 7 - How sea level rose during Holocene. Modified from Vacchi et al. (2016).....21

Figure 8 - a) Mean annual rainfall (in mm): the data collected cover the entire period from 1961 to 2010.With two red rectangles are indicated, starting from the West, the area near Pigna

Municipality, where Tana di Badalucco cave is situated, and the Finalese area where the remaining three studied caves are located. Modified from ARPAL (2013). b) Mean temperatures (in °C) for the sole Finalese area, as obtained from the ARPAL site (Regione Liguria, 2021). No data were available for the other area. c) Mean annual frost days, i.e. the days with a minimum temperature below 0 ° C. What was said for a) also applies here. Modified from ARPAL (2013).....24

Figure 9 – Tana di Badalucco cave location and geology (a); Tana di Badalucco cave plan and sections, one of its synonyms is reported (b) (from Calandri et al., 1979). 27

Figure 10 - Geological and geographical framework of the study area. 31

Figure 11 – Pre-Pliocene chronostratigraphic chart with focus on the Miocene Epoch. Pliocene, Pleistocene and Holocene are not reported here. 34

Figure 12 - Legend of the geological map of the Finalese area. The geological formations are in alphabetical order. 35

Figure 13 - Calcare di Finale Ligure fm. ("Pietra di Finale", Finale Ligure limestone) outcrop. Detail of the Monte Carmo member. 38

Figure 14 - a) Plan of Arma degli Zerbi (modified from Farinazzo (1999)). b) The entrance to the cave. 39

Figure 15 - The four sections as drawn by prof. Negrino.....40

Figure 16 - a) Plan of the cave, with the arrow indicating the position of corridor 3 (from Bichet (1987)). b) The detail of the first portion of the cave, including corridor 3, with the reference squares shown. 43

Figure 17 - The entrance hall of Caverna delle Fate. a) Here it is possible to see the detail of the entrance, with the recent wall. b) The back of the entrance hall. 44

Figure 18 - Plan of corridor 3. f1-2-3: hearths. Sections A, B and C are also shown. 45

Figure 19 - a) Section A stratigraphy (Echassoux et al., 1989). b) Section B stratigraphy, in red the micromorphological samples position from Bichet (1987). Modified from (Bichet, 1987)...46

Figure 20 - Section C stratigraphy, modified from Bichet (1987). In red micromorphological samples position in (Bichet, 1987). 47

Figure 21 - Section A as drawn by (Bichet, 1987). Here it is possible to see all layers' names. 48

Figure 22 - Arma delle Manie cave. a) The context of the cave. b) The entrance to the cave. Only the gated part has been studied. Arma delle Manie is one of the largest caves in western Liguria. 50

Figure 23 - Arma delle Manie cave studied area planimetry. 51

Figure 24 – Arma delle Manie's first stratigraphy. Modified from Arobba et al. (1976). Highlighted in yellow the seven stratigraphic layers. 52

Figure 25 – Magnetic properties study of Arma delle Manie infillings, from Djerrab & Camps (2010). 54

Figure 26 - Caverna delle Fate and Arma delle Manie infillings climatic and chronological evolution, based on multidisciplinary results. From Psathi (2003). 54

Figure 27 - Here are some of the different stages of field work. a) Recognition and study of the stratigraphic section. b) Cleaning of the section, in order to well expose the deposit. c) Description of the stratigraphy, in particular, Munsell colour recognition in this case. d) Notes on the position of the micromorphological samples. 57

Figure 28 - Sampling. a) Block obtained from two levels by digging around the desired portion. b) Application of plaster jackets on undisturbed sample. 58

Figure 29 - Various steps of grain size determination procedure are shown. a) The samples are oven-dried. b) Subsequently sieved using different mesh sizes. c) Preparation of the fine fraction for the sedigraph (All pictures by me, except for the last one by Mr. Demergasso). 59

Figure 30 - Tana di Badalucco stratigraphy and Munsell colours, sample position and levels. the stratigraphy as presented here is to be intended as a synthesis of the different sections individuated in the field. 64

Figure 31 - Tana di Badalucco cave plan with sections indication. 65

Figure 32 - Sampling of sections 2 and 3. a) Section 2 with four of the five samples taken. TB B was sampled before the photograph was taken, from beneath sample TB C. b) Sampling in section 3. It is evident how the sampled level is the only one still in place in this part of the cave. 67

Figure 33 - Stratigraphic sections and division into levels of stratigraphies. White rectangles indicate the micromorphological samples taken. 76

Figure 34 - Section 2, level 1 in detail: in this figure it is easier to appreciate the clear limit, with little charcoal fragments, and, with two asterisks for clarity, one tooth and one big charcoal fragment in place. 77

Figure 35 - Sections 3 and 4 with the micromorphological samples position. 78

Figure 36 - Section 3. At about 60 cm from the surface it is possible to see a lithic instrument in place. 79

Figure 37 - Arma degli Zerbi cave fine earths' textures. 81

Figure 38 - Grain size analysis results (in %) for the first two sections of Arma degli Zerbi cave. 82

Figure 39 - Grain size analysis results (in %) for the last two sections of Arma degli Zerbi cave. 83

Figure 40 - XRD analysis results for Arma degli Zerbi. This is the graphical representation of Table 6. 86

Figure 41 - Section 4 microfacies presentation. Only the L thin section is excluded from this figure. Thin sections' position are meant only to convey the relative relations between them. ...95

Figure 42 - Caverna delle Fate stratigraphy. At the top right it is also possible to see the exact location of the three stratigraphies in corridor 3. The micromorphological samples are indicated with a red rectangle. 99

Figure 43 - Section FC and its peculiar appearance. The perspective changes level 1 lower limit position. 102

Figure 44 - Grain size analysis results (in %) of section FB and FC of Caverna delle Fate cave. 103

Figure 45 - Grain size analysis results (in %) for section FA of Caverna delle Fate cave. 104

Figure 46 - Caverna delle Fate cave fine earths' textures. 105

Figure 47 - XRD analysis results for Caverna delle Fate deposits. All data are in percentages. 106

Figure 48 - Arma delle Manie cave stratigraphic section. Crosses indicate the sampling points for radiocarbon dating. In several positions the perspective creates optical illusions that could impact on depths of the levels. 120

Figure 49 - The peculiarity of the limit between level D (upper part) and level C (lower part). 121

Figure 50 - Grain size analysis results for the first half of the samples from Arma delle Manie cave..... 124

Figure 51 - Grain size analysis results for the second part of the samples from Arma delle Manie cave..... 125

Figure 52 - XRD analysis results. This is the graphical representation of Table 9. 126

Figure 53 - Thin section GH from Arma delle Manie cave, with all mF numbers, as used in the description. The original aspect of GH is in figure. 130

Figure 54 - Arid and then humid temperate MFT. a-b) In this microphotograph it is possible to note the large amount of coarse material of this MFT, the presence of small clay pedofeatures and the granostriated b-fabric. (Always PPL and XPL) c-d) Parallel microlaminated clay coatings with traces of manganese. e-f) Dusty parallel microlaminated clay coatings in contact with the voids.

g-h) In the centre a small coprolite is present, recognizable thanks to the characteristic yellowish aspect in PPL and isotropic in XPL, typical of phosphates. 140

Figure 55 – Microphotograph from the Cold and human influence MFT. a-b) In this microphotograph it is possible to notice the well-developed platy microstructure of t.s. B, in PPL and XPL. c-d) Vesicles, like those clearly visible in the centre, are one of the distinctive features of a deposits influenced by frost action. Thin section G, PPL and XPL. e-f) A bone fragment, bearing the clear signs of burning, marks is placed in the centre of thin section B, PPL and XPL. g-h) A large fragment of charcoal from section F. PPL and XPL. 142

Figure 56 - Microphotograph from the Cold and bioturbation MFT. a-b) In this microphotograph it is possible to notice the platy microstructure (partly reworked by bioturbation) of t.s. F. PPL and XPL. c-d) In t.s. D a single silt capping was observed on a weathered rock fragment. e-f) A coprolite with quartz grains inside of it is easily discernible thanks to its yellowish colour in PPL and isotropic behaviour in XPL. g-h) Nonlaminar clay infillings, probably result of water passage. PPL and XPL. 144

Figure 57 - Microphotograph from the Humid temperate MFT. a-b)Typical signs of humidity are visible, such as manganese-rich pedofeatures. Inside the aggregate it is also possible to notice a calcite infilling, another sign linked to humidity. PPL and XPL. c-d) Another pedofeature, but this time a dusty clay coating. PPL and XPL. e-f) In this case it is possible to see two different pedofeatures, one on top of the other: a calcite hypocoating and, in contact with the void, a partial infilling of calcite. PPL and XPL. 146

Figure 58 - a-b) Microphotographs of t.s. l. It is possible to see, above, a fragment of bone, surrounded by apatite (more easily appreciated in XPL) and below a fragment of slightly altered limestone. It is interesting to see how the influence of apatite decreases as we approach the carbonate rock. Thin section l, PPL and XPL. c-d) In t.s. c, especially towards its lower part, there are numerous fragments of charcoal, an example in microphotograph. CM MFT. PPL and XPL. e-f) Also belonging to the CM MFT, a large fragment of bone bearing burn marks. T.s. f mF II. PPL and XPL. g-h) At the bottom right, there is a part of a larger coprolite. MOO MFT, t.s. section 4 mF V. PPL and XPL. 151

Figure 59 - a-b) Thin section e (MOO MFT), belonging to the second phase of animal occupation. In the microphotograph one of the many large fragments of bones is present. PPL and

XPL. c-d) Microfacies III of section 4, also of the second phase of animal occupation and MOO MFT. In this case, it is possible to see, in the centre, an apatite nodule, probably the result of bones and animal excrement alteration. On the left there is a fragment of limestone from the "Calcare di Finale" formation, recognizable thanks to the presence of coral fossils. PPL and XPL. e-f) In the microphotograph it is possible to appreciate more aspects of the mF IV: the moderately separated granular microstructure, the presence of charcoal, perhaps organic matter and probably other burned material, as well as fragments of limestone and quartz grains. PPL and XPL. g-h) In the lower part there is a carnivore excrement with the typical yellowish-greyish colour and a little bone fragment in its upper part. In the upper part, the porous crumbs aggregates can be seen. The b-fabric is crystallitic-undifferentiated, maybe due to the high phosphates content. PPL and XPL. 152

Figure 60 - a-d) In the first four microphotographs it is possible to notice the clayey pedofeatures from section 4 mF II (YD MFT). It is evident that they are fractured and not in equilibrium with the current surface. These are surrounded by limestone fragments of different sizes. PPL and XPL. e-f) In t.s. b it is possible to note the presence of a silt capping placed above a rock fragment. It is also possible to state that it is silt capping as the deposition of the material above shows a sedimentation different from that of the surrounding aggregates. The presence of such a figure implies the action of frost. PPL, XPL. g-h) Porous crumbs aggregates are present and it is possible to notice the platy overprint present in this t.s. (b, GC MFT). PPL, XPL. 154

Figure 61 - Section 1, but viewed from the south facing side. The large amount of bones and charcoals present in the lower portion is evident. 155

Figure 62 - a-b) On the right an aggregate in t.s. d mF II (CM MFT) showing signs of reddening (although in the microphotograph it is not very evident), while on the left there is a small fragment of charcoal. PPL, XPL. c-d) Still from the same t.s., a large fragment of charcoal and, further down, a fragment of fossiliferous limestone. PPL, XPL. e-f) From the t.s. a (CW MFT). It is possible to see multiple levels of carbonate deposition. In this case, the calcite began to settle on top of an aggregate rich in bone fragments. PPL, XPL. g-h) From the same t.s.. Different levels, with different development of mineral habit, of calcite. PPL, XPL.....156

Figure 63 - The figure (the first of three) shows the deposits of the Arma degli Zerbi cave considered, divided by the relative chronology proposed. From the oldest to the most recent levels. 158

Figure 64 - The figure (the second of three) shows the deposits of the Arma degli Zerbi cave considered, divided by the relative chronology proposed. From the oldest to the most recent levels. “Not signalled” is to be considered as not indicated in the figure. 159

Figure 65 - The figure (the last of three) shows the deposits of the Arma degli Zerbi cave considered, divided by the relative chronology proposed. From the oldest to the most recent levels. 160

Figure 66 - Already from the FC thin section it is possible to notice the transition between level 1 and 2. The limits and fragments belonging to level 2 within level 1 are marked with a white dashed line. A) Level 1 is characterized by the presence of coprolites, one of which is also quite large, partly visible in the microphotograph. PPL, XPL. b) In the microphotograph it is possible to see the visible signs of the erosion that occurred at the contact between the two levels. In this case the different silt laminae are fragmented and mixed with aggregates from the top. PPL, XPL. c) In this case, the different silt laminae are shown. PPL, XPL. 162

Figure 67 - a) In the first microphotograph it is possible to see a reaction rim on a big grain of calcite. T.s. FA 12. PPL, XPL. b) Mn hypocoatings in t.s. FA 13a. PPL, XPL. c) Mn hypocoatings in t.s. FB 3. PPL, XPL.....165

Figure 68 - a) Microphotograph of one of the different clay pedofeatures present. In particular t.s. FB 3. PPL, XPL. b) Part of the thick clay coating in FA 13b indicating a previously exposed surface. PPL, XPL. c) Only part of the cryptocrystalline phosphatic coating present in t.s. FB 3, always indicating a previously exposed surface. PPL, XPL. 166

Figure 69 - Some examples of terra rossa fragments. The names of the thin section of origin are reported.....168

Figure 70 – Microphotographs of t.s. FA 13a showing two examples of the anthropogenic material found in this thin section. PPL, XPL. a) A bone fragment showing signs of burning. b) One thin charcoal fragment. PPL, XPL.....169

Figure 71 - Level FB 2. a) This is one of the thin sections from this level. b) The microphotograph shows the aggregates surrounded, but in this case, not touched, by the calcitic palisade fabric. PPL, XPL. c) Only part of the silt capping from FB 2, with the detail of the sand size quartz grain. PPL, XPL. d) Particular of a bone fragment in this level. PPL, XPL.....170

Figure 72 - PC MFT. A) Thin section FA 11. B) Microphotograph showing a portion of t.s. FA 11 with moderately separated granular microstructure. PPL, XPL. C) From t.s. FA 9b, porous crumbs with a platy overprint and calcitic pedofeatures. PPL, XPL. D) A small part of the big bone completely replaced by calcite. In microphotograph are evident the calcitic veins. PPL, XPL. 171

Figure 73 – Microphotographs from SC MFT. A) Porous crumbs aggregates surrounded by carbonates. It is possible to discern a vague platy overprint (t.s. FA 9a). PPL, XPL. B) In t.s. FA 6 it is possible to see the peculiar aggregates' arrangement, the great presence of carbonatic pedofeatures and a single coprolite. PPL, XPL. c) Porous crumbs and calcitic meniscus in t.s. 3. PPL, XPL. D) Part of a bone fragment on the left and the phosphatic material on the right. T.s. 4. PPL, XPL. E) Little charcoal fragment in t.s. 4. PPL, XPL. 174

Figure 74 - Thin section VI scan (a) and microphotographs. B) It is possible to see the prismatic microstructure. PPL, XPL. C) It is still possible to appreciate the prismatic microstructure and the presence of a little charcoal fragment. PPL, XPL. 176

Figure 75 - Microphotographs from the BC MFT. A) The well-developed platy microstructure in t.s. III. PPL, XPL. B) In t.s. II few coarsening up infillings are present. PPL, XPL. C) Pure clay coatings in t.s. V. PPL, XPL. D) A less developed platy microstructure in t.s. IV and, on the right, a charcoal fragment. PPL, XPL. 178

Figure 76 - CL MFT scanned thin sections and microphotographs. B)In this microphotograph the platy microstructure and a little rock fragment showing the peculiar vertical orientation are displayed. PPL, XPL. C)Another microphotograph to present the platy microstructure of the t.s. PPL, XPL. e) One dusty clay coating is presented here. It is also possible to see two sand size rock fragments. PPL, XPL. F) The upper part of t.s. B exhibits a certain degree of cementation. PPL, XPL. 181

Figure 77 - DC MFT scanned thin sections and microphotographs. A) Thin section CD scan. The aggregates and part of the coarse fraction are recognisable to the naked eye. B) Part of a big charcoal and one little burnt bone fragment. It is also possible to see the presence of porous crumbs. PPL, XPL. C) The dual colour (yellowish and reddish) of few clayey pedofeatures present in t.s. CD. PPL, XPL. D) Thin section E scan. On the left some big bone fragments, on the right part of a jaw and carnivore teeth. E) On the left, part of a big bone fragment, on the right one big charcoal fragment. PPL, XPL. F) Evidence of cementation of this MFT. PPL, XPL. 183

Figure 78 – Thin section GH scan and microphotographs. B) Silty laminae from mF 1. PPL, XPL. C) Single spaced equal enaulic microstructure of mF3. PPL, XPL. 184

Table index

Table 1 - A non-exhaustive table of cave sediments types divided for origin and nature. * indicates high likelihood, - indicates low likelihood of finding. Modified from (Goldberg and Sherwood, 2006). 25

Table 2 - A non-exhaustive table of processes occurring inside a cave. Modified from (Goldberg and Sherwood, 2006). 26

Table 3 - Recognition of the nature of the material (thanks to prof. Arobba, Museo Archeologico del Finale) and dating of coals from the four studied sections of Arma degli Zerbi cave deposits. 41

Table 4 - Frequency and abundance estimates from Macphail & Goldberg (2017). In bold the change applied here. 62

Table 5 - Microfacies types (MFT) and simplified descriptions to highlight crucial aspects for interpretation of results for Tana di Badalucco cave deposits. 68

Table 6 - Semi-quantitative XRD analysis results for Arma degli Zerbi cave deposits. All numbers shown are percentages. The abbreviations for minerals are those suggested by Whitney and Evans (2010). 85

Table 7 - Microfacies types (MFT) and simplified descriptions to highlight crucial aspects for interpretation of results for Arma degli Zerbi cave deposits. ("n.d." for not detectable, f-1 for single occurrence) 88

Table 8 - Microfacies types (MFT) and simplified descriptions to highlight crucial aspects for interpretation of results for Caverna delle Fate cave deposits. 108

Table 9 - Semi-quantitative XRD analysis results for Arma delle Manie cave deposits. All numbers shown are percentages. 126

Table 10 - Radiocarbon datings for Arma delle Manie deposits. 127

Table 11 - Microfacies types (MFT) and simplified descriptions to highlight crucial aspects for interpretation of results for Arma delle Manie cave deposits. (“n.r.” for not recognisable). 128

Table 12 - Summary and simplified table of the results obtained within this thesis for all four caves. 189

Bibliography

Abbassi, M. *et al.* (1998) 'Distribution and evolution of Arvicola Lacepede, 1799 (Rodentia, Mammalia) from France and Liguria during the Middle and the Upper Pleistocene', *Quaternaire*. Association Francaise pour l'Etude du Quaternaire, 9(2), pp. 105–116. doi: 10.3406/quate.1998.1594.

Abbassi, M. and Brunet-Lecomte, P. (1997) 'Terricola fatio 1867 (Arvicolidae, rodentia) from five sequences of the south east of France and Liguria', *Quaternaire*, 8(1), pp. 3–12. doi: 10.3406/quate.1997.1553.

Aldeias, V. *et al.* (2014) 'Deciphering site formation processes through soil micromorphology at Contrebandiers Cave, Morocco', *Journal of Human Evolution*. Academic Press, 69(1), pp. 8–30. doi: 10.1016/j.jhevol.2013.12.016.

Aldeias, V. *et al.* (2016) 'How heat alters underlying deposits and implications for archaeological fire features: A controlled experiment', *Journal of Archaeological Science*, 67, pp. 64–79. doi: 10.1016/j.jas.2016.01.016.

Alhaique, F. (1994) 'Taphonomic analysis of the faunal remains from the "P" and "M" layers of the Arene Candide cave (Savona, Italy)', in *The upper Pleistocene deposit of the Arene Candide (Savona, Italy) : new studies on the 1940-42 excavations*, pp. 263–296. Available at: https://www.researchgate.net/publication/284651001_Taphonomic_study_of_the_faunal_remains_from_the_M_and_P_layers_of_the_Arene_Candide_Savona_Italy (Accessed: 26 January 2021).

Alonso-Zarza, A. M. and Tanner, L. H. (2010a) *Carbonates in continental settings - Geochemistry, Diagenesis and Applications, Developments in Sedimentology*.

Alonso-Zarza, A. M. and Tanner, L. H. (2010b) *in Carbonates in Continental Settings: Facies, Environments and Processes*.

Alperson, N. and Hovers, E. (2005) 'Differential use of space in the Neanderthal site of Amud Cave, Isreal', *Eurasian Prehistory*, 3(1), pp. 3–22.

Altomare, A. *et al.* (2008) 'QUALX: A computer program for qualitative analysis using powder diffraction data', *Journal of Applied Crystallography*, pp. 815–817. doi: 10.1107/S0021889808016956.

Altomare, A. *et al.* (2015) 'QUALX2.0: A qualitative phase analysis software using the freely

available database POW-COD', *Journal of Applied Crystallography*. International Union of Crystallography, 48(2), pp. 598–603. doi: 10.1107/S1600576715002319.

Amandola, F. (1995) *Il deposito della Grotta delle fate (Finale Ligure): problematiche geologiche e paleoclimatiche*. Università degli Studi di Genova.

Anderson, D. E., Goudie, A. and Parker, A. (2013) *Global environments through the quaternary: exploring evironmental change*. Oxford University Press, USA.

Andreucci, S. *et al.* (2014) 'Evolution and architecture of a west mediterranean upper pleistocene to holocene coastal apron-fan system', *Sedimentology*, 61(2), pp. 333–361. doi: 10.1111/sed.12058.

Angelone, C., Moncunill-Solé, B. and Kotsakis, T. (2020) 'Fossil Lagomorpha (Mammalia) of Italy: Systematics and biochronology', *Rivista Italiana di Paleontologia e Stratigrafia*. Universita degli Studi di Milano, 126(1), pp. 157–187. doi: 10.13130/2039-4942/13014.

Angelucci, D. E. and Zilhão, J. (2009) 'Stratigraphy and formation processes of the upper pleistocene deposit at gruta da oliveira, almonda karstic system, Torres Novas, Portugal', *Geoarchaeology*, 24(3), pp. 277–310. doi: 10.1002/gea.20267.

Antoine, P. *et al.* (2009) 'High-resolution record of the last climatic cycle in the southern Carpathian Basin (Surduk, Vojvodina, Serbia)', *Quaternary International*, 198(1–2), pp. 19–36. doi: 10.1016/j.quaint.2008.12.008.

Armenteros, I. (2010) 'Chapter 2 Diagenesis of Carbonates in Continental Settings', *Developments in Sedimentology*. Elsevier, pp. 61–151. doi: 10.1016/S0070-4571(09)06202-5.

Arnaud, J. (2013) *Etude des restes mandibulaires d'Homo neanderthalensis de Guattari, Caverna delle Fate et San Francesco d'Archi*. Università degli Studi di Ferrara.

Arobba, D. *et al.* (1976) 'Le Mànie', in *Archeologia in Liguria*, pp. 133–144.

Arobba, D. *et al.* (2018) 'New evidence on the earliest human presence in the urban area of Genoa (Liguria, Italy): A multi-proxy study of a mid-Holocene deposit at the mouth of the Bisagno river', *Holocene*, 28(12), pp. 1918–1935. doi: 10.1177/0959683618798107.

Arobba, D. and Caramiello, R. (2008) 'Il "Cimitero degli orsi" della grotta della Bàsura. Analisi palinologica del deposito', in *Toirano e la Grotta della Bàsura. Conoscere, conservare e gestire il patrimonio archeologico e paleontologico. Toirano, 26-28 ottobre 2000*. Toirano, pp. 37–43. Available at: http://www.museoarcheologicodelfinale.it/pdf/arobba/2008_cimiteroorsibasura.pdf (Accessed: 4 January 2021).

ARPAL (2013) *Atlante climatico della Liguria*. Edited by G. Agrillo and V. Bonati. Genova: ARPAL. Available at: https://www.arpal.liguria.it/contenuti_statici//clima/atlante/Atlante_climatico_della_Liguria.pdf.

Arrhenius, G. (1953) 'Sediment cores from the east pacific', *GFF*, pp. 115–118. doi: 10.1080/11035895309454862.

Arrhenius, G. (1961) *25. PELAGIC SEDIMENTS*.

Badino, F. *et al.* (2020) 'An overview of Alpine and Mediterranean palaeogeography, terrestrial ecosystems and climate history during MIS 3 with focus on the Middle to Upper Palaeolithic transition', *Quaternary International*. Elsevier Ltd, 551, pp. 7–28. doi: 10.1016/j.quaint.2019.09.024.

Bahn, P. G. (1977) 'Seasonal migration in South-west France during the late glacial period', *Journal of Archaeological Science*. Academic Press, 4(3), pp. 245–257. doi: 10.1016/0305-4403(77)90092-9.

Bar-Matthews, M. *et al.* (1999) 'The Eastern Mediterranean paleoclimate as a reflection of regional events: Soreq cave, Israel', *Earth and Planetary Science Letters*, 166(1–2), pp. 85–95. doi: 10.1016/S0012-821X(98)00275-1.

Bar-Yosef, O. *et al.* (1992) 'The Excavations in Kebara Cave, Mt. Carmel [and Comments and Replies]', *Current Anthropology*. University of Chicago Press, 33(5), pp. 497–550. doi: 10.1086/204112.

Bardají, T. *et al.* (2009) 'Sea level and climate changes during OIS 5e in the Western Mediterranean', *Geomorphology*, 104(1–2), pp. 22–37. doi: 10.1016/j.geomorph.2008.05.027.

Barta, G. (2011) 'Secondary carbonates in loess-paleosoil sequences: A general review', *Central European Journal of Geosciences*, 3(2), pp. 129–146. doi: 10.2478/s13533-011-0013-7.

Baumgartner, M. *et al.* (2014) 'NGRIP CH4 concentration from 120 to 10 kyr before present and its relation to a δ15N temperature reconstruction from the same ice core', *Climate of the Past*. European Geosciences Union, 10(2), pp. 903–920. doi: 10.5194/cp-10-903-2014.

Becker, D. *et al.* (2015) 'LGM paleoenvironment of Europe - Map', *CRC806-Database*. doi: 10.5880/SFB806.15.

Becker, P. *et al.* (2017) 'A study of the Würm glaciation focused on the Valais region (Alps)', *Geographica Helvetica*, 72(4), pp. 421–442. doi: 10.5194/gh-72-421-2017.

Bellini, C., Mariotti-Lippi, M. and Montanari, C. (2009) 'The Holocene landscape history of

the NW Italian coasts', *Holocene*, 19(8), pp. 1161–1172. doi: 10.1177/0959683609345077.

Benjamin, J. *et al.* (2017) 'Late Quaternary sea-level changes and early human societies in the central and eastern Mediterranean Basin: An interdisciplinary review', *Quaternary International*. Elsevier Ltd, pp. 29–57. doi: 10.1016/j.quaint.2017.06.025.

Benyarku, C. A. and Stoops, G. (2005) *Guidelines for preparation of rock and soil thin sections and polished sections*. Lleida: Departament de Medi Ambient i Ciències del Sòl, Universitat de Lleida.

Bergadà, M. M., Villaverde, V. and Román, D. (2013) 'Microstratigraphy of the Magdalenian sequence at Cendres Cave (Teulada-Moraira, Alicante, Spain): Formation and diagenesis', *Quaternary International*, 315, pp. 56–75. doi: 10.1016/j.quaint.2013.09.017.

Berto, C., Santaniello, F. and Grimaldi, S. (2019) 'Palaeoenvironment and palaeoclimate in the western Liguria region (northwestern Italy) during the Last Glacial. The small mammal sequence of Riparo Mochi (Balzi Rossi, Ventimiglia)', *Comptes Rendus - Palevol*. Elsevier Masson SAS, 18(1), pp. 13–23. doi: 10.1016/j.crpv.2018.04.007.

Bertran, P. *et al.* (2016) 'A map of Pleistocene aeolian deposits in Western Europe, with special emphasis on France', *Journal of Quaternary Science*. John Wiley and Sons Ltd, 31(8), pp. 844–856. doi: 10.1002/jqs.2909.

Bianchi, N., Rellini, I. and Traverso, A. (2015) 'Pigna. Grotta Giacheira e Tana di Badalucco: la ripresa delle ricerche', V, pp. 128–130. Available at: https://iris.unige.it/handle/11567/831896?mode=full.43#.XH_ZwjrSK70.

Biancotti, A. and Motta, M. (1988) 'Morfotettonica dell'Altopiano delle Mànie e zone circostanti (Liguria Occidentale)', *Supplementi di geografia fisica e dinamica quaternaria*, I, pp. 45–68.

Bichet, V. (1987) *Contribution à l'étude sédimentologique du remplissage karstique de la Caverna delle Fate (Ligurie italienne)*. Museum national d'histoire naturelle.

Biltekin, D. *et al.* (2019) 'Vegetation and climate record from Abric Romaní (Capellades, northeast Iberia) during the Upper Pleistocene (MIS 5d−3)', *Quaternary Science Reviews*. Elsevier Ltd, 220, pp. 154–164. doi: 10.1016/j.quascirev.2019.07.035.

Bini, A. (2005) 'I ghiacciai del Passato', in *I Ghiacciai di Lombardia. Evoluzione e attualità*, pp. 11–19. Available at: https://www.researchgate.net/publication/274377689 (Accessed: 24 August 2020).

Bini, A., Tognini, P. and Zuccoli, L. (1998) 'Rapport entre karst et glaciers durant les

glaciations dans les vallées préalpines du Sud des Alpes', *Karstologia : revue de karstologie et de spéléologie physique*, 32(1), pp. 7–26. doi: 10.3406/karst.1998.2422.

Boni, A. *et al.* (1971) *Note illustrative della Carta Geologica d'Italia alla scala 1: 100.000, foglio 92–93 Albenga-Savona*. Roma.

Boni, P., Mosna, S. and Vanossi, M. (1968) *La 'Pietra di Finale' (Liguria Occidentale)*. Pavia: Pavia - Tipografia del libro.

Bosellini, A., Mutti, E. and Ricci Lucchi, A. (1989) *Rocce e successioni sedimentarie, Ed. UTET, Torino*.

Braillard, L., Guélat, M. and Rentzel, P. (2004) 'Effects of bears on rockshelter sediments at Tanay Sur-les-Creux southwestern Switzerland', *Geoarchaeology*. Wiley Periodicals, Inc. Published online in Wiley Interscience, 19(4), pp. 343–367. doi: 10.1002/gea.10123.

Branch, N. P. (2013) 'Early-Middle Holocene vegetation history, climate change and human activities at Lago Riane (Ligurian Apennines, NW Italy)', *Vegetation History and Archaeobotany*, 22(4), pp. 315–334. doi: 10.1007/s00334-012-0384-9.

Branch, N. P. *et al.* (2014) 'The Neolithisation of Liguria (NW Italy): An environmental archaeological and palaeoenvironmental perspective', *Environmental Archaeology*. Maney Publishing, 19(3), pp. 196–213. doi: 10.1179/1749631414Y.0000000024.

Branch, N. P. and Marini, N. A. F. (2014) 'Mid-Late Holocene environmental change and human activities in the northern Apennines, Italy', *Quaternary International*. Elsevier Ltd, 353(1), pp. 34–51. doi: 10.1016/j.quaint.2013.07.053.

Brenchley, P. J. and Harper, D. A. T. (2010) *Palaeoecology: Ecosystems, environments, and evolution*, *Nature*. Edited by Chapman & Hall. Available at: https://www.amazon.it/gp/product/1138418730/ref=dbs_a_def_rwt_hsch_vapi_taft_p1_i0 (Accessed: 14 December 2020).

Brewer, R. (1964) *Fabric and mineral analysis of soils*. Wiley. Available at: https://books.google.it/books?id=A_fwAAAAMAAJ.

Brönnimann, D., Ismail-Meyer, K., *et al.* (2017) 'Excrements of Herbivores', in *Archaeological Soil and Sediment Micromorphology*. Chichester, UK: John Wiley & Sons, Ltd, pp. 55–65. doi: 10.1002/9781118941065.ch6.

Brönnimann, D., Pümpin, C., *et al.* (2017) 'Excrements of Omnivores and Carnivores', in *Archaeological Soil and Sediment Micromorphology*. Chichester, UK: John Wiley & Sons, Ltd, pp. 67–81. doi: 10.1002/9781118941065.ch7.

Brook, E. J., Sowers, T. and Orchardo, J. (1996) ‘Rapid variations in atmospheric methane concentration during the past 110,000 years’, *Science*. American Association for the Advancement of Science, 273(5278), pp. 1087–1091. doi: 10.1126/science.273.5278.1087.

Brown, A. *et al.* (2013) ‘Geomorphology of the Anthropocene: Time-transgressive discontinuities of human-induced alluviation’, *Anthropocene*. Elsevier, pp. 3–13. doi: 10.1016/j.ancene.2013.06.002.

Brugal, J. P. *et al.* (2020) ‘Pleistocene herbivores and carnivores from France: An updated overview of the literature, sites and taxonomy’, *Annales de Paleontologie*. Elsevier Masson SAS, 106(2), p. 102384. doi: 10.1016/j.annpal.2019.102384.

Bullock, P. (1985) *Handbook for soil thin section description*. Waine Research. Available at: https://books.google.it/books?id=ONdOAQAAIAAJ.

Burjachs, F. *et al.* (2012) ‘Palaeoecology of Neanderthals during Dansgaard-Oeschger cycles in northeastern Iberia (Abric Romaní): From regional to global scale’, *Quaternary International*, 247(1), pp. 26–37. doi: 10.1016/j.quaint.2011.01.035.

Burke, A. *et al.* (2017) ‘Risky business: The impact of climate and climate variability on human population dynamics in Western Europe during the Last Glacial Maximum’, *Quaternary Science Reviews*. Elsevier Ltd, 164, pp. 217–229. doi: 10.1016/j.quascirev.2017.04.001.

Calandri, G. and Camprendon, R. (1982) *Geologia e carsismo dell’Alta Val Nervia e Argentina (Liguria occidentale): guida escursione*. Comune di Imperia. Assessorato alle attività culturali ; Gruppo speleologico imperiese C.A.I. Available at: https://books.google.it/books?id=ZtQ9MwEACAAJ.

Calandri, G., Crippa, C. and Ramella, L. (1979) ‘Lo Sgarbu di Barraico in val Nervia (Provincia di Imperia)’, (XXII), pp. 3–13.

Campo, B., Amorosi, A. and Vaiani, S. C. (2017) ‘Sequence stratigraphy and late Quaternary paleoenvironmental evolution of the Northern Adriatic coastal plain (Italy)’, *Palaeogeography, Palaeoclimatology, Palaeoecology*. Elsevier B.V., 466, pp. 265–278. doi: 10.1016/j.palaeo.2016.11.016.

Canti, M. G. (2017a) ‘Charred Plant Remains’, in *Archaeological Soil and Sediment Micromorphology*. Chichester, UK: John Wiley & Sons, Ltd, pp. 141–142. doi: 10.1002/9781118941065.ch15.

Canti, M. G. (2017b) ‘Coal’, in *Archaeological Soil and Sediment Micromorphology*. Chichester, UK: John Wiley & Sons, Ltd, pp. 143–145. doi: 10.1002/9781118941065.ch16.

Canti, M. G. and Brochier, J. É. (2017) ‘Plant Ash’, in *Archaeological Soil and Sediment Micromorphology*. Chichester, UK: John Wiley & Sons, Ltd, pp. 147–154. doi: 10.1002/9781118941065.ch17.

Carobene, L., Firpo, M. and Rovere, A. (2008) ‘Le variazioni ambientali nell’area di Vado Ligure dal Neolitico ad oggi’, *Alpine and Mediterranean Quaternary*, 21(2), pp. 433–456. Available at: https://www.researchgate.net/publication/242398614 (Accessed: 21 October 2020).

Carrion, J. S. and Sanchez-Gomez, P. (1992) ‘Palynological Data in Support of the Survival of Walnut (Juglans regia L.) in the Western Mediterranean Area During Last Glacial Times’, *Journal of Biogeography*. JSTOR, 19(6), p. 623. doi: 10.2307/2845705.

Casazza, G. *et al.* (2008) ‘Ecological and historical factors affecting distribution pattern and richness of endemic plant species: The case of the Maritime and Ligurian Alps hotspot’, *Diversity and Distributions*. John Wiley & Sons, Ltd, 14(1), pp. 47–58. doi: 10.1111/j.1472-4642.2007.00412.x.

Cassoli, P. F. and Tagliacozzo, A. (1994) ‘I macromammiferi dei livelli Tardopleistocenici delle Arene Candide’, *Quaternaria Nova*, pp. 101–262. Available at: https://www.researchgate.net/publication/284391958_I_macromammiferi_dei_livelli_tardopleistocenici_delle_Arene_Candide_Savona_Italia_considerazioni_paleontologiche_e_archeozoologiche (Accessed: 21 January 2021).

Cauche, D. *et al.* (2004) ‘Présentation techno-typologique des industries moustériennes de Ligurie italienne’, in *Section 5 : Le Paléolithique Moyen : sessions générales et posters*. BAR International, pp. 19–27. Available at: https://hal.archives-ouvertes.fr/hal-00485178 (Accessed: 14 October 2020).

Cauche, D. (2007) ‘Les cultures moustériennes en Ligurie italienne : analyse du matériel lithique de trois sites en grotte’, *Anthropologie*, 111(3), pp. 254–289. doi: 10.1016/j.anthro.2007.05.002.

Cauche, D. (2012) ‘Productions lithiques et comportements techno-économiques de groupes humains acheuléens et moustériens en région liguro-provençale’, *Comptes Rendus - Palevol*. No longer published by Elsevier, 11(7), pp. 519–527. doi: 10.1016/j.crpv.2011.12.008.

Cheddadi, R. and Khater, C. (2016) ‘Climate change since the last glacial period in Lebanon and the persistence of Mediterranean species’, *Quaternary Science Reviews*. Elsevier Ltd, 150, pp. 146–157. doi: 10.1016/j.quascirev.2016.08.010.

Cheng, H. *et al.* (2009) ‘Ice age terminations’, *Science*, 326(5950), pp. 248–252. doi:

10.1126/science.1177840.

Chiarenza, N. (2007) ‘Mountains and shore: sites and communication routes of Copper Age western Liguria’, in *HIDDEN LANDSCAPES OF MEDITERRANEAN EUROPE Cultural and methodological biases in pre-and protohistoric landscape studies*. Siena, p. 293.

Ciccacci, S. (2015) *Le Forme del Rilievo*. Available at: https://scholar.google.it/scholar?hl=it&as_sdt=0%2C5&q=%22le+forme+del+rilievo%22+author%3Aciccacci&btnG= (Accessed: 21 March 2021).

Clark, P. U. *et al.* (2013) ‘Mechanisms for an ~7-Kyr Climate and Sea-Level Oscillation During Marine Isotope Stage 3’, in *Ocean Circulation: Mechanisms and Impacts - Past and Future Changes of Meridional Overturning*. American Geophysical Union, pp. 209–246. doi: 10.1029/173GM15.

Cohen, K. M. *et al.* (2013) ‘The ICS international chronostratigraphic chart’, *Episodes*, 36(3), pp. 199–204. doi: 10.18814/epiiugs/2013/v36i3/002.

Combourieu-Nebout, N. *et al.* (2015) ‘Climate changes in the central Mediterranean and Italian vegetation dynamics since the Pliocene’, *Review of Palaeobotany and Palynology*, 218, pp. 127–147. doi: 10.1016/j.revpalbo.2015.03.001.

Cortesogno, L. *et al.* (1998) ‘The Variscan post-collisional volcanism in Late Carboniferous-Permian sequences of Ligurian Alps, Southern Alps and Sardinia (Italy): A synthesis’, *Lithos*, 45(1–4), pp. 305–328. doi: 10.1016/S0024-4937(98)00037-1.

Courty, M.-A. (2001) ‘Microfacies analysis assisting archaeological stratigraphy’, in *Earth sciences and archaeology*. Springer, pp. 205–239.

Courty, M.-A. A., Goldberg, P. and Macphail, R. (1990) *Soils and micromorphology in archaeology*, *Soils and micromorphology in archaeology*. Wiley. doi: 10.1097/00010694-199012000-00014.

Courty, M.-A. and Vallverdu, J. (2001) ‘The Microstratigraphic Record of Abrupt Climate Changes in Cave Sediments of the Western Mediterranean’, *Geoarchaeology - An International Journal*, 16(5), pp. 467–499. doi: 10.1002/gea.1002.

Cremaschi, M. *et al.* (1990) ‘Sedimentary and pedological processes in the Upper Pleistocene loess of northern Italy. The Bagaggera sequence’, *Quaternary International*. Pergamon, 5(C), pp. 23–38. doi: 10.1016/1040-6182(90)90022-V.

Cremaschi, M. *et al.* (2015) ‘Age, soil-forming processes, and archaeology of the loess deposits at the Apennine margin of the Po plain (northern Italy): New insights from the Ghiardo area’,

Quaternary International, 376, pp. 173–188. doi: 10.1016/j.quaint.2014.07.044.

Cremaschi, M. and Van Vliet-Lanoë, B. (1990) 'Traces of frost activity and ice segregation in Pleistocene loess deposits and till of northern Italy: Deep seasonal freezing or permafrost?', *Quaternary International*. Elsevier, 5(C), pp. 39–48. doi: 10.1016/1040-6182(90)90023-W.

Cruise, G. M. *et al.* (2009) 'Lago di Bargone, Liguria, n Italy: A reconstruction of Holocene environmental and land-use history', *Holocene*. SAGE PublicationsSage UK: London, England, 19(7), pp. 987–1003. doi: 10.1177/0959683609343142.

Dallagiovanna, G. *et al.* (2011) *NOTE ILLUSTRATIVE della CARTA GEOLOGICA D'ITALIA alla scala 1:50.000 CAIRO MONTENOTTE*.

Dallagiovanna, G. *et al.* (2012) 'Carta Geologica alla scala 1:25000 Foglio 257 "Dolceacqua" e Foglio 270 "Ventimiglia" con note illustrative.', pp. 1–76. Available at: https://arts.units.it/handle/11368/2768327#.XH_ytTrSK70.

Dansgaard, W. *et al.* (1982) 'A new Greenland deep ice core', *Science*. American Association for the Advancement of Science, 218(4579), pp. 1273–1277. doi: 10.1126/science.218.4579.1273.

Davis, B. A. S. *et al.* (2003) 'The temperature of Europe during the Holocene reconstructed from pollen data', *Quaternary Science Reviews*. Elsevier Ltd, 22(15–17), pp. 1701–1716. doi: 10.1016/S0277-3791(03)00173-2.

Davis, P. T., Menounos, B. and Osborn, G. (2009) 'Holocene and latest Pleistocene alpine glacier fluctuations: a global perspective', *Quaternary Science Reviews*, 28(21–22), pp. 2021–2033. doi: 10.1016/j.quascirev.2009.05.020.

Decarlis, A. *et al.* (2013) 'Stratigraphic evolution in the Ligurian Alps between Variscan heritages and the Alpine Tethys opening: A review', *Earth-Science Reviews*, pp. 43–68. doi: 10.1016/j.earscirev.2013.07.001.

Defleur, A. R. and Desclaux, E. (2019) 'Impact of the last interglacial climate change on ecosystems and Neanderthals behavior at Baume Moula-Guercy, Ardèche, France', *Journal of Archaeological Science*, 104, pp. 114–124. doi: 10.1016/j.jas.2019.01.002.

Ding, Z. L. *et al.* (1999) 'Climate instability during the penultimate glaciation: Evidence from two high-resolution loess records, China', *Journal of Geophysical Research: Solid Earth*, 104(B9), pp. 20123–20132. doi: 10.1029/1999jb900183.

Ditlevsen, P. D., Ditlevsen, S. and Andersen, K. K. (2002) 'The fast climate fluctuations during the stadial and interstadial climate states', *Annals of Glaciology*, 35, pp. 457–462. doi: 10.3189/172756402781816870.

Djerrab, A. and Camps, P. (2010) ‘Propriétés magnétiques du remplissage de la Caverna delle Manie (Finale Ligurie, Italie)’, *ArchéoSciences*, 34(1), pp. 81–96. doi: 10.4000/archeosciences.2648.

Djerrab, A. and Hedley, I. (2010) ‘Magnetic mineral study of the prehistoric site of caverna delle fate (finale, liguria, Italy)’, *Quaternaire*. Association Française pour l’Étude du Quaternaire, 21(2), pp. 165–180. doi: 10.4000/quaternaire.5534.

Dodero, C. (2017) *L’ Arma degli Zerbi (Finale Ligure, Savona): revisione stratigrafica e inquadramento crono-culturale dei materiali archeologici*. Università degli Studi di Genova.

Drees, C. *et al.* (2010) ‘Multiple glacial refuges of unwinged ground beetles in Europe: Molecular data support classical phylogeographic models’, in *Relict Species: Phylogeography and Conservation Biology*. Springer-Verlag Berlin Heidelberg, pp. 199–215. doi: 10.1007/978-3-540-92160-8_11.

Drysdale, R. N. *et al.* (2004) ‘Palaeoclimatic implications of the growth history and stable isotope (δ18O and δ13C) geochemistry of a Middle to Late Pleistocene stalagmite from central-western Italy’, *Earth and Planetary Science Letters*, 227(3–4), pp. 215–229. doi: 10.1016/j.epsl.2004.09.010.

Dumitru, O. A. *et al.* (2018) ‘Climate variability in the western Mediterranean between 121 and 67 ka derived from a Mallorcan speleothem record’, *Palaeogeography, Palaeoclimatology, Palaeoecology*. Elsevier B.V., 506, pp. 128–138. doi: 10.1016/j.palaeo.2018.06.028.

Durand, N. *et al.* (2018) ‘Calcium Carbonate Features’, in *Interpretation of Micromorphological Features of Soils and Regoliths*. Elsevier, pp. 205–258. doi: 10.1016/b978-0-444-63522-8.00009-7.

Echassoux, A. *et al.* (1989) ‘Les nouvelles fouilles dans le gisement moustérien de la Caverna delle Fate (Finale, Ligurie italienne)’, *L’Homme de Neandertal*, 6, pp. 49–58.

Emiliani, C. (1955) ‘Pleistocene Temperatures’, *The Journal of Geology*, 63(6), pp. 538–578. doi: 10.1086/626295.

Epstein, S. *et al.* (1951) ‘Carbonate-water isotopic temperature scale’, *Bulletin of the Geological Society of America*. Geological Society of America, 62(4), pp. 417–426. doi: 10.1130/0016-7606(1951)62[417:CITS]2.0.CO;2.

Erhart, H. (1955) ‘“Biostasie” et “Rhexistasie”. Esquisse d’une théorie sur le rôle de la pédogenèse en tant que phénomène géologique’, *Comptes rendus hebdomadaires des séances de l’Académie des Sciences de Paris*, 241(18 (31 octobre 1955)), pp. 1218–1220. Available at:

https://scholar.google.com/scholar?q=Biostasie et rhexistasie. Esquisse dune théorie sur le rôle de la pédogenèse en tant que phénomène géologique (Accessed: 5 March 2021).

Fabio Scarciglia *et al.* (2009) 'The role of human impacts and Holocene climate change in the Santuario della Madonna Cave (Calabria)Il ruolo dell'impatto antropico e del clima olocenico nella Grotta del Santuario della Madonna (Calabria)Impacts d'origine anthropique et forçages climatiq', *Méditerranée*. OpenEdition, (112), pp. 137–143. doi: 10.4000/mediterranee.3395.

Falguères, C., Yokoyama, Y. and Bibron, R. (1990) 'Electron spin resonance (ESR) dating of hominid-bearing deposits in the Caverna delle Fate, Ligure, Italy', *Quaternary Research*, 34, pp. 121–128. doi: https://doi.org/10.1016/0033-5894(90)90077-X.

Farinazzo, R. (1999) 'Scavi archeologici all'Arma di Zerbi', *Stalattiti e stalagmiti*, 25, pp. 64–66.

Farrand, W. R. (2001) 'Sediments and Stratigraphy in Rockshelters and Caves: A Personal Perspective on Principles and Pragmatics', *Geoarchaeology - An International Journal*. John Wiley & Sons, Ltd, 16(5), pp. 537–557. doi: 10.1002/gea.1004.

Federici, P. R. and Pappalardo, M. (2006) 'Evidence of Marine Isotope Stage 5.5 highstand in Liguria (Italy) and its tectonic significance', *Quaternary International*, 145–146, pp. 68–77. doi: 10.1016/j.quaint.2005.07.003.

Figueiral, I. and Terral, J. F. (2002) 'Late quaternary refugia of mediterranean taxa in the Portuguese estremadura: Charcoal based palaeovegetation and climatic reconstruction', *Quaternary Science Reviews*. Pergamon, 21(4–6), pp. 549–558. doi: 10.1016/S0277-3791(01)00022-1.

Fitzsimmons, K. E., Marković, S. B. and Hambach, U. (2012) 'Pleistocene environmental dynamics recorded in the loess of the middle and lower Danube basin', *Quaternary Science Reviews*. Pergamon, 41, pp. 104–118. doi: 10.1016/j.quascirev.2012.03.002.

Flückiger, J. *et al.* (2008) 'Modeled seasonality of glacial abrupt climate events', *Climate Dynamics*, 31(6), pp. 633–645. doi: 10.1007/s00382-008-0373-y.

Flückiger, J., Knutti, R. and White, J. W. C. (2006) 'Oceanic processes as potential trigger and amplifying mechanisms for Heinrich events', *Paleoceanography*, 21(2). doi: 10.1029/2005PA001204.

Folk, R. L. (1980) *Petrology of sedimentary rocks*. Hemphill publishing company.

Ford, D. and Williams, P. (2013) *Karst Hydrogeology and Geomorphology*, *Karst Hydrogeology and Geomorphology*. doi: 10.1002/9781118684986.

Fosse, P. *et al.* (2004) 'Denning behaviour of "modern" brown bear (Ursus arctos, L.) in caves: biological and paleontological considerations from French Pyrenean sites', in *Cahiers Scientifiques. Hors Série*. Department du Rhone - Museum, Lyon, pp. 171–182. Available at: https://www.persee.fr/doc/mhnly_1762-8024_2004_act_2_1_1412?pageid=t1_177 (Accessed: 9 March 2020).

Fratianni, S. and Acquaotta, F. (2017) 'The Climate of Italy', in *World Geomorphological Landscapes*. Springer, pp. 29–38. doi: 10.1007/978-3-319-26194-2_4.

Giacobini, G. *et al.* (1984) 'Neanderthal child and adult remains from a Mousterian deposit in Northern Italy (Caverna delle fate, finale ligure)', *Journal of Human Evolution*, 13(8), pp. 687–707.

Gillieson, D. (1996) *Caves: processes, development and management*. Malden, Massachusetts: Blackwell Publishing Ltd. Available at: https://books.google.it/books?hl=it&lr=&id=Lp-TIIZ_GpAC&oi=fnd&pg=PR5&dq=grain+size+analysis+in+caves&ots=US3GxP-R9f&sig=1bus6qMzqv46APJi8f5DSY3pMOw (Accessed: 18 February 2021).

Goldberg, P. (2000) 'Micromorphology and site formation at Die Kelders Cave I, South Africa', *Journal of Human Evolution*. Academic Press, 38(1), pp. 43–90. doi: 10.1006/jhev.1999.0350.

Goldberg, P. *et al.* (2001) 'Site formation processes at Zhoukoudian, China', *Journal of Human Evolution*. Academic Press, 41(5), pp. 483–530. doi: 10.1006/jhev.2001.0498.

Goldberg, P. *et al.* (2009) 'Bedding, hearths, and site maintenance in the Middle Stone Age of Sibudu Cave, KwaZulu-Natal, South Africa', *Archaeological and Anthropological Sciences*, 1(2), pp. 95–122. doi: 10.1007/s12520-009-0008-1.

Goldberg, P., Berna, F. and Chazan, M. (2015) 'Deposition and Diagenesis in the Earlier Stone Age of Wonderwerk Cave, Excavation 1, South Africa', *African Archaeological Review*, 32(4), pp. 613–643. doi: 10.1007/s10437-015-9192-9.

Goldberg, P. and Macphail, R. I. (2013) *Practical and Theoretical Geoarchaeology*, *Practical and Theoretical Geoarchaeology*. John Wiley & Sons. doi: 10.1002/9781118688182.

Goldberg, P. and Sherwood, S. C. (2006) 'Deciphering human prehistory through the geoarcheological study of cave sediments', *Evolutionary Anthropology*. Wiley Online Library, 15(1), pp. 20–36. doi: 10.1002/evan.20094.

Greenland Ice-core Project (GRIP) Members (1993) 'Climate instability during the last interglacial period recorded in the GRIP ice core', *Nature*, 364(6434), pp. 203–207. doi: 10.1038/364203a0.

Grootes, P. M. *et al.* (1993) ‘Comparison of oxygen isotope records from the GISP2 and GRIP Greenland ice cores’, *Nature*, 366(6455), pp. 552–554. doi: 10.1038/366552a0.

Guido, M. A. *et al.* (2020) ‘Climate and vegetation dynamics of the Northern Apennines (Italy) during the Late Pleistocene and Holocene’, *Quaternary Science Reviews*. Elsevier Ltd, 231, p. 106206. doi: 10.1016/j.quascirev.2020.106206.

Habel, J. C., Dieker, P. and Schmitt, T. (2009) ‘Biogeographical connections between the Maghreb and the Mediterranean peninsulas of southern Europe’, *Biological Journal of the Linnean Society*. Oxford Academic, 98(3), pp. 693–703. doi: 10.1111/j.1095-8312.2009.01300.x.

Heinrich, H. (1988) ‘Origin and consequences of cyclic ice rafting in the Northeast Atlantic Ocean during the past 130,000 years’, *Quaternary Research*. Cambridge University Press, 29(2), pp. 142–152. doi: 10.1016/0033-5894(88)90057-9.

Hemming, S. R. (2004) ‘Heinrich events: Massive late Pleistocene detritus layers of the North Atlantic and their global climate imprint’, *Reviews of Geophysics*. Blackwell Publishing Ltd, 42(1), p. 43. doi: 10.1029/2003RG000128.

Herries, A. I. R. and Fisher, E. C. (2010) ‘Multidimensional GIS modeling of magnetic mineralogy as a proxy for fire use and spatial patterning: Evidence from the Middle Stone Age bearing sea cave of Pinnacle Point 13B (Western Cape, South Africa)’, *Journal of Human Evolution*. Academic Press, 59(3–4), pp. 306–320. doi: 10.1016/j.jhevol.2010.07.012.

Holt, B. *et al.* (2019) ‘The Middle-Upper Paleolithic transition in Northwest Italy: new evidence from Riparo Bombrini (Balzi Rossi, Liguria, Italy)’, *Quaternary International*. Elsevier Ltd, 508, pp. 142–152. doi: 10.1016/j.quaint.2018.11.032.

Hošek, J. *et al.* (2015) ‘An integrated rock-magnetic and geochemical approach to loess/paleosol sequences from Bohemia and Moravia (Czech Republic): Implications for the Upper Pleistocene paleoenvironment in central Europe’, *Palaeogeography, Palaeoclimatology, Palaeoecology*. Elsevier, 418, pp. 344–358. doi: 10.1016/j.palaeo.2014.11.024.

Houmark-Nielsen, M. (1994) ‘Late Pleistocene stratigraphy, glaciation chronology and Middle Weichselian environmental history from Klintholm, Møn, Denmark’, *Bulletin of the Geological society of Denmark*. Available at: https://www.researchgate.net/publication/237624217 (Accessed: 25 March 2021).

Housley, R. A. *et al.* (1997) ‘Radiocarbon evidence for the Lateglacial Human Recolonisation of Northern Europe’, *Proceedings of the Prehistoric Society*, 63, pp. 25–54. doi: 10.1017/s0079497x0000236x.

Hughes, T. (1996) ‘Can ice sheets trigger abrupt climatic change?’, *Arctic and Alpine Research*, 28(4), pp. 448–465. doi: 10.2307/1551856.

Huijzer, A. S. and Isarin, R. F. B. (1997) ‘The reconstruction of past climates using multi-proxy evidence: An example of the Weichselian pleniglacial in northwest and central Europe’, *Quaternary Science Reviews*, 16(6), pp. 513–533. doi: 10.1016/S0277-3791(96)00080-7.

Isetti, G. and de Lumley, H. (1962) ‘L’industria litica della caverna delle Fate’, *Rivista Ingauna e Intemelia*, XVI(1–4), pp. 1–15.

Issel, A. (1892) *Liguria: geologica e preistorica*. A. Forni.

Issel, A. (1908) *Liguria preistorica*. Genova: a cura della Società ligure di Storia Patria. Available at: http://archive.org/details/attidellasociet40sociuoft%5Cnhttp://it.wikisource.org/wiki/Liguria_preistorica (Accessed: 14 April 2020).

Johnsen, S. J. *et al.* (1992) ‘Irregular glacial interstadials recorded in a new Greenland ice core’, *Nature*, 662(August), pp. 311–313.

Joseph, P. and Lomas, S. A. (2004) ‘Deep-water sedimentation in the Alpine Foreland Basin of SE France: New perspectives on the Grès d’Annot and related systems - An introduction’, *Geological Society Special Publication*, 221, pp. 1–16. doi: 10.1144/GSL.SP.2004.221.01.01.

Kamel, O. M. (2019) ‘Iron behavior in fersiallitic soil during the Quaternary and their paleo environmental significance northern Tunisia’, in *International Meeting on Paleoclimate: Change and Adaptation*. Macao, Portugal. Available at: http://www.pacadnetwork.com/itm/images/sampledata/Domeniu/AreaDomeniu8_.pdf#page=61 (Accessed: 9 February 2021).

Kaniewski, D. *et al.* (2005) ‘Upper Pleistocene and Late Holocene vegetation belts in western Liguria: An archaeopalynological approach’, *Quaternary International*. Elsevier Ltd, 135(1 SPEC. ISS.), pp. 47–63. doi: 10.1016/j.quaint.2004.10.023.

Kaniewski, D., Renault-Miskovsky, J. and de Lumley, H. (2004) ‘Madonna dell’Arma (San Remo, Italy): Local expression of the Ligurian vegetation during the Middle Palaeolithic’, *Geobios*, 37(5), pp. 583–593. doi: 10.1016/j.geobios.2003.05.003.

Kaniewski, D., Renault-Miskovsky, J. and de Lumley, H. (2005) ‘Palaeovegetation from a Homo neanderthalensis occupation in Western Liguria: Archaeopalynology of Madonna dell’Arma (San Remo, Italy)’, *Journal of Archaeological Science*, 32(6), pp. 827–840. doi: 10.1016/j.jas.2004.12.005.

Karatsori, E. (2003) *Environnement vegetal de l'homme fossile et climats en Ligurie pendant le dernier cycle climatique et le postglaciaire*. Available at: https://www.theses.fr/2003MNHN0004 (Accessed: 14 October 2020).

Karatsori, E. *et al.* (2005) 'Environnement de l'Homme de Néandertal en Ligurie au Pléistocène supérieur. Analyse pollinique de la Caverna delle Fate (Finale Ligure, Italie)', *Comptes Rendus - Palevol*. No longer published by Elsevier, 4(5), pp. 395–404. doi: 10.1016/j.crpv.2005.03.006.

Karkanas, P. *et al.* (2000) 'Diagenesis in prehistoric caves: The use of minerals that form in situ to assess the completeness of the archaeological record', *Journal of Archaeological Science*. Academic Press, 27(10), pp. 915–929. doi: 10.1006/jasc.1999.0506.

Karkanas, P. (2002) 'Micromorphological Studies of Greek Prehistoric Sites: New Insights in the Interpretation of the Archaeological Record', *Geoarchaeology - An International Journal*, 17(3), pp. 237–259. doi: 10.1002/gea.10012.

Karkanas, P. *et al.* (2007) 'Evidence for habitual use of fire at the end of the Lower Paleolithic: Site-formation processes at Qesem Cave, Israel', *Journal of Human Evolution*, 53(2), pp. 197–212. doi: 10.1016/j.jhevol.2007.04.002.

Karkanas, P. (2017) 'Guano', in *Archaeological Soil and Sediment Micromorphology*. Chichester, UK: John Wiley & Sons, Ltd, pp. 83–89. doi: 10.1002/9781118941065.ch8.

Karkanas, P. and Goldberg, P. (2010) 'Site formation processes at Pinnacle Point Cave 13B (Mossel Bay, Western Cape Province, South Africa): Resolving stratigraphic and depositional complexities with micromorphology', *Journal of Human Evolution*. Academic Press, 59(3–4), pp. 256–273. doi: 10.1016/j.jhevol.2010.07.001.

Karkanas, P. and Goldberg, P. (2013) 'Micromorphology of Cave Sediments', in *Treatise on Geomorphology*. Elsevier Inc., pp. 286–297. doi: 10.1016/B978-0-12-374739-6.00120-2.

Karkanas, P. and Goldberg, P. (2017) 'Cave Settings', in Gilbert, A. (ed.) *Encyclopedia of Earth Sciences Series*. Dordrecht: Springer, pp. 108–118. doi: 10.1007/978-1-4020-4409-0_151.

Karkanas, P. and Goldberg, P. (2018) 'Phosphatic Features', in *Interpretation of Micromorphological Features of Soils and Regoliths*. Elsevier, pp. 323–346. doi: 10.1016/b978-0-444-63522-8.00012-7.

Kehl, M. *et al.* (2018) 'The rock shelter Abrigo del Molino (Segovia, Spain) and the timing of the late Middle Paleolithic in Central Iberia', *Quaternary Research (United States)*. Cambridge University Press, 90(1), pp. 180–200. doi: 10.1017/qua.2018.13.

Kindler, P. *et al.* (2014) 'Temperature reconstruction from 10 to 120 kyr b2k from the NGRIP

ice core', *Climate of the Past*, 10, pp. 887–902. doi: 10.5194/cp-10-887-2014.

Kjellström, E. *et al.* (2010) 'Simulated climate conditions in Europe during the Marine Isotope Stage 3 stadial', *Boreas*. John Wiley & Sons, Ltd, 39(2), pp. 436–456. doi: 10.1111/j.1502-3885.2010.00143.x.

Koç, D. E., Svenning, J. C. and Avcı, M. (2018) 'Climate change impacts on the potential distribution of Taxus baccata L. in the Eastern Mediterranean and the Bolkar Mountains (Turkey) from Last Glacial Maximum to the future', *Eurasian Journal of Forest Science*. doi: 10.31195/ejejfs.435962.

Kottek, M. *et al.* (2006) 'World Map of the Köppen-Geiger climate classification updated', *Meteorologische Zeitschrift*, pp. 259–263. doi: 10.1127/0941-2948/2006/0130.

Krajcarz, M. T. *et al.* (2016) 'Loess in a cave: Lithostratigraphic and correlative value of loess and loess-like layers in caves from the Kraków-Czestochowa Upland (Poland)', *Quaternary International*. Elsevier Ltd, 399, pp. 13–30. doi: 10.1016/j.quaint.2015.08.069.

Kühn, P. *et al.* (2018) 'Textural Pedofeatures and Related Horizons', in *Interpretation of Micromorphological Features of Soils and Regoliths*. Elsevier, pp. 377–423. doi: 10.1016/b978-0-444-63522-8.00014-0.

Leger, E. (2011) *Interpretazione tecnologica ed economica dell'industria litica dell'Arma delle Manie (strati V, IV, III, II) - i livelli musteriani dello Stadio Isotopico 3*. Università degli Studi di Ferrara, Università degli Studi di Modena e Reggio Emilia, Instituto politecnico de Tomar.

Lisiecki, L. E. and Stern, J. V. (2016) 'Regional and global benthic δ18O stacks for the last glacial cycle', *Paleoceanography*. Blackwell Publishing Ltd, 31(10), pp. 1368–1394. doi: 10.1002/2016PA003002.

Lowe, J. J. (2001) 'Abrupt climatic changes in Europe during the last glacial-interglacial transition: The potential for testing hypotheses on the synchroneity of climatic events using tephrochronology', *Global and Planetary Change*. Elsevier B.V., 30(1–4), pp. 73–84. doi: 10.1016/S0921-8181(01)00079-0.

Lowe, J. J. *et al.* (2008) 'Synchronisation of palaeoenvironmental events in the North Atlantic region during the Last Termination: a revised protocol recommended by the INTIMATE group', *Quaternary Science Reviews*, 27(1–2), pp. 6–17.

Lowe, J. and Walker, M. (2014) *Reconstructing quaternary environments*, *Reconstructing Quaternary Environments*. Taylor and Francis. doi: 10.4324/9781315797496.

de Lumley, H. *et al.* (2008) 'Les cultures acheuléennes et moustériennes dans les Alpes-

Maritimes et en Ligurie', *Archéologies transfrontalières : Alpes du sud, Côte d'Azur, Piémont et Ligurie : bilan et perspectives de recherche : actes du colloque de Nice, 13-15 décembre 2007*, 1(3), pp. 11–20.

De Lumley, M. A. and Giacobini, G. (2013a) 'Les néandertaliens de la Caverna delle Fate (Finale Ligure, Italie). I - Chronostratigraphie, restes squelettiques', *Anthropologie*, 117(3), pp. 273–304. doi: 10.1016/j.anthro.2013.05.003.

De Lumley, M. A. and Giacobini, G. (2013b) 'Les néandertaliens de la Caverna delle Fate (Finale Ligure, Italie). II - Les dents', *Anthropologie*. Elsevier Masson, 117(3), pp. 305–344. doi: 10.1016/j.anthro.2013.05.002.

Macklin, M. G., Johnstone, E. and Lewin, J. (2005) 'Pervasive and long-term forcing of Holocene river instability and flooding in Great Britain by centennial-scale climate change', *Holocene*, 15(7), pp. 937–943. doi: 10.1191/0959683605hl867ft.

Macphail, R. I. and Goldberg, P. (2017) *Applied Soils and Micromorphology in Archaeology*, *Applied Soils and Micromorphology in Archaeology*. Cambridge University Press. doi: 10.1017/9780511895562.

Mallol, C., Cabanes, D. and Baena, J. (2010) 'Microstratigraphy and diagenesis at the upper Pleistocene site of Esquilleu Cave (Cantabria, Spain)', *Quaternary International*, 214(1–2), pp. 70–81. doi: 10.1016/j.quaint.2009.10.018.

Mallol, C., Mentzer, S. M. and Miller, C. E. (2017) 'Combustion Features', in *Archaeological Soil and Sediment Micromorphology*. Chichester, UK: John Wiley & Sons, Ltd, pp. 299–330. doi: 10.1002/9781118941065.ch31.

Marcelino, V., Schaefer, C. E. G. R. and Stoops, G. (2018) 'Oxic and Related Materials', in *Interpretation of Micromorphological Features of Soils and Regoliths*. Elsevier, pp. 663–689. doi: 10.1016/b978-0-444-63522-8.00023-1.

Marchal, O. *et al.* (2002) 'Apparent long-term cooling of the sea surface in the northeast Atlantic and Mediterranean during the Holocene', *Quaternary Science Reviews*, 21(4–6), pp. 455–483. doi: 10.1016/S0277-3791(01)00105-6.

De Marchi, M. P. (2003) 'Carnivores contribution to quaternary palaeoenvironments. Application to the carnivore community of the Caverna delle Fate (Western Liguria, Italy)', *Quaternaire*. Association Francaise pour l'Etude du Quaternaire, 14(3), pp. 155–161. doi: 10.3406/quate.2003.1739.

Margari, V. *et al.* (2009) 'Character of vegetational and environmental changes in southern

Europe during the last glacial period; evidence from Lesvos Island, Greece', *Quaternary Science Reviews*, 28(13–14), pp. 1317–1339. doi: 10.1016/j.quascirev.2009.01.008.

Mariotti Lippi, M. *et al.* (2007) 'The Massaciuccoli Holocene pollen sequence and the vegetation history of the coastal plains by the Mar Ligure (Tuscany and Liguria, Italy)', *Vegetation History and Archaeobotany*, 16(4), pp. 267–277. doi: 10.1007/s00334-006-0090-6.

Martrat, B. *et al.* (2004) 'Abrupt temperature changes in the Western Mediterranean over the past 250,000 years', *Science*. American Association for the Advancement of Science, 306(5702), pp. 1762–1765. doi: 10.1126/science.1101706.

McAdams, C. *et al.* (2020) 'The Pleistocene geoarchaeology and geochronology of Con Moong Cave, North Vietnam: Site formation processes and hominin activity in the humid tropics', *Geoarchaeology*. John Wiley and Sons Inc., 35(1), pp. 72–97. doi: 10.1002/gea.21758.

Médail, F. and Diadema, K. (2009) 'Glacial refugia influence plant diversity patterns in the Mediterranean Basin', *Journal of Biogeography*. John Wiley & Sons, Ltd, 36(7), pp. 1333–1345. doi: 10.1111/j.1365-2699.2008.02051.x.

Van Meerbeeck, C. J. *et al.* (2011) 'The nature of MIS 3 stadial-interstadial transitions in Europe: New insights from model-data comparisons', *Quaternary Science Reviews*. Pergamon, 30(25–26), pp. 3618–3637. doi: 10.1016/j.quascirev.2011.08.002.

Mehidi, N. (2005) 'Datation de sites moustériens de Ligurie par les méthodes U/Th et RPE: Abri Mochi et Arma delle Manie'. Available at: https://www.theses.fr/2005MNHN0039 (Accessed: 27 February 2020).

Mentzer, S. M. (2018) 'Caves and Fissures', in *The Encyclopedia of Archaeological Sciences*. Hoboken, NJ, USA: Wiley Online Library, pp. 1–4. doi: 10.1002/9781119188230.saseas0074.

Miller, C. *et al.* (2010) 'Dumping, sweeping and trampling: experimental micromorphological analysis of anthropogenically modified combustion features', *Faculty of Science, Medicine and Health - Papers: part A*, pp. 25–37. Available at: https://ro.uow.edu.au/smhpapers/3080.

Miller, K. G. *et al.* (2011) 'Sea level and ice volume variations from continental margin and deep-sea isotopic records', *Oceanography*, 24(2), pp. 40–53. doi: 10.5670/oceanog.2011.26.

Mojtabavi, S. *et al.* (2019) 'A first chronology for the East GReenland Ice-core Project (EGRIP) over the Holocene and last glacial termination', *Climate of the Past Discussions*, 16, pp. 1–22. doi: 10.5194/cp-2019-143.

Mol, D., de Vos, J. and van der Plicht, J. (2007) 'The presence and extinction of Elephas antiquus Falconer and Cautley, 1847, in Europe', *Quaternary International*, 169–170(SPEC.

ISS.), pp. 149–153. doi: 10.1016/j.quaint.2006.06.002.

Molinari, I., Montinari, G. and Rossi, G. (2012) *Grotta Torello/Tuvetto o Tana di Badalucco, Pigna (IM) - Un contesto disperso*. M. Convent, *Archeologia in Liguria*. M. Convent. Genova: SAGEP.

Moncel, M. H. *et al.* (2015) 'Evaluating the integrity of palaeoenvironmental and archaeological records in MIS 5 to 3 karst sequences from southeastern France', *Quaternary International*, 378, pp. 22–39. doi: 10.1016/j.quaint.2013.12.009.

Montanari, C. *et al.* (2014) 'Storia dell'ambiente costiero del Mar Ligure sulla base di analisi biostratigrafiche', *Studi costieri*, 22, pp. 209–223.

Moreno, A. *et al.* (2012) 'Northern Iberian abrupt climate change dynamics during the last glacial cycle: A view from lacustrine sediments', *Quaternary Science Reviews*, 36, pp. 139–153. doi: 10.1016/j.quascirev.2010.06.031.

Morley, M. W. *et al.* (2019) 'Hominin and animal activities in the microstratigraphic record from Denisova Cave (Altai Mountains, Russia)', *Scientific Reports*, 9(1). doi: 10.1038/s41598-019-49930-3.

Moussous, A., Valensi, P. and Simon, P. (2014) 'Identification de l'ivoire de Proboscidiens des grottes des Balzi Rossi (Ligurie, Italie) à partir de la méthode des lignes de Schreger', *Bulletin du Musée d'Anthropologie préhistorique de Monaco*, 54, pp. 83–90.

Murialdo, G., Cabella, R. and Arobba, D. (2019) *PIETRA DI FINALE Una risorsa naturale e storica del Ponente ligure a cura di*. Finale Ligure.

Negrino, F. *et al.* (2018) 'L'Arma degli Zerbi (Finale Ligure): un sito riscoperto', in IIPP (ed.) *LIII RIUNIONE SCIENTIFICA DELL'ISTITUTO ITALIANO DI PREISTORIA E PROTOSTORIA*. Genova, p. 87.

Nejman, L. *et al.* (2017) 'Hominid visitation of the Moravian Karst during the Middle-Upper Paleolithic transition: New results from Pod Hradem Cave (Czech Republic)', *Journal of Human Evolution*. Academic Press, 108, pp. 131–146. doi: 10.1016/j.jhevol.2017.03.015.

Nejman, L. *et al.* (2018) 'Cave deposits as a sedimentary trap for the Marine Isotope Stage 3 environmental record: The case study of Pod Hradem, Czech Republic', *Palaeogeography, Palaeoclimatology, Palaeoecology*, 497, pp. 201–217. doi: 10.1016/j.palaeo.2018.02.020.

Nichols, G. (2009) *Sedimentology and stratigraphy*. Available at: https://books.google.it/books?hl=it&lr=&id=zl4L7WqXvogC&oi=fnd&pg=PP10&dq=nichols+1999+sedimentology+and+stratigraphy&ots=l4DjSO8sxd&sig=XdxP4CzpLHqg5Lqsbtpq0HHzL

d4#v=onepage&q=nichols 1999 sedimentology and stratigraphy&f=false (Accessed: 18 February 2021).

Nicosia, C. and Stoops, G. (2017) *Archaeological Soil and Sediment Micromorphology*, *Archaeological Soil and Sediment Micromorphology*. John Wiley & Sons. doi: 10.1002/9781118941065.

Nielsen-Marsh, C. M. and Hedges, R. E. M. (2000) 'Patterns of diagenesis in bone I: The effects of site environments', *Journal of Archaeological Science*. Academic Press, 27(12), pp. 1139–1150. doi: 10.1006/jasc.1999.0537.

North Greenland Ice Core Project members (2004) 'High-resolution record of Northern Hemisphere climate extending into the last interglacial period', *Nature*. Nature Publishing Group, 431(7005), pp. 147–151. doi: 10.1038/nature02805.

Obreht, I. *et al.* (2017) 'Shift of large-scale atmospheric systems over Europe during late MIS 3 and implications for Modern Human dispersal', *Scientific Reports*. Nature Publishing Group, 7(1), pp. 1–10. doi: 10.1038/s41598-017-06285-x.

Oliva, M. *et al.* (2018) 'Permafrost conditions in the Mediterranean region since the Last Glaciation', *Earth-Science Reviews*. Elsevier B.V., pp. 397–436. doi: 10.1016/j.earscirev.2018.06.018.

Onoratini, G. *et al.* (2012) 'The Barma Grande cave (Grimaldi, Vintimiglia, Italy): From Neandertal, hunter of " Elephas antiquus" , to Sapiens with ornaments of mammoth ivory', *Quaternary International*, 255, pp. 141–157. doi: 10.1016/j.quaint.2011.05.015.

De Pascale, A. (2008) 'Le prime esplorazioni nelle caverne ossidere del Finalese: tracce, ipotesi e scoperte ad opera di Issel, Perrando, Morelli, Rovereto, Rossi, Amerano...', in *La nascita della Paletnologia in Liguria*. Bordighera, pp. 233–248.

Pascucci, V., Sechi, D. and Andreucci, S. (2014) 'Middle Pleistocene to Holocene coastal evolution of NW Sardinia (Mediterranean Sea, Italy)', *Quaternary International*. Elsevier Ltd, 328–329(1), pp. 3–20. doi: 10.1016/j.quaint.2014.02.018.

Peel, M. C., Finlayson, B. L. and McMahon, T. A. (2007) 'Updated world map of the Köppen-Geiger climate classification', *Hydrology and Earth System Sciences*, 11(5), pp. 1633–1644. doi: 10.5194/hess-11-1633-2007.

Perotti, C. R., Seno, S. and Vanossi, M. (1994) 'The crust-mantle boundary in the Ligurian area: geological and geodynamic implications', *Bollettino di Geofisica Teorica ed Applicata*, 36(141–144), pp. 63–75. Available at: http://www3.ogs.trieste.it/bgta/pdf/bgta36.141-

144_PEROTTI.pdf (Accessed: 20 October 2020).

Perotti, E. *et al.* (2012) 'A tectonically-induced Eocene sedimentary mélange in the West Ligurian Alps, Italy', *Tectonophysics*. Elsevier, 568–569, pp. 200–214. doi: 10.1016/j.tecto.2011.09.005.

Petit, R. J. *et al.* (2003) 'Glacial refugia: Hotspots but not melting pots of genetic diversity', *Science*. American Association for the Advancement of Science, 300(5625), pp. 1563–1565. doi: 10.1126/science.1083264.

Pisias, N. G. and Moore, T. C. (1981) 'The evolution of Pleistocene climate: A time series approach', *Earth and Planetary Science Letters*. Elsevier, 52(2), pp. 450–458. doi: 10.1016/0012-821X(81)90197-7.

Pissart, A. (1970) 'Les phénomènes physiques essentiels liés au gel, les structures périglaciaires qui en résultent et leur signification climatique', *Annales de la Société géologique de Belgique*, 93, pp. 7–49. Available at: https://popups.uliege.be/0037-9395/index.php?id=6149 (Accessed: 3 March 2020).

Profe, J. *et al.* (2016) 'Geochemistry unravels MIS 3/2 paleoenvironmental dynamics at the loess–paleosol sequence Schwalbenberg II, Germany', *Palaeogeography, Palaeoclimatology, Palaeoecology*. Elsevier B.V., 459, pp. 537–551. doi: 10.1016/j.palaeo.2016.07.022.

Psathi, E. (2003) *Les sites d'Arma delle Manie et de la Caverna delle Fate (Ligurie, Italie). Etudes paléontologiques, archéozoologique et biostratigraphique de la grande faune.* Available at: https://www.theses.fr/2003MNHN0006 (Accessed: 14 October 2020).

Pye, K. (1984) 'Loess', *Progress in Physical Geography*, 8(2), pp. 176–217. doi: 10.1177/030913338400800202.

Quiles, J. and Monchot, H. (2004) 'Sex-ratio et analyse des mélanges d'Ursus spelaeus (Carnivora, Ursidae) du gisement pléistocène supérieur de Fate (Ligurie, Italie). Implications paléobiologiques', *Annales de Paleontologie*, 90(2), pp. 115–133. doi: 10.1016/j.annpal.2004.03.001.

Quinif, Y. (2006) 'COMPLEX STRATIGRAPHIC SEQUENCES IN BELGIAN CAVES : CORRELATION WITH CLIMATIC CHANGES DURING THE MIDDLE, THE UPPER PLEISTOCENE, AND THE HOLOCENE', *Geologica Belgica*, 9(3–4), pp. 231–244.

Ramsey, C. B. (2009) 'Bayesian analysis of radiocarbon dates', *Radiocarbon*. University of Arizona, 51(1), pp. 337–360. doi: 10.1017/s0033822200033865.

Ramstein, G. *et al.* (2007) 'How cold was Europe at the Last Glacial Maximum? A synthesis

of the progress achieved since the first PMIP model-data comparison', *Climate of the Past*. European Geosciences Union, 3(2), pp. 331–339. doi: 10.5194/cp-3-331-2007.

Rasmussen, S. O. *et al.* (2014) 'A stratigraphic framework for abrupt climatic changes during the Last Glacial period based on three synchronized Greenland ice-core records: Refining and extending the INTIMATE event stratigraphy', *Quaternary Science Reviews*. Elsevier Ltd, 106, pp. 14–28. doi: 10.1016/j.quascirev.2014.09.007.

Raymo, M. E. (1992) 'Global Climate Change: A Three Million Year Perspective', in *Start of a Glacial*. Springer Berlin Heidelberg, pp. 207–223. doi: 10.1007/978-3-642-76954-2_15.

Regione Liguria (2021) *Ambiente in Liguria: meteo*. Available at: http://www.cartografiarl.regione.liguria.it/SiraQualMeteo/Fruizione.asp (Accessed: 27 January 2021).

Reimer, P. J. *et al.* (2013) 'IntCal13 and Marine13 Radiocarbon Age Calibration Curves 0–50,000 Years cal BP', *Radiocarbon*, 55(4), pp. 1869–1887. doi: 10.2458/azu_js_rc.55.16947.

Rellini, I. (2007) *SUOLI E PALEOSUOLI DELLA LIGURIA OCCIDENTALE: ALCUNI ESEMPI E LORO APPLICAZIONI PALEOAMBIENTALI*. Università degli Studi di Genova.

Rellini, I. *et al.* (2009) 'Extending westward the loess basin between the Alps and the Mediterranean region: Micromorphological and mineralogical evidences from the Northern slope of the Ligurian Alps, Northern Italy', in *Geografia Fisica e Dinamica Quaternaria*, pp. 103–116. Available at: http://www.glaciologia.it/wp-content/uploads/FullText/full_text_32_1/13_GFDQ_32_1_Rellini_103_116.pdf (Accessed: 18 January 2021).

Rellini, I. *et al.* (2013) 'Climate and environmental changes recognized by micromorphology in Paleolithic deposits at Arene Candide (Liguria, Italy)', *Quaternary International*. Pergamon, 315, pp. 42–55. doi: 10.1016/j.quaint.2013.05.050.

Rellini, I. *et al.* (2014) 'Frost activity and ice segregation in a palaeosol of the Ligurian Alps (Beigua Massif, Italy): Evidence of past permafrost?', *Geografia Fisica e Dinamica Quaternaria*, 37(1), pp. 29–42. doi: 10.4461/GFDQ.2014.37.4.

Rellini, I. *et al.* (2015) 'Petroplinthite formation in a pedosedimentary sequence along a northern Mediterranean coast: from micromorphology to landscape evolution', *Journal of Soils and Sediments*, 15(6), pp. 1311–1328. doi: 10.1007/s11368-014-0896-2.

Rellini, I. *et al.* (2020) 'Micromorphological investigations at Scaloria Cave (Puglia, South-east Italy): new evidences of multifunctional use of the space during the Neolithic', *Archaeological*

and Anthropological Sciences, 12(1). doi: 10.1007/s12520-019-01005-0.

Ricci Lucchi, M. (2008) 'Vegetation dynamics during the Last Interglacial-Glacial cycle in the Arno coastal plain (Tuscany, western Italy): location of a new tree refuge', *Quaternary Science Reviews*. Pergamon, 27(27–28), pp. 2456–2466. doi: 10.1016/j.quascirev.2008.09.009.

Ricci, M. (1988) 'Pigna nella preistoria', in *Pigna e il suo territorio*. (Cartoguide De Agostini), p. 21.

Ricci, M. (2011) 'Grotte de Badalucco', in *Les premiers peuplements de la Côte d'Azur et de la Ligurie*. Colomars. De Lumley H. – De Lumley M. A., pp. 92–93.

Roberts, N. *et al.* (2004) 'Holocene climate, environment and cultural change in the circum-Mediterranean region', in R. W. Battarbee et al. (ed.) *Past Climate Variability through Europe and Africa*. Springer, Dordrecht, The Netherlands., pp. 343–362. doi: 10.1007/978-1-4020-2121-3_17.

Roberts, N. (2014) *The Holocene: an environmental history*. Third Edit. Edited by Wiley Blackwell. Oxford. doi: 10.5860/choice.52-0859.

Roberts, N. *et al.* (2018) 'Human responses and non-responses to climatic variations during the last Glacial-Interglacial transition in the eastern Mediterranean', *Quaternary Science Reviews*. Elsevier Ltd, 184, pp. 47–67. doi: 10.1016/j.quascirev.2017.09.011.

Rodríguez-Ochoa, R. *et al.* (2019) 'Relict periglacial soils on Quaternary terraces in the Central Ebro Basin (NE Spain)', in *Permafrost and Periglacial Processes*. John Wiley and Sons Ltd, pp. 364–373. doi: 10.1002/ppp.2005.

Rohling, E. J., Marino, G. and Grant, K. M. (2015) 'Mediterranean climate and oceanography, and the periodic development of anoxic events (sapropels)', *Earth-Science Reviews*, 143, pp. 62–97. doi: 10.1016/j.earscirev.2015.01.008.

Rousse, S. *et al.* (2006) 'Holocene centennial to millennial-scale climatic variability: Evidence from high-resolution magnetic analyses of the last 10 cal kyr off North Iceland (core MD99-2275)', *Earth and Planetary Science Letters*, 242(3–4), pp. 390–405. doi: 10.1016/j.epsl.2005.07.030.

Rousseau, D.-D. *et al.* (2018) 'European Loess Records ☆', in *Reference Module in Earth Systems and Environmental Sciences*, pp. 1–17. doi: 10.1016/b978-0-12-409548-9.11136-4.

Rousseau, D. D. *et al.* (2017) 'Eurasian contribution to the last glacial dust cycle: How are loess sequences built?', *Climate of the Past*, 13(9), pp. 1181–1197. doi: 10.5194/cp-13-1181-2017.

Rovere, A. *et al.* (2011) 'Underwater geomorphology of the rocky coastal tracts between Finale Ligure and Vado Ligure (western Liguria, NW Mediterranean Sea)', *Quaternary International*, 232(1–2), pp. 187–200. doi: 10.1016/j.quaint.2010.05.016.

Royer, A. *et al.* (2016) 'Investigating the influence of climate changes on rodent communities at a regional-scale (MIS 1-3, Southwestern France)', *PLoS ONE*, 11(1). doi: 10.1371/journal.pone.0145600.

Ruddiman, W. F. and McIntyre, A. (1973) 'Time-transgressive deglacial retreat of polar waters from the North Atlantic', *Quaternary Research*, 3(1), pp. 117–130. doi: 10.1016/0033-5894(73)90058-6.

Salari, L. (2010) 'Lateglacial bats from the "M" layers of the Arene Candide Cave (Liguria, Italy)', *Rivista Italiana di Paleontologia e Stratigrafia*, 116(1), pp. 119–138. doi: 10.13130/2039-4942/5944.

Saltzman, B. and Maasch, K. A. (1988) 'Carbon cycle instability as a cause of the Late Pleistocene Ice Age Oscillations: Modeling the asymmetric response', *Global Biogeochemical Cycles*. John Wiley & Sons, Ltd, 2(2), pp. 177–185. doi: 10.1029/GB002i002p00177.

Saltzman, B. and Verbitsky, M. (1994) 'Late Pleistocene climatic trajectory in the phase space of global ice, ocean state, and CO2: Observations and theory', *Paleoceanography*, 9(6), pp. 767–779. doi: 10.1029/94PA02289.

Sancho, C. *et al.* (2004) 'Morphological and speleothemic development in Brujas Cave (Southern Andean Range, Argentine): Palaeoenvironmental significance', *Geomorphology*. Elsevier, 57(3–4), pp. 367–384. doi: 10.1016/S0169-555X(03)00166-1.

Schwander, J. *et al.* (1997) 'Age scale of the air in the summit ice: Implication for glacial-interglacial temperature change', *Journal of Geophysical Research Atmospheres*. Blackwell Publishing Ltd, 102(16), pp. 19483–19493. doi: 10.1029/97jd01309.

Scott, K. M. *et al.* (2004) 'Optimal methods for estimating kinetic isotope effects from different forms of the Rayleigh distillation equation', *Geochimica et Cosmochimica Acta*, 68(3), pp. 433–442. doi: 10.1016/S0016-7037(03)00459-9.

Sessa, E. *et al.* (2019) 'Microstratigraphic Records as Tools for the Detection of Climatic Changes in Tana di Badalucco Cave (Liguria, NW Italy)', *Geosciences*, 9(6), p. 276. doi: 10.3390/geosciences9060276.

Sessa, E., Bona, F. and Angiolini, L. (2021) 'Frost action and human occupation during the Late Pleistocene in the Italian Southern Alps: micromorphological evidences from the Caverna

Generosa cave', *Italian Journal of Geosciences*. SOCIETA' GEOLOGICA ITALIANA, 140(2), pp. 1–16. doi: 10.3301/IJG.2020.28.

Shackleton, N. J. (1967) 'Oxygen isotope analyses and Pleistocene temperatures re-assessed', *Nature*, 215, pp. 15–17.

Shackleton, N. J. *et al.* (2003) 'Marine isotope substage 5e and the Eemian interglacial', in *Global and Planetary Change*, pp. 151–155. doi: 10.1016/S0921-8181(02)00181-9.

Shahack-Gross, R. *et al.* (2008) 'Formation processes of cemented features in Karstic Cave sites revealed using stable oxygen and carbon isotopicanalyses: A case study at middle paleolithic Amud Cave, Israel', *Geoarchaeology*. John Wiley & Sons, Ltd, 23(1), pp. 43–62. doi: 10.1002/gea.20203.

Shahack-Gross, R. *et al.* (2014) 'Evidence for the repeated use of a central hearth at Middle Pleistocene (300ky ago) Qesem Cave, Israel', *Journal of Archaeological Science*. Academic Press, 44(1), pp. 12–21. doi: 10.1016/j.jas.2013.11.015.

Shumm, S. A. (1991) *To Interpret the Earth: Ten Ways to Be Wrong*. doi: 10.2307/3515401.

Simões, C. D., Carvalho, A. F. and Tente, C. (2020) 'Neolithic geoarchaeology at Penedo dos Mouros Rockshelter: Mid-Holocene site formation, diagenesis and human activity at the foothills of Serra da Estrela (Portugal)', *Geoarchaeology*. John Wiley and Sons Inc., 35(4), pp. 503–521. doi: 10.1002/gea.21785.

Šolcová, A. *et al.* (2020) 'Abrupt vegetation and environmental change since the MIS 2: A unique paleorecord from Slovakia (Central Europe)', *Quaternary Science Reviews*, 230. doi: 10.1016/j.quascirev.2020.106170.

Sommer, R. and Benecke, N. (2004) 'Late- and Post-Glacial history of the Mustelidae in Europe', *Mammal Review*. Blackwell Publishing Ltd, pp. 249–284. doi: 10.1111/j.1365-2907.2004.00043.x.

Sommer, R. and Benecke, N. (2005) 'Late-Pleistocene and early Holocene history of the canid fauna of Europe (Canidae)', *Mammalian Biology*. Elsevier GmbH, 70(4), pp. 227–241. doi: 10.1016/j.mambio.2004.12.001.

Sommer, R. S. and Nadachowski, A. (2006) 'Glacial refugia of mammals in Europe: evidence from fossil records', *Mammal Review*. Blackwell Publishing Ltd, 36(4), pp. 251–265. doi: 10.1111/j.1365-2907.2006.00093.x.

Sorin, L. *et al.* (2010) 'Late Pleistocene palaeoclimatic and palaeoenvironmental reconstruction of the Dead Sea area (Israel), based on speleothems and cave stromatolites', *Quaternary Science*

Reviews. Pergamon, 29(9–10), pp. 1201–1211. doi: 10.1016/j.quascirev.2010.01.018.

Spötl, C. and Mangini, A. (2002) 'Stalagmite from the Austrian Alps reveals Dansgaard-Oeschger events during isotope stage 3: Implications for the absolute chronology of Greenland ice cores', *Earth and Planetary Science Letters*, 203(1), pp. 507–518. doi: 10.1016/S0012-821X(02)00837-3.

Stani, G. *et al.* (2009) 'Evidence of syn-sedimentary tectonic activity in the «flysch di Ventimiglia» (Ligurian Alps foredeep basin)', *Bollettino della Societa Geologica Italiana*. GeoScienceWorld, 128(2), pp. 467–472. doi: 10.3301/IJG.2009.128.2.467.

Stanley, D. J. (1975) 'Submarine canyon and slope sedimentation (Gres d'Annot) in the French Maritime Alps', in *IX Congres Int. Sedimentol. Nice France*, p. 129pp. doi: -.

Steffensen, J. P. *et al.* (2008) 'High-resolution greenland ice core data show abrupt climate change happens in few years', *Science*, 321(5889), pp. 680–684. doi: 10.1126/science.1157707.

Stoops, G. (2003) *Guidelines for analysis and description of soil and regolith thin sections*. Soil Science Society of America. Available at: https://books.google.it/books?id=8c1OAQAAIAAJ.

Stoops, G., Langohr, R. and Van Ranst, E. (2020) 'Micromorphology of soils and palaeosoils in Belgium. An inventory and meta-analysis', *Catena*. Elsevier B.V. doi: 10.1016/j.catena.2020.104718.

Stoops, G., Marcelino, V. and Mees, F. (2010) *Interpretation of Micromorphological Features of Soils and Regoliths*. Elsevier. Available at: https://books.google.it/books?id=HMCyfrxixdoC.

Stoops, G., Marcelino, V. and Mees, F. (2018a) *Interpretation of Micromorphological Features of Soils and Regoliths*. Elsevier. Available at: https://books.google.it/books?id=AZSZDgAAQBAJ.

Stoops, G., Marcelino, V. and Mees, F. (2018b) 'Micromorphological Features and Their Relation to Processes and Classification', in *Interpretation of Micromorphological Features of Soils and Regoliths*. Elsevier, pp. 895–917. doi: 10.1016/b978-0-444-63522-8.00030-9.

Svendsen, J. I. *et al.* (2004) 'Late Quaternary ice sheet history of northern Eurasia', in *Quaternary Science Reviews*, pp. 1229–1271. doi: 10.1016/j.quascirev.2003.12.008.

Tagliacozzo, A. *et al.* (2012) 'Archaeozoological evidence of subsistence strategies during the Gravettian at Riparo Mochi (Balzi Rossi, Ventimiglia, Imperia - Italy)', *Quaternary International*, 252, pp. 142–154. doi: 10.1016/j.quaint.2011.03.059.

Todisco, D. and Bhiry, N. (2008) 'Micromorphology of periglacial sediments from the Tayara

site, Qikirtaq Island, Nunavik (Canada)', *Catena*, 76(1), pp. 1–21. doi: 10.1016/j.catena.2008.08.002.

TS-Creator (2020). Available at: https://timescalecreator.org/index/index.php (Accessed: 15 December 2020).

Urey, H. C. (1947) 'The thermodynamic properties of isotopic substances. Liversidge lecture, delivered before the Chemical Society in the Royal Institution on December 18th, 1946', *Journal of the Chemical Society (Resumed)*. The Royal Society of Chemistry, (0), pp. 562–581. doi: 10.1039/jr9470000562.

Vacchi, M. *et al.* (2016) 'Multiproxy assessment of Holocene relative sea-level changes in the western Mediterranean: Sea-level variability and improvements in the definition of the isostatic signal', *Earth-Science Reviews*, pp. 172–197. doi: 10.1016/j.earscirev.2016.02.002.

Valensi, P. *et al.* (2008) 'LA GROTTE DE SANTA LUCIA SUPERIORE (TOIRANO, LIGURIE, ITALIE). LES FAUNES PENDANT LE PLÉISTOCÈNE SUPÉRIEUR ANCIEN', in *Toirano e la Grotta della Basùra, Atti del Convegno, Toirano, 26-28 ottobre 2000*. Bordighera, pp. 159–169. Available at: https://d1wqtxts1xzle7.cloudfront.net/53637701/2008-Valensi-et-al-SantaLuciaSuperiore.pdf?1498227679=&response-content-disposition=inline%3B+filename%3DLa_grotte_de_Santa_Lucia_Superiore_Toira.pdf&Expires=1611253606&Signature=Q3SW~y-7SFZvbEwtQbS-1PMpQzUbc (Accessed: 21 January 2021).

Valensi, P. (2009) 'Evolution of large mammal populations in west mediterranean Europe during middle and upper pleistocene. A regional example: French and Italian Southern ALPS', *Quaternaire*. Association Française pour l'Étude du Quaternaire, 20(4), pp. 551–567. doi: 10.4000/quaternaire.5368.

Valensi, P., Crégut-Bonnoure, E. and Defleur, A. (2012) 'Archaeozoological data from the Mousterian level from Moula-Guercy (Ardèche, France) bearing cannibalised Neanderthal remains', *Quaternary International*, 252, pp. 48–55. doi: 10.1016/j.quaint.2011.07.028.

Valensi, P. and Psathi, E. (2004) 'Faunal exploitation during the Middle Palaeolithic in South-eastern France and North-western Italy', *International Journal of Osteoarchaeology*, 14(3–4), pp. 256–272. doi: 10.1002/oa.760.

Vallverdú-Poch, J. and Courty, M. A. (2012) 'Microstratigraphic analysis of level J deposits: A dual paleoenvironmental-paleoethnographic contribution to paleolithic archeology at the Abric Romaní', in *Vertebrate Paleobiology and Paleoanthropology*. Springer, pp. 77–133. doi: 10.1007/978-94-007-3922-2_4.

Vandenberghe, J. *et al.* (1998) ‘Short climatic oscillations in a western European loess sequence (Kesselt, Belgium)’, *Journal of Quaternary Science*, 13(5), pp. 471–485. doi: 10.1002/(SICI)1099-1417(1998090)13:5<471::AID-JQS401>3.0.CO;2-T.

Vesica, P. L. *et al.* (2000) ‘Late Pleistocene Paleoclimates and sea-level change in the Mediterranean as inferred from stable isotope and U-series studies of overgrowths on speleothems, Mallorca, Spain’, *Quaternary Science Reviews*, 19(9), pp. 865–879. doi: 10.1016/S0277-3791(99)00026-8.

Villagran, X. S. *et al.* (2017) ‘Bone and Other Skeletal Tissues’, in *Archaeological Soil and Sediment Micromorphology*. Chichester, UK: John Wiley & Sons, Ltd, pp. 9–38. doi: 10.1002/9781118941065.ch1.

Vliet-Lanoë, B. Van (2010) ‘Frost Action’, in *Interpretation of Micromorphological Features of Soils and Regoliths*. Elsevier, pp. 81–108. doi: 10.1016/B978-0-444-53156-8.00006-4.

Van Vliet-Lanoë, B. (2013) *Cryosphère, Histoire et environnements de notre ère glaciaire, Ed. Vuibert*. Vuibert.

Van Vliet-Lanoë, B. and Fox, C. A. (2018) ‘Frost action’, in *Interpretation of micromorphological features of soils and regoliths*. Elsevier, pp. 575–603. doi: 10.1016/B978-0-444-63522-8.00020-6.

Van Vliet-Lanoe, B., Fox, C. A. and Gubin, S. V (2004) ‘Micromorphology of cryosols’, in *Cryosols*. Springer, pp. 365–390.

Van Vliet-Lanoë, B. and Hallegouët, B. (2001) ‘European permafrost at the LGM and at its maximal extent’, in *Permafrost Response on Economic Development, Environmental Security and Natural Resources*. Dordrecht: Springer Netherlands, pp. 195–213. doi: 10.1007/978-94-010-0684-2_13.

Van Vliet-Lanoë, B., Coutard, J. -P and Pissart, A. (1984) ‘Structures caused by repeated freezing and thawing in various loamy sediments: A comparison of active, fossil and experimental data’, *Earth Surface Processes and Landforms*, 9(6), pp. 553–565. doi: 10.1002/esp.3290090609.

van Vliet, B. and Langohr, R. (1981) ‘Correlation between fragipans and permafrost with special reference to silty Weichselian deposits in Belgium and northern France’, *CATENA*. Elsevier BV, 8(2), pp. 137–154. doi: 10.1016/0341-8162(81)90002-3.

Voelker, A. H. L. (2002) ‘Global distribution of centennial-scale records for Marine Isotope Stage (MIS) 3: A database’, *Quaternary Science Reviews*. Pergamon, 21(10), pp. 1185–1212. doi: 10.1016/S0277-3791(01)00139-1.

Waelbroeck, C. *et al.* (2002) 'Sea-level and deep water temperature changes derived from benthic foraminifera isotopic records', *Quaternary Science Reviews*. Pergamon, 21(1–3), pp. 295–305. doi: 10.1016/S0277-3791(01)00101-9.

Waelbroeck, C. *et al.* (2008) 'Transferring radiometric dating of the last interglacial sea level high stand to marine and ice core records', *Earth and Planetary Science Letters*, 265(1–2), pp. 183–194. doi: 10.1016/j.epsl.2007.10.006.

Weber, M. *et al.* (2018) 'Evidence of warm and humid interstadials in central Europe during early MIS 3 revealed by a multi-proxy speleothem record', *Quaternary Science Reviews*. Elsevier Ltd, 200, pp. 276–286. doi: 10.1016/j.quascirev.2018.09.045.

Whitau, R. *et al.* (2018) 'Home Is Where the Hearth Is: Anthracological and Microstratigraphic Analyses of Pleistocene and Holocene Combustion Features, Riwi Cave (Kimberley, Western Australia)', *Journal of Archaeological Method and Theory*. Springer New York LLC, 25(3), pp. 739–776. doi: 10.1007/s10816-017-9354-y.

White, W. B. (2007) 'Cave sediments and paleoclimate', *Journal of Cave and Karst Studies*, pp. 76–93.

Whitney, D. L. and Evans, B. W. (2010) 'Abbreviations for names of rock-forming minerals', *American Mineralogist*, 95(1), pp. 185–187. doi: 10.2138/am.2010.3371.

Willner, W., Di Pietro, R. and Bergmeier, E. (2009) 'Phytogeographical evidence for post-glacial dispersal limitation of European beech forest species', *Ecography*. John Wiley & Sons, Ltd, 32(6), pp. 1011–1018. doi: 10.1111/j.1600-0587.2009.05957.x.

Wohlfarth, B. *et al.* (2008) 'Rapid ecosystem response to abrupt climate changes during the last glacial period in western Europe, 40-16 ka', *Geology*, 36(5), pp. 407–410. doi: 10.1130/G24600A.1.

Woodward, J. C. and Goldberg, P. (2001) 'The Sedimentary Records in Mediterranean Rockshelters and Caves: Archives of Environmental Change', *Geoarchaeology - An International Journal*, 16(4), pp. 327–354. doi: 10.1002/gea.1007.

Yang, F., Karius, V. and Sauer, D. (2020) 'Short Communication. Quantification of loess proportions in Pleistocene periglacial slope deposits and Holocene colluvium using grain-size data by laser diffractometry', *Journal of Plant Nutrition and Soil Science*. Wiley-VCH Verlag. doi: 10.1002/jpln.201900376.

Zambelli, F. H. (1934) 'La Tana di Badalucco nella Liguria Occidentale', *Le Grotte d'Italia*. (VIII), XII(1–4), pp. 1–11.

Zanchetta, G. *et al.* (2014) ‘Coeval dry events in the central and eastern Mediterranean basin at 5.2 and 5.6ka recorded in Corchia (Italy) and Soreq caves (Israel) speleothems’, *Global and Planetary Change*, 122, pp. 130–139. doi: 10.1016/j.gloplacha.2014.07.013.

Zerboni, A. *et al.* (2018) ‘Towards a map of the Upper Pleistocene loess of the Po Plain Loess Basin (Northern Italy)’, *Alpine and Mediterranean Quaternary*, 31(1), pp. 253–256. Available at: https://www.researchgate.net/publication/325930091.

Zhornyak, L. V *et al.* (2011) ‘Stratigraphic evidence for a “ pluvial phase” between ca 8200-7100 ka from Renella cave (Central Italy)’, *Quaternary Science Reviews*, 30(3–4), pp. 409–417. doi: 10.1016/j.quascirev.2010.12.003.

Appendices

Appendix A: Micromorphological description table

In order to best describe every single thin section's feature, a specific table, as comprehensive as possible, was developed.

Site:

Thin section:

Microstructure and porosity pattern

Microstructure	

Aggregates	Size	Notes (relative % if needed)

Voids	Size	Frequency	Notes

Groundmass

c\f limit	
c\f ratio	
c\f related distribution	

Coarse material

Single mineral grains

Nature	Shape	Alteration	Size	Frequency	Pattern

Compound mineral grains and rock fragments

Nature	Shape	Alteration	Size	Frequency	Pattern

Inorganic residues of biological origin

Nature	Size	Alteration	Abundance	Pattern
Bones				
Shells				
Teeth				
Spherulites				
Biospheroids				
Phytoliths				
Opaline particles				
Hair				

Anthropogenic elements

Nature	Size	Alteration	Abundance	Pattern
Burnt bones				
Charcoal				
Bricks and pottery				
Glass				
Metal fragments				
Ashes				
Lithic artefacts				

Organic components

Residue	Size	Colour	Alteration (see Stoops, 2003)
Organ			
Tissue			
Organic fine material			

Micromass

Nature	Colour	Limpidity	Interference col.	B-fabric

Organic material not included in the groundmass

Type	Alteration	Size	Pattern

Pedofeatures

Ferrous features

Nature	Size	Shape	Abundance	Pattern	Alteration

Manganese features

Nature	Size	Shape	Abundance	Pattern	Alteration

Calcitic features

Nature	Size	Shape	Abundance	Pattern	Alteration

Clayey features

Nature	Size	Shape	Abundance	Pattern	Alteration

Phosphorous features

Nature	Size	Shape	Abundance	Pattern	Alteration

Excrements

Nature	Size	Shape	Abundance	Pattern	Alteration

Other

Nature	Size	Shape	Abundance	Pattern	Alteration

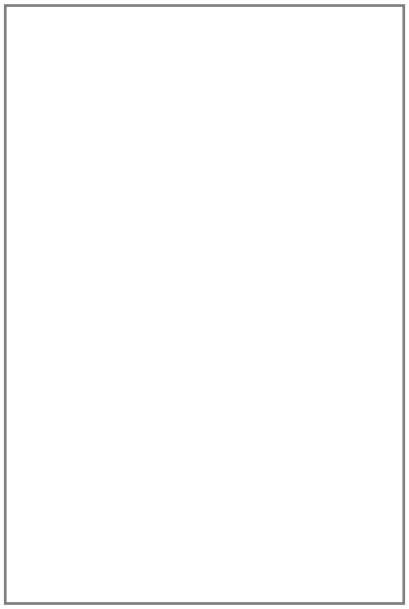

Characteristics:

Appendix B: Micromorphological analysis description

For each thin section a description was created, following Stoops' indications (Stoops, 2003). Here below these descriptions are presented in a schematic way, divided by cave and stratigraphic section.

Tana di Badalucco cave

Section 1:

Thin section TB A1 (MFT: Quartz-rich, reddish clayey deposits, QRC)

Vertical thin section.

Microstructure and porosity

Highly separated subangular blocky microstructure, with subangular blocky peds (2-3 cm). Planes (very fine sand sized, v.f.s.; ±10% of the peds); channels (fine sand, f.s., ±10%); chambers (f.s., ±5%); vughs (v.f.s., ±5%); vesicles (f.s., ±2%).

Groundmass

c/$f_{5\mu m}$ ratio: 40/60; c/f-related distribution pattern: single spaced porphyric.

Coarse material:

Mineral: angular grains of quartz (v.f.s., ±20% of the entire thin section area); angular grains of feldspars (v.f.s., ±5%), both with no signs of weathering. Quartz can sometimes be found in same sized grains lenses. Few tabular, not identifiable (due to weathering) rock fragments are present (medium sand, m.s., ±5%).

Micromass: reddish brown, cloudy clay and iron with granostriated b-fabric.

Pedofeatures

- Typic ferrous nodules, around 100 µm in diameter, no pattern found (±2% of the total area).
- Typic manganese nodules, around 100 µm in diameter, no pattern found (±2%).
- Micritic mammillate nodules, f.s., ±2%.
- Continuous micritic hypocoatings, about 50 µm thick, ±1%.

- Dusty parallel microlaminated clay coatings with sharp extinction lines, in some cases fragmented, about 50 µm thick, ±10%.

Thin section TB A2 (MFT: Quartz-rich, reddish clayey deposits, QRC)

Vertical thin section.

Microstructure and porosity

Subangular blocky microstructure with a single subangular blocky ped (5 cm in diameter); planes (v.f.s., ±10%); channels (f.s., ±5%); chambers (f.s., ±2%); vughs (v.f.s., ±2%).

Groundmass

c/$f_{5\mu m}$ ratio: 40/60; c/f-related distribution pattern: single spaced porphyric.

Coarse material:

Mineral: angular quartz grains (f.s., ±30%); subangular calcite grains (f.s., ±2%), highly altered. Very few tabular, not identifiable (due to weathering) rock fragments (f.s., ±2%).

Micromass: Brown, cloudy clay and iron with granostriated b-fabric.

Pedofeatures

- Typic iron nodules, f.s., ±2%, some are fragmented.
- Manganese (hydr)oxides hypocoatings, v.f.s., ±1%.
- Micritic hypocoatings, v.f.s., ±2%, concentrated in the upper half of the thin section.
- Micritic mammillate nodules, f.s., ±1%, concentrated in the upper half of the thin section, as well.
- Limpid parallel microlaminated clay coatings with sharp extinction lines, v.f.s., ±10%.
- Limpid parallel microlaminated infillings with sharp extinction lines, f.s., ±5%, some are fragmented.
- Cryptocrystalline typic apatite nodules, m.s., ±1%, showing low degree of alteration.

Section 2:

Thin section TB B (Cold and Human influence MFT, CH)

Horizontal thin section.

Microstructure and porosity

Complex microstructure: subangular blocky and platy microstructure, with subangular blocky peds (5 mm), lenticular plates (0.5 mm), porous crumbs (0.5 mm). Planes (v.f.s., ±10%), vughs (v.f.s., ±5%), chambers (f.s., ±5%), channels (f.s., ±5%), vesicles (v.f.s., ±2%).

Groundmass

c/$f_{5\mu m}$ ratio: 40/60; c/f-related distribution pattern: double spaced porphyric.

Coarse material:

Mineral: Two textural classes of quartz grains: one more angular and finer (silt size, s.s., ±10%), the other subangular and bigger (f.s. and m.s., ±10%). Tabular greywacke fragments (m.s., ±10%) with their main axis perpendicular to the ground surface), moderately weathered subangular fossiliferous limestone (f.s., ±5%).

Inorganic residues of biological origin: moderately to highly altered bones (f.s., ±2%); moderately to highly altered bones showing signs of burning (f.s., ±2%).

Micromass: dark brown, cloudy clay with weakly expressed granostriated b-fabric.

Pedofeatures

- Typic ferrous nodules, f.s., ±2%.
- Micritic hypocoatings, v.f.s., ±1%.
- Clay depletion hypocoating, coarse sand (c.s.), ±2%.
- Cryptocrystalline apatite nodules, f.s., ±2%.
- Subrounded excrements of large animals, sometimes clustered, f.s., ±2%.

Thin section TB C (Cold and Bioturbation MFT, CB)

Vertical thin section.

Microstructure and porosity

Complex microstructure: moderately separated subangular blocky and moderately separated crumb microstructure, with subangular blocky peds (pebble size), porous crumbs (f.s.). Vughs (v.f.s., ± 10%); channels (v.f.s., ±5%); planes (s.s., ±5%); chambers (f.s., ±5%).

Groundmass

c/$f_{5\mu m}$ ratio: 40/60; c/f-related distribution pattern: single spaced porphyric.

Coarse material

Mineral: angular quartz grains (v.f.s.-s.s., ±20%). Rounded micritic limestone, highly weathered (v.f.s., ±2%); tabular and subrounded greywacke, highly weathered (v.f.s.-s.s., ±2%).

Micromass: Brown, cloudy clay with granostriated b-fabric.

Pedofeatures

- Typic ferrous nodules, v.f.s., ±5%.
- Manganese (hydr)oxides hypocoatings, dendritic sometimes (s.s., ±1%).
- Micritic hypocoatings (s.s., ±2%).
- Limpid nonlaminated clay coating with diffuse extinction lines, occasionally juxtaposed on Mn hypocoatings (v.f.s., ±2%).
- Limpid nonlaminated clay infilling with diffuse extinction lines, occasionally juxtaposed on Mn hypocoatings (v.f.s., ±2%).
- Clay depletion hypocoating, coarse sand (c.s., ±2%).
- Subrounded excrements of large animals, (m.s., ±2%).

Thin section TB D (Cold and Bioturbation MFT, CB)

Vertical thin section.

Microstructure and porosity

Complex microstructure: moderately separated subangular blocky, moderately separated crumb. Subangular blocky peds (pebble size); porous crumbs (very coarse sand, v.c.s.). Planes (v.f.s., ±10%); complex packing voids (f.s., ±5%); channels (f.s., ±5%); chambers (f.s., ±5%); vughs (v.f.s., ±2%); vesicles (v.f.s., ±2%).

Groundmass

c/$f_{5\mu m}$ ratio: 30/70; c/f-related distribution pattern: double spaced porphyric; locally single spaced coarse enaulic.

Coarse material

Mineral: angular grains of quartz (s.s., ±20%). Fossiliferous rounded limestone, highly altered (m.s., ±2%); tabular greywacke, highly to moderately weathered (m.s., ±2%); highly weathered subangular sandstone (very coarse sand, v.c.s., one occurrence).

Inorganic residues of biological origin: bones (pebble size, one occurrence) at the top of the thin section.

Micromass: Brown, cloudy clay with weakly developed striated b-fabric.

Pedofeatures

- Typic ferrous nodules (v.f.s., ±2%).
- Micritic hypocoating, found only at the bone fragment (v.f.s., ±1%).
- Clayey silt capping, nonlaminated on a highly weathered sandstone grain (200 µm thick).
- Cryptocrystalline apatite nodules (f.s., ±1%).
- Subrounded excrements of large animals, (m.s., ±1%).

Thin section TB E (Humid and Temperate MFT, HT)

Vertical thin section.

Microstructure and porosity

Complex microstructure: moderately separated subangular blocky microstructure and chamber microstructure. Subangular blocky peds, 2 cm in size. Chambers (c.s., ±10%); planes (f.s., ±5%); channels (f.s., ±5%); vesicles (f.s., ±5%); vughs (f.s., ±2%).

Ground mass

c/$f_{5\mu m}$ ratio: 20/80; c/f-related distribution pattern: open porphyric.

Coarse material

Mineral: subangular quartz grains, moderately weathered (two size classes: s.s. and f.s., ±5%); Subangular feldspar grains, moderately to highly weathered (v.f.s., 2%). Subangular limestone, highly weathered (m.s., ±1%).

Micromass: brown, cloudy clay with weakly developed random striated b-fabric.

Pedofeatures

- Typic ferrous nodules (v.f.s., 2%).
- Manganese (hydr)oxides hypocoatings, dendritic sometimes (v.f.s., ±5%).
- Micritic hypocoatings (v.f.s., ±2%).
- Dense and incomplete calcite infilling, with equigranular and xenotopic crystals, fractured (±1 cm, in the top left part of the thin section, ±2%).
- Dusty clay coatings, nonlaminated, diffuse or absence of extinction lines (v.f.s., ±2%).
- Dusty clay infillings, nonlaminated, diffuse or absence of extinction lines (f.s., ±1%).

- Subrounded excrements of large animals, (m.s., ±2%).

Thin section TB F1 (Cold and Bioturbation MFT, CB)

Vertical thin section.

Microstructure and porosity

Moderately separated subangular blocky microstructure. Subangular blocky peds (pebble size, p.s.); plates (c.s.). Chambers (f.s., but one is 1 cm in size, ±20%); planes (v.f.s., ±10%); channels (f.s., ±10%); vughs (f.s., ±10%).

Groundmass

$c/f_{5\mu m}$ ratio: 20/80; c/f-related distribution pattern: open porphyric.

Coarse material

Mineral: Angular quartz grains (s.s., ±10%). Subrounded limestone, highly weathered (m.s., ±10%); subangular greywacke, moderately weathered (m.s. ±5%).

Inorganic residues of biological origin: bones (m.s., ±2%);

Anthropogenic elements: burnt bones (m.s., ±1%); charcoal fragments (f.s., ±2%).

Micromass: dark brown, cloudy clay and calcite with weakly developed striated.

Pedofeatures

- Typic ferrous nodules (f.s., ±2%).
- Micritic hypocoatings (v.f.s., ±2%).
- Cryptocrystalline apatite nodules (v.f.s., ±5%).
- Subrounded excrements of large animals, (m.s., ±1%).

Thin section TB F2 (Cold and Human influence MFT, CH)

Vertical thin section.

Microstructure and porosity

Complex microstructure: moderately separated subangular blocky and moderately separated crumb microstructure. Subangular blocky peds (pebble size, p.s.); porous crumbs (c.s.). Complex packing voids (c.s., ±10%); planes (v.f.s., ±5%); channels (f.s., ±5%); vesicles (f.s., ±5%); vughs (f.s., ±5%).

Groundmass

c/$f_{5\mu m}$ ratio: 30/70; c/f-related distribution pattern: open porphyric and single spaced enaulic.

Coarse material

Mineral: Angular quartz grains (s.s., ±10%). Subrounded limestone, highly weathered (m.s., ±10%); subangular greywacke, moderately weathered (m.s. ±5%).

Inorganic residues of biological origin: bones (m.s., ±2%);

Anthropogenic elements: burnt bones (m.s., ±2%); charcoal fragments (f.s., ±2%); ashes (f.s., ±5%).

Micromass: dark brown, cloudy clay and calcite with weakly developed striated.

Pedofeatures

- Typic ferrous nodules (f.s., ±1%).
- Cryptocrystalline apatite nodules (v.f.s., ±2%).
- Subrounded excrements of large animals (m.s., ±10%).

Section 3:

Thin section TB G (Cold and Human influence MFT, CH)

Vertical thin section.

Microstructure and porosity

Complex microstructure: moderately separated subangular blocky and moderately separated granular microstructure. Subangular blocky peds (cobble size, c.s.); granules (c.s.-v.c.s.). Vughs (m.s., ±10%); complex packing voids (c.s., ±5%); planes (v.f.s., ±5%); channels (f.s., ±5%).

Groundmass

c/$f_{5\mu m}$ ratio: 60/40; c/f-related distribution pattern: close fine enaulic and open porphyric.

Coarse material

Mineral: Angular quartz grains (two size classes: f.s. and m.s., ±15%); calcite grains (m.s., 2%). Angular and subangular fossiliferous limestone, highly weathered (cobble size, ±30%); subangular greywacke, moderately weathered (m.s. ±5%).

Inorganic residues of biological origin: bones (m.s., ±2%);

Anthropogenic elements: burnt bones (f.s., ±1%); charcoal fragments (f.s., ±1%).

Micromass: brown, cloudy clay with weakly developed striated.

Pedofeatures

- Typic ferrous nodules (f.s., ±2%).
- Cryptocrystalline apatite nodules (f.s., ±1%).

Section 1:

Thin section* a *(MFT: Cave wall deposits, CW)

Vertical thin section.

Microstructure and porosity

The microstructure was not detectable and neither aggregates. Channels (fine sand, f.s., ±10%); planes (v.f.s.; ±5%); chambers (c.s., ±2%).

Groundmass

c/$f_{5\mu m}$ ratio: 40/60; c/f-related distribution pattern: single spaced porphyric.

Coarse material:

Mineral: angular and subangular grains of quartz (v.f.s., ±2%), with no signs of weathering. Fossiliferous limestone rock fragments (pebble size, ±20%).

Inorganic residues of biological origin: bones (f.s., ±2%);

Anthropogenic elements: charcoal fragments (f.s., ±5%).

Micromass: greyish brown, speckled mixture of clay and calcite; crystallitic b-fabric.

Pedofeatures

- Typic ferrous nodules, v.f.s., no pattern found (±1% of the total area).
- Sparitic calcite coatings with palisade fabric (equigranular hypidiotopic), m.s., ±50%.
- Micritic nodules, f.s., ±5%.
- Silt nonlaminated coatings with no extinction lines, m.s. in thickness, ±10%.

Section 2:

Thin section* b *(MFT: Greyish and coarse deposit, GC)

Vertical thin section.

Microstructure and porosity

Weakly separated subangular blocky and crumb microstructure, with a platy overprint in the upper part, and with subangular blocky peds (v.c.s.) and porous crumbs (c.s.). Complex packing

voids (v.f.s., ±10%); planes (v.f.s.; ±5%); channels (s.s., ±5%); chambers (f.s., ±2%); regular vughs (s.s., ±2%).

Groundmass

c/$f_{5\mu m}$ ratio: 50/50; c/f-related distribution pattern: Single spaced porphyric - single spaced equal enaulic.

Coarse material:

Mineral: subangular grains of quartz (f.s., ±5%), with no signs of weathering. Fossiliferous and non-fossiliferous subrounded limestone rock fragments (m.s., but with a fragment occupying all the lower part 6x2 cm, ±30%); quartzite subangular and subrounded rock fragments (m.s.; ±10%); subrounded porphyroid rock fragment (v.c.s., one occurrence in the middle lower part of the thin section).

Inorganic residues of biological origin: highly weathered bones (f.s., ±1%);

Anthropogenic elements: highly weathered burnt bones (f.s., ±1%); charcoal fragments (f.s., ±2%).

Micromass: yellowish brown, speckled mixture of calcite, clay and phosphates; undifferentiated-crystallitic b-fabric.

Pedofeatures

- Typic ferrous nodules, no pattern found (s.s., ±1%).
- Manganese (hydr)oxide hypocoatings (v.f.s., ±2%).
- Two silty cappings on two quartz grains (v.c.s.)
- Micritic (equigranular xenotopic) nodules (f.s., ±5%).
- Cryptocrystalline typic apatite nodules (f.s., ±1%).
- Subrounded excrements of large animals, (m.s., ±2%).

Thin section* c *(MFT: Deposits rich in material of organic origin, MOO)

Vertical thin section.

Microstructure and porosity

Weakly separated crumb microstructure, with porous crumbs (m.s.). Complex packing voids (s.s., ±20%); channels (s.s., ±10%); regular vughs (s.s., ±2%).

Groundmass

c/$f_{5\mu m}$ ratio: 40/60; c/f-related distribution pattern: Single spaced equal-coarse enaulic.

Coarse material:

Mineral: subangular grains of quartz (f.s., ±10%), with no signs of weathering; subangular grains of calcite (f.s., ±5%). Fossiliferous subangular and subrounded limestone rock fragments (m.s., but with a 3 cm fragment, ±20%); quartzite subangular and subrounded rock fragments (f.s.; ±5%).

Inorganic residues of biological origin: moderately weathered bones (f.s., ±5%);

Anthropogenic elements: moderately weathered burnt bones (f.s., ±5%); charcoal fragments (f.s., ±2%), bigger fragments in the lower part of the thin section.

Micromass: yellowish brown, speckled mixture of calcite, clay and phosphates; weakly developed crystallitic - undifferentiated b-fabric.

Pedofeatures

- Typic ferrous nodules, no pattern found (s.s., ±2%).
- Manganese (hydr)oxide hypocoatings (s.s., ±1%).
- Micritic (equigranular xenotopic) nodules (s.s., ±5%).
- Subrounded excrements of large animals, (f.s., ±1%).

Section 3:

***Thin section* d**

Vertical thin section.

Two microfacies are present and will be described separately.

Microfacies I: Deposits rich in material of organic origin (MOO)

Microstructure and porosity

Weakly separated subangular blocky microstructure, with weakly developed pedality. Channels (f.s., ±5%); planes (s.s.; ±5%); chambers (f.s., ±2%).

Groundmass

c/$f_{5\mu m}$ ratio: 30/70; c/f-related distribution pattern: Double spaced porphyric.

Coarse material:

Mineral: subangular and angular grains of quartz (f.s., ±5%), with no signs of weathering. Subangular grains of microcline (f.s., ±1%), with low signs of weathering. Fossiliferous and non-fossiliferous subrounded limestone rock fragments (v.c.s., but with fragments up to 2 cm in size, ±20%); quartzite subangular rock fragments (v.c.s.; ±2%).

Inorganic residues of biological origin: bones (f.s., ±5%);

Anthropogenic elements: burnt bones (f.s., ±1%); charcoal fragments (m.s., ±2%).

Micromass: brown grey, speckled mixture of calcite, clay and phosphates; undifferentiated-crystallitic b-fabric.

Organic material not included in the groundmass: one brown burnt plant tissue residue, isotropic (c.s.).

Pedofeatures

- Typic ferrous nodules (s.s., ±1%).
- Coatings with palisade fabric (equigranular hypidiotopic) (f.s.-m.s., ±5%). On rock fragments and in contact with voids.
- Micritic (equigranular xenotopic) nodules (f.s., ±1%).
- Subrounded excrement of large carnivore, (granule size, one occurrence).

Microfacies II: Sediments rich in charred material (CM)

Microstructure and porosity

Moderately separated crumb microstructure, with porous crumbs (f.s.). Compound packing voids (v.f.s., ±20%); channels (f.s., ±5%); planes (f.s.; ±2%).

Groundmass

c/$f_{5\mu m}$ ratio: 30/70; c/f-related distribution pattern: single spaced coarse enaulic.

Coarse material:

Mineral: subangular grains of quartz (f.s., ±5%). Fossiliferous subrounded limestone rock fragments (c.s., ±10%); quartzite subangular rock fragments (f.s.; ±2%).

Inorganic residues of biological origin: bones (v.f.s., ±5%);

Anthropogenic elements: burnt bones (s.s., ±1%); charcoal fragments (f.s., ±10%).

Micromass: light brown (few crumbs show a reddened micromass), speckled mixture of calcite, clay and phosphates; weakly developed crystallitic b-fabric.

Pedofeatures

- Typic ferrous nodules (s.s., ±1%).
- Micritic (equigranular xenotopic) nodules (f.s., ±1%).
- Subrounded excrement of large animals, (c.s., ±2%).

Thin section* e *(MFT: Deposits rich in material of organic origin, MOO)

Vertical thin section.

Microstructure and porosity

Complex: moderately separated crumb structure and subangular blocky structure, with porous crumbs (v.f.s.) and subangular blocky peds (f.s.). Complex packing voids (f.s., ±10%); channels (f.s., ±5%); vughs (v.f.s., ±5%).

Groundmass

$c/f_{5\mu m}$ ratio: 30/70; c/f-related distribution pattern: Single spaced equal enaulic and double spaced porphyric.

Coarse material:

Mineral: subangular grains of quartz (v.f.s., ±10%). Fossiliferous and speleothem subangular limestone rock fragments (c.s., but up to 3 cm, ±20%); quartzite subangular and subrounded rock fragments (v.f.s.; ±5%).

Inorganic residues of biological origin: bones (f.s., ±1%);

Anthropogenic elements: burnt bones (f.s., ±1%); charcoal fragments (v.f.s.-f.s., ±2%).

Micromass: Yellowish grey-very light brown, speckled mixture of calcite, clay and phosphates; crystallitic - undifferentiated b-fabric.

Pedofeatures

- Typic ferrous nodules, no pattern found (v.f.s., ±1%).
- Micritic (equigranular xenotopic) nodules (f.s., ±2%).
- Equigranular xenotopic calcitic infillings (f.s., ±1%).
- Cryptocrystalline typic apatite nodules (f.s., ±1%).

***Thin section* f**

Vertical thin section.

Two microfacies are present and will be described separately.

Microfacies I: Deposits rich in material of organic origin (MOO)

Microstructure and porosity

Moderately separated crumb microstructure, with porous crumbs (v.c.s.). Complex packing voids (f.s., ±10%); channels (s.s., ±5%); vughs (f.s., ±5%).

Groundmass

$c/f_{5\mu m}$ ratio: 20/80; c/f-related distribution pattern: close coarse enaulic.

Coarse material:

Mineral: subangular grains of quartz (f.s., ±5%). Fossiliferous rounded limestone rock fragments (m.s., ±5%).

Inorganic residues of biological origin: bones (f.s., ±2%);

Anthropogenic elements: burnt bones (v.f.s., ±1%); charcoal fragments (f.s., ±2%).

Micromass: Yellowish grey, speckled mixture of calcite, clay and phosphates; crystallitic - undifferentiated b-fabric.

Pedofeatures

- Typic ferrous nodules (f.s., ±1%).
- Manganese (hydr)oxide hypocoatings (s.s., ±2%), along the outlines of the aggregates.
- Micritic (equigranular xenotopic) nodules (m.s., ±5%).
- Cryptocrystalline typic apatite nodules (f.s., ±1%).
- Subrounded excrement of large animals, (c.s., ±1%).

Microfacies II: Sediments rich in charred material (CM)

Microstructure and porosity

Moderately separated crumb microstructure, with porous crumbs (c.s.). Compound packing voids (v.f.s., ±20%); channels (m.s., ±5%).

Groundmass

c/$f_{5\mu m}$ ratio: 40/60; c/f-related distribution pattern: single spaced equal enaulic.

Coarse material:

Mineral: subangular grains of quartz (f.s., ±10%); Subangular grains of calcite (f.s., ±1%). Fossiliferous subrounded limestone rock fragments (v.c.s., ±20%); quartzite subangular rock fragments (m.s.; ±2%); subangular chert rock fragments (m.s., ±1%).

Inorganic residues of biological origin: bones (m.s., ±2%);

Anthropogenic elements: burnt bones (m.s., ±2%); charcoal fragments (m.s., ±2%).

Micromass: brown, speckled mixture of clay, calcite and phosphates; weakly developed crystallitic b-fabric.

Pedofeatures

- Typic ferrous nodules (m.s., ±1%).
- Manganese (hydr)oxide hypocoatings (s.s., ±1%), along the outlines of the aggregates.
- Micritic (equigranular xenotopic) nodules (f.s., ±1%).
- Cryptocrystalline typic apatite nodules (f.s., ±1%).
- Subrounded excrement of large animals, (c.s., one occurrence).

Section 4:

For section 4, a different approach to description will be used: since the same levels have been sampled more than once, we will proceed with a description following the order of the recognized microfacies (following the order presented in Figure 41).

Microfacies I (thin section g) (MFT: Deposits rich in material of organic origin, MOO)

Microstructure and porosity

Weakly separated subangular blocky microstructure, with weakly developed pedality, with subangular blocky peds (c.s.). Channels (f.s., ±10%); complex packing voids (v.f.s., ±5%); planes (s.s.; ±5%).

Groundmass

c/$f_{5\mu m}$ ratio: 30/70; c/f-related distribution pattern: close coarse enaulic.

Coarse material:

Mineral: subangular and angular grains of quartz (f.s., ±5%); subangular grains of calcite (f.s., ±2%). Fossiliferous subrounded limestone rock fragments (m.s., ±10%); quartzite subangular and subrounded rock fragments (f.s.; ±2%).

Inorganic residues of biological origin: bones (f.s., ±1%);

Anthropogenic elements: burnt bones (v.f.s., ±1%); charcoal fragments (f.s., ±1%).

Micromass: brown grey, speckled mixture of calcite, clay and phosphates; undifferentiated-crystallitic b-fabric.

Pedofeatures

- Typic ferrous nodules (v.f.s., ±1%).
- Manganese (hydr)oxide hypocoatings (f.s., ±1%).
- Micritic (equigranular xenotopic) nodules (f.s., ±2%).
- Compound parallel layered typic dusty clay coatings (m.s., one occurrence), fragmented.
- Subrounded excrement of large animals, (granule size, five occurrences).

Microfacies II (thin sections* g, i, h*) (MFT: Yellowish deposit, YD)

Microstructure and porosity

Moderately separated crumb microstructure, with porous crumbs (f.s.) and subangular blocky peds (fine gravel size). Complex packing voids (v.f.s., ±20%); channels (s.s., ±5%); planes (s.s.; ±2%).

Groundmass

c/$f_{5\mu m}$ ratio: 50/50; c/f-related distribution pattern: Single spaced equal enaulic and double spaced porphyric.

Coarse material:

Mineral: subangular grains of quartz (v.f.s., ±10%). Fossiliferous subrounded limestone rock fragments (f.s. but up to cobble size, above all at the limit between mF II and mF III, ±30%); quartzite subangular and subrounded rock fragments (f.s.; ±2%).

Inorganic residues of biological origin: bones (v.f.s., ±2%);

Anthropogenic elements: charcoal fragments (f.s., ±2%).

Micromass: light brown grey, cloudy mixture of calcite and clay; crystallitic b-fabric.

Pedofeatures

- Typic ferrous nodules (f.s., ±1%).
- Manganese (hydr)oxide hypocoatings (s.s., ±1%).
- Micritic (equigranular xenotopic) nodules (v.f.s., ±10%).
- Equigranular hypidiotopic calcite coatings (f.s., ±5%).
- Compound parallel layered typic dusty clay coatings (granule size, ±20%), fragmented.
- Dense incomplete compound parallel layered dusty clay infillings (granule size, ±5%), fragmented.

Microfacies III (thin section* i *and* l*) (MFT: Deposits rich in material of organic origin, MOO)

Microstructure and porosity

Moderately-weakly separated crumb microstructure, with porous crumbs (f.s.) and subangular blocky peds (v.c.s.). Complex packing voids (f.s., ±20%); Channels (v.f.s., ±5%); planes (s.s.; ±2%); chambers (f.s., ±1%).

Groundmass

c/$f_{5\mu m}$ ratio: 30/70; c/f-related distribution pattern: single spaced equal enaulic.

Coarse material:

Mineral: subangular and angular grains of quartz (f.s., ±10%); subangular grains of calcite (f.s., ±1%). Fossiliferous subrounded limestone rock fragments (c.s., ±10%); quartzite subrounded rock fragments (f.s.; ±1%).

Inorganic residues of biological origin: bones (f.s., ±1%);

Anthropogenic elements: burnt bones (f.s., ±1%); charcoal fragments (f.s., ±2%), one fragment is embedded in a brownish aggregate.

Micromass: brown grey, speckled mixture of calcite and clay; weakly developed crystallitic b-fabric.

Pedofeatures

- Typic ferrous nodules (f.s., ±1%).
- Manganese (hydr)oxide hypocoatings (f.s., ±1%).
- Micritic (equigranular xenotopic) nodules (f.s., ±2%).
- Compound parallel layered typic dusty clay coatings (m.s., ±1%), fragmented.
- Cryptocrystalline typic apatite nodules (v.f.s., ±1%).
- Subrounded excrement of large animals, (m.s., ±1%).

Microfacies IV (thin section* i*) (MFT:. Sediments rich in charred material, CM)

Microstructure and porosity

Moderately separated granular microstructure, with granules (m.s.). Complex packing voids (v.f.s., ±30%); planes (s.s.; ±2%); chambers (f.s., ±1%).

Groundmass

c/$f_{5\mu m}$ ratio: 50/50; c/f-related distribution pattern: single spaced equal enaulic.

Coarse material:

Mineral: subangular and angular grains of quartz (v.f.s., ±10%); subangular grains of microcline (f.s., one occurrence). Fossiliferous subrounded limestone rock fragments (f.s., ±20%).

Inorganic residues of biological origin: bones (v.f.s., ±2%);

Anthropogenic elements: burnt bones (v.f.s., ±5%); charcoal fragments (f.s., ±20%).

Micromass: dark brown, dotted-opaque mixture of calcite, organic matter, charcoal, phosphates and clay; undifferentiated-crystallitic b-fabric.

Pedofeatures

- Typic ferrous nodules (f.s., ±1%).
- Micritic (equigranular xenotopic) nodules (s.s., ±2%).

Microfacies V (thin section* i*) (MFT: Deposits rich in material of organic origin, MOO)

Microstructure and porosity

Highly separated crumb and subangular microstructure, with porous crumbs (v.f.s.) and subangular blocky peds (m.s., but also gravel size). Complex packing voids (s.s., ±30%); planes (s.s., ±5%); channels (s.s., ±2%); chambers (f.s., ±1%).

Groundmass

c/$f_{5\mu m}$ ratio: 30/70; c/f-related distribution pattern: double spaced equal enaulic, locally double spaced porphyric.

Coarse material:

Mineral: subangular and angular grains of quartz (m.s., ±10%); subangular grains of calcite (m.s., ±5%). Fossiliferous subangular limestone rock fragments (v.c.s., ±10%); quartzite subangular rock fragments (m.s.; ±1%).

Inorganic residues of biological origin: bones (f.s., ±2%);

Anthropogenic elements: burnt bones (v.f.s., ±2%); charcoal fragments (v.f.s., ±2%).

Micromass: brown, darker in the subangular peds and beige in the crumbs, speckled mixture of calcite, clay and phosphates in the crumbs, clay and calcite in the blocky peds; weakly developed crystallitic b-fabric.

Pedofeatures

- Typic ferrous nodules (f.s., ±1%).
- Micritic (equigranular xenotopic) nodules (f.s., ±5%).
- Typic impure clay nonlaminated coatings (v.f.s., ±1%), fragmented.
- Cryptocrystalline typic apatite coatings (v.f.s., ±1%).
- Subrounded excrement of large animals, (f.s., ±1%).

Thin section* l *(MFT: Deposits rich in material of organic origin, MOO)

Microstructure and porosity

Highly separated crumb microstructure, with porous crumbs (f.s.). Complex packing voids (v.f.s., ±30%); channels (s.s., ±10%); planes (s.s., ±5%).

Groundmass

c/$f_{5\mu m}$ ratio: 30/70; c/f-related distribution pattern: single spaced equal enaulic.

Coarse material:

Mineral: subangular grains of quartz (f.s., ±5%). Fossiliferous subangular limestone rock fragments (c.s., up to cobble size, ±20%); quartzite subangular rock fragments (m.s.; ±5%).

Inorganic residues of biological origin: bones (m.s., ±2%);

Anthropogenic elements: burnt bones (f.s., ±1%); charcoal fragments (f.s., ±1%).

Micromass: yellowish brown, speckled mixture of calcite, clay and phosphates; crystallitic-undifferentiated b-fabric.

Pedofeatures

- Typic ferrous nodules (v.f.s., ±1%).
- Micritic (equigranular xenotopic) nodules (f.s., ±2%).
- Micritic (equigranular xenotopic) hypocoatings (f.s., ±5%).
- Cryptocrystalline typic apatite nodules (f.s., ±1%).
- Subrounded excrement of large animals, (m.s., ±10%).

Section FA

Thin section* FA 3 *(MFT: Strongly cemented deposits, SC)

Vertical thin section.

Microstructure and porosity

Moderately separated crumb microstructure, with porous crumbs (fine gravel); subangular blocky peds (fine gravel). Complex packing voids (f.s., ±20%); channels (v.f.s., ±5%); vughs (v.f.s., ±5%); planes (s.s., ±2%).

Groundmass

c/$f_{5\mu m}$ ratio: 30/70; c/f-related distribution pattern: single spaced coarse enaulic.

Coarse material:

Mineral: angular-subangular grains of quartz (f.s., ±5%); angular grains of calcite (f.s., ±2%); subangular grains of muscovite (v.f.s., ±1%). Fossiliferous and speleothem subangular limestone rock fragments (c.s., up to cobble size, ±10%); quartzite subangular rock fragments (c.s.; ±2%).

Inorganic residues of biological origin: bones (m.s., ±5%);

Anthropogenic elements: burnt bones (f.s., ±1%); charcoal fragments (f.s., ±5%).

Micromass: grey-brown, speckled mixture of calcite, clay and phosphates for the porous crumbs; reddish brown, cloudy mixture of clay and iron for the subangular blocky peds; crystallitic, locally undifferentiated, b-fabric.

Pedofeatures

- Typic ferrous nodules (f.s., ±1%).
- Dendritic Manganese hypocoatings (f.s., ±1%).
- Calcite coatings, with palisade fabric, forming braces between the fabric elements (m.s., ±30%).
- Micritic (equigranular xenotopic) nodules (m.s., ±5%).
- Micritic (equigranular xenotopic) hypocoatings (s.s., ±10%).

- Phosphatic rims on rocks and bones. Cryptocrystalline apatite hypocoatings (v.f.s., ±1%).
- Cryptocrystalline typic apatite nodules (f.s., ±2%).
- Subrounded excrement of large animals (among them are carnivores), (v.c.s., ±5%).

Thin section* FA 4 *(MFT: Strongly cemented deposits, SC)

Vertical thin section.

Microstructure and porosity

Moderately separated crumb microstructure, with porous crumbs (fine gravel); subangular blocky peds (granules). Complex packing voids (m.s., ±10%); channels (v.f.s., ±5%); vughs (f.s., ±2%); planes (s.s., ±2%).

Groundmass

$c/f_{5\mu m}$ ratio: 30/70; c/f-related distribution pattern: single spaced coarse enaulic.

Coarse material:

Mineral: angular-subangular grains of quartz (m.s., ±5%); angular grains of calcite (m.s., ±2%). Fossiliferous subrounded-subangular limestone rock fragments (granule size, ±5%); quartzite subrounded rock fragments (g.s.; ±2%).

Inorganic residues of biological origin: bones (m.s., ±5%); tooth (m.s., one occurrence).

Anthropogenic elements: burnt bones (v.f.s., ±1%); charcoal fragments (f.s., ±5%).

Micromass: light brown, cloudy mixture of calcite, clay and phosphates for the porous crumbs; reddish brown, cloudy mixture of clay and iron for the subangular blocky peds; crystallitic, locally undifferentiated, b-fabric for the porous crumbs, weakly developed granostriated for the subangular blocky peds.

Pedofeatures

- Typic ferrous nodules (m.s., ±1%).
- Dendritic Manganese hypocoatings (f.s., ±1%).
- Typic manganese nodules (m.s., ±1%).
- Calcite coatings, with palisade fabric, forming braces between the fabric elements (f.s., ±40%).

- Phosphatic rims on rocks and bones. Cryptocrystalline apatite coatings (f.s., ±1%).
- Cryptocrystalline typic apatite nodules (f.s., ±1%).
- Subrounded excrement of large animals, (v.c.s., ±5%).

Thin section* FA 6 *(MFT: Strongly cemented deposits, SC)

Vertical thin section.

Microstructure and porosity

Complex: weakly separated subangular blocky microstructure and crumb microstructure, with subangular blocky peds (cobble size) and porous crumbs (v.c.s.). Complex packing voids (m.s., ±5%); planes (f.s., ±5%); channels (v.f.s., ±5%); chambers (m.s., ±2%); vughs (s.s., ±2%).

Groundmass

$c/f_{5\mu m}$ ratio: 30/70; c/f-related distribution pattern: double spaced porphyric - close coarse enaulic.

Coarse material:

Mineral: angular-subangular grains of quartz (from s.s. to pebble size, ±10%); angular grains of calcite (f.s., ±2%); not identifiable (v.f.s., ±1%). Fossiliferous subangular limestone rock fragments (granule size, ±5%); quartzite subangular rock fragments (v.c.s.; ±1%); sandstone angular rock fragments (pebble s.; one occurrence).

Inorganic residues of biological origin: bones (granule s., ±2%).

Anthropogenic elements: charcoal fragments (v.c.s., one occurrence).

Micromass: dark greyish brown, cloudy mixture of calcite, clay and phosphates; weakly developed crystallitic.

Pedofeatures

- Typic ferrous nodules (f.s., ±1%).
- Dendritic Manganese hypocoatings (f.s., ±1%).
- Calcite coatings, with palisade and needle-like fabric, forming braces between the fabric elements (m.s., ±20%).
- Micritic (equigranular xenotopic) hypocoatings (m.s., ±5%).
- Calcite geodic nodules (m.s., ±2%).

- Cryptocrystalline apatite coatings: unsorted, nonlaminated (f.s., ±1%).
- Subrounded excrement of large animals, (m.s., ±2%).

Thin section* FA 9a *(Strongly cemented deposits, SC)

Vertical thin section.

Microstructure and porosity

Weakly separated crumb microstructure, with porous crumbs (granules) and subangular blocky peds (granules). Complex packing voids (m.s., ±10%); channels (v.f.s., ±5%); vughs (f.s., ±2%); planes (v.s., ±2%).

Groundmass

c/$f_{5\mu m}$ ratio: 40/60; c/f-related distribution pattern: Close coarse enaulic.

Coarse material:

Mineral: subrounded-subangular grains of quartz (from v.f.s. to pebble s., ±10%); angular grains of calcite (m.s., ±2%). Fossiliferous subangular limestone rock fragments (granule size, but one fragment is 3 cm, ±5%); quartzite subrounded rock fragments (g.s.; ±2%).

Inorganic residues of biological origin: bones (m.s., ±2%); tooth (c.s., one occurrence) fragmented.

Anthropogenic elements: charcoal fragments (v.c.s., two occurrences).

Micromass: light brown, cloudy mixture of calcite, clay and phosphates for the porous crumbs; reddish brown, cloudy mixture of clay and iron for the subangular blocky peds; crystallitic, locally undifferentiated, b-fabric for the porous crumbs, weakly developed porostriated for the subangular blocky peds.

Pedofeatures

- Typic ferrous nodules (s.s., ±1%).
- Dendritic Manganese hypocoatings (f.s., ±2%).
- Typic manganese nodules (f.s., ±1%).
- Calcite coatings, with palisade and needle-like fabric, forming braces between the fabric elements (f.s., ±20%).
- Limpid parallel microlaminated clay coatings, with sharp extinction lines (f.s., ±1%).

- Limpid parallel microlaminated clay infillings, with sharp extinction lines (f.s., ±1%).
- Cryptocrystalline typic apatite nodules (f.s., ±2%).
- Subrounded excrement of large animals, some carnivores (c.s., ±5%).

Thin section* FA 9b *(MFT: Partly cemented deposits, PC)

Vertical thin section.

Microstructure and porosity

Complex: Weakly separated subangular blocky and weakly separated crumb microstructure, with subangular and angular blocky peds (granules size), porous crumbs (granules size) and granules (granules size). Complex packing voids (m.s., ±10%); channels (m.s., ±5%); planes (m.s., ±5%); chambers (c.s., ±2%); vughs (f.s., ±2%); .

Groundmass

c/$f_{5\mu m}$ ratio: 40/60; c/f-related distribution pattern: single spaced porphyric and single spaced coarse enaulic.

Coarse material:

Mineral: subrounded-subangular grains of quartz (f.s., ±5%); angular grains of calcite (m.s., ±2%); rounded grains of feldspars (m.s., ±1%). Fossiliferous rounded limestone rock fragments (pebble size, ±10%); quartzite rounded rock fragments (g.s.; ±5%).

Inorganic residues of biological origin: bones (m.s., ±2%).

Anthropogenic elements: charcoal fragments (m.s., two occurrences).

Micromass: greyish brown, cloudy mixture of calcite, clay and phosphates; reddish brown, cloudy mixture of clay and iron for certain subangular blocky peds; crystallitic, locally undifferentiated, b-fabric, weakly developed porostriated for certain subangular blocky peds.

Pedofeatures

- Typic ferrous nodules (c.s., ±1%).
- Dendritic Manganese hypocoatings (v.f.s., ±1%).
- Typic manganese nodules (f.s., ±5%).
- Equigranular hypidiotopic sutured micritic nodules (f.s., ±2%).

- Micritic (equigranular xenotopic) hypocoatings (s.s., ±5%).
- Limpid parallel microlaminated clay coatings, with sharp extinction lines (v.c.s., one occurrence).
- Cryptocrystalline typic apatite nodules (f.s., ±1%).
- Cryptocrystalline typic apatite coatings (v.f.s., ±1%).
- Subrounded excrement of large animals, some of carnivores (c.s., ±1%, but one big element, 1 cm).

Thin section* FA 11 *(MFT: Partly cemented deposits, PC)

Vertical thin section.

Microstructure and porosity

Complex: moderately separated angular blocky and moderately separated granular microstructure, with angular blocky peds (pebble size) and granules (m.s.). Complex packing voids (v.f.s., ±10%); channels (m.s., ±10%); planes (c.s., ±10%); vughs (v.f.s., ±2%); .

Groundmass

c/$f_{5\mu m}$ ratio: 30/70; c/f-related distribution pattern: single spaced porphyric and single spaced equal enaulic.

Coarse material:

Mineral: subrounded-subangular grains of quartz (m.s. but up to granule size, ±10%); angular grains of calcite (v.c.s., ±5%); subangular grains of feldspars (m.s., ±1%). Fossiliferous rounded limestone rock fragments (v.c.s. but up to pebble size, ±10%); quartzite rounded rock fragments (v.c.s.; ±1%).

Inorganic residues of biological origin: bones (f.s., ±2%).

Anthropogenic elements: charcoal fragments (m.s., ±1%).

Micromass: greyish brown, cloudy mixture of calcite, clay and phosphates; reddish brown with clay and iron in a few of granules; crystallitic, locally undifferentiated, b-fabric, weakly developed porostriated for certain granules.

Pedofeatures

- Typic ferrous nodules (f.s., ±2%).

- Dendritic Manganese hypocoatings (v.f.s., ±1%).
- Typic manganese nodules (m.s., ±2%).
- Micritic (equigranular xenotopic) hypocoatings (v.c.s., ±20%).
- Sparitic coatings with palisade fabric, in contact with the micritic hypocoatings (f.s., ±5%).
- Equigranular xenotopic mosaic-like calcite infillings (m.s., ±1%).
- Fe-stained nonlaminated clay coating with few quartz fragments (of different sizes), underneath few of the micritic hypocoatings (c.s., ±1%).
- Cryptocrystalline typic apatite coatings (v.f.s., ±1%) (reactions rims on rock fragments).
- Subrounded excrement of large animals, some of which carnivores (f.s., ±2%).

Thin section* FA 12 *(MFT: Reddish brown deposits, RB)

Vertical thin section.

Microstructure and porosity

Complex: highly separated subangular blocky microstructure, with subangular blocky peds (cobble size). Planes (c.s., ±10%); chambers (v.c.s., ±5%); channels (f.s., ±2%); vughs (v.f.s., ±2%).

Groundmass

c/$f_{5\mu m}$ ratio: 40/60; c/f-related distribution pattern: single spaced porphyric.

Coarse material:

Mineral: subrounded-subangular grains of quartz (s.s.-c.s., ±10%); angular grains of calcite (c.s., ±5%); angular grains of feldspars (f.s., ±1%). Fossiliferous rounded limestone and speleothem rock fragments (v.c.s.-pebble size, ±5%); quartzite rounded rock fragments (pebble s.; ±2%); sandstone angular rock fragments (v.c.s.; two occurrences).

Inorganic residues of biological origin: bones (m.s.-granule size, ±2%).

Anthropogenic elements: burnt bones (f.s., ±1%); charcoal fragments (f.s., ±2%), fragmented.

Micromass: brown, cloudy of clay and phosphates; weakly developed porostriated, locally undifferentiated, b-fabric; few aggregates in the groundmass are reddish brown, iron- and clay-rich, with porostriated b-fabric.

Pedofeatures

- Typic ferrous nodules (f.s., ±1%).
- Dendritic Manganese hypocoatings (m.s., ±5%).
- Typic manganese nodules (f.s., ±2%).
- Micritic (equigranular xenotopic sutured) nodules (f.s., ±2%), mainly in the inferior part.
- Fragmented compound layered clay coating (c.s., one occurrence).
- Cryptocrystalline typic apatite coatings (f.s., ±2%) (reactions rims on mineral grains and rock fragments).
- Subrounded excrement of large animals (m.s., ±2%).

Thin section* FA 13a *and the upper part of* FA13b *(MFT: Reddish brown deposits, RB)

Vertical thin section.

Microstructure and porosity

Weakly separated subangular blocky microstructure, with subangular blocky peds (cobble size). Planes (f.s., ±10%, many perpendicular to the ground surface); chambers (m.s., ±5%); channels (f.s., ±5%).

Groundmass

$c/f_{5\mu m}$ ratio: 40/60; c/f-related distribution pattern: close porphyric.

Coarse material:

Mineral: angular grains of quartz (v.f.s., ±20%); angular grains of calcite (v.c.s., ±2%); flakes-like grains of muscovite (s.s., ±1%). Fossiliferous subangular and subrounded limestone rock fragments (granule s., ±5%); quartzite subangular and subrounded rock fragments (c.s.; ±5%).

Inorganic residues of biological origin: bones (f.s., ±5%).

Anthropogenic elements: burnt bones (f.s., ±1%); charcoal fragments (m.s., ±2%); burnt aggregate (granule s., one occurrence).

Micromass: brown, cloudy of clay, phosphates and mica; weakly developed porostriated, locally undifferentiated, b-fabric; few aggregates in the groundmass are reddish brown, iron- and clay-rich, with porostriated b-fabric.

Pedofeatures

- Typic ferrous nodules (v.f.s., ±1%).
- Dendritic manganese (hydr)oxide hypocoatings (m.s., ±5%). Mostly in the inferior part, sometimes associated to bones.
- Nonlaminated dusty and limpid clay infillings (f.s., ±2%).
- Cryptocrystalline typic apatite coatings (f.s., ±2%) (reactions rims on mineral grains and rock fragments).
- Subrounded excrement of large animals (f.s.-granule s., ±5%).

Thin section* FA 13b *(MFT: Reddish brown deposits, RB)

Vertical thin section.

Microstructure and porosity

Weakly separated subangular blocky microstructure, with subangular blocky peds (pebble size). Planes (f.s., ±10%); chambers (c.s., ±5%); channels (f.s., ±5%); vughs (f.s., ±5%).

Groundmass

c/$f_{5\mu m}$ ratio: 40/60; c/f-related distribution pattern: close porphyric, locally single spaced.

Coarse material:

Mineral: angular grains of quartz (f.s., ±20%). Quartzite subrounded rock fragments (c.s.; ±5%); mudrock subrounded rock fragments (c.s., ±1%).

Inorganic residues of biological origin: bones (f.s., ±1%).

Anthropogenic elements: charcoal fragments (v.f.s., ±1%).

Micromass: reddish brown, cloudy, composed of clay and little of phosphates; weakly developed porostriated, locally undifferentiated, b-fabric.

Pedofeatures

- Typic ferrous nodules (v.f.s., ±1%).
- Dendritic manganese (hydr)oxide hypocoatings (m.s., ±2%).

- Parallel compound layered clay and silt coatings (c.s. but up to v.c.s., ±5%). Mainly along a straight line. Partly fragmented.
- Cryptocrystalline typic apatite coatings (v.f.s., ±1%).
- Subrounded excrement of large animals (m.s., ±5%).

Section FB

Thin section* FB 2 *(MFT: Cave wall deposits, CW)

Horizontal thin section

Microstructure and porosity

Weakly separated subangular blocky microstructure, with subangular blocky peds (pebble size). Planes (f.s., ±10%); chambers (c.s., ±5%); channels (f.s., ±5%); vughs (f.s., ±5%).

Groundmass

$c/f_{5\mu m}$ ratio: 20/80; c/f-related distribution pattern: open porphyric.

Coarse material:

Mineral: angular grains of quartz (f.s., ±10%). Fossiliferous subangular and subrounded limestone rock fragments (f.s., ±1%); quartzite subangular and subrounded rock fragments (f.s.; ±1%).

Inorganic residues of biological origin: bones (c.s. but two fragments are cobble size, ±5%).

Anthropogenic elements: charcoal fragments (v.f.s., ±1%).

Micromass: brown, cloudy, composed of clay and a little of phosphates; weakly developed porostriated, locally undifferentiated, b-fabric. Some portions along the calcite coatings show a light brown micromass and a weakly developed crystallitic b-fabric.

Pedofeatures

- Typic ferrous nodules (v.f.s., ±1%).
- Dendritic manganese (hydr)oxide hypocoatings (v.f.s., ±2%).
- Compound layered equigranular xenotopic calcitic coatings (c.s., ±20%). Beneath the other carbonate pedofeatures classes.

- Compound layered equigranular hypidiotopic calcitic coatings (c.s., ±10%). Between the other two carbonate pedofeatures classes described.
- Equigranular idiotopic calcitic coatings (c.s., ±20%). Usually above the other two carbonate pedofeatures classes.
- Silt capping, nonlaminated (v.c.s., one occurrence).
- Cryptocrystalline typic apatite nodules (v.f.s., ±1%).
- Subrounded excrement of large animals (m.s., ±2%).

Thin section* FB3 *(MFT: Reddish brown deposits, RB)

Vertical thin section.

Microstructure and porosity

Spongy and weakly separated crumb microstructure, with subangular blocky peds (cobble size, weakly developed pedality) and crumb (v.c.s., weakly developed pedality). Channels (m.s., ±10%); vughs (f.s., ±10%); planes (f.s., ±5%); chambers (m.s., ±5%);

Groundmass

c/$f_{5\mu m}$ ratio: 30/70; c/f-related distribution pattern: single spaced porphyric.

Coarse material:

Mineral: angular grains of quartz (v.f.s., ±20%); angular grains of muscovite (s.s., ±1%). Quartzite subangular and subrounded rock fragments (c.s.; ±5%).

Inorganic residues of biological origin: bones (c.s., ±2%).

Anthropogenic elements: charcoal fragments (c.s., ±2%).

Micromass: brown-reddish brown, cloudy, composed of clay and phosphates; weakly developed granostriated, locally undifferentiated, b-fabric; few aggregates in the groundmass are reddish, iron- and clay-rich, with striated b-fabric.

Pedofeatures

- Typic ferrous nodules (f.s., ±1%).
- Dendritic manganese (hydr)oxide hypocoatings (s.s., ±1%).
- Typic manganese (hydr)oxide nodules (f.s., ±2%).
- Sparitic coatings with palisade fabric (equigranular hypidiotopic)(c.s., ±5%).

- Sparitic infillings with palisade fabric (equigranular hypidiotopic)(c.s., ±2%).
- Nonlaminated limpid clay coatings with diffuse extinction lines (v.f.s., ±10%).
- Cryptocrystalline typic apatite infilling (m.s., 1 occurrence: it cuts the thin section in half).
- Subrounded excrement of large animals (c.s., ±5%).

Section FC

***Thin section* FC**

Vertical thin section.

Two microfacies are present and they actually represent level 1 and level 2 of the stratigraphic section. They will be described separately.

Microfacies 1 (Pale yellow deposit, PY)

Microstructure and porosity

Moderately separated subangular blocky microstructure, with subangular blocky peds (cobble size). Compound packing voids (v.c.s., ±10%); planes (m.s., ±10%); chambers (c.s., ±5%); channels (m.s., ±5%).

Groundmass

c/$f_{5\mu m}$ ratio: 40/60; c/f-related distribution pattern: single spaced porphyric.

Coarse material:

Mineral: angular and subangular grains of quartz (f.s., ±10%). Quartzite, subangular and subrounded, rock fragments (c.s.; ±2%).

Inorganic residues of biological origin: bones (f.s., ±1%).

Micromass: greenish yellow, cloudy, composed of clay, calcite and phosphates; undifferentiated b-fabric.

Pedofeatures

- Typic ferrous nodules (v.f.s., ±1%).
- Dendritic manganese (hydr)oxide hypocoatings (m.s., ±1%).
- Typic micritic (equigranular xenotopic) nodules (c.s., ±2%). Isotropic in XPL.

- Clay and silt coatings, compound layered, laminae are parallel and extinction lines are absent (pebble s., ±10%). Only in the lower part of the mF.
- Cryptocrystalline typic apatite nodules, mammillate (c.s., ±2%).
- Subrounded excrement of large animals (v.c.s., ±20%).

Microfacies 2 (Laminated silt, LS)

Microstructure and porosity

Moderately separated angular blocky microstructure, with angular blocky peds (cobble size). Planes (v.c.s., ±10%); chambers (c.s., ±5%); channels (v.f.s., ±2%); vughs (s.s., ±2%).

Groundmass

$c/f_{5\mu m}$ ratio: 60/40; c/f-related distribution pattern: close porphyric.

Coarse material:

Mineral: angular and subangular grains of quartz (s.s., ±50%); flake-like grains of muscovite (s.s., ±2%).

Micromass: reddish brown, speckled, composed of clay, micas and iron; unistrial b-fabric.

Pedofeatures

- Typic ferrous nodules (s.s., ±1%), only in the finer layers.
- Typic micritic (equigranular xenotopic) nodule (pebble s., one occurrence). Isotropic in XPL.
- Cryptocrystalline typic apatite nodules (f.s., ±2%).
- Crescent apatite coating (c.s., ±1%).
- Subrounded excrements (c.s., ±2%). Predominantly in the upper part of the mF.

Thin section* GH *(MFT: Reddish brown deposit MFT, RB)

Vertical semi-mammoth thin section.

Four microfacies were recognised. Microfacies 1 coincides with level H, the rest of them belong to level G. They will be described separately.

Microfacies 1

Microstructure and porosity

Moderately separated angular blocky microstructure, with angular blocky peds (pebble size). Planes (c.s., ±5%); chambers (v.c.s., ±5%); channels (m.s., ±2%).

Groundmass

c/$f_{5\mu m}$ ratio: 50/50; c/f-related distribution pattern: Varying (it depends on the lamina) between close porphyric and open porphyric.

Coarse material:

Mineral: angular grains of quartz (s.s., ±40%).

Anthropogenic elements: charcoal fragments (c.s., two occurrences). Found in the coarser laminae.

Micromass: reddish brown, speckled, composed of clay and quartz; stipple speckled b-fabric.

Pedofeatures

- Calcitic coatings with palisade fabric (equigranular hypidiotopic) (v.c.s., ±1%).
- Calcitic infillings with palisade fabric (equigranular hypidiotopic) (v.c.s., ±2%).

Microfacies 2

Microstructure and porosity

Weakly separated subangular blocky microstructure, with subangular blocky peds (granule size). Planes (f.s., ±10%); channels (m.s., ±5%).

Groundmass

c/$f_{5\mu m}$ ratio: 30/70; c/f-related distribution pattern: Single spaced porphyric.

Coarse material:

Mineral: angular grains of quartz (f.s., ±20%).

Anthropogenic elements: charcoal fragments (c.s., ±5%).

Micromass: reddish brown, cloudy, composed of clay; stipple speckled b-fabric.

Pedofeatures

- Manganese (hydr)oxide typic nodules (f.s., ±1%).
- Calcitic coatings with palisade fabric (equigranular hypidiotopic) (v.c.s., ±2%). Fragmented.

Microfacies 3

Microstructure and porosity

Single spaced equal enaulic microstructure, with porous crumbs (v.c.s.). Complex packing voids (m.s., ±10%); channels (s.s., ±2%).

Groundmass

c/$f_{5\mu m}$ ratio: 60/40; c/f-related distribution pattern: Single spaced equal enaulic.

Coarse material:

Mineral: subangular grains of quartz (v.c.s., ±50%). Quartzite, subangular and tabular, rock fragments (v.c.s.; ±1%).

Anthropogenic elements: charcoal fragments (v.c.s., two occurrences).

Micromass: reddish brown, speckled opaque, composed of clay and iron; weakly developed stipple speckled b-fabric.

Pedofeatures

- Manganese (hydr)oxide dendritic hypocoatings (m.s., ±1%).
- Calcitic coatings with palisade fabric (equigranular hypidiotopic) (v.c.s., ±5%). Fragmented.
- Mammillate excrements (v.c.s., ±1%).

Microfacies 4

Microstructure and porosity

Moderately separated subangular blocky microstructure, with subangular blocky peds (granule size). Complex packing voids (f.s., ±5%); planes (f.s., ±2%); channels (v.f.s., ±2%); chambers (f.s., ±2%).

Groundmass

c/$f_{5\mu m}$ ratio: 20/80; c/f-related distribution pattern: Open porphyric.

Coarse material:

Mineral: angular grains of quartz (s.s., ±10%).

Anthropogenic elements: charcoal fragments (f.s., 1%).

Micromass: reddish brown, speckled opaque, composed of clay and iron; weakly developed stipple speckled b-fabric.

Pedofeatures

- Manganese (hydr)oxide digitate nodules (f.s., ±1%).
- Parallel laminated micropan (moving towards the surface: silt, impure clay, dusty clay). On the contact between the last mF 4 and the last mF 3. (1 mm thick x 15 mm long; one occurrence).
- Fragmented limpid-impure clay parallel laminated coating (m.s., ±2%). Fragmented.

Thin section* AM E *(MFT: Dark, cemented deposit MFT, DC)

Vertical thin section.

Microstructure and porosity

Weakly separated subangular blocky microstructure, with subangular blocky peds (pebble size) and porous crumbs (granule size). Planes (v.f.s., ±10%); vughs (f.s., ±5%); channels (s.s., ±5%).

Groundmass

c/$f_{5\mu m}$ ratio: 50/50; c/f-related distribution pattern: doble spaced porphyric.

Coarse material:

Mineral: subangular grains of quartz (f.s., ±2%). Limestone subrounded rock fragments (f.s.; ±10%).

Inorganic residues of biological origin: bones (cobble size, ±30%); teeth (cobble size, two occurrences); hair (3 mm long; one occurrence), in the uppermost part of the t.s..

Anthropogenic elements: charcoal fragments (v.c.s., ±10%); burnt aggregates (v.c.s., ±5%).

Micromass: Two kinds of micromass: one dark brown, cloudy, composed of clay and charcoal, with an undifferentiated b-fabric; the other brown, cloudy, composed of clay and carbonates, with crystallitic b-fabric.

Pedofeatures

- Typic ferrous nodules (m.s., ±2%).
- Dendritic manganese (hydr)oxide hypocoatings (f.s., ±1%).
- Calcitic coatings, equigranular xenotopic (s.s., ±2%).
- Calcitic infillings, equigranular xenotopic (f.s., ±5%).
- Limpid nonlaminated clay coatings with no extinction lines (f.s., ±1%). When a calcite coatings is also present, the clay coating is found between the ped and the $CaCO_3$ coating. Fragmented.
- Limpid nonlaminated clay infillings with no extinction lines (f.s., ±2%). Fragmented.

Thin section* AM C *(MFT: Dark, cemented deposit MFT, DC)

Vertical thin section.

Microstructure and porosity

Complex: Weakly separated crumb microstructure and weakly separated granular microstructure, with porous crumbs (granule size) and granules (granule size). Complex packing voids (m.s., ±10%); channels (f.s., ±5%).

Groundmass

c/$f_{5\mu m}$ ratio: 40/60; c/f-related distribution pattern: Single spaced coarse enaulic.

Coarse material:

Mineral: subangular grains of quartz (s.s., ±5%). Limestone subangular rock fragments (c.s.; ±20%); schist subangular rock fragments (c.s.; one occurrence).

Inorganic residues of biological origin: bones (m.s., ±5%).

Anthropogenic elements: charcoal fragments (c.s. but one element is pebble size, ±10%); burnt bones (m.s., ±10%); burnt aggregates (granule s., ±2%); lithic artefact remain (granule s., one occurrence), upper part of the t.s..

Micromass: dark brown, cloudy, composed of clay, calcite and charcoal, with a stipple speckled, undifferentiated at traits, b-fabric.

Pedofeatures

- Typic ferrous nodules (f.s., ±1%).
- Calcitic coatings, equigranular xenotopic (f.s., ±20%).
- Limpid parallel laminated (alternating yellowish and reddish laminae) clay coating with diffuse extinction lines (f.s., ±5%). On voids, aggregates and mineral grains.

Thin section* AM B *(MFT: Reworked loess MFT, RL)

Vertical thin section.

Microstructure and porosity

Complex: Weakly separated crumb microstructure and weakly separated granular microstructure, with porous crumbs (granule size) and granules (granule size). Complex packing voids (f.s., ±10%); chambers (v.c.s., ±10%); vughs (v.f.s., ±5%); planes (f.s., ±5%); channels (f.s., ±2%).

Groundmass

c/$f_{5\mu m}$ ratio: 40/60; c/f-related distribution pattern: close coarse enaulic.

Coarse material:

Mineral: subangular grains of quartz (s.s., ±20%); flake-like grains of mica (s.s., ±5%). Limestone (speleothem) subangular rock fragments (c.s.; ±10%).

Inorganic residues of biological origin: bones (f.s., ±1%); shell (c.s.; one occurrence).

Anthropogenic elements: charcoal fragments (f.s., two occurrences).

Micromass: yellowish grey, cloudy, composed of clay and carbonates, with weakly developed crystallitic b-fabric.

Pedofeatures

- Typic ferrous nodules (f.s., ±1%).
- Manganese (hydr)oxide hypocoatings (s.s., ±1%).
- Calcitic infillings, equigranular xenotopic (s.s., ±10%).
- Limpid/dusty clay coatings, nonlaminated, with diffuse extinction lines (s.s., ±5%). Underneath the calcite infillings.

Thin section* AM A *(MFT: Reworked loess MFT, RL)

Vertical thin section.

Microstructure and porosity

Weakly separated platy microstructure, with plates (pebble size) and subangular blocky peds (pebble size). Planes (v.f.s., ±10%); vughs (f.s., ±10%); chambers (v.c.s., ±5%); channels (f.s., ±2%).

Groundmass

c/$f_{5\mu m}$ ratio: 30/70; c/f-related distribution pattern: double spaced porphyric.

Coarse material:

Mineral: subangular and angular grains of quartz (f.s., ±10%); flake-like grains of mica (s.s., ±1%). Limestone (fossiliferous and speleothem) subangular, subrounded and tabular rock fragments (granule s.; ±10%), some elements seem oriented with their main axis perpendicular to the ground; quartzite subrounded and subangular rock fragments (v.c.s.; ±5%); schist subrounded and subangular rock fragments (v.c.s.; ±2%).

Inorganic residues of biological origin: bones (f.s., ±10%); shell (c.s.; one occurrence).

Anthropogenic elements: charcoal fragments (f.s., ±1%).

Micromass: yellowish grey, cloudy, composed of clay and carbonates, with weakly developed crystallitic b-fabric.

Pedofeatures

- Typic ferrous nodules (f.s., ±1%).

- Micritic (equigranular xenotopic) nodules (granule s., ±5%).
- Calcitic dense incomplete infillings, equigranular xenotopic (granule-pebble size, ±5%).
- Dusty parallel microlaminated clay coatings with diffuse extinction (s.s., ±1%).

Thin section* AM II *(MFT: Brown clay MFT, CC)

Vertical thin section.

Microstructure and porosity

Moderately-weakly separated platy microstructure, with plates (pebble size) and subangular blocky peds (granule size). Planes (v.f.s., ±10%); chambers (v.c.s., ±10%); vesicles (c.s., ±2%); channels (c.s., ±2%); vughs (c.s., ±2%).

Groundmass

c/$f_{5\mu m}$ ratio: 40/60; c/f-related distribution pattern: double spaced porphyric.

Coarse material:

Mineral: subangular and angular grains of quartz (s.s., ±20%); angular grains of mica (s.s., ±10%). Limestone (fossiliferous and speleothem) subangular rock fragments (c.s.; ±5%), some elements seem oriented with their main axis perpendicular to the ground; quartzite subrounded rock fragments (v.c.s.; ±1%).

Inorganic residues of biological origin: bones (c.s. with one big fragment 23 mm long, ±5%); hair (1 mm long; one occurrence), in the middle part of the t.s..

Anthropogenic elements: charcoal fragments (c.s., ±1%); burnt bones (m.s., ±2%).

Micromass: brown, speckled, composed of clay, with weakly developed porostriated b-fabric.

Pedofeatures

- Typic ferrous nodules (m.s., ±1%).
- Typic manganese (hydr)oxide nodules (f.s., ±1%).
- Clay coarsening (from dusty clay parallel lamination, to chaotically disposed silt sized quartz) dense incomplete infilling (granule size, one occurrence in the lower part of the t.s.).

- Limpid parallel microlaminated clay coatings with diffuse extinction lines (s.s., ±1%). Mainly in the lower part of the t.s..

Thin section* AM III *(MFT: Brown clay MFT, CC)

Vertical thin section.

Microstructure and porosity

Moderately separated platy microstructure, with plates (pebble size). Planes (v.f.s., ±10%); channels (c.s., ±5%), some are oblong; chambers (c.s., ±10%); vughs (f.s., ±2%); vesicles (f.s., ±2%).

Groundmass

c/$f_{5\mu m}$ ratio: 40/60; c/f-related distribution pattern: single spaced porphyric.

Coarse material:

Mineral: subangular and angular grains of quartz (s.s., ±20%). Limestone (fossiliferous) subrounded rock fragments (v.c.s.; ±2%); schist subangular-tabular rock fragments (v.c.s.; ±2%); quartzite subrounded rock fragments (c.s.; ±1%).

Inorganic residues of biological origin: bones (f.s., ±1%).

Anthropogenic elements: charcoal fragments (f.s., ±1%); burnt bones (v.f.s., ±1%).

Micromass: brown, cloudy, composed of clay, with weakly developed cross-striated b-fabric.

Pedofeatures

- Typic ferrous nodules (f.s., ±1%).
- Manganese (hydr)oxide hypocoatings (s.s., ±1%).
- Clay coarsening (from dusty clay parallel lamination, to chaotically disposed silt sized quartz) dense incomplete infilling (v.c.s., ±1%).

Thin section* AM IV *(MFT: Brown clay MFT, CC)

Vertical thin section.

Microstructure and porosity

Moderately separated platy and weakly separated subangular blocky microstructure, with plates (v.c.s.) and subangular blocky peds (granule s.). Planes (f.s., ±10%); channels (f.s., ±5%); chambers (c.s., ±5%); vesicles (f.s., ±2%).

Groundmass

c/$f_{5\mu m}$ ratio: 30/70; c/f-related distribution pattern: double spaced porphyric.

Coarse material:

Mineral: subangular grains of quartz (m.s., ±10%). Limestone (fossiliferous) subangular rock fragments (v.c.s.; ±5%); schist subangular-tabular rock fragments (v.c.s.; ±2%).

Inorganic residues of biological origin: bones (m.s., ±2%).

Anthropogenic elements: charcoal fragments (v.c.s., ±5%); burnt bones (c.s., ±5%), one big fragment seems calcined.

Micromass: brown, cloudy, composed of clay, with weakly developed porostriated b-fabric.

Pedofeatures

- Typic ferrous nodules (c.s., ±2%).
- Manganese (hydr)oxide nodules (s.s., ±1%).

Thin section* AM V *(MFT: Brown clay MFT, CC)

Vertical thin section.

Microstructure and porosity

Moderately separated platy and weakly separated subangular blocky microstructure, with plates (granule size) and subangular blocky peds (pebble size). Planes (f.s., ±10%); vesicles (m.s., ±10%); channels (f.s., ±5%); chambers (c.s., ±2%).

Groundmass

c/$f_{5\mu m}$ ratio: 30/70; c/f-related distribution pattern: double spaced porphyric.

Coarse material:

Mineral: subangular grains of quartz (f.s., ±10%); subangular grains of calcite (f.s., ±2%). Limestone (fossiliferous) subangular, subrounded and tabular rock fragments (granule s.; ±10%); quartzite subangular rock fragments (granule s.; ±2%); not recognisable subangular-tabular rock fragments (granule s.; ±2%). Few tabular limestone fragments are disposed on a line, as already seen in the field.

Inorganic residues of biological origin: bones (m.s., ±5%).

Anthropogenic elements: charcoal fragments (v.c.s., ±2%); burnt bones (m.s., ±1%).

Micromass: reddish brown, cloudy, composed of clay, with weakly developed porostriated b-fabric.

Pedofeatures

- Typic ferrous nodules (m.s., ±1%).
- Manganese (hydr)oxide quasicoatings (s.s., ±1%).
- Limpid parallel microlaminated clay coatings with sharp extinction lines (s.s., ±1%).

Thin section* AM VI *(MFT: Brown clay MFT, BC)

Vertical thin section.

Microstructure and porosity

Weakly-moderately separated prismatic microstructure, with prismatic peds (pebble size). Planes (f.s., ±10%); chambers (v.c.s., ±5%); channels (f.s., ±2%); vughs (f.s., ±2%).

Groundmass

c/$f_{5\mu m}$ ratio: 40/60; c/f-related distribution pattern: single spaced porphyric.

Coarse material:

Mineral: subangular and subrounded grains of quartz (m.s., ±10%); angular grains of calcite (f.s., ±2%); subangular and subrounded grains of plagioclase (f.s., ±2%). Limestone (fossiliferous and speleothem) subangular, subrounded and tabular rock fragments (granule s.; ±20%); quartzite subrounded rock fragments (granule s.; ±2%); not recognisable subrounded rock fragments (v.c.s.; ±1%). All the mineral elements are positioned with their main axis perpendicular to the ground surface.

Inorganic residues of biological origin: bones (f.s., ±2%).

Anthropogenic elements: charcoal fragments (f.s., ±2%); burnt bones (f.s., ±2%).

Micromass: reddish brown, cloudy, composed of clay, with weakly developed granostriated b-fabric.

Pedofeatures

- Typic ferrous nodules (f.s., ±1%).
- Micritic (equigranular xenotopic) nodules (f.s., ±1%).
- Dusty parallel microlaminated clay coatings with sharp extinction lines (s.s., ±1%).
- Loose continuous infilling of granule size peds (two occurrences).